LITHOSPHERIC MODIFICATION OF FLOOD BASALT MAGMAS: A CHEMO STRATIGRAPHIC ANALYSIS OF THE EOCENE TO EARLY OLIGOCENE FLOOD BASALT PROVINCE IN EAST AFRICA

By

Ronald Alexander Steiner

A DISSERTATION

Submitted to
Michigan State University
in partial fulfillment of the requirements
for the degree of

Geological Sciences – Doctor of Philosophy

2022

ABSTRACT

LITHOSPHERIC MODIFICATION OF FLOOD BASALT MAGMAS: A CHEMO STRATIGRAPHIC ANALYSIS OF THE EOCENE TO EARLY OLIGOCENE FLOOD BASALT PROVINCE IN EAST AFRICA

By

Ronald Alexander Steiner

Continental large igneous provinces (LIP) are among the largest magmatic events on Earth, manifesting at the surface as stacks of monotonous flood basalt lavas. There are two distinct flood basalt episodes evident in East Africa, both considered related to the African Large Low Shear Velocity Province (LLSVP). This dissertation focuses on flood basalts from the Eocene Initial Phase - generated as a result of the initial interaction between material rising from the African LLSVP and the African lithosphere. In chapter 2 we present a geographically well-distributed geochemical dataset of these flood basalts to refine the regional volcano-stratigraphy into three distinct units: (1) Akobo Basalts (49.4 -46.6 Ma), representing the initial phase of flood basalt volcanism derived from the melting of lithospheric-mantle metasomes, (2) Amaro Basalts (45.2-39.58 Ma) representing the early main phase of flood basalt volcanism derived from the melting of the upwelling thermochemical anomaly, and (3) Gamo-Makonnen magmatic unit (38-28 Ma) representing the mature main phase of flood basalt volcanism that has undergone significant processing within the lithosphere. The focused intrusion of these main phase magmas over 10 m.y. preconditioned the African lithosphere for the localization of strain. Focusing of strain into the region occupied by this continental LIP may have contributed to the initial extension in SW Ethiopia associated with the East African Rift.

Chapter 3 presents crystal chemistry from a stratigraphically well-constrained series of 54 flood basalts, permitting a temporal insight into the development of one the best-

preserved continental LIP. The stratiform mafic lavas exposed in northern Kenya consist of alternating aphyric and plagioclase-rich lava packages consistent with periods of eruption punctuated by volcanic hiatuses, where magmas stall and crystallize plagioclase at medium to shallow crustal levels. Plagioclase exhibit little intra-crystal or intra-sample compositional diversity. Intra-crystal equilibrium calculations for Sr and Ti indicate internal chemical equilibrium, requiring storage at high temperature over a prolonged time interval (10,000-100,000 years). Using a series of interlinked partial crystal fractionation models, we find the balance between recharge and evacuation, and diffusive equilibration within a shallow magmatic system controls the composition of plagioclase in these flood basalts. We conclude that the shallow fractionation system modulates eruptive cycles and constitutes a critical component of continental LIPs.

Chapter 4 explores how magma flux influences lava compositions using the first chemo-stratigraphic section of these flood basalts. We find that the geochemical variability within the lavas parallels the existing petro-stratigraphic framework, and is consistent with a common parental magma composition. We interpret the variability in lava compositions as reflecting open-system magma differentiation processes and use mass balance equations to construct numerical models to resolve this variability. We identify three volcano-stratigraphic units that record the initial, main, and terminal phases of flood basalt volcanism. We find that the three volcano-stratigraphic units exhibit a progressive decrease in the magnitude of magma recharge over time. This cycle of activity parallels similar petrographic observations from the Oligocene Traps Phase of the NW Ethiopian Plateau, thereby suggesting a similar progression in the development of a continental flood basalt magma plumbing system at both locales.

I dedicate this work to my daughter Riley. She has always known the geology department and this work has been as much her life for this time as my own. Her growing passion for rocks and volcanos served as encouragement to continue through difficult times and persevere. I also dedicate this work to Megan, who has supported this mad dream with equal devotion and effort. Finally, I would also like to dedicate this work to the friends who came together during hardship, supported each other, and helped make this journey a bright one.

ACKNOWLEDGEMENTS

This work was supported by the United States National Science Foundation (EAR-1551872 and EAR-1734884), the National Aeronautics and Space Administration Michigan Space Grant Consortium student research grant, 2019, the Michigan State University Dissertation Completion Fellowship, and the Warren and Anneliese Undergraduate Research Award. I would also like to recognize the support of Big Rock Exploration for the gracious release time that allowed this work to continue.

We extend our gratitude to the late Frank Brown for providing basalt samples from the Turkana region and to the Geological Survey of Canada for providing access to the archived Omo River Project samples materials used in this study. Collection of field samples in Turkana, Kenya was made possible by Saint Patrick's Center for Nomadic Girls, our guide and driver John, and the communities of the Turkana region.

This work was made possible by the valuable contributions of collaborators Guillaume Girard, Todd Lydic, John Kappelman, Cynthia Ebinger, Nick Rogers, Nicholas Mariita, Liam Peterson, and Rayn Phillips. This work was also made possible by patient guidance of my advisor, Tyrone Rooney, and my committee members, Susannah Dorfman, Allen McNamara, Songqiao Wei, and Micheal Velbel.

TABLE OF CONTENTS

LIST OF TABLES

LIST OF FIGURES

1. INTRODUCTION AND BACKGROUND

1.1 Introduction

Continental flood basalts (CFB), which are among the largest magmatic events on Earth, rarely record lava compositions that can be considered primary (Cox, 1980; Villiger et al., 2004). Such an observation requires prolonged residence and differentiation of magmas within the lithosphere. The impact of such processes is profound: (a) significant volumes of dense material fractionated from transient magmas may greatly alter both the bulk composition and thermal state of the crust as well as contribute to the formation of structures such as High Velocity Lower-crust; (b) the construction of a magmatic plumbing system may impact how magma degasses and over what timescales, with implications for climate change caused by such events; (c) components of the magmatic plumbing systems are recognized as the host of significant economic mineral deposits such as Noril'sk-Talanakh beneath the Siberian flood basalt province and those of the Duluth Complex associated with the Keweenawan flood basalt province (Naldrett, 2010). It is therefore apparent that resolving the development and processes contributing to a magmatic plumbing system within a CFB province has application beyond igneous systems.

The lifecycle of a CFB is typically <10 Ma, during which, >1 million km^3 of lava and intrusive material may be formed (Coffin and Eldholm, 1993). Magmatism is not uniformly distributed throughout this interval. The CFB system is episodic, evolving through a series of phases over its lifetime (Jerram and Widdowson, 2005). The temporal evolution of a CFB event can divided be three phases: Initial phase, Main phase, and the Termination/Diminishing phase (Jerram and Widdowson, 2005; Self et al., 1997). Volcanism during Initial and

Termination/Diminishing phases are similar in that they are characterized by small volume eruptions of predominantly alkaline lavas. During the Main phase of volcanism, the greatest proportion of lavas erupt, ~70% of the total lava volume (Jerram and Widdowson, 2005). The Main phase lavas exhibit a shift toward moderately evolved, transitional to tholeiitic compositions (Ernst, 2014). The evolved magmas erupted during the Main phase of volcanism suggests a large volume of magma has spent a prolonged period within the magma differentiation system. Therefore, understanding the physical and chemical conditions of that magma differentiation system is a key component to better understand the evolution of a CFB province.

The plumbing systems of CFB provinces must transmit large volumes of magma through the lithosphere in a relatively short interval (Jerram and Widdowson, 2005; Self et al., 1997). This assertion is supported by observations of large economic deposits that formed beneath CFB provinces where the volume of silicate magma required to create the deposit far exceeds the volume of the host intrusion (e.g., Eagle Mine, Michigan) (Ding et al., 2012). The necessity of a high flux of magma through the magmatic plumbing system has two important implications: (1) it requires an interconnected system that is efficient at storing, transporting, and hybridizing magmas, and (2) differentiation paths are defined by an aggregate of processes, and are not limited to fractional crystallization and assimilation (Lee et al., 2014). Resolving these magmatic processes requires a comprehensive examination that includes not only fractional crystallization and assimilation, but also the effect of magma recharge and evacuation (eruption) (Griselin et al., 1997; Jean et al., 2013; Lassiter et al., 1995; Lightfoot et al., 1990; Peng et al., 1994; Yu et al., 2015). Many flood basalt provinces exhibit lava compositions that are remarkably homogeneous, with a decoupling in major and trace element behaviors. Consequently, probing of the magmatic

system using such erupted lava compositions requires more complex modeling than typically considered in most magmatic systems, and has been achieved through recharge-evacuation-assimilation-fractional crystallization (REAFC) models (e.g. Bohrson et al., 2014; Lee et al., 2014).

Advancements in the understanding of the magmatic plumbing system beneath CFB provinces has come from studies of the Oligocene CFB province in East Africa (Krans et al., 2018). This relatively well-studied flood basalt province has typically been ascribed to the interaction of a mantle plume with the African lithosphere (e.g., Beccaluva et al., 2009; Hofmann et al., 1997; Kieffer et al., 2004; Natali et al., 2016; Pik et al., 1999; Rooney, 2017). However, this province was not the first manifestation of Cenozoic magmatic activity in East Africa. A thick sequence of stratiform mafic lavas erupted in southern Ethiopia and northern Kenya approximately 15 Ma prior to the Oligocene CFB province (Davidson, 1983; Ebinger et al., 1993; George et al., 1998; WoldeGabriel, 1988). The relative paucity of parallel studies upon this Eocene province (Ebinger et al., 1993; George et al., 1998; George and Rogers, 2002; Stewart and Rogers, 1996) is due in part to difficulties with access to the region. With the recognition that the Eocene province represents a volumetrically significant fraction of magmatism within the Ethiopian-Arabian Large Igneous Province (Rooney, 2017), there is an urgent need to examine the origin of the Eocene event and establish its relationship to the subsequent Oligocene CFB.

Existing information on the Eocene CFB province follows the same basic outline as the Oligocene CFB province to the north. Historical observations lacked geochemical constraints to divide lavas and, instead, relied upon stratigraphic observations (Mohr and Zanettin, 1988). The Oligocene CFB province was divided into two main stratigraphic units: the older Ashangi and

the younger Aiba. However, the lack of continuity in stratigraphic markers, including the contact between the Ashangi and Aiba units (Mohr, 1983), resulted in ambiguity as to the regional volcanic succession. Parallel studies examining the stratigraphic succession in the Eocene CFB province suffer from similar complications of stratigraphic continuity, but with the additional complexity of bookcase faulting in southern Ethiopia (Davidson, 1983; Ebinger et al., 1993). Recent insights on the Oligocene CFB province have come from detailed geochemical studies, that have recognized compositional zoning within the province (e.g., Pik et al., 1998). Comparable studies within the Eocene CFB province do not exist preventing a petrologic comparison between the two CFB provinces.

The goal of this dissertation is to utilize geographically and stratigraphically constrained whole-rock geochemical datasets, petrographic observations, and mineral composition datasets from flood basalt lavas to probe the petrologic evolution the Eocene Initial Phase's magma plumbing system. Chapter 2 will revise the existing magmatic stratigraphy for the Eocene Initial Phase lavas, explore the open-system differentiation processes, and discuss the impacts of flood basalt magmatic systems on the lithosphere. Chapter 3 seeks to define a petro-stratigraphy in a well constrained stratigraphic section of flood basalt lavas, examine the variation in mineral compositions through the stratigraphy, and evaluate modification of flood basalt magmas due to crystal-liquid diffusive equilibration. Chapter 4 will examine the same section of flood basalt lavas as chapter 3, but will instead utilize whole-rock lava compositions to probe the magma plumbing system using open-system numerical models.

1.2 Background

1.2.1 Regional Geology

1.2.1.1 Lithospheric Structure and Tectonic history East Africa Prior to Cenozoic Rifting

The predominant crustal architecture of East Africa was constructed during the Pan-African Orogeny, and has a significant influence on the distribution of Cenozoic magmatism, (Purcell, 2018). The Pan-African Orogeny resulted in Tibetan-style continental collision (Burke and Dewey, 1972) eventually culminating in the assembly of the super continents Gondwana and Pannotia between 1200 and 550 Ma (Cutten, 2002; Stein and Goldstein, 1996). Early phases of orogenic activity began with the accretion of island arcs and microcontinents, constructing what would eventually become the African mobile belts. Subsequent full-scale continental collision thickened the lithosphere and formed the structures that exhibit considerable control on Cenozoic magmatism in East Africa (Purcell, 2018; Stern, 1994). The NW-NNW trending shear zones and metamorphic fabrics observed today in the Mozambique Mobile belt results in parallel orientation of Cenozoic dike intrusions, thereby controlling the distribution of lavas at the surface (Abdelsalam and Stern, 1996; Davidson, 1983; Maguire et al., 2006; McWilliams, 1981; Rooney, 2019a; Stern, 1994). While the metamorphic fabrics clearly influence Cenozoic dike orientations and the locations of volcanic centers, the Pan-African Orogeny has a more profound secondary impact on magmatism when coupled with rifting events during the Mesozoic.

East Africa experienced another profound modification of the lithosphere during the mid to late Mesozoic, subsequently affecting the distribution of Cenozoic magmatism (Ebinger et al., 2000). Mesozoic rift systems in Africa represent a complex series of extensional events relating to the breakup of Gondwana and the separation of Madagascar. Of particular interest for the northern parts of the East Africa, the focus region of this study, are the Mesozoic rifts of Sudan

(Muglad, Melut, and Pibor rifts) and Kenya (Anza Graben) (Figure 1.1; Bosworth, 1992; Purcell, 2018). Extension within the Sudan rifts and the Anza Graben began in the late Cretaceous representing a shift in the tectonic stresses giving these basins a NW-SE orientation (Bosworth, 1992). It is possible the Sudan rifts and Anza Graben are accessing the same broad Pan-African suture or shear zone given the systems are along strike. However, there is a curious gap in Turkana, Kenya where neither system can be traced directly requiring a stepped or transitional series of N-S structures (Ebinger et al., 2000; Ebinger and Ibrahim, 1994). Such an observation may explain the shift from NW striking Mesozoic structures to the sub-meridional rifts of the East African Rift System. The tectonic table-setting of structural domains in Turkana may have permitted EARS rifting to begin there (Ebinger et al., 2000; Purcell, 2018). Additionally, the resultant thinned lithosphere from the formation of the late Mesozoic basins may contribute to distribution of magmatism during the Eocene and Oligocene flood basalt events in East Africa (Ebinger and Sleep, 1998).

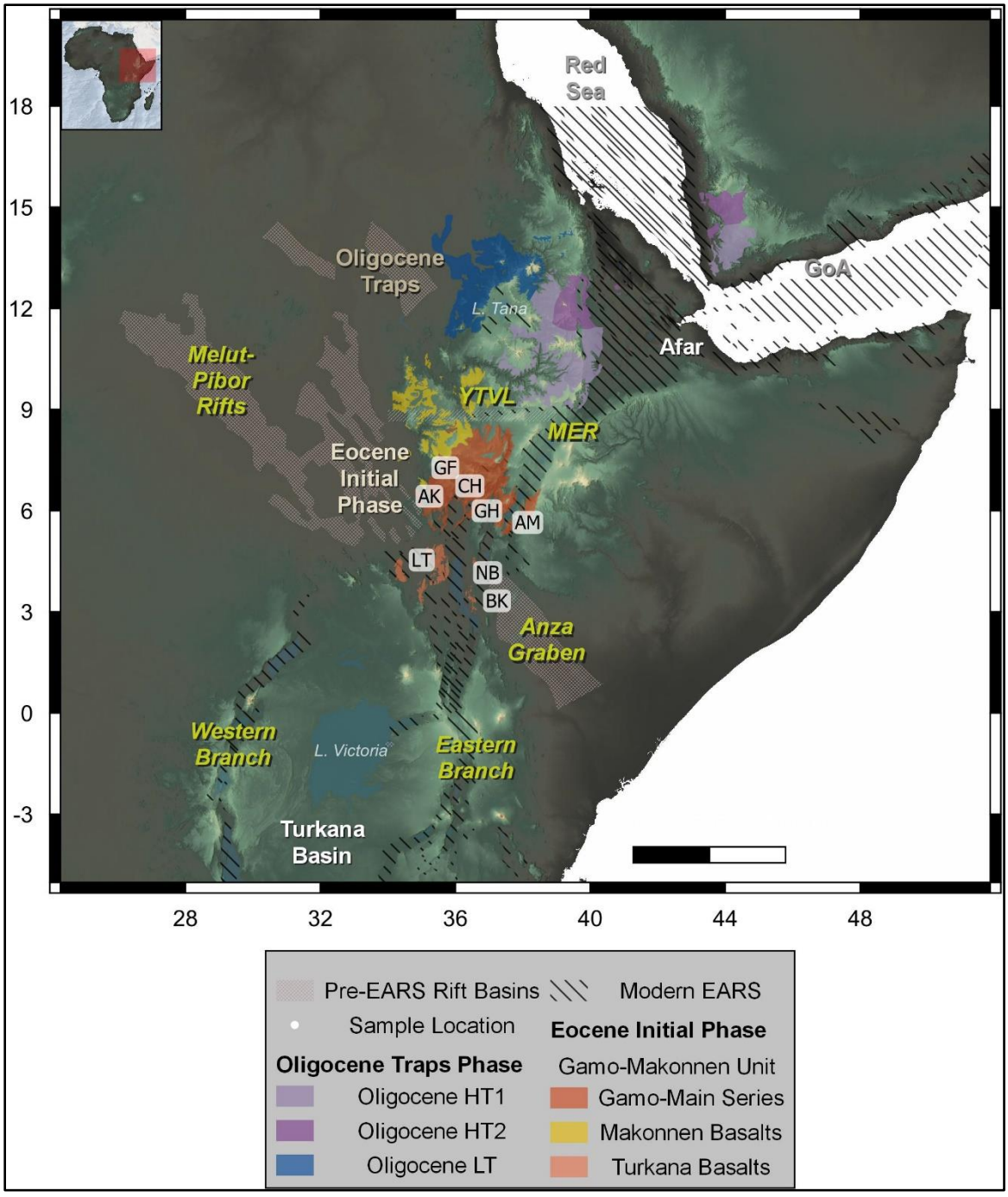

Figure 1.1 - Distribution of the Eocene and Oligoene flood basalt provinces in East Africa. Abbreviations: Amaro Region (AM), Balsea Koromoto (BK), Chebera (CH), Gidole Horst (GH), Gura Ferda (GF), Gulf of Aden (GoA), Lokitaung (LT), Main Ethiopian Rift (MER), Nabwall Hills (NB), Hashed regions denote Mesozoic rift basins and Cenozoic rift basins.

1.2.1.2 Paleogene Magmatic History of Southern Ethiopia and Northern Kenya

Modern magmatism in East Africa is typically restricted to the modern rift basins or adjoining rift margins and is limited in aerial extent. Prior to rift development, widespread shield volcanism impacted much of the northern portion of the East African rift (Rooney, 2017). However, the most pronounced magmatic events during the Cenozoic are unconnected to the rift. Flood basalts occupy a vast area in the northern EARS from Turkana to Yemen (Figure 1; Baker et al., 1996; Raphaël Pik et al., 1998; Rooney, 2017). The most well-known of these events, centered on the NW Ethiopian Plateau was active during the Oligocene from ca. 29-31 Ma (Abbate et al., 2014; Baker et al., 1996; Hofmann et al., 1997; Rochette et al., 1998; Rooney, 2017; Ukstins et al., 2002). However, a second earlier event commenced ca. 45 Ma during the Eocene (Ebinger et al., 1993; George et al., 1998; George and Rogers, 2002). This study focuses upon this Eocene event and its relationship to the subsequent Oligocene flood basalts.

Prior studies have used the terminology of a 'Pre-Rift Sequence' to refer to the flood basalt activity and related magmatic events in SW Ethiopia between ca 50-28Ma (Davidson and Rex, 1980; Davidson, 1983; George and Rogers, 2002). The 'Pre-Rift Sequence' represents between 200 to over 1500 meters stratigraphic section and are composed of dominantly stratiform mafic lavas with silicic intercalations that increase in frequency towards the upper flows. Widely mapped sub-divisions were originally recognized on the basis of petrographic characteristics, and later K-Ar isotopic age determinations as: the Akobo basalts (49.4 ±1.9 Ma to 46.6 ±2.0 Ma), the Main Series (42.7±2.0 Ma to 32.7 ±1.3 Ma), and the Makonnen Basalt (34.8 ±1.3 to 28.8 ±1 Ma) (Davidson, 1983). Subsequent refinement of the temporal constraints of the Eocene CFB came from $^{40}Ar/^{39}Ar$ techniques whereby the stratigraphic sequence in the vicinity of the Amaro graben was re-interpreted as the Amaro (45-39 Ma) and Gamo lavas (39-

34 Ma) (Ebinger et al., 1993; George et al., 1998). These units have been geochemically well-characterized (George and Rogers, 2002; Stewart and Rogers, 1996); in contrast no parallel data exist for the 'Pre-Rift Sequence'. For this reason, there remains ambiguity as to the relationship between the mapped units comprising the Eocene CFB, and the subsequent temporally refined units around the Amaro horst.

The nomenclature for describing rocks of Eocene and early Oligocene age in southern Ethiopia has not been standardized in the literature. The Ethiopian Geologic Survey continued to use the mapped distribution of Eocene-Oligocene rocks as determined by Davidson (1983) but choose to reassign those units into a broader context. The Akobo, lowest in the Davidson section, was correlated to the Ashangi formation of the Oligocene traps (Tefera et al., 1996). The overlying Main Series was transformed into the Jimma volcanics featuring a lower basaltic and upper mostly silicic unit, which covers most of the southern Ethiopian highlands. The Makonnen Basalts of Davidson (1983) were redefined and expanded to include all basalts of Oligocene age in southern Ethiopia that lie upon crystalline basement rocks. Notably, the distribution of the Makonnen Basalts appears limited only to the region south of the Abbay river (Figure 1.1).

1.2.2 The Pre-Rift Sequence of the southwest Ethiopian Plateau: existing stratigraphic and temporal constraints

The lowest unit in the 'Pre-Rift Sequence' are the flows of the Akobo Basalts, which are comprised of a limited number of flows that erupted directly onto the Precambrian/Paleozoic basement. The Akobo basalts are limited in areal extent, occurring near Surma along the flanks of the Akobo and Kari river valleys (Figure 1.1). Dated by Davidson and Rex (1980) to 46.6-49.4 Ma, the Akobo are the oldest Cenozoic lavas recognized from SW Ethiopia, and may be among the oldest lavas in the EARS. These early lavas are characterized by an unusual

phenocryst assemblage in comparison to the subsequent units, consisting of abundant large, strongly zoned titaniferous clinopyroxene and olivine (Davidson, 1983). The abundance of early forming pyroxene and occurrence of analcime suggest the Akobo lavas are of an alkaline affinity (Davidson, 1983). The Akobo lavas are separated from the overlying Main Series by a thick sequence of silicic volcanic material (Davidson, 1983).

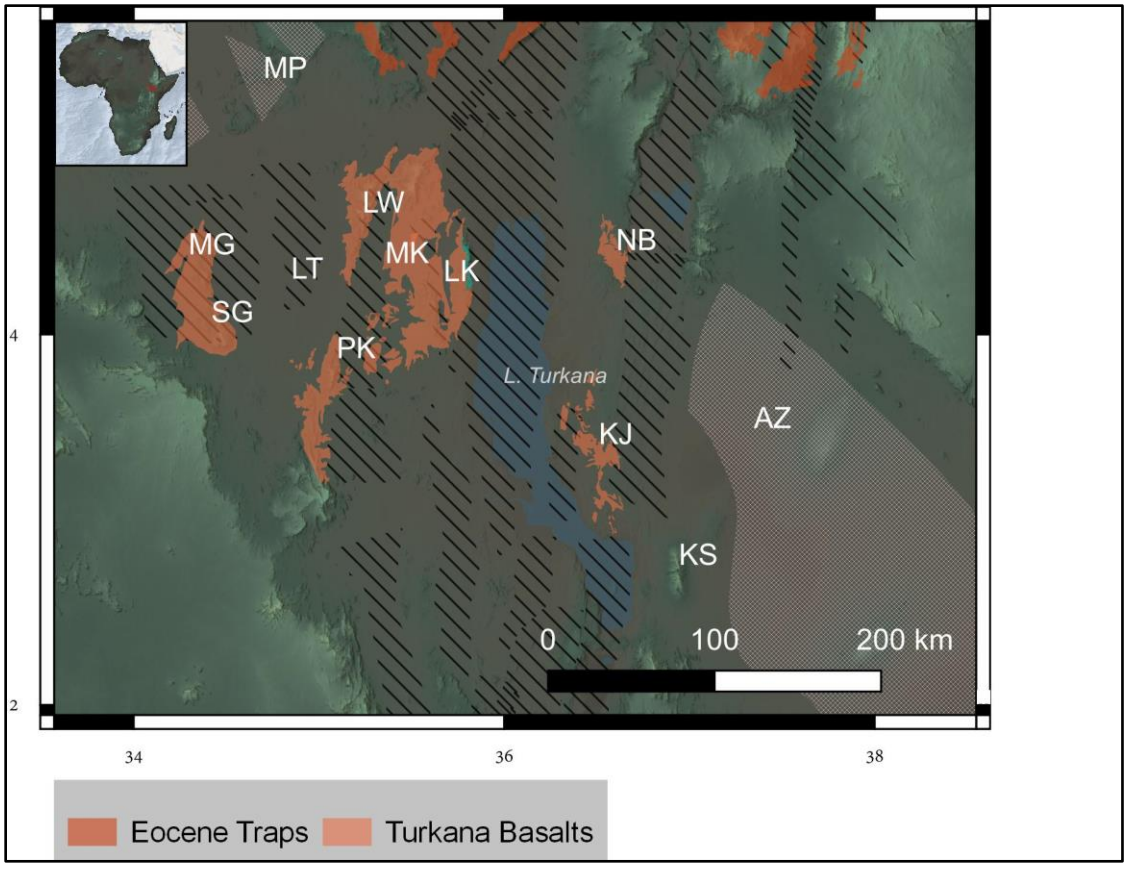

Figure 1.2 - Distribution of Eocene-Oligocene aged mafic volcanics in Turkana, Kenya. Abbreviations: Anza Graben (AZ), Kajong (KJ), Kulal Shield (KS), Lokitaung (LK), Lokwanamur (LK), Lotikipi Plain (LT), Melut-Pibor Rift System (MP), Mogila (MG), Murorith-Kalin (MK), Nabwal Hills (NB), Peleketch (PK), Songot (SG).

The 'Pre-Rift Sequence' is dominantly composed of the stratiform basalts and silicic volcanics of the Main Series. This series of flood basalts covers a broad area extending from

Gidiole Highlands, west and northwest to the Surma plain and Gura Ferda (figure 1; Davidson, 1983). The 200 to 1500 meter thick basaltic sequences of the Main Series are typically exposed along west-facing escarpments of highland regions. Where exposed, the basal flows are almost ubiquitously erupted onto a red-basal sandstone developed on the Precambrian basement (Davidson, 1983). The age of those basal lavas range from 33.9 to 42.7 Ma, while in the silicic lavas of the upper parts of the section, material can be as young as 32.7 Ma (Davidson and Rex, 1980). Distinct from the older Akobo basalt, the majority of flows within the Main Series are aphyric to weakly porphyritic. Where flows are porphyritic, the dominant phases are plagioclase and olivine with rare clinopyroxene. Highly porphyritic plagioclase-rich flows are evident, but uncommon (Davidson, 1983). Mineral assemblages indicate these lavas are transitional to tholeiitic in composition. A period of uplift and erosion resulted in the development of a weathered horizon capping the Main Series lavas, onto which the youngest of the 'Pre-Rift Sequence' is erupted (Davidson, 1983).

The Makonnen Basalts are the youngest flows associated with the 'Pre-Rift Sequence'. The Makonnen Basalts, as described by Davidson (1983), cap a series of plateaus near Chebera and Mt. Shasha, south of the Yerer-Tullu Wellel Volcanic Lineament (YTVL) (Figure 1.1). The unbroken section of basalt locally reaches 700 m. Flows were erupted onto a basal paleosol that developed atop both the Precambrian basement and the tilted flows of the Main Series, representing an angular unconformity between the two basalt sequences. The hiatus in activity is reflected in the ca. 31.8 Ma average age determination for the Makonnen Basalts, suggesting a younger age than much of the Main Series (Davidson and Rex, 1980). Notably, there is no evidence for silicic volcanism within the Makonnen Basalt sequence. Phenocrysts are rare in the Makonnen lavas, which are dominantly aphyric but may be ophitic in places. In contrast to

plagioclase within lavas of the Main Series (Davidson, 1983), rare plagioclase phenocrysts within the Makonnen Basalts are not zoned and rarely occur with olivine. Following the eruption of the Makonnen Basalts, there is a hiatus in mafic volcanism in southern Ethiopia until the mid-Miocene (Rooney, 2017).

1.2.3 The Eocene Amaro and Gamo flood basalts of southern Ethiopia: Existing Stratigraphic and Temporal Constraints

Several sections of stratiform basalts are exposed along the flanks of the Southern Main Ethiopian Rift and the Broadly Rifted Zone that are contemporaneous with the 'Pre-Rift Sequence' of the southwestern Ethiopian Plateau (Figure 1.1). The type sections for these lavas are in the Amaro region, but additional exposures are found throughout the Broadly Rifted Zone west of the Gidiole Highlands (Figure 1.1). Initially recognized as Eocene in age (WoldeGabriel et al., 1991; Yemane and Yohunie, 1987; Zanettin, 1978), the stratiform volcanics of the SMER represent 500 m of predominantly basalt, outcropping along steep escarpments. It was recognized that the sequence consisted of two units that are distinctive in their petrographic character. The lowest stratigraphic unit in the SMER is termed the Amaro Basalt, which erupted as much as 250 m of stratiform basalt over a red basal sandstone. Predominantly porphyritic, the Amaro Basalts commonly contain both olivine and plagioclase phenocrysts with rare clinopyroxene, consistent with a tholeiitic fractionation sequence (George and Rogers, 2002). After a short hiatus in basaltic volcanism, locally marked by the Arba Minch Tuff, there is a shift in petrologic character to marginally more evolved compositions with the eruption of the Gamo Basalts. Petrologically distinct from the underling Amaro Basalt, the Gamo lavas are typically aphyric to weakly olivine porphyritic and generally more alkaline in composition.

The geochronologic significance of the boundary between the Amaro and Gamo Basalts remained uncertain until the application of ^{40}Ar-^{39}Ar techniques (Ebinger et al., 1993). Ebinger et al. (1993) redefined the stratigraphy by recognizing a temporal break between an older Amaro Basalt and younger Gamo Basalt. The Amaro lavas exhibit a range in ages from 45.2 to 39.8 Ma (Ebinger et al., 1993; George et al., 1998), the second oldest Cenozoic volcanic material. The Gamo lavas date 35 to 37.9 Ma and are capped by the 33 Ma Amaro Tuff, which blankets much of the Eocene-early Oligocene section in SW Ethiopia (Davidson, 1983; Ebinger et al., 1993).

The link between the two established stratigraphic frameworks (i.e. 'Pre-Rift Sequence' and Amaro Basalt-Gamo Basalt) is ambiguous. While there are clear temporal similarities between the sequences, the lack of geochemical constraints within the 'Pre-Rift Sequence', and pervasive book-case faulting within the Broadly Rifted Zone, have limited regional correlations. A notable overlap between the sequences is evident - Ebinger et al. (2000) expanded the Amaro-Gamo division westward into areas previously mapped by Davidson (1983), by correlating the widespread stratigraphic occurrence of stratiform basalts being overlain by a thick silicic tuff. The silicic tuff was interpreted by Ebinger et al. (2000) to be the Amaro tuff and inferred the underlying lavas to be the Gamo Basalts. Further examination of the 'Pre-Rift Sequence' lavas from a geochemical perspective can help to confirm the hypothesis of Ebinger et al. (2000) and further expand said hypotheses into the remainder of SW Ethiopia.

1.2.4 The Eocene-Early Oligocene "Turkana Basalts" of Northern Kenya: existing Stratigraphic and Temporal Constraints

Thick sequences of basaltic lava of Eocene to Oligocene age occur throughout Turkana, Kenya (Brown and McDougall, 2011). Early descriptions of stratiform volcanics in Turkana can be found in Cavendish (1898), Arambourg (1932), and Champion (1937) who note a thick sequence

of basaltic lavas overlying coarse-grained rift-filling sandstones. Fuchs (1939) provided the first detailed discussion on the occurrence of stratiform basaltic material west of Lake Turkana, but focused on the underlying fossil-bearing sandstones. However, correlations between the various lava sequences were tenuous due the broad biostratigraphic age determinations used at the time, indicating an age between the late Cretaceous to the Miocene (Fuchs, 1939). It was not until detailed stratigraphic/geochronologic analyses of lavas throughout the Turkana region that the age and distribution of Eocene to Oligocene aged lavas were recognized. Occurrences east of Lake Turkana (Figure 1.2) are known from the Nabwal Hills/Asille Highlands region (34.8-33.5 Ma; Brown and Mcdougall, 2011) and the Kajong region (~39 Ma; Furman et al., 2006). However, the thickest sequences of Eocene-Oligocene mafic lavas are found west of Lake Turkana in the highlands surrounding the Lotikipi Basin (Figure 1.2). The best constrained section occurs in the Lokitaung Gorge, where age-determinations indicate eruption ages between 37-28 Ma (Brown and Mcdougall, 2011; Tiercelin et al., 2012; Walsh and Dodson, 1969). The ages of the remaining stratiform lava occurrences surrounding the Lotikipi basin are considered to be minimum ages, as determinations were made from either the overlying rhyolites or a single age within the section and include: Morurith-Kalin (32-29 Ma; McDougall and Brown, 2009) the Peleketch (>27 Ma; McDougall and Brown, 2009), and Songot-Mogila mountains (31.7-32.5 Ma; Brown and Jicha, 2016) (31.7-32.5 Ma; Brown and Jicha, 2016). These data show significant number of occurrences of Eocene-Oligocene aged lava are found in Turkana, however, the petrologic relationship between these occurrences cannot be determined due to a lack of modern geochemical studies in the region.

The paucity of geochemical studies in the Turkana region has hindered placing those lavas into the greater context of Cenozoic magmatism in East Africa (Rooney, 2017). The

earliest geochemical work on the region recognized a range of lava compositions from silica-undersaturated to transitional lavas but this work was restricted to major elements and is of limited utility (Bellieni et al., 1981). Modern studies have primarily focused on the east side of Lake Turkana in the Kajong and Kulal Shield regions where lavas range in age from 39 Ma through to the present. Of interest to this study are the Eocene Belesa Koromto lavas which have been examined using modern geochemical techniques (Furman et al., 2006). Based on their incompatible trace element characteristics, these are divided into two geochemical groups. The first, termed group A, exhibits modest incompatible trace element enrichment and is broadly consistent with Type-Ib pattern of Rooney (2017). Group B lavas are alkaline in composition and have elevated incompatible trace element patterns with superimposed negative anomalies in alkali metals, consistent with type II magmas of Rooney (2017). These observations along with recent work recognized the Belsea Koromto Group B magmas are broadly like the Akobo basalts of southern Ethiopia (Steiner et al., 2019) and may represent an early alkaline phase of volcanism prior to the Main Phase of flood basalt activity. The Group A lavas, being type Ib, are similar to flood basalt compositions from the Eocene flood basalt province to the north (Rooney, 2017). With additional sampling of the remaining Eocene-Oligocene basalt sequences, it will be possible to close the gap in geochemical knowledge in this region and place the Turkana lavas into the greater context magmatism in East Africa.

Filling the sampling gap could not be accomplished with existing sample suites requiring the collection of a new, detailed suite of lava samples from the Turkana region. During the summer of 2018, we conducted a five-week sampling campaign in western Turkana that focused primarily on collecting stratigraphic sections of Eocene-Oligocene lavas. Of primary interest were outcropping lava sections surrounding the Lotikipi plain, which are hypothesized to be the

surface expression of a synform hosting more than 1000 meters of basaltic section (figure 2; Wescott et al., 1999). Two well-constrained (Peleketch and Lokitaung Gorge) sections and one partially constrained section (Songot-Mogila) were collected from these outcroppings. Of these, the Lokitaung Gorge section is the most stratigraphically complete, extending from the lower-contact with the Cretaceous sediments to the upper contact with what may be lavas associated with the Early Miocene Resurgence (Rooney, 2017). For this reason, I choose to examine the flood basalt lavas of the Lokitaung Gorge to fill some of the gaps in the geochemical and petrologic knowledge of Eocene-Oligocene magmatic activity in Turkana, Kenya

2. INITIAL CENOZOIC MAGMATIC ACTIVITY IN EAST AFRICA: NEW GEOCHEMICAL CONSTRAINTS ON MAGMA DISTRIBUTION WITHIN THE EOCENE CONTINENTAL FLOOD BASALT PROVINCE

Reprinted with permission from the Geological Society of London, Journal of the Geological Society, Initial Cenozoic Magmatic Activity in East Africa: New Geochemical Constraints on Magma Distribution within the Eocene Continental Flood Basalt Province, R. A. Steiner et al. 2022

2.1 Introduction

Continental large igneous provinces (LIPs), which are among the largest magmatic events on Earth, rarely record lava compositions that can be considered primary (Cox, 1980; Villiger et al., 2004). Such an observation requires residence and differentiation of magmas within the lithosphere evidenced by voluminous crystal cumulates within numerous intrusive complexes (Charlier et al., 2015). The impacts of such processes are profound: (a) significant volumes of dense material fractionated from transient magmas may greatly alter the bulk composition, hydration state, and thermal state of the continental crust, as well as contribute to the formation of structures such as High Velocity Lower Crust, all of which have uncertain feedbacks on rheology and continental rifting (Farnetani et al., 1996; Larsen et al., 2018; Montési, 2013; Ridley and Richards, 2010; Thybo and Artemieva, 2013); (b) the structure of a magmatic plumbing system may impact how magma degasses and over what timescales, with implications for climate change caused by such events (Self et al., 2005); (c) LIP plumbing systems are recognized as the host of significant economic mineral deposits such as Noril'sk-Talanakh beneath the Siberian LIP and those of the Duluth Complex associated with the Keweenawan LIP of North America (Naldrett, 2010). It is therefore apparent that resolving the processes contributing to the development of a magmatic plumbing system within a LIP has application beyond igneous systems to strain localization within continental interiors and exploration for economic mineral deposits.

The plumbing systems of LIPs must transmit large volumes of magma through the lithosphere in a relatively short interval (Jerram and Widdowson, 2005; Self et al., 1997). This assertion is supported by observations of large economic deposits that formed within LIPs where the volume of silicate magma required to create the deposit far exceeds the volume of the host intrusion (e.g. Eagle Mine, Michigan; Ding et al., 2012). The necessity for a high flux of magma through the magmatic plumbing system requires an interconnected system that is efficient at storing, transporting, and hybridizing magmas (Griselin et al., 1997; Jean et al., 2013; Lassiter et al., 1995; Lightfoot et al., 1990; Peng et al., 1994; Yu et al., 2015). LIP's lava compositions are therefore defined by an aggregate of processes, and are not limited to fractional crystallization and assimilation (e.g. Lee et al., 2014). Many continental LIPs exhibit lava compositions that are remarkably homogeneous with little variation from flow to flow in terms of major elements, although trace elements may exhibit more variability. Lava compositions show that major and trace elements appear to have decoupled from trends typically observed during fractional crystallization (Cox, 1980; Kieffer et al., 2004; Paces, 1990; Villiger et al., 2004). Probing the magmatic plumbing system of LIPs using such lava compositions thus requires the application of recharge-evacuation-assimilation-fractional crystallization (REAFC) models (e.g. Bohrson et al., 2014; Lee et al., 2014; Nishimura, 2019).

Continental LIPs are frequently highly eroded and dissected, with poor preservation of erupted sequences, which make probing their magmatic plumbing systems challenging (Ernst, 2014). Among the best-preserved LIPs is the Ethiopian-Arabian Large Igneous Province, which is dominated by distinct Eocene and Oligocene continental flood basalt provinces or continental LIP events. Among these two events, the Oligocene Ethiopian continental LIP, which coincided with the initial opening of the southern Red Sea rift at 30 Ma, has been the focus of more

intensive study. Advancements in the understanding of the magmatic plumbing system within the Oligocene continental LIP has come from detailed petro-stratigraphic studies of flow-by-flow lava sequences (Kieffer et al., 2004; Krans et al., 2018; Pik et al., 1999), and their emplacement with respect to initial rift opening (Ukstins et al., 2002; Wolfenden et al., 2005). Trace element and isotopic studies have further shown that the Oligocene continental LIP is likely the result of an interaction of a mantle plume with the African lithosphere (Beccaluva et al., 2009; Kieffer et al., 2004; Natali et al., 2016; Pik et al., 1999). However, the Oligocene continental LIP was not the first manifestation of Cenozoic magmatic activity in East Africa. A thick sequence of stratiform primarily mafic lavas erupted in southern Ethiopia and northern Kenya approximately 15 m.y. prior to the Oligocene continental LIP, roughly synchronous with the intrusion of kimberlites in central Africa (Ebinger et al., 2017). The relative paucity of parallel studies upon this Eocene continental LIP (Ebinger et al., 1993; George et al., 1998; George and Rogers, 2002; Stewart and Rogers, 1996) is due, in part, to difficulties with access to the region. With the recognition that the Eocene continental LIP represents approximately 25% of magmatism within the broader Ethiopian-Arabian LIP (Ebinger et al., 1993; Rooney, 2017), there is a need to examine the origin of the Eocene event and establish its relationship to the subsequent Oligocene continental LIP, as well as plateau uplift and strain localization as rifting initiated in East Africa (e.g. Kounidis et al., 2021; Faccenna et al., 2019; Pik et al., 2008).

Here we present a geochemical study of the Eocene continental LIP utilizing samples collected during the original mapping of the region in the 1970s (Davidson et al., 1973; Davidson, 1983). This sample suite allows for the most complete geochemical examination of the Eocene continental LIP to date. Through major and trace element characterization of these lavas, we find remarkable homogeneity in lava compositions erupted over a wide area. Using

existing volcano-stratigraphy, we show that the majority of flood basalt lavas of the Eocene continental LIP, including the heretofore enigmatic "Makonnen Basalts" (Davidson, 1983; Rooney, 2017), share a common composition consistent with the Gamo Basalt unit (George and Rogers, 2002). We show that the broad geographic distribution of this relatively homogenous basaltic composition is consistent with the main phase of flood basalt activity within the Eocene continental LIP. We present an REAFC model constraining the magmatic system during the main phase of LIP volcanism that allows erupted lava compositions to be derived from a common primitive magma. The period over which the common primitive magma must have been recharging the REAFC system is considerably longer than a typical continental LIP. We assess the impact of this long-lived magmatic system on the thermal and compositional state of the crust and examine the implications for subsequent rifting of the African continent.

2.2 Background

2.2.1 Regional Overview

Holocene-recent magmatism associated with the East African Rift system south of the Red Sea is typically of limited areal extent and generally is restricted to rift basins and uplifted rift flanks, both onshore and in the Indian Ocean (Corti et al., 2019; Ebinger, 2020). Geophysical studies of the East African mantle reveal a seismic low-velocity zone above a mantle transition zone of relatively uniform thickness and broad distribution (Reed et al., 2016; Thompson et al., 2015). Such observations are interpreted as the upwelling of chemically distinct, volatile-rich material (Reed et al., 2016; Thompson et al., 2015) consistent with a mantle plume, however the geometry of the upwelling plume material is not well-defined and might not be representative of its geometry throughout Cenozoic (e.g., Boyce et al., 2021; Chang et al., 2020). Ambient noise

and surface wave tomography, receiver function analyses, and limited controlled source seismic studies, with different techniques imaging the top and bottom of the accreted magmatic material, indicate that the crust beneath the Ethiopian plateau has been extensively underplated by mafic intrusions (e.g. Kounidis et al., 2021; Chambers et al., 2019; Lavayssière et al., 2018). Estimates of lithospheric thickness from surface wave tomography and mantle xenolith data are 100-88 km, respectively, suggesting moderate thinning of Pan-African lithosphere associated with heating and subsequent stretching (Priestley et al., 2008). These studies indicate that a profound degree of modification of the East African crust and mantle must have occurred prior to the onset modern magmatism.

A rich geochronological and geochemical framework has demonstrated that magmatism in East Africa has been both more volumetrically significant and more widely distributed than would be assumed from studies of modern magmatism (Baker et al., 1971; Brotzu et al., 1984; Brown and McDougall, 2011; Davidson et al., 1973; Ebinger et al., 1993; Furman et al., 2006; Guth, 2013; Hackman et al., 1990; Hofmann et al., 1997; Key and Watkins, 1988; Kieffer et al., 2004; Morley et al., 1992; Natali et al., 2013; WoldeGabriel et al., 1991). Using these studies, a recent synthesis has identified specific pulses of widespread basaltic magmatism at ca. 4 Ma, 10-12 Ma, and 20-26 Ma in the rift system East of the Tanzania craton (Rooney, 2020a, 2020b, 2020c). Each discrete magmatic pulse is linked with an extensional episode, providing a decompression melting mechanism for magma generation (Rooney, 2020b), however the volume of material erupted is suggestive of persistent elevated mantle potential temperature of the East African upper mantle (Armitage et al., 2015; Ferguson et al., 2013; Rooney et al., 2012). The most voluminous and widely distributed Cenozoic magmatic events in East Africa pre-date these pulses and occur during the Eocene and Oligocene (Abbate et al., 2014; Baker et al., 1996;

Ebinger et al., 1993; George et al., 1998; George and Rogers, 2002; Hofmann et al., 1997; Pik et al., 1998; Rochette et al., 1998; Rooney, 2017; Ukstins et al., 2002). The flood basalt sequences of the Eocene and Oligocene continental LIPs record the most anomalous mantle potential temperatures and have geochemical signatures consistent with a derivation from the lower mantle (Pik et al., 1999; Rooney et al., 2012). It is therefore apparent that studies of the initial magmatic events provide insight into the long-term thermo-chemical perturbation of the East African upper mantle, with relevance to modern studies of melt generation within the East African Rift.

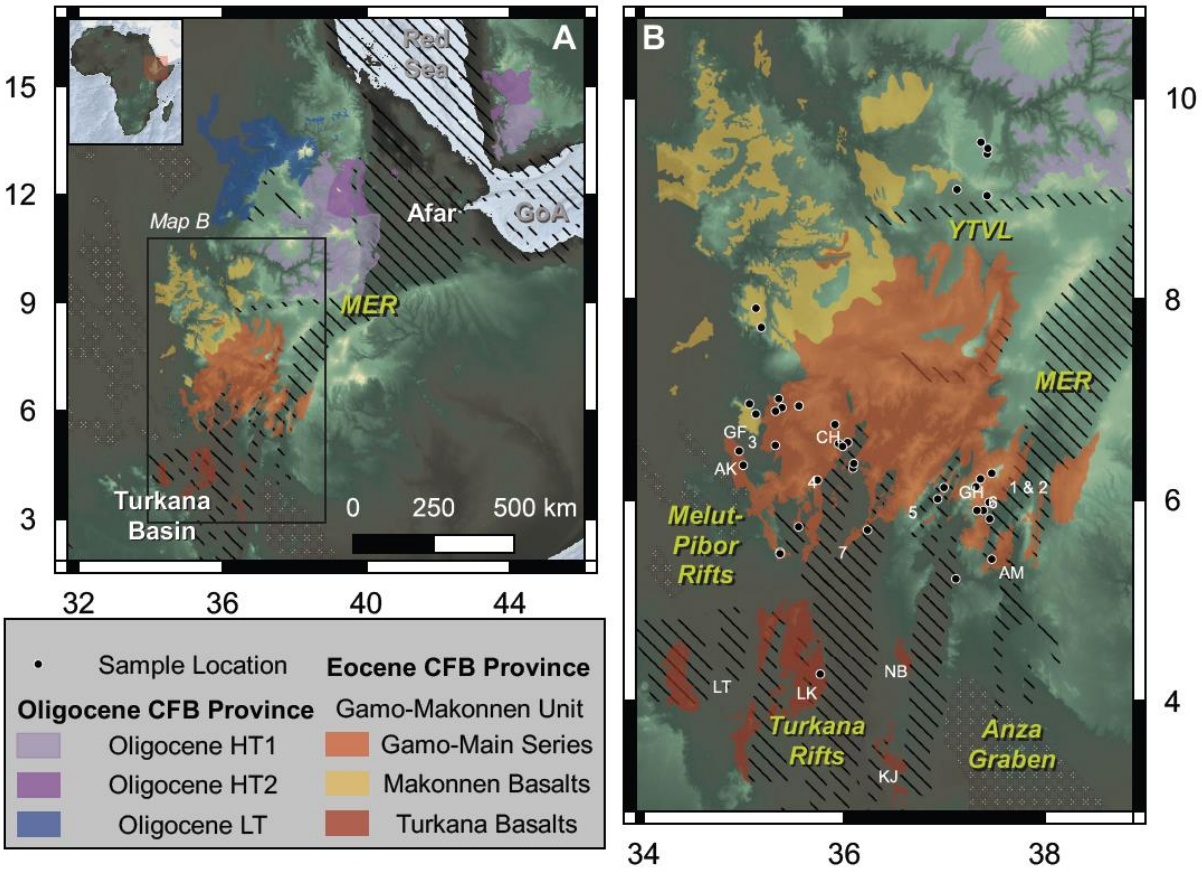

Figure 2.1 – Distribution of the Eocene and Oligoene flood basalt provinces in East Africa. Abbreviations: Akobo Basalts (AK), Amaro Region (AM), Chebera (CH), Gidole Horst (GH), Gura Ferda (GF), Kajong (KJ), Lokitaung town (LK), Lotikipi Basin (LT), Nabwal Hills (NB), Yerer Tullu-Wellel Volcanic Lineament (YTVL). Locations for sections 1-7 described in figure 2.5 correspond to numerals. The distribution of the Akobo Basalts and the Amaro Basalts are not pictured due to their small footprint at the map scale presented here. Hashed regions denote rift basins.

2.2.2 Existing stratigraphic and temporal constraints for the SW Ethiopian and northern East African Plateaus

Exposures of flood basalt sequences are facilitated by the ~18 Ma-Recent normal faulting and flank uplift across the region, which was accompanied by much smaller volume magmatism localized to the faulted rift valleys (Ebinger et al., 2000; Morley et al., 1992; WoldeGabriel et al., 1991). Paleaogene extension west of Lake Turkana remains enigmatic, and includes inversion of Mesozoic rift basins (Morley et al., 1999b, 1999a). The existing nomenclature for describing volcanic rocks of Eocene and Early Oligocene age in SW Ethiopia has not been standardized in the literature. Prior studies have used the terminology of a 'Pre-Rift Sequence' to refer to the flood basalt activity and related magmatic events in SW Ethiopia between ca. 50-28 Ma (Davidson and Rex, 1980; Davidson, 1983; George and Rogers, 2002). The 'Pre-Rift Sequence' represents several hundred to over 1500 meters stratigraphic section, composed of dominantly stratiform mafic lavas with silicic intercalations that increase in frequency towards the upper flows (Davidson, 1983). Widely mapped sub-divisions were originally recognized on the basis of petrographic characteristics, and later K-Ar isotopic age determinations as: (1) The Akobo Basalts (49.4 ±1.9 Ma to 46.6 ±2.0 Ma); (2) The Main Series (42.7±2.0 Ma to 32.7 ±1.3 Ma); and (3) The Makonnen Basalt (34.8 ±1.3 to 28.8 ±1 Ma) (Davidson, 1983). The Ethiopian Geological Survey has continued to use the mapped distribution of Eocene-Oligocene rocks as determined by Davidson (1983), but chose to reassign those units into a broader context. The Akobo Basalts, lowest in the Davidson section, were correlated to the Ashangi formation of the Oligocene continental LIP (Tefera et al., 1996). The overlying Main Series was transformed into the Jimma Volcanics, featuring a lower basaltic and upper mostly silicic unit, which covers most of the southern Ethiopian highlands. The Makonnen Basalts of Davidson (1983) were redefined

and expanded to include all basalts of Oligocene age in SW Ethiopia that lie upon crystalline basement rocks (Tefera et al., 1996). Subsequent examination of the correlative ages between the Makonnen Basalts (~34.8-28.1 Ma) and the Oligocene continental LIP (~32-27 Ma) led Rooney (2017) to hypothesize a link between the two, noting that additional geochemical and geochronological work was required to confirm this hypothesis.

2.2.3 The Eocene Amaro and Gamo Basalts of southern Ethiopia existing stratigraphic and temporal constraints

Several sections of stratiform basalts are exposed along the flanks of the Southern Main Ethiopian Rift and the rift basins of SW Ethiopia and northern Kenya that are contemporaneous with the 'Pre-Rift Sequence' of the SW Ethiopian Plateau (Figure 2.1). Unlike the 'Pre-Rift sequence', which was a broad regional compilation, these sections of stratiform basalts were examined using detailed stratigraphic, geochronologic, and geochemical techniques (Ebinger et al., 2000, 1993; George et al., 1998; George and Rogers, 2002; Stewart and Rogers, 1996). The type-sections for these lavas are in the Amaro region, but additional exposures are found west of the Gidole Highlands (GH, Figure 2.1). Initially recognized as Eocene in age (WoldeGabriel et al., 1991; Yemane and Yohunie, 1987; Zanettin, 1978), the sequence consists of two units that are distinctive in their petrographic character: (A) The lower Amaro Basalt, which erupted as much as 250 m of stratiform basalt over a red basal sandstone. Predominantly porphyritic, the Amaro Basalts commonly contain both olivine and plagioclase phenocrysts with rare clinopyroxene, consistent with a tholeiitic fractionation sequence (George and Rogers, 2002); (B) After a short hiatus in basaltic volcanism, locally marked by the silicic Arba Minch Tuff, there is a shift in petrologic character to marginally more evolved compositions with the eruption of the Gamo Basalts (Ebinger et al., 1993). Petrologically distinct from the underlying Amaro

Basalt unit, the Gamo Basalt lavas are typically aphyric to weakly olivine porphyritic and generally more alkaline in composition.

Subsequent refinement of the temporal constraints of the Eocene continental LIP came from $^{40}Ar/^{39}Ar$ techniques, whereby a temporal break between an older Amaro Basalt and younger Gamo Basalt was recognized. The Amaro Basalt lavas exhibit a range in ages from 45.2 (±1.4) to 39.8 (±0.8) Ma (Ebinger et al., 1993; George et al., 1998). The Gamo Basalts (39.8 ± 0.6 Ma to 34.1 ± 0.5 Ma) are capped by the 33 Ma Amaro Tuff that blankets much of the Eocene-early Oligocene geologic section in SW Ethiopia (Davidson, 1983; Ebinger et al., 1993).

The relationship between the two established stratigraphic frameworks (i.e. 'Pre-Rift Sequence' and Amaro-Gamo Basalts) is ambiguous. While there are clear temporal similarities between the sequences, the lack of geochemical constraints from lavas in SW Ethiopia created difficulties in correlating flood basalt stratigraphy across the multiple magmatic basins that developed after eruption (Davidson et al., 1976; Ebinger et al., 2000). A notable overlap between the sequences is evident: Ebinger et al. (2000) correlated the widespread stratigraphic occurrence of stratiform basalts being overlain by a thick silicic tuff from a large eruption of an unknown volcano thereby expanding the Amaro-Gamo Basalts classification west of the Gidole Highlands (Figure 2.1) into regions mapped by Davidson (1983). The silicic tuff was interpreted by Ebinger et al. (2000) to be the Amaro Tuff and inferred the underlying lavas to be the Gamo Basalts. Further examination of the 'Pre-Rift Sequence' lavas from a geochemical perspective can help to confirm the hypothesis of Ebinger et al. (2000) and further expand this designation into the remainder of SW Ethiopia.

2.2.4 Stratiform Basalts in northern Kenya

The Turkana region of northern Kenya encompasses multiple exposures of stratiform mafic lavas that are contemporaneous with those in southern and southwestern Ethiopia (Brown and McDougall, 2011; Davidson, 1983; Furman et al., 2006; McDougall and Watkins, 2006; WoldeGabriel et al., 1991; Zanettin et al., 1983). A recent synthesis of East African Rift magmatism (Rooney, 2017) tentatively divides the stratiform lavas of the Turkana region into the regional magmatic pulses of the Eocene Initial and Oligocene Traps phases. The Eocene initial phase in Turkana begins with the eruption the Balsea Koromto basalts (39.2-35.2 Ma; Furman et al., 2006; Wilkinson, 1988) in the Kajong region. Also included in the Eocene Initial Phase are the Nabwal formation (34.3 Ma; McDougall and Watkins, 2006) and Turkana Volcanics near Lokitaung town (31.1-36 Ma; Bellieni et al., 1981; McDougall and Brown, 2009; Morley et al., 1992; Tiercelin et al., 2012) (LK, Figure 2.1). Mafic lavas tentatively attributed to the Oligocene Traps phase outcrop on the perimeter of the Lotikipi Basin (Rooney, 2017; Wescott 1999, Brown and Jicha 2016; Brown and Mcdougall, 2011). The assignation of these lavas to the Oligocene Traps phase was based upon age determinations of silicic volcanics (32.5-31.7 Ma; Brown and Jicha, 2016) that overlie the stratiform mafic lavas. Seismic reflection surveys in western Turkana support the possibility that the stratiform lavas surrounding the Lotikipi basin may be correlative to those near Lokitaung town (Morley et al., 1999b; Wescott et al., 1999) (Figure 2.1).

While there is clear temporal correlation between the stratiform lavas in southern/southwestern Ethiopia and those in Turkana, the paucity of geochemical data prevents a robust conclusion of their relationship. The Turkana Volcanics at Lokitaung and the Nabwal formation are near the border with Ethiopia (Figure 2.1) making a correlation with the Amaro-

Gamo sequence possible, though, existing geochemical information is limited to major elements (Bellieni et al., 1986; Tiercelin et al., 2012). Extant trace element geochemical studies in Turkana from this time period focused upon the Balsea Koromto (Furman 2006) that have a distinctive trace element signature inconsistent with existing lavas from southern Ethiopia. However, the Balsea Koromto lavas near Kajong are more than 150km farther southeast than the Turkana Volcanics (KJ, Figure 2.1.), making geographically broad interpretations on the relationship of contemporaneous lavas in Turkana with those in Ethiopia difficult. Additional geochemical data from the Turkana Volcanics can help to contextualize the Turkana stratiform lava's connection to the Eocene continental LIP lavas erupted in southern Ethiopia.

2.3 Methods

In order to compare lavas of the 'Pre-Rift Sequence' and the Amaro/Gamo Basalt division, we have undertaken a modern geochemical study of previously collected samples. The 'Pre-Rift Sequence' is represented by The Omo River Project sample suite (Davidson, 1983). Samples of this suite were collected between 1972 and 1974 during a collaborative Ethiopian Geological Survey- Geological Survey of Canada expedition to formerly inaccessible areas of SW Ethiopia between 4^{o} and 8^{o}N. In this study we have utilized thin section off-cuts loaned from the Geological Survey of Canada. We have re-created the sample catalog from original archive documentation and linked the sample numbers to location information provided at the time of sample collection. Given the collection period pre-dates GPS, the sample coordinates are those of 'stations' from the original catalog that were located by aerial photography (Figure 2.1). All metadata associated with this sample suite is linked to its IGSN catalogue number.

The small size of the remnant material available for study and need for sample archiving required geochemical analysis to be performed with in-situ analytical methods. Their relatively low crystallinity allows the use of a wide beam laser-ablation (LA)-ICP-MS technique as a proxy for bulk rock analyses. A total of 34 samples were trimmed, and fragments were mounted in 25mm epoxy molds and polished. The polished sample fragments were analysed simultaneously by LA-ICP-MS for major and trace elements using a 15x15 cm two-volume cell-equipped Teledyne Photon Machines Analyte G2 excimer laser coupled to a Thermo Scientific ICAP Q ICP-MS at Michigan State University. Given the assumed inhomogeneity of the samples, fifteen, 1mm long by 150 μm wide surface ablation scans were collected from each sample in order to obtain a representative geochemical characterization. The 15 scans from each sample were then scrutinized statistically, using the following methodology, to ensure they were representative of a "whole rock" composition. Standard deviations were calculated from each sample's 15 scans. Those individual scans whose compositions fell out of 5% relative standard deviation of their sample average composition were considered suspect and reviewed in the microscope. If the same scan was determined to have intersected a non-representative amount of crystal phases it was omitted from the average composition calculation and is not reported in this study. Out of 310 line-scans a total of eight were identified as problematic and removed from their respective sample averages. Further details on standard reference materials and their reproducibility, and the validated data can be found in the supplemental materials.

The geochemical data for the Omo River Project suite collected using the method discussed above are broadly comparable to conventional whole-rock powder techniques, evidenced by the overlap in X-Y variation diagrams with data from Amaro-Gamo Basalts and the Oligocene continental LIP (supplementary X-Y plots). Our new raster line data does deviate

from the regional dataset, clustering lower concentrations of TiO_2 and Al_2O_3 but remains within the overall spread of existing data. Importantly, despite minor shifts in select major elements, trace elements abundances and spider diagram patterns (Figures 3 and 4) are comparable to whole-rock analyses of contemporary lavas in southern Ethiopia and northern Kenya. Given the similarity of these analyses to regional geochemical data it is evident that data collected using this novel method are consistent with data collected by standard whole-rock methods. The Amaro-Gamo Basalts units have previously been examined for major and trace elements (George and Rogers, 2002; Stewart and Rogers, 1996). These previous studies determined major and trace element abundances through combined XRF and INAA techniques, with a subset of samples analysed by more precise ICP-MS methods. Here we present new whole-rock ICP-MS data for a total of 20 samples that were re-analysed for 38 trace elements at Open University using techniques described in Rogers et al. (2006).

To expand the spatial distribution of the known Eocene-Oligocene sample suite from Southern Ethiopia, we collected new whole-rock major and trace element data from a suite of samples acquired during several sampling campaigns to the Yerer Tullu-Wellel Volcanic Lineament (3096 and 3098), Southern Main Ethiopian Rift (3124, 3125, 3126, 3152 and 3153), and Lokitaung, Kenya (TOR0000NO, collected by Dr. Frank Brown). Samples were cut, polished to remove saw marks, and cleaned in an ultrasonic bath before crushing in a steel jaw crusher. Crushed material was powered in a Bico ceramic disk mill. Dried powers were then mixed with Li-Tetraborate flux and fused into glass disks following procedures detailed in Rooney et al., (2011). Major element analysis of fused disks was performed on a Bruker S4 Pioneer XRF spectrometer. Trace element concentrations were collected on these same disks by LA-ICP-MS using the apparatus described above, following procedures of Rooney et al. (2015).

Detailed information of standards and analytical replicates for XRF and ICP-MS analyses can be found in supplemental documents.

2.4 Results

2.4.1 Overview of Geochemical Results

Geochemical data from this study can be divided, based on whole rock major element compositions, into two coherent lava groups: (1) a transitional to alkaline population (basalt to trachybasalt) constituting the majority of the dataset, and (2) a smaller population of tholeiitic basalts (Le Maitre, 1989). Alkaline samples are commonly more evolved (4-6 wt. % MgO) and exhibit high TiO_2 and Zr. The tholeiitic basalt sub-group is generally more primitive (6.5-10 wt. % MgO) and is consistently less enriched in TiO_2 and Zr than the alkaline samples. Trace element patterns show similar behavior among the datasets: most samples exhibit a convex upward primitive mantle normalised pattern with variability in incompatible trace element enrichment (Figure 2.3). To a first order, incompatible trace element profiles reflect the major elements and split the dataset into two groups: a dominantly tholeiitic group and a dominantly alkaline group. The tholeiitic group (Amaro Basalts) has a depleted and flatter profile in both primitive mantle normalised and chondrite normalised REE diagrams. The dominantly alkaline group (Gamo Basalts, Akobo Basalts, Main Series, Makonnen Basalts, Turkana Volcanics) has more enriched incompatible trace elements in primitive mantle normalised diagrams and steeper profile in chondrite normalised REE diagrams.

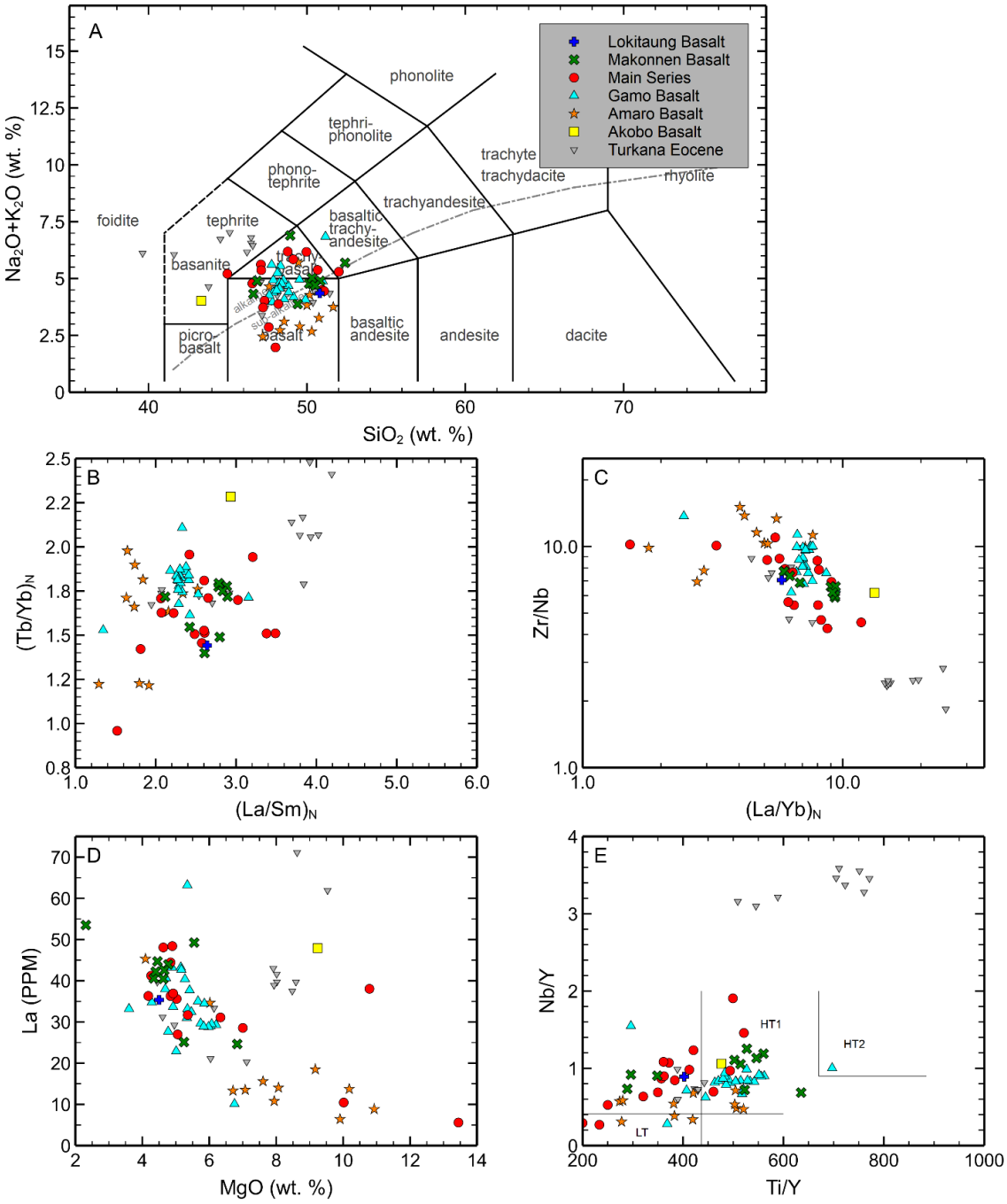

Figure 2.2 – Selected bivariant diagrams showing the major and trace element distribution of Eocene flood basalts. The Main Series and Makonnen samples broadly conform to the existing geochemical framework of the Amaro Basalt and Gamo Basalt units. The Akobo Basalt is similar to those of the Turkana Eocene lavas (Furman et al. 2006).

2.4.2 Southern Ethiopia: Amaro – Gamo Basalts

2.4.2.1 Amaro Basalts

Our new data on the Amaro and Gamo Basalts clarify and expand the geochemical patterns previously established. Consistent with this model, the tholeiitic Amaro basalts exhibit more primitive compositions with higher MgO (~7-11 wt. %) and a marked depletion in the most incompatible trace elements in comparison to other units from SW Ethiopia. This depletion is evident in the chondrite normalised pattern (Figure 2.4), showing a relatively flat slope in the LREE, and HREE: $(La/Sm)_{CN}$ = 1.2-2.0, and $(Tb/Yb)_{CN}$ = 1.3-2.0. Amaro Basalt samples plot within the depleted domain, defined in terms of elevated Zr/Nb and low La/Yb values (Figure 2.2). The primitive mantle normalised pattern of the Amaro Basalts is dominated by the superimposed, pronounced positive anomalies in certain LILE (e.g. Ba) over the generally depleted composition of the other incompatible trace elements (Figure 2.3). On the basis of these primitive mantle normalised patterns, Amaro Basalt lavas classify as Group Ib based upon the collation of Rooney (2017).

2.4.2.2 Gamo Basalts

Consistent with the established Amaro-Gamo Basalt geochemical framework, the alkaline Gamo Basalts exhibit modestly evolved compositions with lower MgO (4-6 wt. %) and enriched trace element characteristics. Modest enrichment is visible in chondrite normalised diagrams where the Gamo Basalts have a flat profile that is steeper than the Amaro basalt $(La/Sm)_{CN}$=2.2-2.5 and $(Tb/Yb)_{CN}$=1.6-2.1). The Gamo Basalts plot near the Amaro Basalts in Zr/Nb vs. La/Yb, but are displaced to more enriched values (Figure 2.2). Primitive mantle normalised diagrams show a convex upward pattern, with positive Ba and Pb, and negative K anomalies (Figure 2.3). Internal variation within the Gamo Basalt dataset is small, evidenced by the narrow range

between the 1st and 3rd quartiles in figure 2.3. Rooney (2017) noted that the Gamo Basalt lavas are not entirely consistent with the Type Ib magma group due to the enrichment in trace elements, a feature common to the Type III magma group.

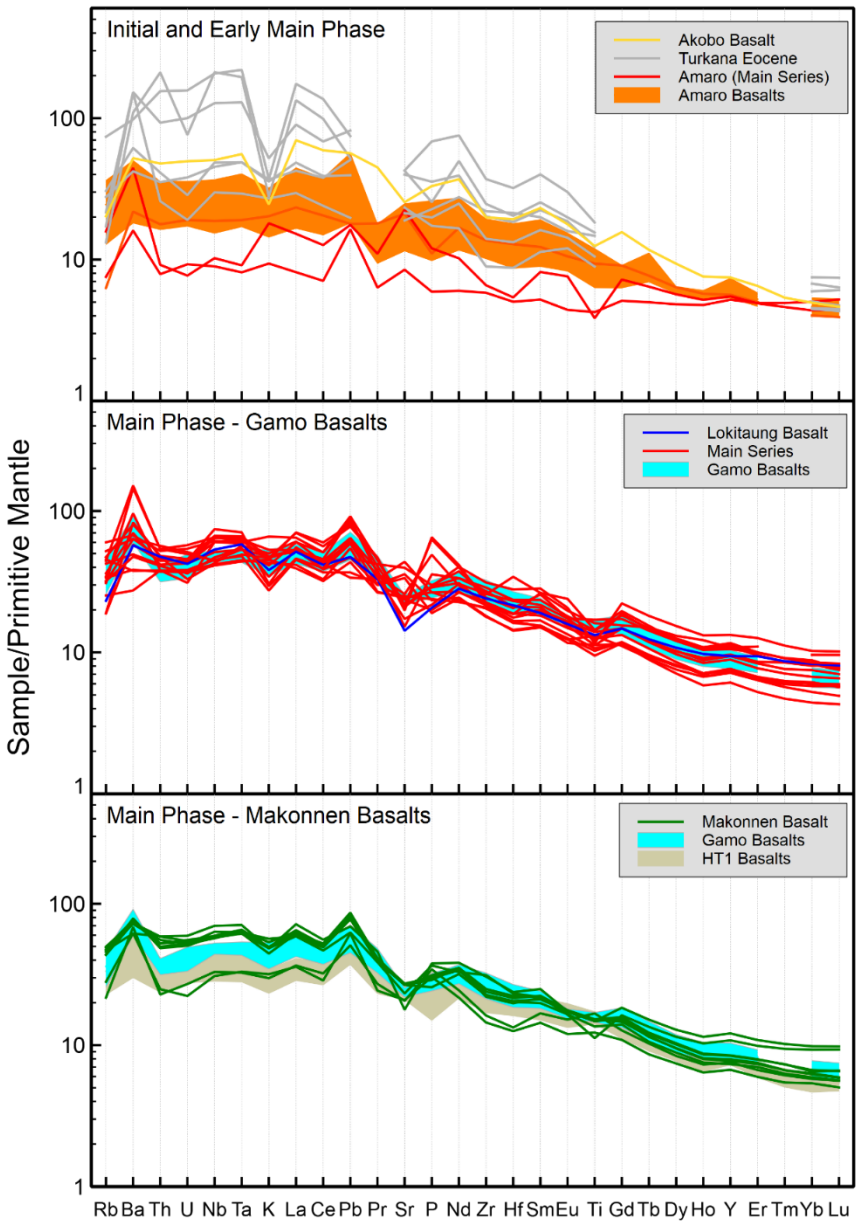

Figure 2.3 – Primitive mantle normalised spider diagrams showing the incompatible trace element patterns for flood basalt samples from the Eocene and Oligocene Ethiopian flood basalt provinces with greater than 4% MgO. Fields for existing Amaro, Gamo, and Oligocene HT1 lava compositions were calculated from the 1st and 3rd quartiles. Primitive mantle composition from Sun and McDonough (1989).

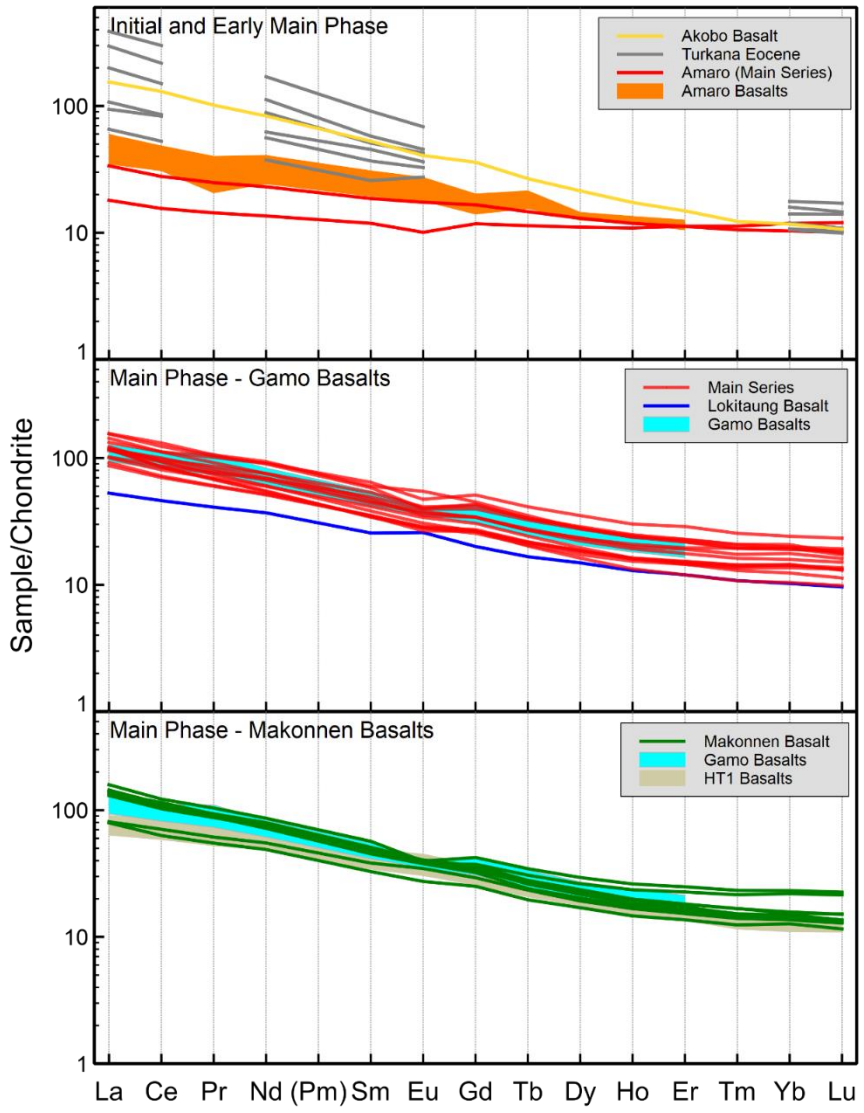

Figure 2.4 – Chondrite normalised spider diagrams showing the REE patterns for flood basalt samples from the Eocene and Oligocene Ethiopian flood basalt provinces with greater than 4% MgO. Fields for existing Amaro Basalt, Gamo Basalt, and Oligocene HT1 lava compositions were calculated from the 1st and 3rd quartiles. Chondrite normalization from Boynton (1984). (Pm calculated from geometric mean of Nd-Sm and does not represent analytical values).

2.4.3 Southwestern Ethiopia: Stratiform Basalts of the Omo Region

2.4.3.1 Akobo Basalt

Trace element behavior for the strongly alkaline Akobo Basalt is unlike other Eocene magmatic units in SW Ethiopia due to its strong enrichment in incompatible trace elements. The Akobo Basalts exhibit a steep REE profile (Figure 2.4) displacing the $(Tb/Yb)_{CN}$-$(La/Sm)_{CN}$ ratio to values near the Turkana Eocene field of Furman et al. (2006) (Figure 2.2). Similar behavior is noted in Zr/Nb-La/Yb space where the Akobo Basalts plot toward the Turkana Eocene lavas and a more enriched domain (Figure 2.2). Primitive mantle normalised patterns show enrichment in the incompatible elements and depletion in K but lack the distinctive Ba and Pb of the Amaro-Gamo Basalt units (Figure 2.3). The Akobo Basalt trace element patterns classify as a Type II magma (Rooney, 2017), similar to the HT2 Oligocene flood basalts (Beccaluva et al., 2009; Natali et al., 2016; Pik et al., 1999) and lithosphere-derived lavas from Kenya and Ethiopia (Rooney, 2020b).

2.4.3.2 Main Series

Most of the Main Series samples are transitional to alkaline in composition (Figure 2.2) and show evidence of being evolved: 4-6 wt. % MgO and 2.5-4 wt. % TiO_2. Trace elements in these Main Series samples exhibit more enriched characteristics consistent with the Gamo Basalts, evident in the greater slope of the REEs $(La/Sm)_{CN}$=1.5-8 and $(Tb/Yb)_{CN}$=1-2.1). Chondrite normalised REE diagrams show a weak negative Eu anomaly (Figure 2.3) on an otherwise flat pattern. These data plot in La/Yb versus Zr/Nb toward more enriched values, overlapping with data from the Gamo Basalts (Figure 2.2). Primitive mantle normalised diagrams show these Main Series data exhibit a modestly enriched pattern, with positive anomalies in Ba and Pb similar to patterns of the Gamo Basalts. As with the Gamo Basalts, this pattern does not comport

with the magma type grouping of Rooney (2017). When examined with the 1st and 3rd quartiles for the distribution of data for known Gamo Basalt samples, it is apparent that the Main Series and Gamo Basalts share the same geochemical signature. Given the similarities between the Main Series lavas and the Gamo Basalts, we hereby assign most of the Main Series samples to the Gamo Basalt.

The samples classified as the Main Series are dominantly transitional to alkaline in composition, except for a subset of samples that are sub-alkaline (Figure 2.2). The two sub-alkaline samples (TOR0000GG and TOR0000H9) appear somewhat more primitive, plotting at greater concentrations of MgO wt. % and lower TiO_2 and P_2O_5. These data show depleted trace element characteristics as evidenced by the shallow slope through the REEs (Figure 2.4) and low values of $(La/Sm)_{CN}$ (Figure 2.2). Similar behavior is observed in Zr/Nb versus La/Yb where these two samples plot toward more depleted values. Trace element patterns in primitive mantle normalised diagrams exhibit positive anomalies in Ba and Pb superimposed on a broadly depleted convex upward pattern (Figure 2.3). Such characteristics are consistent with Type Ib magmas of Rooney (2017) and LT magmas (Kieffer et al., 2004; Pik et al., 1999, 1998). The data from these two samples consistently plot near the Amaro Basalts in X-Y variation diagrams and are sub-parallel with the Amaro Basalt trace element patterns detailed above. Therefore, we assign these two samples to the Amaro Basalt unit characterized geochemically by previous studies (George and Rogers, 2002).

2.4.3.3 Makonnen Basalt

The data for the Makonnen Basalts are transitional to alkaline in composition (Figure 2.2), have MgO between 4.5 and 6 wt. % and generally resemble the Gamo basalts. Variation diagrams versus MgO show the Makonnen Basalts overlap with data from the Gamo Basalts

(e.g. CaO, and P_2O_5), while trace element data for these samples indicate modest enrichment in La/Yb versus Zr/Nb and an REE slope within the range of the Gamo Basalts ($(La/Sm)_{CN}$ =2.1-2.9 versus $(Tb/Yb)_{CN}$=1.4-1.7). Trace elements normalised to primitive mantle are similar to those defined by the 1st and 3rd quartile of the Gamo Basalt data, showing a convex upward pattern with modest enrichment in the incompatible trace elements and superimposed positive Ba and Pb anomalies (Figure 2.3). Given the similarities between the Makonnen Basalts and the Gamo Basalts, the two are considered to be the same magmatic unit that we define as the Gamo-Makonnen magmatic unit (Figure 2.5).

2.4.4 Turkana Volcanics near Lokitaung

A single sample of the Turkana Volcanics near Lokitaung was analyzed for major and trace elements (TOR0000NO). This sample is a transitional basalt that contains 4.5% MgO and 2.9 % TiO_2 indicating a moderate degree of evolution. Trace element data indicate moderate enrichment in La/Yb versus Zr/Nb and REE element slope comparable to the Gamo Basalts $(La/Sm)_{CN}$ =2.6 versus $(Tb/Yb)_{CN}$=1.4. Primitive mantle normalised patterns (Sun and Mcdonough 1989; Figure 2.3) for the Turkana Volcanics are parallel to, and within the 1st-3rd quartile range for the Gamo Basalts. Due the similarity in geochemical characteristics between the Gamo Basalt and the Turkana Volcanics, we tentatively assign the Turkana Volcanics to the Gamo-Makonnen magmatic unit with the caveat that this assignation is based upon a single analysis and requires further study to confirm the relationship.

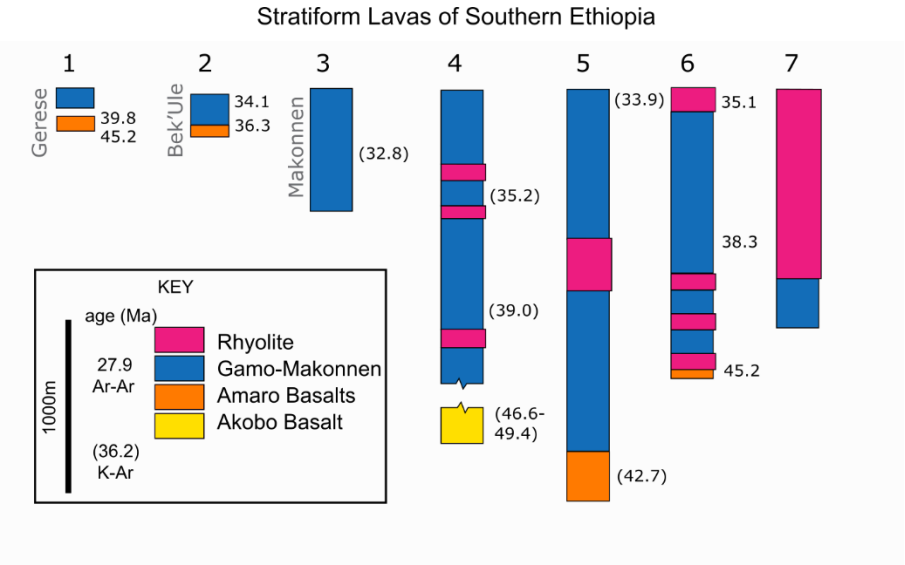

Figure 2.5 – Idealized magmatic stratigraphy of southern Ethiopia modified from Rooney (2017). Stratigraphic relationships derived from field observations and geochronology (Davidson and Rex, 1980; Davidson, 1983; Ebinger et al., 1993; George et al., 1998; George and Rogers, 2002; WoldeGabriel et al., 1991). The Akobo Basalt are included in section 4 only to show the temporal relationship between the Gamo-Makonnen unit and the Akobo Basalts.

2.5 Discussion

The regional scale geochemical dataset presented here permits a synthesis of the two systems by which Paleaogene volcanic rocks of southern and SW Ethiopia are described, and it provides tentative links to NW Kenya stratigraphic sequences. The existing country-scale map of Ethiopia utilizes a stratigraphic sequence for the Eocene units of SW Ethiopia based upon regional scale mapping and geochronology, dominantly undertaken by The Omo River Project surveys during the 1970s (Davidson and Rex, 1980; Davidson, 1983). Subsequent and more detailed mapping, geochemical characterization, and precise $^{40}Ar/^{39}Ar$ geochronology of discrete volcano-stratigraphic sections established an alternate stratigraphy based upon the Amaro Basalt and

Gamo Basalt units (Ebinger et al., 1993; George et al., 1998). The resolution of these two schemes into a unified volcano-stratigraphic sequence (Figure 2.5) has heretofore not been possible due to a lack of regional-scale geochemical characterization of the lavas in SW Ethiopia.

The newly resolved volcano stratigraphy in southern and SW Ethiopia allows for the interpretation of magmatic processes within the poorly characterized Eocene continental LIP. We expand upon the work of George and Rogers (2002) in the Amaro-Gamo region and explore the origin of the remarkable homogeneity in erupted lava compositions that are found throughout the region and persist for ~10 Ma. While the duration of volcanism does extend into the Oligocene, we utilize the term Eocene continental LIP to reflect the onset of this magmatic pulse, Eocene Initial Phase, as defined by Rooney (2017). We examine the impact of persistent and voluminous magmas staging within the crust by assessing the thermal and compositional state of the crust as a prelude to rift development. We interpret these observations within a developing paradigm of an East African upper mantle that is more complicated, both thermally and compositionally, than can be accommodated by the mantle plume head-tail model (e.g., Pik et al., 2006; Bastow et al., 2008; Chang and van der Lee, 2011; French and Romanowicz, 2015).

2.5.1 Unified Eocene Stratigraphy

2.5.1.1 Earliest Alkaline Magmatism (>45 Ma)

There is a growing recognition that pre-flood basalt small-volume alkaline magmatism may be more common in East Africa than initially considered. Instances of such activity are observed in the Oligocene continental LIP located on the NW Ethiopian Plateau, where Krans et al. (2018) identified a clinopyroxene-phyric alkaline basaltic sequence at the base of the Oligocene continental LIP. The Akobo Basalts, which occur at the base of the Eocene continental LIP flood

basalt sequence, share a similar petrographic character and contain abundant large, strongly zoned titaniferous clinopyroxene and olivine. We interpret these small volume alkaline events as representing the initial phase of flood basalt (LIP) volcanism, as defined in the tripartite division of Jerram and Widdowson (2005).

We show that the Akobo Basalts are the most silica-undersaturated lavas in the Eocene stratigraphy in SW Ethiopia (Figure 2.2), and exhibit a Type II lava pattern (Rooney, 2017). The Type II lava patterns evident in the Akobo Basalts suggest a likely origin within a metasomatized amphibole-bearing lithospheric mantle, which may have been thermo-barically destabilized by the Afar plume, and either melted in-situ or foundered into the upper mantle (Furman et al., 2016; Rooney et al., 2017, 2014). Broadly compositionally-equivalent magmatism is also evident at the southern edge of the Eocene continental LIP in Turkana (Kenya). The Balsea Kormoto (35-39 Ma; Furman et al., 2006) lavas are dominantly silica-undersaturated Type II lavas that are located East of Lake Turkana in the Kajong region (KJ, Figure 2.1). These lavas have been similarly interpreted as being derived from metasomatized lithospheric mantle (Furman et al., 2016; Rooney, 2017, 2010). The younger ages of these rocks suggests this style of magmatism may persist during the main flood basalt episode in more distal portions of the province.

2.5.1.2 Amaro Basalts (45-39 Ma)

Following the Akobo Basalts, ~ 250-300 m of moderately evolved stratiform basalts were erupted to form the Amaro Basalts. Prior studies have noted the prevalence of these Amaro Basalts in the region surrounding the Amaro horst, and constrained the eruption of the Amaro Basalts within a window of about 5 Ma (45.2-38.58 Ma; Ebinger et al., 1993; George et al., 1998). An important unknown in earlier studies has been the potential wider spatial distribution

of the Amaro Basalt lavas than is currently understood. Prior to this study, the geochemical characterization necessary to assign lavas to the Amaro Basalts was limited to sections along the flanks of the Ethiopian Rift, extending as far west as the Mago Basin (Figure 2.1). We interpret these primitive lavas as representing the early stage of the main phase of flood basalt volcanism, as defined in the tripartite division of Jerram and Widdowson (2005).

The new dataset we present expands the spatial coverage of geochemically characterized lavas within the province (Figure 2.1). Previous nomenclature for these lavas assigned them to the undifferentiated 'Main Series' (~43-34 Ma) of the Pre-Rift Sequence (Davidson, 1983), which temporally occupies the same time window assigned to both the Amaro Basalts (45.2-39.58 Ma) and Gamo Basalts (38-34 Ma; Ebinger et al., 1993; George et al., 1998). Examination of the Main Series samples shows that lavas with Amaro-like compositions (Figure 2.3) are dominantly restricted in spatial distribution, focused on the region flanking the Ethiopian Rift (Figure 2.1). An important outcome of these observations is the confirmation that the locus of volcanism during the early stages of the flood basalt event is towards the Amaro horst (George and Rogers, 2002).

2.5.1.3 Gamo Basalts (38-34 Ma)

Following the eruption of the Amaro Basalts, there is a hiatus in basaltic volcanism that is represented by the Arba Minch tuff from an unknown volcanic centre (>39 Ma; Ebinger et al., 1993). Flood basalt volcanism (Gamo Basalts) recommenced with the eruption of a relatively more evolved suite of basaltic lavas and intercalated tuffs. The age range of the Gamo Basalts (38-34 Ma; Ebinger et al., 1993; George et al., 1998) overlaps the Main Series lavas (~43-34 Ma) of the 'Pre-Rift Sequence' (Davidson, 1983). Despite this temporal overlap, the genetic relationship between the two sequences has been unclear due to the lack of geochemical

constraints on Main Series lavas. Our new results show that most Main Series lava samples geochemically resemble the Gamo Basalts. We therefore assign the majority of the Main Series to the Gamo Basalts, thereby refining the previous *en masse* assignation of the Main Series to Amaro Basalt-Gamo Basalt Sequence (Rooney, 2017). This observation vastly improves the constraints on the spatial distribution of the Gamo Basalt unit, which are now shown to occupy much of the province and comprises up to 1500 m of lava flows and silicic volcaniclastics (Davidson, 1983; Rooney, 2017). The widespread distribution of silicic volcaniclastics erupted from unidentified volcanic centres (Amaro Tuff, Ebinger et al., 1993; Jvr unit, Tefera et al., 1996) was used by Ebinger et al. (2000) to suggest the Gamo basalts extended into SW Ethiopia. Our observations of similar geochemical characteristics between the Main Series of SW Ethiopia and the Gamo Basalts support the hypothesis of Ebinger et al. (2000).

Contemporaneous stratiform lavas in the Turkana region of northern Kenya (Figure 2.1) also exhibit Gamo Basalt-like geochemical characteristics. These lavas are represented in this study by a sample from the lower-most flows of the gorge east of Lokitaung town, estimated to be ~36 Ma (Brown and McDougall, 2011). This lava exhibits a primitive mantle normalised pattern nearly identical to that of the Gamo Basalt suite (Figure 2.3). Therefore, we tentatively assign the Lokitaung Basalts to the Gamo Basalt group and recognize that the limited geochemical data from Eocene-Oligocene lavas in the Turkana region prevents more robust conclusions. Additional geochemical characterization of the stratiform basalts in Turkana is required to fully evaluate the potential connection between those lavas and the neighboring Gamo Basalts.

2.5.1.4 Makonnen Basalts (34 – 28 Ma)

The Makonnen Basalts are the youngest stratigraphic unit associated with the 'Pre-Rift Sequence' of SW Ethiopia (Davidson, 1983). The prior stratigraphic separation of the Makonnen Basalts from the underlying Main Series (now Gamo Basalts) was the result of an angular unconformity between the two units (Davidson, 1983). This temporal break is reflected in the ca. 31.8 Ma average age determination for the Makonnen basalts, suggesting a younger age than much of the Main Series (Davidson and Rex, 1980) and Gamo Basalts (38-34 Ma; Ebinger et al., 1993; George et al., 1998). As with previous stratigraphic units within the 'Pre-Rift Sequence', the relationship between the Makonnen Basalts and the Amaro Basalt-Gamo Basalt Sequence has been unclear.

We have now shown that the Makonnen Basalts and the Gamo Basalts share a common geochemical signature and are hereby treated as a single magmatic unit (Gamo-Makonnen magmatic unit) for the purposes of exploring the magma genesis of the Eocene continental LIP. This amalgamation has implications for the distribution of Eocene continental LIP lavas in time and space. The Gamo-Makonnen grouping covers nearly the entire footprint of the Eocene continental LIP (Figure 2.1), making this group the most volumetrically significant unit in SW Ethiopia. Additionally, the Gamo-Makonnen unit occupies a broad time window, potentially extending from 38-28 Ma. We interpret these homogenous, relatively evolved lavas as representing the main phase of flood basalt volcanism, as defined in Jerram and Widdowson (2005). In the following discussion, we examine how homogenous lava compositions could be erupted over a broad spatial and temporal window through the examination of the magmatic processes impacting magma compositions during the Paleaogene in East Africa.

2.5.2 Lithospheric Modification of Magmas in the Eocene Province

Utilizing the newly established magmatic stratigraphy for the Eocene continental LIP, (Figure 2.5), it is now possible to examine the magmatic conditions present during the main phase of activity across the whole of the province (~320,000 km^2, Rooney, 2017). Prior work hypothesized that the Amaro Basalt and Gamo Basalt primary magmas are derived from sub-lithospheric reservoirs. Heterogeneity between the two primary magmas was thought to result from differential degrees of fractional crystallization of a primary magma (George and Rogers, 2002). With the recognition that recharge-evacuation-assimilation-fractional crystallization (REAFC) processes may impose significant heterogeneity in the composition of lavas in continental LIPs (Paces, 1990; Turner et al., 1999; Yu et al., 2015), we explore the possibility that the Amaro and Gamo Basalts are derived from a common primary magma.

2.5.2.1 Melt Generation during the Eocene in Southern Ethiopia

The current model explaining the origin of the Eocene continental LIP focuses upon differing intensive parameters of melting and polybaric fractionation to generate lava compositions for the Amaro Basalt and Gamo-Makonnen units (George and Rogers, 2002). The melting conditions during the eruption of the Amaro Basalts were determined by George and Rogers (2002) to be consistent with experimental compositions derived by 3-7% fractional melting of the primitive mantle between 1.5-2 GPa at approximately 1480°C. Melt fractions decrease to ~2% during the eruption of the Gamo Basalts 5-10 m.y. later. As noted by George and Rogers (2002) the pressure and temperature of melting require an elevated mantle potential temperature beneath southern Ethiopia at the time of eruption, consistent with the presence of a mantle thermochemical anomaly during this time (Ebinger and Sleep, 1998; George et al., 1998; Rooney et al., 2012).

2.5.2.2 Conceptual model of the magmatic differentiation system in the Eocene Province

The primary compositional difference between the Amaro and Gamo Basalts units is thought to be imparted by their degree of differentiation. The Gamo Basalts are recognized as being more differentiated than the Amaro Basalts, an interpretation supported by the lower MgO (wt. %) and greater trace element abundances of the Gamo Basalts (George and Rogers, 2002; Stewart and Rogers, 1997). George and Rogers (2002) indicate that assimilation is not the primary agent of differentiation in the Amaro-Gamo magmatic system as it would require unreasonable amounts of assimilant to be incorporated given the bulk composition of the lavas. Additionally, a simple fractional crystallization sequence cannot be accommodated due to the seemingly contradictory petrographic observations and major element characteristics (George and Rogers, 2002). The Amaro and Gamo lavas are noted to contain gabbroic fractionation products that likely formed at shallow depths. However, compositional data indicate a correlation between MgO and the ratios of Sc/Yb and CaO/Al_2O_3 that is contradictory to evolution in a shallow magmatic system. Both ratios decrease with decreasing MgO, an observation consistent with deep fractionation of clinopyroxene (George and Rogers; 2002 and citations therein). MELTS models (Ghiorso and Sack 1995) similarly demonstrate the control of deep fractionation on Amaro-Gamo compositions which lie along the 0.5 GPa liquid line of descent (George and Rogers, 2002). The presence of plagioclase phenocrysts formed at shallow depths coupled with evidence of deep clinopyroxene fractionation led George and Rogers (2002) to conclude that the Amaro-Gamo Basalts evolved by polybaric differentiation pathways. The Amaro-Gamo primary magmas underwent deep fractionation of clinopyroxene and olivine prior to being released to higher crustal levels where gabbroic differentiation occurred forming the crystal cargo observed in the lavas.

Our new results based upon a series of observations of the Gamo-Makonnen magmatic unit are difficult to interpret within the existing magma genesis model for the Eocene-Oligocene lavas in southern Ethiopia. Firstly, our results show that the Gamo-Makonnen lavas are a single magmatic unit representing the large volume main phase of flood basalt volcanism that began in the Eocene and extended into the Oligocene. This observation is difficult to reconcile with the existing magma genesis model for the Eocene continental LIP that suggests the primary magma of the Gamo-Makonnen unit is generated by a smaller degree of mantle melting. Second, as noted by George and Rogers (2002) and this study, the Gamo-Makonnen unit is remarkably homogenous in terms of major and trace element characteristics. It is unlikely, given the new broader spatial and temporal constraints on the Gamo-Makonnen magmatic unit, that fractional crystallization can account for the observed compositional homogeneity. The wide spatial distribution of the Gamo-Makonnen unit would require many closed magmatic systems evolving along an identical differentiation pathway. Additionally, the long temporal window occupied by the Gamo-Makonnen lavas requires these presumably identical magmatic systems to either: (1) evolve only to the composition of the erupted lavas and remain there for the duration of eruption, or (2) new magmatic systems must be formed that also follow the identical differentiation pathway. Additional processes must be active in the magmatic system of the Eocene continental LIP that can reconcile the differentiation pathway identified by George and Rogers (2002) and the broad spatial and temporal constraints from this contribution.

The magmatic systems of continental LIPs are long-lived and modify transient magma through several magmatic processes. Several lines of evidence support a largely open system, in contrast to isolated closed ‘magma chamber’ systems. While fractional crystallization is widely recognized as one of the primary processes contributing to magma differentiation, additional

mechanisms including assimilation of crustal material play an important role (e.g. Bohrson and Spera, 2001; Spera and Bohrson, 2001). However, there is a growing recognition that the closed magma chamber model for differentiation may not accurately represent the large, high-flux magmatic systems of LIPS (Bohrson et al., 2020, 2006; Krans et al., 2018; Paces, 1990; Steiner and Streck, 2019; Streck and Grunder, 2012; Turner et al., 1999; Yu et al., 2015). The magmatic differentiation system of continental LIPs undergo episodic recharge and evacuation that results in hybridized magmas, whose evolutionary pathway is defined by the balance of recharge/evacuation and fractional crystallization/assimilation. For example, where fractional crystallization outpaces the recharge of magma into the system, the resultant lavas will progress toward more evolved compositions. During periods of high magma-recharge rates, the influx of new, primitive magma will drive lava compositions toward less evolved compositions, an effect not likely under closed-system differentiation. Furthermore, when recharge and crystal fractionation are balanced, the magmatic system reaches a steady or buffered state, erupting lavas whose composition remains constant over time. Critically, the buffering of individual elements is strongly dependent on their degree of compatibility, where compatible elements will quickly reach a buffered state while incompatible elements take longer (Lee et al., 2014). Lavas erupted from a buffered REAFC dominated system can exhibit significant enrichment and/or variability in incompatible trace elements abundances with limited variation in compatible elements (Lee et al., 2014). This subtle interplay between the REAFC components may explain the geochemical trends observed in the Eocene continental LIP.

2.5.2.3 Numerical modelling of magma differentiation in the Eocene Province

To probe the processes active within the Gamo-Makonnen magmatic system and to reveal constraints as to the potential flux of magma from the mantle, we undertook REAFC modeling of

the Gamo-Makonnen magmatic system. To allow for efficient exploration of the model parameter space, we developed a Python implementation of the base equations for a constant mass box model developed by Lee et al. (2014). Our model examines REAFC, AFC, assimilation, and fractionation crystallization solutions over a range of evacuation, recharge, assimilation, and crystallization conditions. The primary model outcomes are liquid lines of descent representing each of these processes. For AFC, assimilation, and fractionation crystallization, these liquid lines of descent represent evolution of a single magma chamber without mass addition or subtraction. REAFC modelling requires a persistent magma chamber where mass is continuously added (recharged) or removed (evacuated). Lee et al. (2014) described a complete mass exchange within the magma chamber as an 'overturn'. Liquid lines of descent for REAFC models therefore represent the composition of the residual liquid that has been hybridized over potentially multiple overturns. As the number of overturns increases, the REAFC solutions trend towards a steady state that is termed 'buffered'.

Conceptually, we explored whether the Gamo-Makonnen Basalts can be produced by REAFC modification from an Amaro Basalt composition. To that end, we presume the initial magma chamber composition and recharging magma composition is equivalent to a primitive Amaro Basalt lava. We do not utilize previously calculated primary Amaro Basalt compositions (George and Rogers, 2002) given the presumption that some olivine loss would occur in the lower crust, prior to entering the REAFC system. The assumed assimilant is an average middle crustal composition (Rudnick and Gao, 2003).

Fractional crystallization parameters were set to include crystallizing phases of olivine, clinopyroxene, plagioclase, and Fe-Ti oxides, reflective of those noted in petrographic descriptions and genetic models of previous studies (Davidson, 1983; George and Rogers, 2002).

The examined range of modal abundances for crystallizing phases are as follows: olivine 0.22-0.8, clinopyroxene 0.15-0.5, plagioclase 0-0.3, while Fe-Ti oxides were held constant at 0.05 (where the proportion of Ilm/Mt = 9).

To examine the change in magma composition as a result of REAFC processes, we examined a suite of both compatible and incompatible elements that are sensitive to the crystallization specific phases or are indicative of assimilation. For the compatible elements we chose to examine MgO as a proxy for the degree of differentiation and Ni and Cr to probe the fractionation of mafic phases, whereby Ni and Cr partition into olivine or clinopyroxene, respectively. The behavior of incompatible elements was examined through: (1) Sr, which is affected primarily by the fractionation of plagioclase, (2) Nb, which is sensitive to Fe-Ti oxides or assimilation, and (3) La, which behaves incompatibly throughout the range of MgO concentrations examined by this study. Partition coefficients between minerals and basaltic liquid used by this study are described by: (Bougault and Hekinian, 1974; Ewart and Griffin, 1994; Green et al., 2000; McCallum and Charette, 1978; McKenzie and O'Nions, 1991; Nielsen et al., 1992; Paster et al., 1974; Ringwood and Essene, 1970).

The REAFC model presented here assumes the system is at constant-mass requiring equivalency of input (recharge and assimilation) and output (fractional crystallization and eruption) parameters. This constant mass assumption results in a hybrid parameter wherein there is a continuous balance between the degree of recharge and evacuation. Three REAFC parameters were examined over a range of values: (1) fractional crystallization, which varied from 20-98%, (2) eruption/recharge, which varied from 0-78%, and (3) assimilation, which varied from 0-15%. Within this parameter space, three solutions resulted in liquid lines of descent that bracket the cluster of data defined by the Gamo-Makonnen composition.

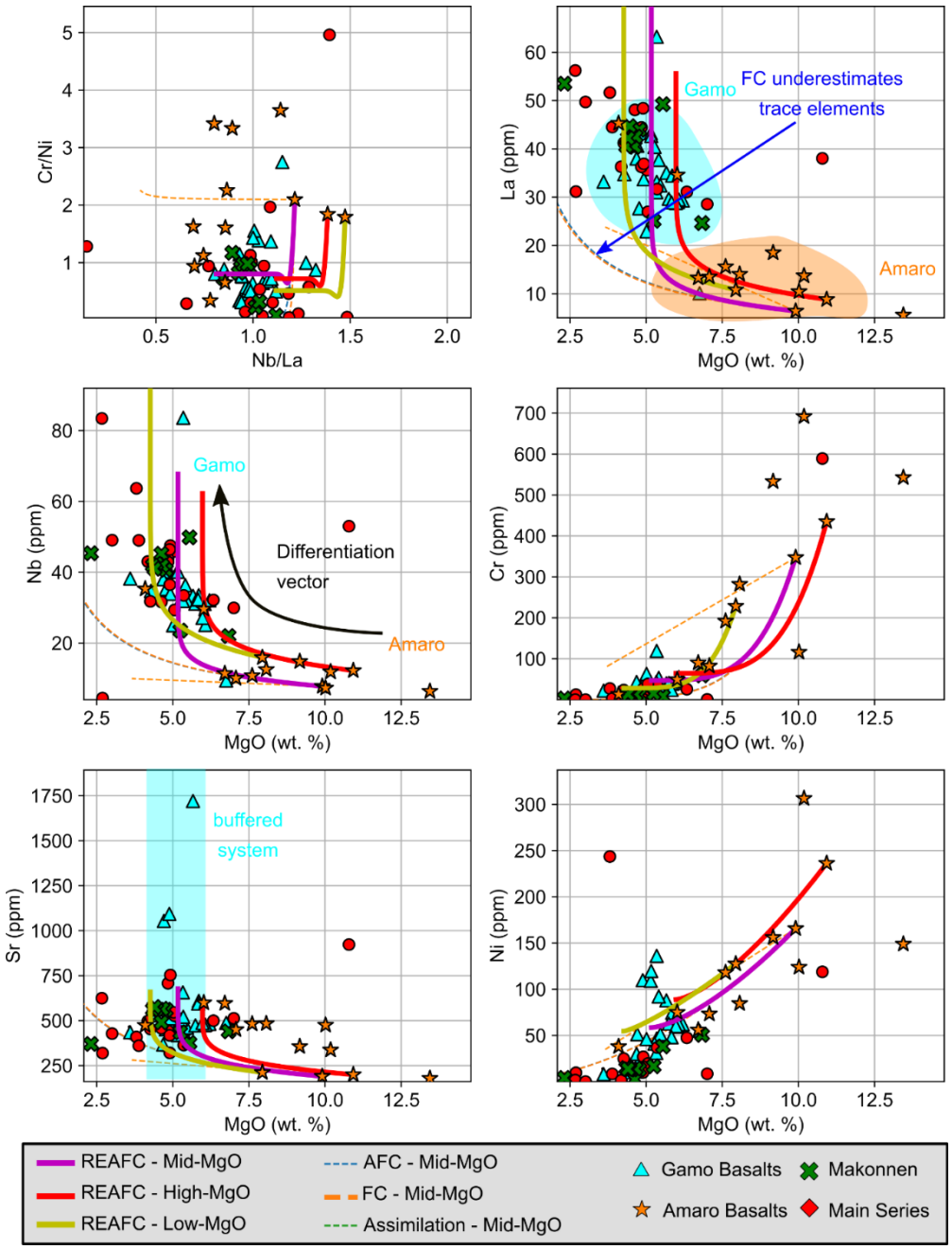

Figure 2.6 – REAFC controlled-liquid lines of descent (LLD) were calculated for several Amaro lava compositions resulting in a series of solutions that bracket samples of the Gamo-Makonnen magmatic unit. Through REAFC magmatic differentiation, Gamo-Makonnen lava compositions can be derived from a primitive Amaro magma.

The modelled liquid lines of descent for fractional crystallization, pure assimilation, and AFC fail to provide solutions that adequately reproduce the Gamo-Makonnen dataset. These solutions yield liquid lines of descent that contain an insufficient concentration of incompatible trace elements to pass through the Gamo-Makonnen dataset (Figure 2.6). In contrast, REAFC models do provide a sufficient enrichment in incompatible trace elements such that model curves pass through the observed data. However, a single initial/recharge magma composition cannot generate an array of curves that circumscribe the observed dataset.

An explanation for the failure of REAFC curves to circumscribe the data, despite significant leverage in model parameter variability, reflects an important principle of REAFC models – the potential to fractionate the behavior of elements based upon compatibility. Specifically, the degree of compatibility of any element within the fractionating phases impacts the point at which that element may become buffered and no longer vary with continued REAFC processing. Each element examined reaches buffered conditions at different points during the evolution of the magmatic system. Compatible trace elements and MgO become buffered within three overturns, consequently, these elements rapidly reach steady state within the magma chamber. The results of our modelling illustrate the necessity for three different initial/recharge magma compositions to accommodate the observed compatible element characteristics. The rapid buffering of MgO prevents any single model solution from exhibiting a traditional liquid line of descent whereby MgO would fall with progressive melt evolution (Figure 2.6). Our REAFC model results instead reach a minimum buffered MgO value below which the magma compositions will not fall, irrespective of further differentiation within the magma system. These model outcomes have further implications for coupled variation in MgO versus incompatible trace element concentrations – notably it is possible to generate a wide range of incompatible

trace element concentrations (and ratios) at common values of MgO from a single primitive magma composition. The implication of these observations is that the initial/recharge magma composition may vary within the Gamo-Makonnen magmatic unit.

Three solutions from our REAFC modelling bracket the majority of the Gamo-Makonnen data (Figure 2.6). The primary difference among these three solutions is the composition of the initial and recharging magma:

(1) Low MgO solution. The initial/recharge magma was ~8 wt. % MgO (sample RG93-73). The fractionating modal assemblage was: 0.22 olivine, 0.60 clinopyroxene, 0.13 plagioclase, 0.05 ilmenite+magnetite. REAFC parameters of fractional crystallization 90%, recharge 8%, assimilation 2%.

(2) Middle MgO solution. The initial/recharge magma was 10 wt. % MgO (sample RG93-75). The fractionating modal assemblage was: 0.32 olivine, 0.50 clinopyroxene, 0.13 plagioclase 0.05 ilmenite+magnetite. REAFC parameters of fractional crystallization 96%, recharge 2%, assimilation 2%.

(3) High MgO solution. The initial/recharge magma was ~11 wt. % MgO (sample RG93-74). The fractionating modal assemblage was: 0.32 olivine, 0.50 clinopyroxene, 0.13 plagioclase 0.05 ilmenite+magnetite. REAFC parameters of fractional crystallization 92%, recharge 6%, assimilation 2%.

While three distinctive initial/recharge magmas were required to capture the variance in the Gamo-Makonnen geochemical data, other model parameters (REAFC proportions, modal assemblage, etc..) did not vary significantly between solutions. The model parameters for all three best-fit solutions showed that fractional crystallization is the dominant process controlling

the liquid lines of descent (90-96 %), while recharge/evacuation (2-8 %), and assimilation (2%) exhibited less control.

2.5.2.4 REAFC Model Validation and Implications

The REAFC modeling results presented here support a previous hypothesis explaining high Ni concentrations within the Gamo-Makonnen lavas as the result of high-pressure fractionation of clinopyroxene (George and Rogers, 2002). Specifically, the fractionating assemblage used for our pure fractional crystallization, assimilation, AFC, and REAFC models is dominated by clinopyroxene (modal abundance between 50-60%). Despite the modal abundance of clinopyroxene used, pure fractional crystallization, assimilation, and AFC fail to replicate the Ni concentrations in the Gamo-Makonnen lavas. However, the REAFC solutions result in the observed high Ni concentrations that occur at modest MgO contents, comparable to the Gamo-Makonnen dataset. This effect is the result of Ni becoming buffered in the magmatic system. A similar outcome is observed for Cr where only REAFC can reproduce the Cr concentrations in the Gamo-Makonnen lavas. The REAFC modeling results confirm that fractionation of clinopyroxene played an important role in the evolution of the Gamo-Makonnen lavas (George and Rogers, 2002), but further refine the mechanism by which magma differentiation proceeded.

The variable buffering of individual elements within the REAFC system can explain the observed differences in incompatible trace element ratios between the Amaro Basalts and the Gamo-Makonnen unit. Previous study of the incompatible trace element and isotopic characteristics of the Amaro and Gamo Basalts indicated it was not possible to generate the Gamo Basalts from the Amaro Basalts through differentiation (George and Rogers, 2002). Our fractional crystallization results support this assertion in that Nb/La values are insufficiently low to capture the Gamo-Makonnen dataset. However, through REAFC, a greater diversity of Nb/La

values is possible. The heterogeneity in incompatible trace element ratios between the Amaro Basalts and the Gamo-Makonnen unit can be explained by differential buffering of these elements. Differences in the interval at which a particular incompatible trace element may buffer – e.g., La between 50 and 90 overturns; Nb between 40 and 60 overturns – will result in variance in the ratios of incompatible trace elements.

A final implication of the model results is the potential origin of the Gamo-Makonnen lavas. Our initial rationale for undertaking REAFC modelling was to examine the hypothesis of whether the Gamo-Makonnen lavas could be derived from the Amaro Basalt magmas through differentiation. The primary difference between the Amaro Basalts and the Gamo-Makonnen unit is the incompatible trace element enrichment. Our REAFC model resolves the origin of the observed incompatible trace element enrichment that defines the Gamo-Makonnen magmatic unit as resulting from continued recharge and differentiation within the magma plumbing system (Figure 2.6). Incompatible trace elements fail to buffer until 20-90 overturns have occurred, while MgO buffers after three overturns. Such modeling outcomes suggest that while MgO and compatible elements may remain constant, the concentration of incompatible trace elements may exhibit substantial variability. The primary outcome of our modelling is that the incompatible trace element concentrations observed in the Gamo-Makonnen lavas can be produced from a parental magma equivalent to the composition of the Amaro Basalt magmas (Figure 2.6).

2.5.3 Development of the of the Main phase of the Eocene Flood Basalt Magmatic System

2.5.3.1 Initial Immature Magmatic System

The maturation of a magmatic plumbing system is best probed when a temporal magmatic record exists. The flood basalt component of continental LIPs provide an unusually complete

record of magmatic conditions within the lithosphere. The existing stratigraphic constraints show that the earliest manifestations of volcanism within the Eocene continental LIP are represented by the Akobo Basalts (49-46 Ma). These basalts, which exhibit a clear Type II magma signature (Rooney et al., 2017), are derived from the sub-continental lithospheric mantle either through direct melting or foundering of the material into the asthenosphere. The relatively shallow depth of origin of the Akobo Basalts (i.e., within the sub-continental lithospheric mantle) may conflict with the clear evidence of significant fractionation of HREE within the data we present (Tb_{CN}/Yb_{CN} ~2.3). Such fractionation may be considered reflective of deep mantle melting within the garnet zone, if interpreted on the basis of a peridotite melting paradigm. However, fractionated HREE values are commonly seen within melts derived from continental lithosphere metasomes where garnet is inferred to be absent (Rooney, 2020c; Rooney et al., 2017). With a single sample it is difficult to establish the nature of the magmatic plumbing system during this initial phase, but the limited distribution of this unit is indicative of a poorly developed magmatic plumbing system.

The transition from the initial phase to the main phase of flood basalt volcanism is represented by the Amaro Basalts (45-39 Ma). The initial conditions under which magmatic differentiation occurred during the main phase within the African lithosphere is preserved in the geochemical characteristics of the Amaro Basalts. We propose that the magmatic system active during Amaro Basalt event was dominated by early crystallization of olivine; a secondary, less pronounced, nascent magma system formed at mid-upper crustal levels wherein plagioclase, clinopyroxene, and further olivine fractionates (George and Rogers, 2002). We interpret the diversity in the Amaro Basalt lava compositions as reflecting the relative immaturity of this magmatic system; the lack of an extensive and continuous mid-crustal differentiation system

permits melt extraction at various degrees of evolution from a variety of staging chambers throughout the crust (Figure 2.7).

It is not currently possible to probe the melting conditions within the Akobo Basalt unit due to ambiguities as to the precise modal mineralogy of its lithospheric mantle source. However, existing constraints on magma generation conditions during the subsequent Amaro Basalt phase indicate a relatively high degree of melting to generate the magmas entering the nascent flood basalt plumbing system. The primary Amaro Basalt magmas are hypothesized to be a 6-8% partial melt of a mantle exhibiting elevated mantle potential temperature (~1500 °C) (George and Rogers, 2002; Rooney et al., 2012). This requires a shift in the source of magmatism from the lithosphere to the sub-lithospheric reservoir coincident with the transition from initial to main phase volcanism in the Eocene continental LIP.

2.5.3.2 Development of a Mature Magmatic System during the Main phase

The eruption of the Gamo-Makonnen magmatic unit (38-28 Ma) is coincident with a profound change in the regional magmatic plumbing system reflective of the maturation of the magma plumbing system during the main phase of flood basalt volcanism. We show that the compositional characteristics of the Gamo-Makonnen lavas can be effectively described by a mature REAFC system within the crust. The efficiency of these magmatic plumbing systems is evident when considering the composition of the erupted products; Gamo-Makonnen lavas are more homogenous than the prior Amaro Basalts and are universally evolved (4.5-6 wt. % MgO), requiring extensive magma hybridization and fractional crystallization. Given the mass removal required during magmatic differentiation within such a system, the flux of magma into the lithosphere during the mature main phase (in comparison to the Amaro Basalt phase) must be far greater than the volume difference in erupted lavas alone. We have shown that the Gamo-

Makonnen lavas represent the most volumetrically important unit within the Eocene continental LIP, with the implication that a significantly greater volume of magma moved through the magmatic plumbing system in comparison to the prior Amaro Basalt phase.

The inferred increase of magma volume entering the lithosphere during the Gamo-Makonnen phase has implications for the state of the East African mantle during the main phase of flood basalt volcanism during the Eocene and Oligocene. Increased magma volume during the Gamo-Makonnen event may be achieved through either: (1) a greater degree of melting of the same mantle volume that melted during the Amaro Basalt event, or (2) through melt generation in a larger volume of mantle. The first model is improbable, as a higher degree of melting will result in primitive lavas with even less enrichment in incompatible trace elements than the Amaro Basalts – contrary to observations of enriched lavas from the Gamo-Makonnen unit. The second model may be achieved by decompression melting of the plume material either through thermo-mechanical erosion of the continental lithosphere by the plume itself, or thinning of the continental lithosphere by extension.

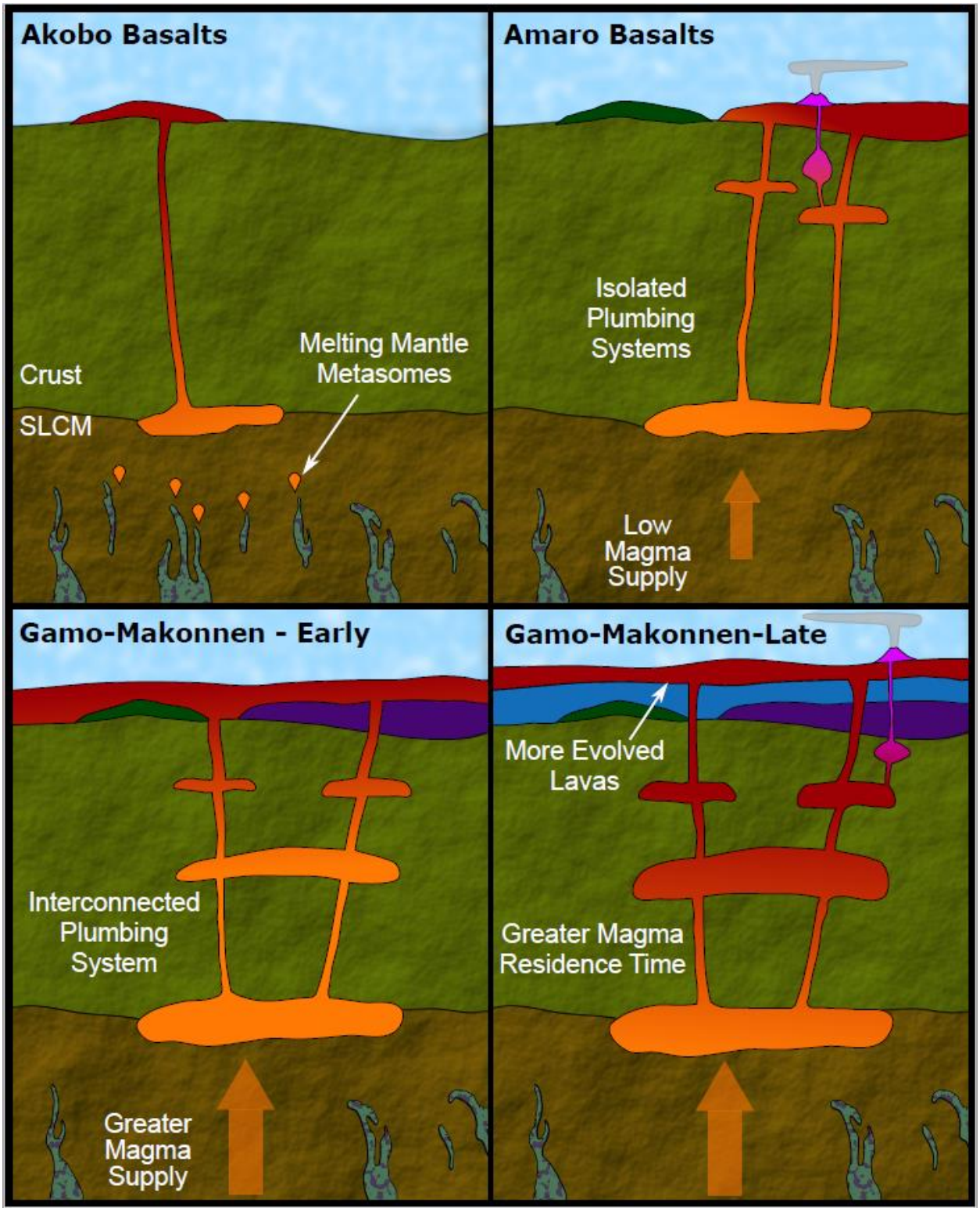

Figure 2.7 – Cartoon describing the evolution of the magmatic plumbing system of the Eocene continental LIP. The Akobo Basalts were derived from the destabilization metasomes within the

Figure 2.7 (cont'd)

lithospheric mantle in response to the impingement of a mantle plume on the base of the lithosphere. These initial phase lavas are small in volume and restricted in spatial distribution. The Amaro Basalts represent the onset of main phase of volcanism and are the first Eocene continental LIP lavas derived predominantly from sub-lithospheric reservoirs. Increased melt contributions from the plume feed a magmatic plumbing system that is poorly connected and inefficient at processing magmas. The resultant lavas are mostly primitive but heterogenous in composition. Poor conductivity of recharging magma results in localized advanced differentiation evidenced by the Arba Minch Tuff. The early stages of the Gamo-Makonnen were the onset of an efficient magma plumbing system likely fed by an increased supply of magma. Abundant, interconnected magma chambers efficiently differentiate and homogenize magmas during this period. The resulting lavas were homogenous and modestly lava compositions observed in the Gamo-Makonnen magmatic unit. During the Gamo-Makonnen late stage, the magmatic plumbing system was more efficient at differentiating magmas, resulting in the progressively more evolved lavas observed in the Gamo Basalts (George and Rogers, 2002). Eventual shut-down of the magmatic system is heralded by the eruption of the widespread Amaro Tuff, the result of advanced differentiation possible due to a lack of magma recharge.

George and Rogers (2002) noted that some lithospheric thinning in addition to anomalously hot asthenosphere was required to explain the Palaeogene magmatism. Confirmation of the onset of rifting in this part of Africa is complicated by the superposition of a largely amagmatic Mesozoic rift zone and the magma-rich Cenozoic rift system. Thermal subsidence modelling of the Mesozoic rifting in South Sudan and NW Kenya indicate that a lithospheric thin zone most likely underlay westernmost Ethiopia and the region of the Turkana

depression (e.g. Ebinger and Sleep, 1998; Hendrie et al., 1994; Mechie et al., 1994). Basins in the Mesozoic Anza graben east of Lake Turkana showed uplift, erosion, and inversion in a time interval loosely bracketed between 40 and 25 Ma (Morley et al., 1999a). Basins west of Lake Turkana experienced fault-controlled subsidence by roughly 35 Ma, based on paleontological analyses of well data, and stratigraphic ties to surface outcrops (Morley et al., 1999b; Talbot et al., 2004). Fission track data suggest a protracted period of uplift and erosion from ~54 Ma, with clear indications of footwall uplift by ~30 Ma (Boone et al., 2019). The amount of lithospheric stretching in Palaeogene time predicted by subsidence modelling is small (~10%, Emishaw and Abdelsalam, 2019; Hendrie et al., 1994)). The pre-rift lithospheric structure as well as minor stretching within and adjacent to the Mesozoic rift system, therefore, may have served to enhance melting across a much broader region where some minor additional extension occurred (e.g. Ebinger and Sleep, 1998; Hendrie et al., 1994). As outlined above and in Figure 2.7a, the hydration state of the subcontinental lithospheric mantle (SCLM) may have played a critical role in the localization of the first pulse of magmatism, which occurred within NNW-trending terranes accreted during the Pan-African orogeny (Davidson, 1983). We interpret the increase in magma generation between 38 and 28 Ma as interaction of a deep mantle upwelling with a pre-existing lithospheric thin zone which began to extend, focusing decompression melting of a thermochemically anomalous material to areas with developing magmatic plumbing systems from the initial heating phase. The dikes and sills from the Eocene continental LIP magmatism probably provided warmer, weaker zones for subsequent intrusions, and served to localize the surface expression of magmatism, and may explain the relatively minor crustal contamination of later sequences (George and Rogers, 2002). Thus, the long-lived Gamo-Makonnen sequence with moderate magma production rates exploited the Akobo and Amaro horst plumbing systems,

further preconditioning the lithosphere for strain localization as Arabia separated from Africa during the Oligocene. Dynamic processes led to initial extension in the East African rift south of Afar during the early Miocene.

While the transition to a mature plumbing system is coincident with a significant increase in magma volumes, the magmatic system continued to evolve throughout the main phase of Eocene volcanism. The existing dataset shows no clear spatial clustering of Main phase lavas wherein erupted compositions at one locale are best accommodated with a specific input composition. Instead, the variance in samples requires that the three different initial magma types are widely distributed throughout the province. Examination of potential temporal heterogeneity in the magmatic system is more complex and limited by the lack of clear stratigraphic constraints for most samples. Insights into the continued development of the magmatic plumbing system is revealed by the examination of the Bek'ule (1, Figure 2.1) stratigraphic section, which consists of ~200 m of stratigraphy correlating to 3.5 Ma of time (George and Rogers, 2002). A series of six Gamo Basalt lava samples from this section show lava compositions that become gradually more evolved, decreasing from 6 wt. % MgO in the older flows to ~4 wt. % in the younger flows. These lavas are representative of the entire range of compositions evident within the Gamo-Makonnen dataset. Such an observation suggests some temporal variation in the initial/recharge magma compositions entering the REAFC system, which are becoming more evolved over time, likely reflecting increased residence time (and olivine and clinopyroxene removal) in the deeper part of the magmatic plumbing system. Further refinement of the temporal evolution of the magmatic plumbing system during the main phase requires more complete stratigraphic sampling of lavas from well constrained lava sections.

2.5.4 Connection to the Oligocene Flood Basalt Province

2.5.4.1 Stratigraphic parallels between the Eocene and Oligocene Provinces

The range of radiogenic age dates (34.8-28.8 Ma) recorded from the Makonnen Basalts of the Gamo-Makonnen magmatic unit show that the eruption of this stratigraphic unit is contemporaneous with the ca. 32–27 Ma Oligocene continental LIP described along the Red Sea margins (Abbate et al., 2014; Baker et al., 1996; Hofmann et al., 1997; Kappelman et al., 2003). On the basis of proximity and these existing geochronological constraints, Rooney (2017) hypothesized that the Makonnen Basalts may have been associated with the Oligocene continental LIP but noted additional geochemical data was needed to confirm this tentative assignation. The new geochemical data we present clearly show that the Makonnen Basalts are magmatically continuous with the Gamo Basalts, forming the Gamo-Makonnen magmatic unit as the predominant composition within the Eocene Province. This conclusion, however, does not preclude a genetic association between the Gamo-Makonnen magmatic unit and the Oligocene continental LIP.

The stratigraphic similarities between the Makonnen Basalts and the Oligocene continental LIP warrant further exploration. The observation of an angular unconformity and paleosol suggests a potential temporal break between the eruption of the Gamo and Makonnen Basalts; these features have been seen elsewhere in the NW Ethiopian Plateau. The initial stratigraphic division of magmatism on the NW Ethiopian plateau recognized that the lower Ashangi was separated from the Aiba flood basalts by an angular unconformity (Mohr and Zanettin, 1988; Zanettin et al., 1980). This observation resulted in the initial division of the Oligocene flood basalts, though this division was ambiguous elsewhere in the province (Mohr, 1983). It is therefore evident that an angular unconformity exists at ca. 30 Ma in both provinces,

consistent with evidence of localized extension throughout the region during this period (Bosworth, 1992; Bosworth and Morley, 1994; Hendrie et al., 1994; Purcell, 2018; Tiercelin et al., 2012; Wolfenden et al., 2005).

2.5.4.2 Geochemical Parallels between the Eocene and Oligocene Provinces

One of the more pronounced features of the Oligocene continental LIP is a distinct spatial zoning of magma types. Stratigraphic units within the flood basalts of the Oligocene continental LIP have been divided on the basis of their magmatic composition. The Ashangi-Aiba stratigraphic units of the Oligocene Province were divided into HT1, HT2, and LT magmatic units (Figure 2.1) (Beccaluva et al., 2009; Pik et al., 1999, 1998). However, the geometry of the geochemical zonation within the Oligocene continental LIP is complicated due to dissection of the volcanic pile during the opening of the Red Sea and East African Rift (Bellahsen et al., 2003; Wolfenden et al., 2005). Several zonation geometries have been proposed for the Oligocene continental LIP including an E-W bilateral arrangement (Pik et al., 1998) and a "bullseye pattern" of magma types (Furman et al., 2016). On the NW Ethiopian plateau, there is a well-defined bilateral zonation between the LT and HT magma types, where the LT lavas occur only in the west and the HT lavas occur in the east (Pik et al., 1998). Subsequent refinement of the distribution of the HT1 and HT2 lavas resulted in the recognition of a radial component, whereby the HT2 lavas appear to be centered on a volcanic plateau that once linked Ethiopia and Yemen (Beccaluva et al., 2009; Natali et al., 2011). These observations were later reinterpreted by Furman et al. (2016) to represent a bullseye pattern, where the HT2 lavas are centrally located. Examination of flood basalts on the southeastern plateau indicates that volcanism may have initiated somewhat later than the rest of the province and dominantly erupted lavas of an HT affinity (Nelson et al., 2019). These studies thus demonstrate that there is a spatial component to

the distribution of magma types in the Oligocene continental LIP , but the geometry of this zonation may differ depending on which magma types are being compared.

Defining a parallel zonation within the Eocene continental LIP has not previously been possible due to a lack of geographically distributed geochemical sampling. Our results suggest there is some ambiguity as to whether the Eocene continental LIP could be considered to be zoned in the same manner. There are three broad magma types within the Eocene continental LIP: the Type II magmas of the Akobo Basalts and the Balsea Koromto lavas; the depleted-Type Ib of the Amaro Basalts; and the enriched-Type Ib of the Gamo-Makonnen magmatic unit (Rooney, 2017). The Type II lavas in the Eocene continental LIP, which are compositionally equivalent to the HT2 lavas from the Oligocene continental LIP, appear to be volumetrically minor components. The limited volume of Eocene Type II magmas is in stark contrast to the compositionally equivalent HT2 Oligocene lavas, which occupy a large portion of the northern Oligocene continental LIP, extending into Yemen (Beccaluva et al., 2009; Natali et al., 2016; Pik et al., 1999). This dichotomy may relate to the mechanism by which HT2 Oligocene magmas were formed – either through lithosphere foundering (Furman et al., 2016), or in situ melting of the lithospheric mantle (Rooney, 2017; Rooney et al., 2014). Regardless of the potential mechanisms of origin, it is evident that Type II lavas within the Eocene continental LIP do not form a clear spatial domain. If interpreted solely on spatial distribution, it is possible that the more primitive Type Ib Amaro Basalts appear spatially constrained in comparison to the more evolved Type Ib Gamo-Makonnen lavas. However, this spatial zonation is also temporal. Therefore, the Eocene continental LIP does not exhibit the same type of zonation evident within the Oligocene continental LIP.

HT1 lavas from the Oligocene continental LIP compositionally overlap with the Gamo-Makonnen magmatic unit; the HT1 and Gamo-Makonnen lavas exhibit primitive mantle normalised patterns that are broadly sub-parallel (Figure 2.3). There is a subtle variance between the majority of samples within the Gamo-Makonnen magmatic unit, which exhibit a less fractionated MREE/LREE slope, and the HT1 lavas, which exhibit a more fractionated pattern. This dichotomy is particularly acute when considering the Gamo-Makonnen lava samples from the southern part of the Eocene continental LIP (Main Series/Gamo Basalt stratigraphic unit), which exhibit the least fractionated REE profile. Curiously, as we have noted above, fractionation of REEs within the Gamo-Makonnen magmatic unit increases with proximity to the Oligocene continental LIP (i.e., the Makonnen Basalt stratigraphic unit). A significant barrier in properly comparing the Gamo-Makonnen unit to the HT1 unit is poor sample coverage and the great diversity of lava compositions exhibited by the HT1 lavas. Notably, the broad diversity in compositions evident within the HT1 lava suite is distinct from the relative homogeneity of the Gamo-Makonnen unit. It remains unclear if the HT1 lava samples actually represent the main phase of volcanism within the continental LIP. Therefore, comparison with the Gamo-Makonnen unit may be of limited utility.

The LT lavas of the Oligocene continental LIP exhibit some parallels to the Gamo-Makonnen magmatic unit. Specifically, relative homogeneity of the LT lavas suggests the potential operation of an REAFC system. The LT lavas are classified as Type Ia (Rooney, 2017) and therefore show some broad similarities with the Type Ib magmas of the Gamo-Makonnen unit. However, Type Ia lavas tend to exhibit a greater depletion in most incompatible trace elements with significant anomalies in Ba and Sr in comparison with Type Ib magmas. These observations could tentatively point to similarities in the lavas contributing to the Eocene and

Oligocene continental LIP , with some degree of heterogeneity imposed by differing REAFC systems. However, the lack of parallel REAFC modeling on the Oligocene continental LIP prevents more firm conclusions at this time.

2.5.4.3 Structure of the Magma System and Implications for Rifting of the African Continent

Well-developed magmatic plumbing systems are recognized as being open, transcrustal systems consisting of interconnected intrusions extending from, in some cases, the upper mantle to the upper-most kilometers of the crust (e.g. Cashman et al., 2017). Our work provides new insights into the initiation and evolution of these lithospheric-scale systems, and, indirectly, their role in extensional strain localization. Resolving the crustal levels at which magmas stall are particularly important for understanding how the crust may respond to the large volume of magmas that transit the lithosphere during LIP events, and those magmas may change the composition of the continental crust. Insight into the distribution of intrusions can be drawn from the mineral modes crystallizing within those intrusions (Morse, 1980). Shallow portions of a continental flood basalt magmatic system, exemplified by the Duluth Complex of Northern Minnesota (Miller and Ripley, 1996; Miller et al. 2002), are dominated by plagioclase crystallization forming troctolites and gabbros (Morse, 1980). However, in the deeper parts of the plumbing system, clinopyroxene is favored (Morse, 1980). The Seiland Igneous Complex in Norway is an example of a lower crustal-upper mantle conduit system that transported tens of thousands of km^3 of magma into the shallower parts of the system (Larsen et al. 2018; Bennet et al., 1986; Grant et al. 2016). Olivine-clinopyroxene cumulates are the predominant rock type in the Seiland Igneous Complex (Larsen et al., 2018) and are inferred to exemplify the deeper portions of the magmatic plumbing system in a continental LIP that transitions to a rift zone.

When interpreted within this conceptual framework, the mineral modes required to explain magmatism within the Eocene province are evidence of deep fractionation. Specifically, we have demonstrated that the mass fraction of crystallizing phases required to form the geochemical compositions of lavas within Eocene continental LIP are dominated by clinopyroxene and olivine: 0.22-0.32 ol, 0.5-0.6 cpx, 0.13 plag, and 0.05 oxides. These mass fractions of minerals are consistent with previous studies that interpreted deep-fractionation of clinopyroxene and olivine as strong controls on lava compositions (George and Rogers, 2002). Consequently, we propose that the deep, clinopyroxene-rich component of the magma system feeding the Eocene continental LIP makes up a larger proportion of the fractionating system than the shallower, plagioclase rich component.

Considering the proportions of minerals crystallizing from the REAFC models, and the likely lithologies predicted from the Duluth Complex (shallow) and from the ultramafic component of the Seiland Igneous Complex (deep), we can estimate the volume of material trapped in shallow and deep parts of the magmatic system. Before estimations of the proportion of deep versus shallow intrusion can be performed, the total volume of intruded material needs to be determined. Our REAFC calculations require 2-8% of the total magma be erupted meaning 92-98 % of the total magma remains in the lithosphere as fractionated products. Estimates on the amount of erupted material in the Eocene continental LIP are ~350,000 km^3 (Rooney, 2017). These eruptive volumes translate to a total magma volume ~7 million km^3, of which ~6.65 million km^3 form intrusions throughout the transcrustal magmatic system. If we then assume that the mass fractions of fractionated products calculated by REAFC models presented in this study reflect the approximate depth of emplacement of magmas, it is possible to estimate the volume of intrusive material at left behind at shallow and deep crustal levels as well as in the SCLM.

Crystallization within the Duluth Complex is thought to have occurred between 7.4 and 11.1 km (Miller and Weiblen, 1990) and is dominated by plagioclase-rich assemblages with lesser olivine (dominantly troctolites; Miller et al. 2002). For this reason, we consider the mass fraction of minerals sequestered within the Eocene continental LIP's shallow system to be plagioclase (mass fraction = 0.13) and a portion of olivine (mass fraction = 0.0325), representing a troctolite lithology crystallizing 80% plagioclase and 20% olivine. This translates to an intrusive volume of 1.4 $x10^6$ km^3 (equivalent to a mass of ~4.8 x 10^{18} kg). The ultramafic intrusions of the Seiland Igneous complex are considered to be the deep crustal roots of Central Iapetus Magmatic Province, intruding between 25-35 km depth, spanning the crust-mantle boundary (Larsen et al. 2018). These deep ultramafic conduits are dominated by clinopyroxene and olivine cumulates (see citations in Larsen et al. 2018). Therefore, we ascribe the crystallizing mass fraction in the deep component of the Eocene continental LIP to dominantly clinopyroxene (mass fraction = 0.6) with the remaining balance assigned to olivine (mass fraction = 0.2875). The deep portion of the magmatic system contains the remaining balance of magma, 5.2 X 10^6 km^3 (equivalent to a mass of ~1.8 x 10^{19} kg). The conclusion that deeper parts of the LIP magmatic system are larger and, therefore, sequester more mass is unsurprising considering geophysical observations of ~10 km-thick high-velocity underplates beneath Ethiopian plateau and LIPs (Farnetani et al., 1996; Maguire et al., 2006; Thybo and Artemieva, 2013).

The volume of magma released from these deep fractionation systems to shallower crustal levels may be relatively small, but these magmas can have a disproportionate effect on the thermal state of the upper crust. Compared to the relatively hot and dense lower crust, even small volumes of magma intruded in the relatively cool and less dense shallow crust can have a significant impact on crustal rheology (Blundy and Annen, 2016; Schmeling and Wallner, 2012).

2.5.4.4 Eocene Continental Large Igneous Province and the African LLSVP

The redefined stratigraphy for the Eocene continental LIP requires the main phase of eruption to have taken place over ~10 m.y., far exceeding the <1-3 m.y. main phase of some LIPs. The observation of a 10 m.y.-long main phase is most likely linked to the initiation of extension and lithospheric stretching, and be linked to mantle upwelling beneath cold, stable continental lithosphere. High melt production rates for 2-3 m.y. above a 1000 km-wide plume head is predicted from models (e.g. Campbell and Griffiths, 1990), and observed in some areas (e.g. Jerram and Widdowson, 2005). The rate of melt extraction from the plume head and entrained ambient mantle during the main phase decreases rapidly with time due to either loss of thermal energy or buoyancy to rise and undergo decompression melting (Campbell and Griffiths 1990). In the case of the Deccan and Parana-Etendeka LIPs, each undergo a period of <1-3 m.y characterized by high volcanic flux consistent with rapid melting of the hot mantle plume, yet both are associated with lithospheric thinning during the high magma production phase. The main phase of flood basalt volcanism within the Deccan LIP may have been as short as 750,000 years (Schoene et al., 2019). For the Parana-Etendeka region, significant lithospheric extension occurred during plume head dissipation (e.g., Harry & Sawyer, 1992). The key difference in NE Africa is that little or no lithospheric stretching occurred during the 10 m.y. of slow magma production rates. The highest magma production rates at 32-27 Ma in the Oligocene continental LIP correspond to the onset of crustal extension in what is now the southern Red Sea and Gulf of Aden (Wolfenden et al., 2005), whereas extension in East Africa initiated much later, and exploited the pre-existing crustal magmatic plumbing systems which may have been thermally weakened.

Our results suggest that upwellings from the African LLSVP, often termed the African Superplume (e.g., Ebinger and Sleep, 1998), impinged on cold thick lithosphere which was too strong to extend, or where far-field extension was weak. Instead, melting occurred within pre-existing thin zones of the Mesozoic-Paleaogene Central African rift zone. Lithospheric imaging beneath the area shows a NW–SE-trending high-wavespeed band in southern Ethiopia at <200 km depth, interpreted as refractory Proterozoic lithosphere that has likely influenced the localization of rifting (Kounidis et al., 2021). Only with 10 m.y. of thermal thinning of the lithosphere, and with the development of a widespread system of dikes and sills did lithosphere weaken (e.g., Bialas et al., 2010) to enable rift initiation between 30 and 25 Ma. We present evidence from REAFC models showing that recharge of fresh magma into the magmatic system of the Eocene continental LIP is required to form the erupted lava compositions. The consistency of these lavas compositions through time means that the input of new magma into the system, and by necessity melt generation in the upper mantle, must have been persistent throughout the duration of mafic volcanism. Persistent melting is consistent with elevated mantle potential temperature recorded in lavas in throughout East Africa (Rooney et al., 2012) indicating broad contamination of the upper mantle by warm, upwelling material, potentially derived from the African LLSVP. Contamination of the East African upper mantle by the African LLSVP appears to be widespread, as evidenced by noble gas isotopic characterizations (Haldorssen et al. 2014) and the convergence of radiogenic isotope arrays on a composition broadly equivalent to the Afar Plume (Rooney, 2020c). The broad distribution of high-temperature, LLSVP derived material is consistent with geophysical observations of a broad thermochemical anomaly present within the East African upper mantle (e.g. Bastow et al., 2008; Boyce et al., 2021; Chang et al., 2020). The modern, widespread thermochemical anomaly may have first interacted with the

African lithosphere during the Eocene, providing a means to generate the magma supply required to maintain the long-lived magmatic system that formed the Eocene continental LIP in East Africa.

2.6 Conclusions

The Eocene continental LIP of SW Ethiopia and northern Kenya is the earliest volcanic manifestation of the interaction between a rising mantle thermochemical anomaly associated with the African LLSVP and the East African lithosphere. The dataset presented herein represents the most geographically distributed suite of lava samples from the Eocene continental LIP, and thus presents an opportunity to resolve an outstanding question of whether geochemical zonation exists within this province that is similar to that observed within the later Oligocene continental LIP . We find that the geochemical variability across the Eocene continental LIP is rather limited – most of the erupted lavas exhibit a trace element pattern that is broadly consistent with the previously characterized Gamo Basalts. An important exception to this homogenous distribution are the Amaro Basalts, which occur in a small area in the east of the province but predate the main phase represented by the Gamo Basalts. The existing data thus show that the Eocene continental LIP lacks the strong geochemical zonation found in the Oligocene continental LIP.

We have shown that lavas of the Eocene continental LIP can be united under a single volcano-stratigraphic framework that records the magmatic evolution of the province. The Cenozoic volcano-stratigraphic record in SW Ethiopia begins at ~49 Ma with the small-volume eruption of the alkaline Akobo Basalts, which we interpret as the result of melting of destabilized mantle metasomes derived from continental lithosphere (Beccaluva et al., 2009; Rooney, 2020c;

Rooney et al., 2017, 2014). The occurrence of early-alkaline volcanism is observed in other LIPs (e.g. Parana-Entendeka, Jerram and Widdowson, 2005) including the neighboring province on the NW Ethiopian plateau but is eventually overwhelmed by more voluminous magmas associated with flood basalt eruptions (Jerram et al., 1999, 2000). Prior geochronologic studies have shown that subsequent flood basalt-style volcanism begins with the eruption of the Amaro Basalt (~45-39 Ma), which we suggest is derived from a relatively immature magmatic plumbing system. Subsequent widespread magmatism (~38-28 Ma) is the amalgamation of several stratigraphic units: the Gamo Basalts, the Main Series, and the Makonnen Basalts. We have shown that the major and trace element characteristics of all three stratigraphic units show limited variability and are thus geochemically indistinguishable. Consequently, we combine the Gamo Basalts, the Main Series, and the Makonnen Basalts into a single magmatic unit termed the Gamo-Makonnen magmatic unit.

With an increasing awareness that lavas erupted during main phase volcanism within a LIP may be impacted by complex differentiation (Bohrson et al., 2020, 2014; Lee et al., 2014; Yu et al., 2015) processes, we undertook REAFC magma modelling to constrain the origin of the Gamo-Makonnen magmatic unit. We find that the erupted compositional range of the Gamo-Makonnen Magmatic unit can be produced via REAFC processes. Critically, our modelling shows that the Gamo-Makonnen lavas may be produced from starting compositions equivalent to Amaro Basalt lavas. The implication of these results is the potential continuity of primitive magma compositions supplying the magma differentiation system during the main phase of volcanism for the Eocene continental LIP. The continuity of magma supply during the eruption of the Gamo-Makonnen magmatic unit indicates prolonged melting of mantle-derived material,

exceeding the main phase eruptive cycle for a typical continental LIP. Such an observation provides valuable insight into the character of the East African upper mantle.

Cenozoic flood basalts in East Africa provide an unusual opportunity to probe material rising from one of the largest structures on the planet – the African LLSVP (Rooney, 2017). Prolonged magma supply feeding the Gamo-Makonnen magmatic unit combined with the subsequent eruption of the neighboring Oligocene continental LIP is suggestive an upper mantle that is being influenced by thermo-chemically anomalous material over broad spatial and temporal scales. It is possible that material rising from the African LLSVP has contaminated much of East African upper mantle, a hypothesis supported by the widespread isotopic signatures of plume-like material and elevated mantle potential temperatures throughout the region (Rooney, 2020c). The eruption of the Eocene continental LIP marks start of a relationship between the African lithosphere and material derived from the deep mantle that will impact the geologic history of East Africa through modern times. Magmas generated as a result of the interaction of material derived from the African LLSVP and the African lithosphere during the Palaeogene had a profound impact on the thermal and compositional state of the East African crust, contributing to the rupture of the African continent and the formation of the East African Rift system. The intrusion of magmas that would erupt to form Akobo and Amaro basalts created preferred conduits for subsequent main phase lavas of the Gamo-Makonnen magmatic unit. The relative homogeneity of the Gamo-Makonnen lavas is evidence for a magmatic system that underwent magma recharge and mixing, processes that require magma injections into existing magma bodies. Critically, the 10 m.y. long period of magma injection during this phase was required to create the zones of weakness in the African lithosphere and SCLM that would focus

strain during Oligo-Miocene extension. These zones of weakness may have been an important component in focusing strain, facilitating the initiation of the East African Rift system.

3. MESSENGERS FROM THE MAGMA CHAMBERS: PETRO-STRATIGRAPHIC ANALYSIS OF PLAGIOCLASE-RICH FLOOD BASALT LAVAS IN TURKANA, KENYA

3.1 Introduction

Continental large igneous provinces (LIPs) are the largest magmatic events on Earth, commonly erupting >100,000 km^3 of lava over periods of <1 to 3 m.y. (Cox, 1980; Ernst, 2014). The rapid eruption of such large volumes of basaltic magma has resulted in various origin hypotheses that range from mantle plumes to lithospheric delamination (Anderson, 2005; Beccaluva et al., 2009; Furman and Graham, 1999). While much attention has thus been focused on constraining these mantle processes in LIPs, the eruption of large volumes of magmas may also impose profound changes on the continental lithosphere (Dufek and Bergantz, 2005; Karakas and Dufek, 2015; Karlstrom and Richards, 2011). Notably, the composition of lavas in these continental LIPs requires extensive differentiation to have occurred within the continental lithosphere (Charlier et al., 2015; Cox, 1980; De Min et al., 2018; George and Rogers, 2002; Pik et al., 1998; Villiger et al., 2004; Wolff et al., 2008). The existence of this magmatic differentiation system facilitates one of the largest terrestrial transfers of mass and thermal energy from the upper mantle to surface (Blundy and Annen, 2016; Jerram and Widdowson, 2005; Self et al., 1997), resulting in significant compositional and thermal perturbation of surrounding lithosphere that may influence rift development (Harry and Sawyer, 1992; Karakas and Dufek, 2015).

The magmatic systems feeding continental LIPs transport and differentiate magmas throughout the lithosphere (Ernst, 2014; Krans et al., 2018). For example, deep, high density cumulates can form “underplates” or regions of "high velocity lower crust" consistent with the staging of magmas and crystal fractionation at depth (Farnetani et al., 1996; Larsen et al., 2018;

Montési, 2013; Ridley and Richards, 2010; Thybo and Artemieva, 2013). The most unambiguous examples of magma differentiation bodies within a continental LIPs are layered mafic intrusions such as Skaergaard, the Bushveld intrusion, and the Duluth Complex (Charlier et al., 2015). Due to complexities related to the accumulation of crystallized material (e.g., erosion of the cumulate pile, sub-intrusions), the temporal record of magmatic processes may not be well preserved within these intrusive bodies (Latypov et al., 2020; Mungall et al., 2016; Robb and Mungall, 2020). However, stratigraphic sequences of mafic lavas that form continental flood basalt provinces can be used to probe the changes in the magmatic system through time (Davis et al., 2021; e.g., Kieffer et al., 2004; Krans et al., 2018; Streck and Grunder, 2012).

Continental flood basalt lavas, and their crystal cargo, represent material extracted from the crustal differentiation system, providing a more complete temporal record of differentiation processes (Higgins and Chandrasekharam, 2007). The utility of this extracted material in elucidating the temporal evolution of a continental LIP's magmatic system is well documented in existing chemo-stratigraphic (Davis et al., 2021; Elkins-Tanton et al., 2007; Vanderkluysen et al., 2011) and petro-stratigraphic studies (Higgins and Chandrasekharam, 2007; Krans et al., 2018). Chemo-stratigraphic studies of continental LIPs examine the liquid component of the magmatic system and provide a cumulative record of all process that have produced the lava (e.g., Davis et al., 2021). Petro-stratigraphic studies, which focus primarily on the crystal cargo carried within erupted lavas, are particularly useful in probing the conditions of the magma differentiation system in which the crystals formed. In particular, the crystals can preserve a record of their interaction with different liquid compositions (e.g., Costa and Dungan, 2005; Nielsen et al., 2020; Zellmer et al., 2003). When compared to other complex magmatic settings such as continental arcs, compositional variations in liquids within continental LIP differentiation

systems are more subtle and have heretofore been somewhat more challenging to interpret (e.g., Kieffer et al., 2004; Pik et al., 1998; Wolff et al., 2008). Recent developments in constraining plagioclase-liquid partition coefficients and new strategies for investigating element diffusion within crystals now permit insights into these subtle compositional variations, and provide a novel window into the magmatic differentiation system of the largest eruptions on Earth (Cherniak and Watson, 2020; Nielsen et al., 2020, 2017; Zellmer et al., 1999).

East Africa represents one of the best regions in which to examine the temporal variation of lavas within a continental LIP (Krans et al., 2018; Rooney, 2017). This province is relatively young (45 Ma – present), with extensive preservation of exposed continuous stratigraphic sections of lavas; (Davidson, 1983; Ebinger et al., 1993; George et al., 1998; George and Rogers, 2002; Hofmann et al., 1997). Insights derived from the Oligocene-aged continental LIP have found spatial zonation in lava composition, with evidence of episodic pulses in magmatism (Furman et al., 2016; Pik et al., 1998). However, there exists a paucity of parallel studies on the earlier phase of magmatic activity, which began during the Eocene (Davidson, 1983; Ebinger et al., 1993; George et al., 1998; George and Rogers, 2002; Steiner et al., 2021). Recent geochronologic work has shown that a significant volume of Eocene continental LIP exists within the Turkana Depression (Brown and Jicha, 2016; McDougall and Brown, 2009). The Lokitaung Gorge (Figure 3.1) in northwestern Turkana exposes a complete volcano-stratigraphic record, extending from the basal contact with older sediments, to terminal silicic volcanoclastics. We leverage this continuous record of magmatism preserved at Lokitaung to investigate the magmatic differentiation system of the Eocene Continental LIP.

The study area preserves a continuous, 790m volcano-stratigraphic section of Eocene LIP flood basalt lavas exposed in the Lokitaung Gorge. We establish a detailed a petro-stratigraphic

history of magmatism within the Gorge based upon lava textures in 54 flows. These data show that the volcanic stratigraphy at Lokitaung was erupted in three broad magmatic pulses, separated by packages of plagioclase-rich lavas. We present a laser-ablation ICP-MS dataset of 545 plagioclase crystal analyses from 15 representative flows. These data show that individual lavas contain plagioclase compositions consistent with a homogenous crystal population, but that these populations change through the stratigraphy. We interpret these observations as the result of the storage and equilibration of a plagioclase-rich mush system at persistently elevated temperatures (>1100°C). We examine the role of plagioclase-liquid equilibration in modifying the composition of flood basalt magmas in a series of interlinked equilibrium recharge, evacuation, assimilation, and fractional crystallization models. Our work shows that crystal-liquid interaction profoundly impacts the magmatic differentiation system in continental LIPs, and that equilibrium crystallization models may provide more realistic insights into how such systems evolve.

3.2 Background

Cenozoic magmatism associated with the African-Arabian LIP extends throughout East Africa and Yemen (Figure 3.1) and is thought to be related to material rising from the African Large Low Shear Velocity Province (Ebinger, 2020; Reed et al., 2016; Thompson et al., 2015). Modern magmatism in the region is centered on the Eastern and Western Branches of the East African Rift System and takes the form of linear chains of cinder cones, or large central volcanoes located within the rift basin (Corti et al., 2019; Ebinger, 2020). There are three broad pulses of basaltic magmatism in East Africa that are associated with the development of the East African Rift System (Rooney, 2020a, 2020b, 2020c, 2017): the Early Miocene Resurgence (26.9

– 22 Ma) and associated Samburu Event (20–16 Ma) (Abbate et al., 2014; Boschetto et al., 1992; Furman et al., 2006a; Kieffer et al., 2004); Mid-Miocene Resurgence (12 – 9 Ma) (Itaya and Sawada, 1987; Tatsumi and Kimura, 1991); and the Stratoid Phase (4 – 0.5 Ma) (Corti et al., 2019; Ebinger et al., 2000; Gathogo et al., 2008). Consistent with observations of other LIPs, the early phases of Cenozoic magmatism in the African-Arabian LIP are characterized by the eruption of voluminous flood basalt (Ebinger et al., 1993; Mohr, 1983; Rooney, 2017). The most well-known of these flood basalt events is the Oligocene traps phase (~33.0 – 27 Ma) of activity, which formed the Ethiopian Flood Basalts on the northwest Ethiopian Plateau, the Somali Plateau, and in western Yemen (Figure 3.1; Abbate et al., 2014; Baker et al., 1996; Hofmann et al., 1997; Ukstins et al., 2002). However, flood basalt magmatism in the region actually began ca. 49 Ma with the formation of the Eocene Initial Phase (49-34 Ma) in southern Ethiopia and northern Kenya (Davidson, 1983; Ebinger et al., 1993; George et al., 1998; WoldeGabriel et al., 1991).

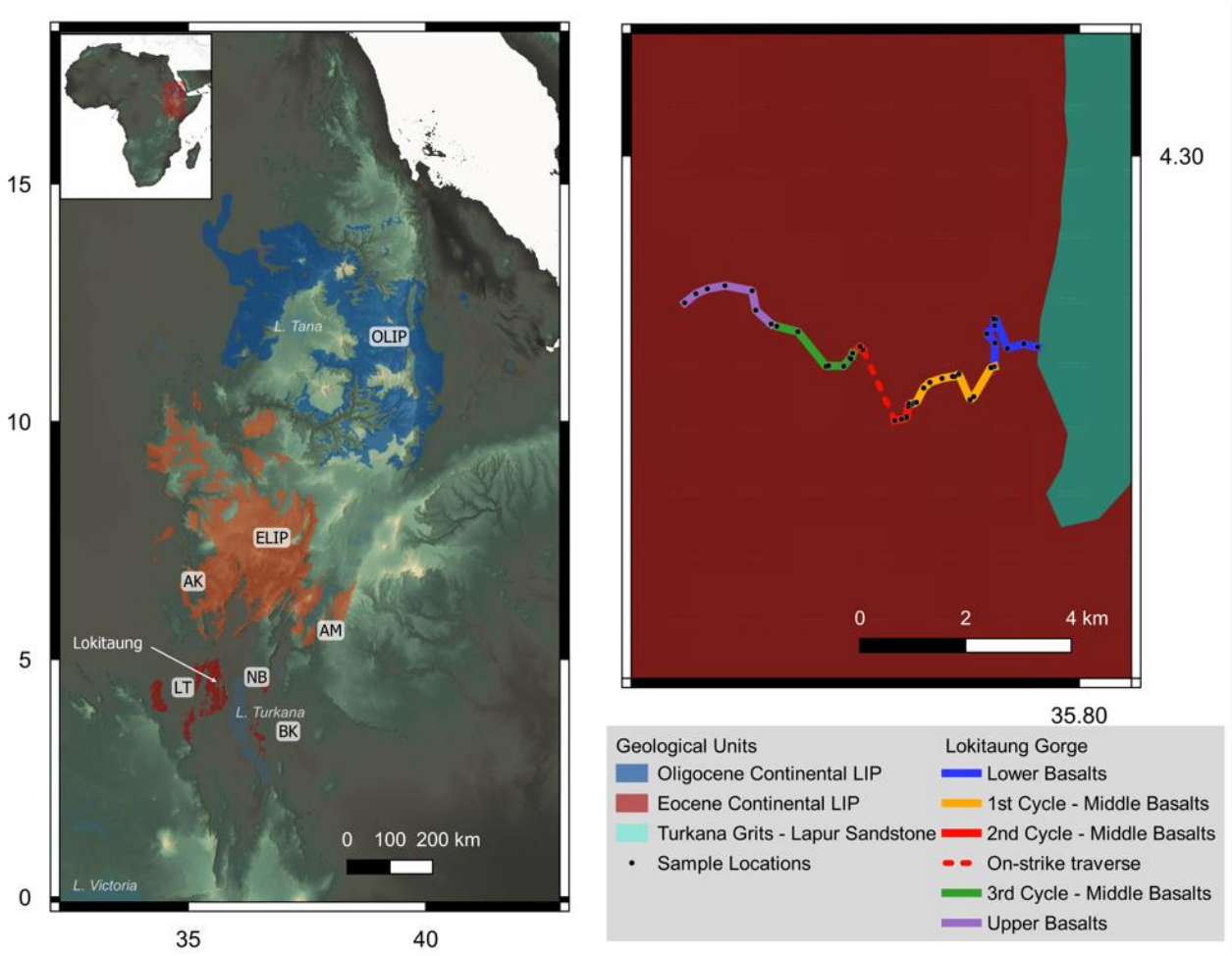

Figure 3.1 – (A) Distribution of continental LIPs in East Africa. Abbreviations: Akobo Basalts (AK), Amaro Region (AM), Balsea Kormoto (BK), Chebera (CH), Eocene Continental LIP (ELIP), Lotikipi Basin (LT), and the Oligocene Continental LIP (OLIP). The distribution of the Akobo Basalts and the Amaro Basalts are not pictured due to their small footprint at the map scale presented here. (B) The Lokitaung Gorge section showing sample locations. The base of the section is to the east where Eocene age lavas overlie older sandstones. Flood basalt lavas dip ~15 degrees to the WSW. Labelled samples represent the first sample in a new magmatic pulse.

Much of the current knowledge of the Eocene Initial Phase is based on data from southern and southwestern Ethiopia (Davidson, 1983; Ebinger et al., 1993; George et al., 1998; George and Rogers, 2002; Steiner et al., 2021), with the exception of spatially-limited geochemical data from east of Lake Turkana (Furman et al., 2006b). In southwestern and southern Ethiopia, the Eocene Initial phase is preserved as the Akobo, Amaro, and Gamo-Makonnen basalts (Ebinger et al., 1993; George et al., 1998; George and Rogers, 2002; Rooney, 2017; Steiner et al., 2021; Stewart and Rogers, 1996), and records the broad evolution of the continental LIP magmatic system. The Akobo basalts are the earliest lavas in the region and comprise a series of clinopyroxene-rich, alkaline lavas that are attributed to the melting of the destabilized lithosphere produced by the initial impingement of a mantle plume on the base of the African lithosphere (Davidson, 1983; Rooney, 2017). The spatially limited Amaro Basalts and widespread Gamo-Makonnen Basalts are transitional tholeiites and are considered to form the main pulse of continental LIP magmatism (Steiner et al., 2021). Both the Amaro and Gamo basalts are thought to originate from plume-influenced mantle melts that have undergone poly-baric differentiation in the African lithosphere (Ebinger et al., 2000, 1993; George et al., 1998; George and Rogers, 2002). This broad evolution of the magmatic system during the Eocene Initial Phase is based primarily upon stratigraphic constraints derived from studies in the Amaro-Gamo region (e.g., Ebinger et al., 1993; George and Rogers, 2002). While useful in resolving large-scale changes in the magmatic system (e.g., transition from one continental LIP phase to another), these studies do not provide sufficiently detailed temporal constraints to resolve changes in the magmatic system during the main pulse of continental LIP activity. Resolving the fine temporal scale of the main pulse of activity requires flow-by-flow stratigraphic samples of the flood basalt sequence.

Stratiform mafic lavas that are contemporaneous to Eocene Initial Phase lavas are recognized from northwestern Kenya. Surface mapping and aerial photography recognized the widespread occurrence of thick stratiform sequences of mafic lavas west of Lake Turkana (Walsh and Dodson, 1969; Figure 3.1). Seismic studies used for petroleum exploration recognized a sub-surface connection in the Lotikipi Basin between outcrops of lava sequences (Morley et al., 1999; Wescott et al., 1999, 1999), thus demonstrating that the stratiform outcrops are part of a large flood basalt sequence in northwestern Kenya. Geochronologic studies of those same outcrops parallel conclusions from the seismic studies and indicate that the lavas were erupted contemporaneously across the region (Brown and Jicha, 2016; Brown and McDougall, 2011; Zanettin et al., 1983). In this area, flood basalt eruptions began at ~ 36 Ma and may have continued to ~31 Ma (Brown and Jicha, 2016; Brown and McDougall, 2011; Tiercelin et al., 2012). The entirety of this geochronologic record as currently known is found only within and above the Lokitaung Gorge (Figure 3.1). Here, the Eocene Initial Phase lavas are bracketed between the contact with the underlying Cretaceous sandstone and the overlying early Miocene lavas. The exposure of the entire flood basalt sequence at Lokitaung permits a detailed temporal examination of the magmatic system feeding the Eocene continental LIP.

3.3 Methods

3.3.1 Stratigraphic Sampling

Lava samples were collected via flow-by-flow sampling of a nearly continuous ~780-meter volcano-stratigraphic section in the Lokitaung Gorge of northwestern Turkana, Kenya (Figure 3.1). The stratiform lavas in the region dip shallowly to the WNW, allowing for the stratigraphic relationships between flows to be readily observed. Flow thicknesses were estimated in the field,

though several flows were sufficiently thick that visual estimation was not possible and thicknesses were then calculated based on dip (~10°) and distance. At a stratigraphic height of 529m, steep waterfalls immediately below the town of Lokitaung required the tracing of flows from the Lokitaung Gorge to the surrounding plain. A marker horizon of a lava flow with paleosol cap was used to ensure stratigraphic position was maintained during this lateral offset of the section. In total, 54 basalt lava flows were sampled. The focus was to collect samples from the dense cores of flow lobes or from the center of massive flows, thus avoiding the highly vesicular and altered marginal areas. Rare occurrences of flows that were severely weathered required sampling for core stones, the interiors of which were less weathered. All samples are recorded in the System for Earth Sample Registration, and sample metadata, including location information, is retrievable using the International Geo Sample Number (IGSN) presented in the Appendix.

3.3.2 Petrographic Classification of Lava Textures

Thin sections were prepared for 54 lava samples and classified based upon micro textures and mineral abundances. The lavas in the Lokitaung section can be divided to a first order based upon the presence of phenocrysts or glomerocrysts into aphyric lavas and crystal rich lavas. Crystal rich lavas are sub-divided into three groups based upon phenocryst/glomerocryst mineralogy (Figure 3.2; appendix 1). The four petrographic groups observed are 1) aphyric (Figure 3.2a), 2) plagioclase porphyritic (Figure 3.2b), 3) plagioclase + clinopyroxene glomerophyric (Figure 3.2c), and 4) large clinopyroxene phyric lavas (Figure 3.2d). Parallel observations of similar textures in other continental LIPs support this classification scheme (Beccaluva et al., 2009; Berg and Klewin, 1988; Camp et al., 2013; Duraiswami et al., 2001; Krans et al., 2018; Lightfoot et al., 1990).

1. Aphyric to weakly porphyritic -

    Aphyric textured lavas are the most abundant petrographic group from the Lokitaung flood basalt section, representing 32 of the 54 lavas examining petrographically. These lavas contain between 0 and 3% phenocryst phases whose mode varies from plagioclase dominated to plagioclase and clinopyroxene. Commonly, aphyric lavas with both plagioclase and clinopyroxene contain glomerocrysts. Groundmass textures found in the aphyric lavas range from microcrystalline to intergranular and are more rarely trachytic.

2. Plagioclase porphyritic

    The second most common petrographic group within the Lokitaung flood basalts are lavas with abundant medium to coarse grained plagioclase. Plagioclase crystals exhibit a range of zoning styles including unzoned crystals, normally zoned, and oscillatory zoned. The plagioclase abundance of these lavas is between 3 and 18%. The distribution of plagioclase abundance within this grouping, however, subdivides these flows into low and high abundances of plagioclase. Flows below 10% phenocrysts are considered to be porphyritic, while those greater than 10% are considered super-porphyritic. In these lavas, plagioclase is observed to occur as single phenocrysts as glomerocrysts composed entirely of plagioclase cumulates. Plagioclase commonly exhibits resorption textures such as sieve texture along with rare embayments and dissolution boundaries within crystals.

3. Plagioclase + clinopyroxene glomerophyric

Limited occurrences of plagioclase and clinopyroxene porphyritic lavas are recognized from the Lokitaung Gorge section. These lavas contain the highest overall abundance of phenocrysts of any lava in the section, some reaching >18% phenocrysts. The proportion of plagioclase to clinopyroxene is about 1:1. Cotectic crystallization textures are commonly observed in these lavas where elongate “bow tie” plagioclase is penetrative and intergrown with granular clinopyroxene (Bryan, 1979; Thy, 1983).

4. Large clinopyroxene porphyritic lavas

Two lavas from the Lokitaung Gorge contain between 7 and 10% large clinopyroxene phenocrysts. Clinopyroxene is commonly zoned and exhibits disequilibrium textures such as sieve and reaction rims. Zonation commonly appears as light green to tan cores surrounded by brown-pink rims. Sieve texture is more common in the rim than in the core of mineral grains. Olivine is observed in these lavas but is subordinate to the abundant clinopyroxene phenocrysts.

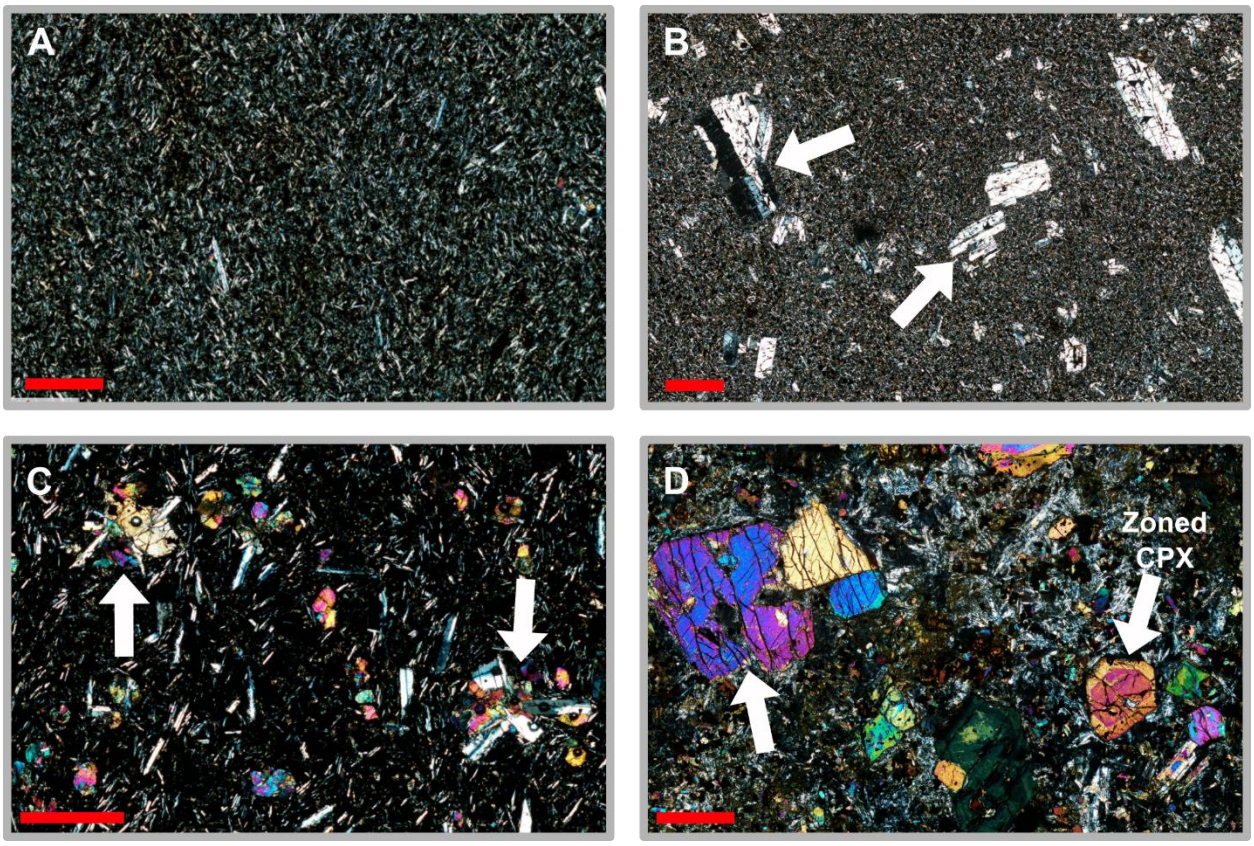

Figure 3.2 – Photomicrographs of representative textures and mineral assemblages from the Lokitaung flood basalts. All images are in XPL, scale bars are 500 µm. (A) Aphyric lava with few to no phenocrysts. Sample TOR0000ZQ from the third cycle of the Middle Basalts. (B) Plagioclase glomerocryst and phenocryst rich lava. Plagioclase indicated by arrows and may be as large as 3mm in this sample. Sample TOR00011F from the first cycle of the Middle Basalts. (C) Clinopyroxene-plagioclase glomerophyric lava containing radiating or "bow tie" glomerocrysts. Sample TOR00011O of the Upper Basalts. (D) Large clinopyroxene bearing lava. Clinopyroxene occurs as both zoned phenocrysts and glomerocrysts (arrows) and are between 250 - >1000 µm in size. Sample TOR00010X from the base of the section in the Lower Basalts.

3.3.3 LA-ICPMS Analyses of Plagioclase

We examined individual and glomerophyric plagioclase grains from crystal-rich lavas from the Lokitaung Gorge by LA-ICPMS at Michigan State University. Analytical methods used in this contribution parallel those of Rooney et al. (2020) and Trestrail et al. (2017). Crystals were ablated with 65 µm spot sizes on standard polished, petrographic thin sections utilizing a Teledyne (Photon-Machines) Analyte G2 excimer laser set at 10 Hz and at a fluence of 4.1 J/cm2, with an energy set point of 3.5 mJ in energy stability mode. The laser ablation system was coupled to a Thermo Scientific ICAP Q ICP-MS instrument for quantitation of major and trace metals. All major and trace element data was normalized to an internal standard of 100% sum of the major element oxides and processed using the Thermo Scientific QTegra software. Instrument drift was monitored by the repeated analysis of fused powder standards JB-2 and BHVO-2G. An NMNH diopside standard was also analyzed as an unknown to monitor matrix effects. The ICP-MS was operated in kinetic energy discrimination (KED) mode using He flux to reduce isobaric interferences. To optimize analytical sensitivity, plagioclase crystals were analyzed solely for those elements known to be enriched in these minerals, enabling precise measurements from a 30 second crystal ablation. Isotopes measured were ^{23}Na, ^{24}Mg, ^{27}Al, ^{28}Si, ^{39}K, ^{42}Ca, ^{49}Ti, ^{51}V, ^{55}Mn, ^{57}Fe, ^{59}Co, ^{85}Rb, ^{88}Sr, ^{89}Y, ^{90}Zr, ^{93}Nb, ^{137}Ba, ^{139}La, ^{140}Ce, ^{141}Pr, ^{146}Nd, ^{153}Eu, ^{157}Gd, ^{172}Yb, ^{175}Lu, ^{178}Hf, and ^{208}Pb.

The host basalt compositions were determined by rastering the groundmass of plagioclase-rich samples by LA-ICPMS (e.g., Svoboda et al., 2021; Steiner et al., 2021). We utilize the groundmass compositions only for major element characterization due to the decoupling of major and trace elements in recharge, evacuation, assimilation, and fractional crystallization (REAFC) dominated systems (e.g., Lee et al. 2014; Yu et al 2015). Additional isotopes measured

for groundmass sampling were ^{31}P, ^{45}Sc, ^{52}Cr, ^{60}Ni, ^{147}Sm, ^{159}Tb, ^{163}Dy, ^{165}Ho, ^{166}Er, ^{169}Tm, ^{181}Ta, ^{232}Th, and ^{238}U. All analytical data can be found in the supplemental files.

3.4 Results

3.4.1 Petrostratigraphy of the Lokitaung Gorge

As noted above, lavas from the Lokitaung Gorge can be divided based on texture and mineralogy into four petrographic groups (Figure 3.2). The primary discriminators among individual petrographic groups is the abundance of phenocrysts phases and the mode of the phenocrysts present. The most common petrographic group is characterized by a lack of abundant phenocryst phases (<3% phenocrysts), termed here as being aphyric (Figure 3.2a). The second most abundant petrographic group is characterized by abundant plagioclase phenocrysts, megacrysts, and/or glomerocrysts (Figure 3.2b; glomerocrysts defined by Krans et al. (2018)). Less common are lavas with either clinopyroxene and/or olivine occurring in a glomerophyric texture with plagioclase (Figure 3.2c). Finally, the last petrographic group includes lavas bearing only clinopyroxene-olivine phenocrysts (Figure 3.2d). Lavas from all petrographic groups exhibit groundmass textures ranging from microcrystalline to intergranular.

The petrographic groups described above are combined with the detailed stratigraphic information collected during sampling and used to create a petrostratigraphic column with flow-by-flow characterization of lavas from Lokitaung Gorge (Figure 3.3a, 3.3b). Based on the petrographic observations presented here, we have identified five petrographic cycles, defined on the basis of the occurrence of plagioclase rich lavas (Figure 3.3a; Krans et al., 2018). These five petrographic cycles are combined into a tripartite division based on common magmatic

conditions contributing to the formation of those lavas: Lower Basalts, Middle Basalts with three sub-units, and Upper Basalts (Fig.3, 4).

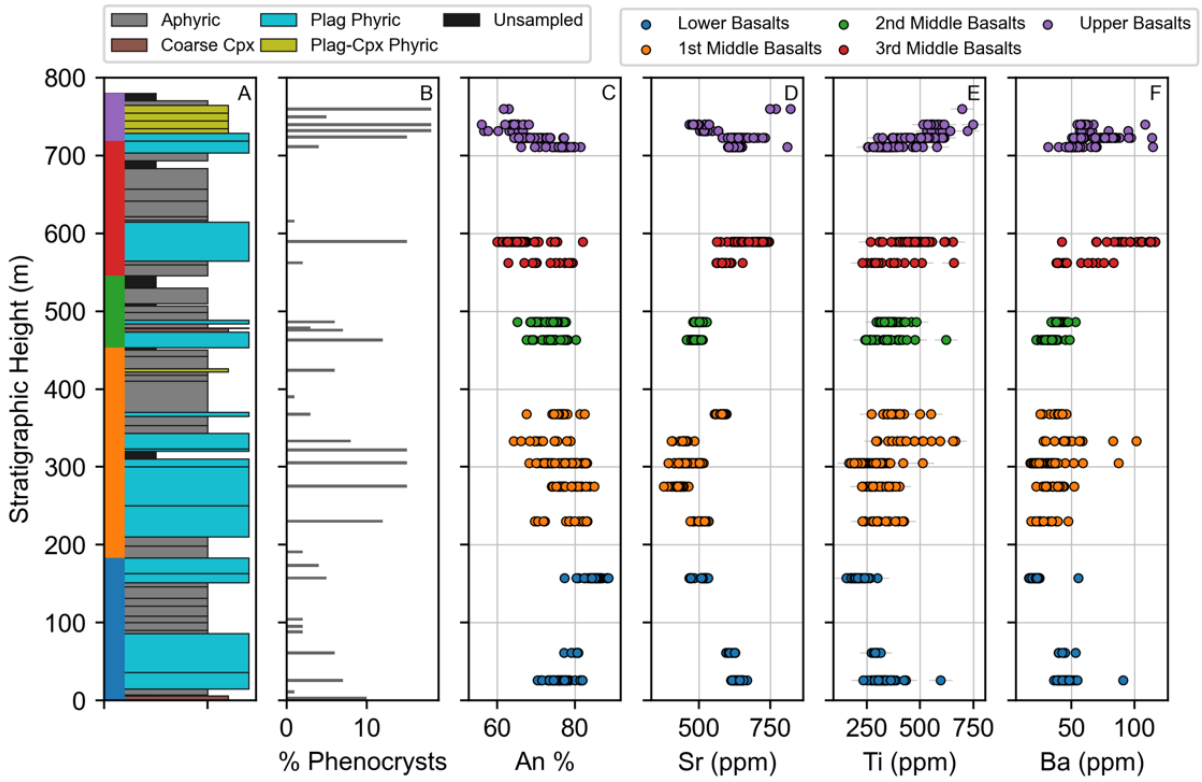

Figure 3.3 – Volcano-stratigraphic column of the Lokitaung section. (A) Lava textures based upon petrographic observations. (B) Phenocryst abundance of lavas based upon petrographic observations. (C) The anorthite composition of plagioclase determined by LA-ICPMS. (D) Sr concentration in plagioclase by LA-ICPMS. (E) Ti concentration in plagioclase by LA-ICPMS. (F) Ba concentration of plagioclase by LA-ICPMS. Error bars for data are plotted where errors are greater than the point size.

3.4.1.1 Lower Basalts

The Lower Basalts sequence is 200m thick and is composed of 13 flows (Figure 3.3). Flow thickness ranges from 6-50 m, with an average of 15 m. Flows are typically massive to blocky

with isolated occurrences of columnar basalts. The first flow in the Lower basalts is the basal lava for the entire section and is in direct contact with the Cretaceous Labur sandstone (Tiercelin et al., 2012). This basal flow contains abundant-zoned clinopyroxene phenocrysts and glomerocrysts (Figure 3.2d) and is of the petrographic group "Large clinopyroxene porphyritic." Overlying the basal flow are 1-4 meters of mudstone and well-sorted sandstone (Figure 3.3). Erupted on top of the sediments are the first occurrences of plagioclase-rich lavas which contain between 6-7% plagioclase (Figure 3.3). Remaining lavas in the Lower Basalts are aphyric to weakly porphyritic and contain between 3-5% plagioclase phenocrysts/glomerocrysts. The upper-most lavas in the Lower Basalts contain "bowtie" clinopyroxene-plagioclase glomerocrysts.

3.4.1.2 Middle Basalts

The Middle Basalts comprise the majority of the Lokitaung Gorge (500m) and extend from 200m to 700m in stratigraphic height and consist of 33 lava flows (Figure 3.3). Flow thicknesses range from 0.5 – 50 m, with an average of 15 m. Flow morphologies include massive, blocky, and columnar lavas along with the occurrence of lobed flows, a morphology not observed in the Lower Basalts. The Middle Basalts are characterized petrographically by the bimodal occurrence of plagioclase-rich and aphyric lavas. Aphyric lavas are the most common textural group in this sequence, although the cyclic occurrence of plagioclase-rich flows are the most distinctive feature of the Middle Basalts (Figure 3.3). These flows are sub-divided into three petrographic cycles termed Cycle 1, Cycle 2, and Cycle 3 (Figure 3.3). The division between the Lower and Middle basalts is marked by a group of highly plagioclase porphyritic lavas (>10% phenocrysts) that define the onset of Cycle 1 of the Middle Basalts. Consisting of five flows, these highly porphyritic lavas average 26 m and are thicker than the other Middle Basalts flows (Figure 3.3).

After 120 m, these highly porphyritic flows give way to the dominantly aphyric lavas which comprise the remainder of the Cycle 1 lavas (Figure 3.3). Cycle 2 lavas are marked by the return to plagioclase rich lavas at 453m height, though the plagioclase rich flows are fewer and thinner than those of Cycle 1. The porphyritic lavas of Cycle 2 also contain a coarse-grained clinopyroxene-phyric lava overlain by aphyric flows until 560m. At 560m height, a 50m thick, plagioclase-rich lava defines the onset of Cycle 3 (Figure 3.3). This early Cycle 3 lava is unique in containing olivine, though plagioclase is the most abundant accounting for >80% of the phenocryst phases. Aphyric flows follow and are dominant until onset the crystal-rich lavas of Upper Basalts at 700m.

3.4.1.3 Upper Basalts

The transition from the Middle Basalts to the Upper Basalts is marked by a 10m thick tuffaceous horizon that also defines the start of the Upper Basalts (Figure 3.3). The tuff is followed by two plagioclase-rich lavas similar to those observed in the previous cycles. The Upper Basalt sequence is 67 m thick and contains 8 lava flows. Flow thicknesses range from 1 to 15m with an average of 8 m. These lavas were sampled along a meandering ephemeral stream in the relatively flat region within the town of Lokitaung (Figure 3.1). Exposure in this area is somewhat limited. Overlying this coarsely-porphyritic flows is a series of lavas characterized by abundant (4-18 modal %) “bow tie” plagioclase + clinopyroxene glomerocrysts (Figure 3.1, 2c). Several, thin aphyric lavas intercalate with the glomerophyric lavas and extend to the top of the flood basalt sequence at 771m. At 771 m, a thick (10 m), partially welded crystal tuff marks the top of the section.

3.4.2 Plagioclase compositions in lavas of the Lokitaung Gorge

A total of 545 plagioclase analyses were collected from 17 lava flows distributed throughout the Lokitaung flood basalt section. Plagioclase compositions range from An_{88} to An_{55} (Figure 3.3c-f). Due to the limited partitioning of elements into plagioclase, many elements commonly used to explore magmatic processes are at or below their detection limits and are of limited utility. Detectable elements exhibit a negative correlation with An content (e.g., Mn, Ti, V, Ba, La), and become more abundant in Ab-rich plagioclase (Figure 3.5). A notable exception is Sr, that uniquely exhibits two distinct trends, a high-Sr and low-Sr, when compared to An-content. Both Sr-trends occur in a comparable range of An-contents and are flat to weakly negatively correlated with An (Figure 3.5). All sample groupings are listed in ascending stratigraphic order.

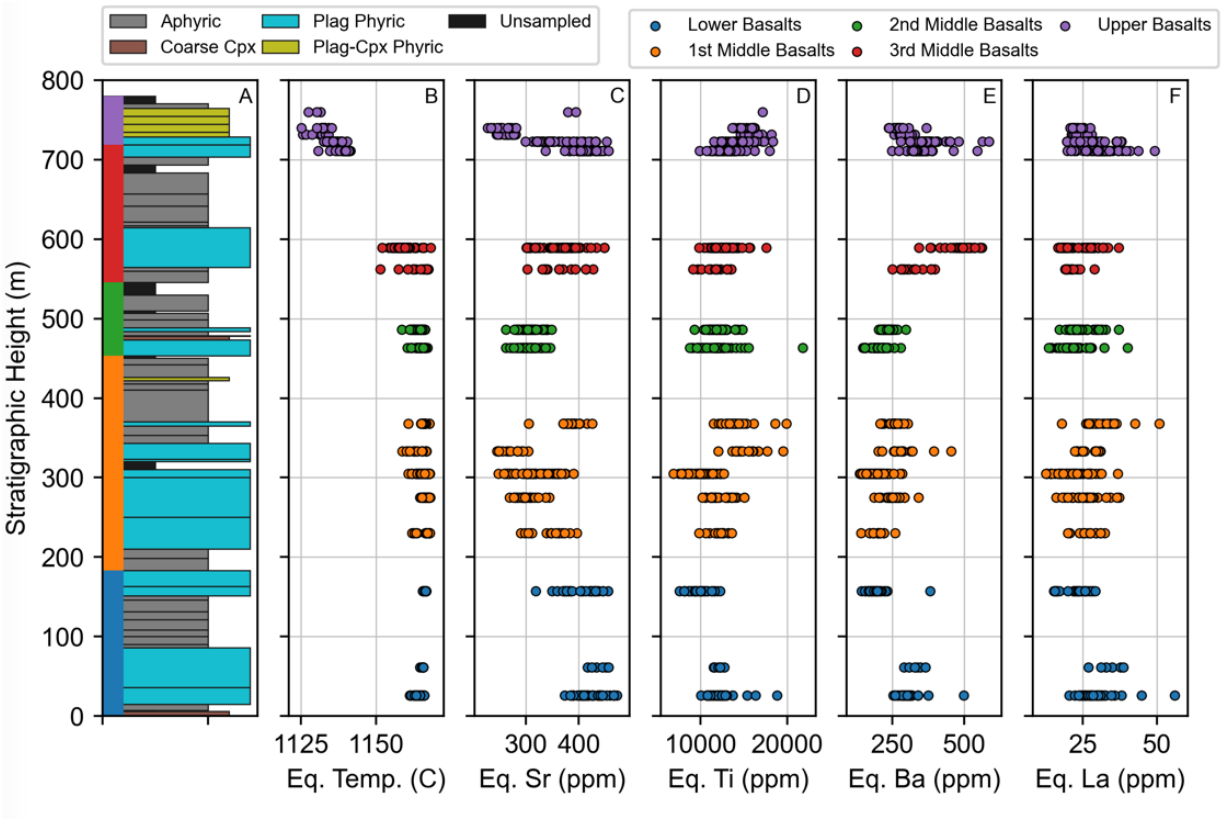

Figure 3.4 – Volcano-stratigraphic column from Lokituang Gorge with values for plagioclase equilibrium temperature and liquid compositions calculated from Nielsen et al. (2020). (A) Lava

Figure 3.4 (cont'd)

textures based upon petrographic observations. (B) Plagioclase equilibrium temperature calculated from Putirka (2008). (C) Sr composition for a liquid in equilibrium with plagioclase crystals. (D) Ti composition for a liquid in equilibrium with plagioclase crystals. (E) Ba composition for the liquid in equilibrium with plagioclase crystals. (F) La composition for the liquid in equilibrium with plagioclase crystals.

3.4.2.1 Lower Basalts

The plagioclase crystals from three lavas in the Lower Basalts were analyzed (TOR000112, TOR000113, and TOR00011B). The plagioclase in the Lower Basalts lavas range from An_{71} to An_{87} (Figure 3.3c), becoming increasingly more An rich upward in the stratigraphy. The concentration of Sr in plagioclase from the Lower Basalts forms two data clusters: (1) between 480-520 ppm and (2) between 600-660 ppm (Figure 3.5). The Sr concentration in plagioclase decreases upward in the stratigraphy of the Lower Basalts (Figure 3.3). The concentrations of La (0.3-1.6 ppm), Ba (16-58 ppm), and Ti (170-420 ppm) all decrease upward in the stratigraphy (Figure 3.3).

3.4.2.2 Middle Basalts

Plagioclase crystals from five plagioclase-rich lavas in Cycle 1 of the Middle Basalts were analyzed (TOR00011F, TOR00011G, TOR00011H, TOR00010V, and TOR00010S). The plagioclase in Cycle 1 of the Middle Basalt lavas range from An_{68} to An_{85}, broadly decreasing in An abundance except for the highest flow, TOR00010S, where the trend shifts to more An-rich compositions (Figure 3.3). The concentration of Sr in plagioclase from Cycle 1 of the Middle Basalts forms two data clusters: (1) between 380-520 ppm, and (2) between 600-660 ppm

(Figure 3.5; TOR00010S only). The Sr concentration in plagioclase exhibit a C-shaped profile, initially decreasing upward in the stratigraphy before increasing in TOR00010S (Figure 3.3). The concentration of La (0.3-1.25 ppm) increases through Cycle 1 of the Middle Basalts, while Ba (18-58 ppm) has a weak D-shaped profile (Figure 3.3). Ti (170-650 ppm) initially decreases upward in the stratigraphy before increasing in lavas TOR00010V and TOR00010S (Figure 3.3).

Plagioclase crystals from two plagioclase-rich lavas in Cycle 2 of the Middle Basalts were analyzed (TOR00010L and TOR00010H). The plagioclase in Cycle 2 of the Middle Basalt lavas range from An_{68} to An_{78} with little change in An content relative to stratigraphic position (Figure 3.3c). The concentration of Sr in plagioclase from Cycle 2 of the Middle basalts is between 440-520 ppm, increasing slightly upward in the stratigraphy (Figure 3.3). The median concentration of La (0.5-1.1 ppm), Ba (20-58 ppm), and Ti (210-450 ppm) increases slightly upward in the stratigraphy (Figure 3.3).

Plagioclase crystals from two plagioclase-rich lavas in Cycle 3 of the Middle Basalts were analyzed (TOR00010C and TOR00010B). The plagioclase in Cycle 3 of the Middle Basalt lavas range from An_{60} to An_{82} with little change in An content relative to stratigraphic position (Figure 3.3c). The concentration of Sr in plagioclase from Cycle 3 of the Middle Basalts is between 550-750 ppm, increasing slightly upward in the stratigraphy due to plagioclase in TOR00010B extending to higher Sr concentrations. The median concentration of La (0.5-1.5 ppm) and Ba (30-100 ppm) increases upward in the stratigraphy while Ti (210-650 ppm) increases only slightly upward.

3.4.2.3 Upper Basalts

Plagioclase crystals from Upper Basalt lavas were analyzed (TOR00011I, TOR00011K, TOR00011L, TOR00011L, TOR00011M, and TOR00011O). The plagioclase in the Upper

Basalt lavas range from An_{71} to An_{87} and decreases in An abundance upwards in the stratigraphy (Figure 3.3). The concentration of Sr in plagioclase from the Upper Basalts forms two clusters: (1) between 480-520 ppm, and (2) 600-660 ppm (Figure 3.5). Sr concentrations decrease upward with the exception of the stratigraphically highest flow, TOR00011O, which contains plagioclase with exceptionally high Sr (>750 ppm) (Figure 3.3d). High and low Sr groups in the Upper Basalts are correlated with two textural occurrences of plagioclase where monomineralic glomerocrysts/phenocrysts are high in Sr while crystals in plagioclase-clinopyroxene glomerocrysts are lower in Sr. The median concentration of La (0.75-1.55 ppm, see appendix 2) does not vary with stratigraphic position. Ba (40-100 ppm) and Ti (240-640 ppm) increases upward in the stratigraphy (Figure 3.3e, f).

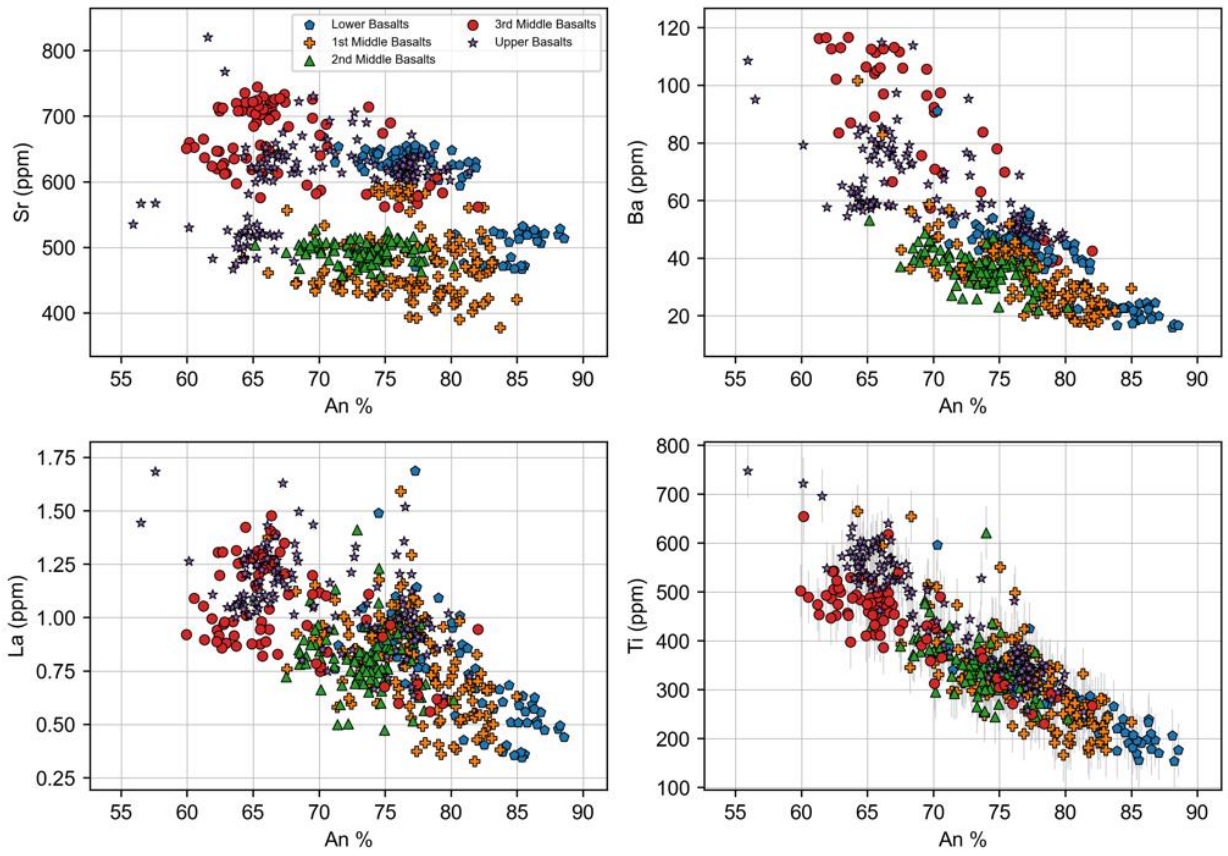

Figure 3.5 - Concentration of select trace elements in plagioclase crystals compared to the crystal's anorthite composition (An%). Most elements exhibit a negative slope, containing lower concentrations of trace elements at higher An contents. Sr is the exception, which exhibits a pair of flat trends defining high and low Sr groups. Error bars for data are plotted where errors are greater than the point size.

3.5 Discussion

3.5.1 Petrographic and Geochemical Stratigraphy of the Lokitaung Gorge Basalts

We have shown that the flood basalt section in the Lokitaung Gorge extends from the contact with the underlying sediments to the termination of continental LIP activity with limited

structural complexity. This unusually complete section presents an opportunity to examine the temporal evolution of the magmatic differentiation processes within one of the youngest examples of a continental LIP. We explore how petrographic models of continental LIP evolution (e.g., Krans et al., 2018) can be enhanced and refined by using observations of crystal chemistry. Using this combined approach, we show that the magmatic system feeding the Lokitaung flood basalts underwent significant oscillations in the proportion of crystallization and magma recharge, consistent with a model of pulsed magmatism.

We have constructed a conceptual model wherein the magmatic system of the continental LIP in this region is dominated by a lower crustal clinopyroxene-rich system and an upper plagioclase-rich system (George and Rogers, 2002; Krans et al., 2018; Larsen et al., 2018; Latypov et al., 2020). Recharge of the upper system is achieved by a flux of magma from the lower system mixing with the existing more evolved magmas in the upper crustal magmatic system (Krans et al., 2018; Latypov et al., 2020). Hiatuses in volcanism permit crystallization within the upper system and the formation of cumulates (Borges et al., 2014; Higgins and Chandrasekharam, 2007; Krans et al., 2018). The widespread occurrence of mono-mineralic plagioclase cumulates within the stratigraphic section requires the continued flux of magmas from the lower crustal system during volcanic hiatuses; otherwise, compositional evolution within the upper magmatic system would result in multiple-saturation (Latypov et al., 2020). The initial occurrence of lavas rich in these mono-mineralic plagioclase-cumulates is indicative of a new pulse of high-magmatic flux wherein the new magmas disrupt and disaggregate cumulates formed during the preceding hiatus (Krans et al., 2018). During these high flux events, aphyric lavas are erupted as the supply of crystals that can be re-mobilized is exhausted (Krans et al., 2018). Changes in the composition of cumulate material erupted can reflect the magnitude of

recharge (Borges et al., 2014; Higgins and Chandrasekharam, 2007). For example, during periods of high-magmatic flux, the bulk composition of the system may shift toward more primitive compositions that, during the next volcanic hiatus, will result in the mono-mineralic cumulates being more primitive (Borges et al., 2014; Nishimura, 2019). We use this conceptual model to describe the temporal evolution of the magmatic system within the Lokitaung Gorge.

3.5.1.1 Lower Basalts Sequence – Establishing the Magmatic System

Examination of the petrographic variation of the crystal cargo carried in continental LIP lavas may be used to probe the establishment of the deep and shallow potions of the magmatic system (Krans et al., 2018). The first lava in the Lokitaung section contains abundant, coarse grained clinopyroxene phenocrysts and glomerocrysts and is uniquely devoid of plagioclase (Figure 3.2). Parallel observations of such clinopyroxene-rich lavas at the base of a flood basalt sequence have been made in southern Ethiopia (Akobo Basalts; Davidson, 1983) and from the NW Ethiopian Plateau (LT Province of the Oligocene Traps; Krans et al., 2018). Where dated, the basal clinopyroxene-rich lavas are not the same age (Davidson, 1983; Hofmann et al., 1997; McDougall and Brown, 2009), suggesting the occurrence of these lavas at the base of a flood basalt sequence records a common process, the establishment of the magmatic system (Krans et al., 2018). The clinopyroxene crystal cargo of these lavas are consistent with derivation from a middle to lower crystal magmatic system where the pressure is sufficient to stabilize the formation of clinopyroxene but not plagioclase (Morse, 1980). Therefore, the occurrence of only clinopyroxene in these early, initial phase lavas indicates that a deep magmatic system is active while the more shallow, plagioclase forming system that dominates the main phase has not yet been established (Jerram and Widdowson, 2005; Krans et al., 2018). A record of the transitions from initial to main phase and eventually to the termination of continental LIP volcanism is

observed in a continuous set of lava flows. Unlike the Akobo Basalts and the Oligocene traps, the section at Lokitaung is continuous, extending from the basal clinopyroxene-rich lava to the terminal silicic volcaniclastics. The apparent temporal continuity of the Lokitaung Gorge lavas permits the examination of the transition from the initial establishment of the magmatic system to the main phase and conclusion of continental LIP activity.

An important observation from Lokitaung is the presence of 1-4m of sediments separating the basal clinopyroxene porphyritic flow from the subsequent plagioclase-phyric flows that dominate the section. Elsewhere, parallel observations of paleosols and sediments followed by plagioclase-rich flows have been interpreted as representing a volcanic hiatus wherein plagioclase accumulated in the shallow magmatic system was later remobilized by the onset of a period of increased magmatic flux (e.g., Krans et al., 2018). This model is supported by observations of a gradual decrease of plagioclase phenocryst/glomerocryst abundance in subsequent lavas followed by the eventual eruption of aphyric flows.

Plagioclase compositions in the Lower Basalts are among the most primitive in the entire stratigraphic section, exhibiting the greatest An content (An_{71} to An_{87}, though five outlier datapoints reach An_{65}; Figure 3.3, 5) and some of the lowest concentrations of elements commonly used as indicators of differentiation (e.g., Ti, REE; Figure 3.3, 5). These observations are consistent with plagioclase derived from a magma that underwent only modest differentiation prior to plagioclase crystallization. It could be expected that progressive establishment of more magma chambers would lead to more efficient storage and differentiation of magmas within the system, leading to progressively more An-poor plagioclase with higher incompatible element abundances through time (Nielson, et al. 2020). However, plagioclase compositions in the Lower Basalts appear to become more primitive up-section (Figure 3.3), increasing from average An_{76}

to An_{81}, with a commensurate decrease in the concentrations of Ti and REEs. These unexpected observations can be accommodated by a high flux of fresh magma into the shallow system, a conclusion consistent with the eruption of aphyric lavas in the sequence. The high flux of fresh magma entering the plagioclase-forming system during this period may exceed the capacity of nascent magma differentiation to evolve the liquid (Streck, 2008; Vance, 1962). The result of continued input is a progressively more primitive hybrid liquid that produces crystals with higher An and lower incompatible trace elements. The possible proportions of recharge to crystallization and the composition of the input magma are not immediately apparent and are explored further in the numerical modeling section.

The final lava flows in the Lower Basalts sequence are characterized by a texture of clinopyroxene-plagioclase glomerocrysts (Figure 3.2c), indicative of cotectic crystallization of plagioclase and clinopyroxene (Bryan, 1979; Thy, 1983). This observation requires that later magmas were further along the liquid line of descent than the earlier lavas that contained mono-mineralic plagioclase cumulates and suggest that the magma supply during the eruption of the final lavas of the Lower Basalts was waning, allowing for the shallowest magmas to differentiate prior to eruption.

3.5.1.2 Middle Flood Basalts – Episodic Eruptions

The Middle Basalts sequence is the main eruptive phase of the Lokitaung section, occurring between 205m and 700m and recording a series of magmatic pulses and volcanic hiatuses delineated by transitions from aphyric to plagioclase-rich lavas. As a group, the Middle Basalts sequence extends to much lower An contents (An_{85} to An_{65}) than the Lower Basalts sequence (Figure 3.3, 5). Ba and REE concentrations are broadly comparable to those of the Lower Basalts, though Ti is displaced toward slightly higher concentrations at a given An content

(Figure 3.5). Sr abundances, however, appear to be decoupled from the rest of the trace elements and divided into high-Sr plagioclase and low-Sr plagioclase groups (Fig 5). While the high-Sr plagioclase resemble plagioclase from the Lower Basalt sequence, the low-Sr plagioclase crystals are a new and distinct feature of the Middle Basalt sequence.

Following the hiatus corresponding to the end of the Lower Basalts sequence, renewed magma supply results in the initial three plagioclase-rich flows of the first pulse of the Middle Basalts sequence (Figure 3.3; 205-320m stratigraphic height). Plagioclase compositions in these lavas are slightly more evolved, displaced to lower An, and have greater incompatible element concentrations (Figure 3.3; Ba, Ti), compared to the latest flows of the Lower Basalts sequence (Figure 3.3). We interpret these crystals as being disaggregated from material accumulated during the waning stages of the Lower Basalts sequence. Magmas that had become trapped by the decrease in flux progressed towards more evolved compositions, forming crystals with increased incompatible element abundances. The two subsequent flows contain crystals that are progressively less anorthitic and have higher concentrations of Ba and Ti (Fig 3). The observed decrease in Sr concentration, coupled with increase in Ti through this sequence, reflects the preferential removal of Sr over Ti during plagioclase crystallization (Cherniak and Watson, 2020; Nielsen et al., 2020, 2017). We therefore interpret the first three flows of the initial pulse of the Middle Basalts sequence as recording a magmatic system where fractionation is the dominant process, presumably due to a reduction in magma flux. The subsequent appearance of aphyric lavas from 320-450m (Figure 3.3) is evidence that the balance has shifted back toward recharge, consistent with previous studies of the Ethiopian Traps (Krans et al., 2018).

The increase in recharge towards the end of the first pulse of the Middle Basalts results in a magmatic system with more primitive magmas (Borges et al., 2014; Higgins and

Chandrasekharam, 2007; Nishimura, 2019). During the subsequent volcanic hiatus at the end of the first pulse, the crystallization of plagioclase should produce compositions that are slightly more An and Sr rich, and contain lower concentrations of Ti and Ba in comparison to earlier magmas. The plagioclase disaggregated from this system and erupted during the initial phases of a new, thinner (75m) second pulse of magmatism are entirely consistent with this model. Few aphyric lavas are found within the second pulse, and those that are present are separated by paleosols and thick tuffaceous horizons. Mafic eruptions cease at 515m stratigraphic height (Figure 3.3). A 20m-thick tuffaceous unit marks the end of the second magmatic pulse and is interpreted as a hiatus in mafic volcanism resultant from a reduction in magma supply to the shallow magmatic system.

Within the plagioclase-rich sequence in this second pulse, at 470m stratigraphic height a thin (~5m) clinopyroxene and olivine rich (ankaramitic) lava erupted onto a hummocky, plagioclase rich flow (Figure 3.3). This lava is petrographically similar to the basal lava of the Lower Basalts (Figure 3.2; zoned clinopyroxene is present), although this flow also contains plagioclase that is presumably entrained in transit to the surface. Based upon the similarity with the basal lava of the Lower Basalts, and interpretations as to the origin of clinopyroxene-bearing lavas in the Ethiopian Traps (Krans et al. 2018), we interpret the ankaramite flow as containing material derived from the lower crustal fractionation system. This observation supports a model wherein the lower crustal fractionation system, whose products were are only observed elsewhere as the first lava of the Lower Basalts, continues to play an important role in the magmatic system.

The low flux evident during the second pulse resulted in a magmatic system with more differentiated magmas that formed the most evolved plagioclase compositions analyzed within

the Middle Basalts sequence. The initial lavas of the third pulse remobilized these crystals, which contain the most albite rich plagioclase (An_{60-70}) as well as the greatest concentrations of Ti and Ba. In addition to evolved plagioclase crystals, the first 50m thick porphyritic flow (Figure 3.3) of the third pulse contains plagioclase, olivine and clinopyroxene glomerocrysts – indicating that the magmatic system at the end of the second pulse evolved sufficiently to permit multiple phase saturation (Charlier et al., 2015; Latypov et al., 2020). Despite an evolved crystal cargo contained within its initial flow, the third pulse is characterized by largely aphyric lavas with rare, fine grained plagioclase indicative of a high-magmatic flux regime. Aphyric lavas extend to 700m stratigraphic height before transitioning to additional plagioclase rich lavas marking the onset of Upper Basalt sequence.

3.5.1.3 Upper Basalts Sequence - Termination of Flood Basalt Activity

The Upper Basalts sequence of the Lokitaung Gorge records the terminal eruptions from the Eocene continental LIP in Turkana. Like previous pulses, the onset of eruption for the Upper Basalts sequence is marked by mono-mineralic plagioclase-glomerophyric lavas (Krans et al., 2018). The composition of plagioclase initially erupted in the Upper Basalts sequence are, unsurprisingly, comparable to the Middle Basalts sequence (Figure 3.3, 5). However, unlike previous resurgences of volcanism, the initial plagioclase-rich lavas are not followed by a period of aphyric eruptions. Instead, lavas of the Upper Basalts contain abundant clinopyroxene-plagioclase glomerocrysts (Figure 3.2d). While such glomerocrysts are observed elsewhere in the section (e.g., youngest flows of the Lower Basalts) the modal abundance of those glomerocrysts does not exceed 1%. However, in the Upper Basalts, clinopyroxene-plagioclase glomerocrysts can reach 15% modal abundance, indicating a fundamental shift in the magmatic system from a shallow-plagioclase forming system to a more evolved system where gabbroic crystallization is

taking place (Thy, 1983). Similarly, the composition of plagioclase cumulates gradually transitions throughout the Upper Basalts sequence toward more evolved compositions (Figure 3.3). Each lava contains plagioclase that is less anorthitic and contains greater concentrations of Ti (Figure 3.3). A commensurate decrease in Sr concentrations similarity indicates that the magmatic system has relatively less input of fresh magma from the lower crustal system. Without fresh magma to maintain the Sr concentrations in the upper crustal magmatic system, the residual magma becomes depleted in Sr as more plagioclase is fractionated.

The paucity of aphyric lavas during the eruption of the Upper Basalts and dominance of shallowly derived cumulate material suggests that contributions from the deeper magmatic system are less voluminous, causing magmas to stage for longer periods of time prior to eruption. During this interval, gabbroic fractionation occurs and forms the plagioclase-clinopyroxene cumulates that are observed in the lavas. Input of new magma ceases, and the final event is a 10m thick, welded crystal tuff. The termination of magma supply from the lower crust marks the end of continental LIP activity preserved within the Lokitaung Gorge.

3.5.2 Plagioclase as a probe of the upper crustal magmatic system at Lokitaung Gorge

3.5.2.1 Testing the hypothesis: plagioclase-rich lavas record diverse crystal populations

The interpretation that plagioclase-rich lavas contain disaggregated cumulate material derived from a previous pulse of magmatism requires an open magmatic system. For example, a pulse of magma may interact with liquids and solids remaining from the previous pulse. Given the ubiquity of plagioclase within section at Lokitaung Gorge, it is reasonable to explore the possibility that plagioclase crystals record this complexity in the form of distinct crystal populations. Identification of diverse crystal populations requires examining the distribution of

plagioclase compositions within individual lavas and comparing discrete populations to those in other lavas.

Albite (Ab)-anorthite (An) zoning in plagioclase crystals is typically well-developed, in part due to the low diffusivity of Ca and Na components (Grove et al., 1984; Liu and Yund, 1992). Such low diffusivity might also preserve evidence of antecrystic plagioclase within lava flows (e.g., Shcherbakov et al., 2011). Common petrographic observations of plagioclase crystals from the Lokitaung Gorge include normal and oscillatory zoning (often superimposed on the broader normal zoning patterns). The broad normal-zoning in plagioclase grains is supported by intra-crystal compositional analyses where crystal cores are 5-10% more An-rich than crystal mantles or rims, consistent with a simple magma fractionation model (Hibbard, 1995). The observation of oscillatory zoning in anorthite content may provide evidence of several injections of fresh magma into magma differentiation bodies (Krans et al., 2018; Óskarsson et al., 2017; Pearce, 1994; Pearce and Kolisnik, 1990), where injections of fresh magma temporarily reverse the effect of crystal fractionation, allowing more An-rich plagioclase to overgrow less An-rich zones. The outcome of these observations is that there are a range of potential An-Ab compositions imposed upon a crystal during its formation, and that these compositional ranges often overlap between different lavas. Thus, while crystal populations within individual lavas provide clear stratigraphic variability in An-Ab, the identification of a single antecryst using such information is more challenging (Cooper and Reid, 2008; Streck, 2008).

Nielson et al. (2020) demonstrated the utility of both plagioclase major and trace element composition in identifying populations of crystals derived from distinct magmas. While a direct comparison of major and trace element concentration differences between crystals might provide some insights as to discrete populations, partitioning of trace elements into plagioclase is

variable and based upon anorthite content, pressure, and temperature (Dohmen and Blundy, 2014, 2014; Nielsen et al., 2017; Singer et al., 1995). An alternative approach was followed by Nielson et al. (2020), who utilized a large dataset of plagioclase compositions from MORB lavas and estimated the diverse and distinct equilibrium liquid compositions that formed the crystals. Here we apply a similar methodology to identify plagioclase populations that may be derived from previous magma pulses in the Lokitaung Gorge.

The methodology from Nielson (2020) and Nielson (2017) requires that temperature and pressure conditions be estimated in order to calculate the trace element compositions of the equilibrium liquid. To ascertain the degree of equilibrium between the groundmass and plagioclase phenocrysts and, therefore, the validity of derivative temperature and pressure estimates, we applied equilibrium calculations from Putrika (2008). The validity of temperature estimates (Putirka, 2008: eqn. 26;) can be determined from the temperature dependent An-Ab exchange K_D as calculated by equation 28b of Purtika (2008). The expected An-Ab K_D at equilibrium for temperatures above 1050°C is 0.28 ± 0.11. We find that the An-Ab exchange K_D for groundmass liquid-plagioclase pairs for our dataset are 0.23 ± 0.10. Using the predicted temperatures from equation 26 (Putirka, 2008) at 1158°C ± 11, we can conclude that plagioclase-liquid pairs are at or near equilibrium with respect to the temperature dependent exchange of An-Ab. Therefore, temperature estimates used for plagioclase-liquid equilibrium compositions are valid.

Estimates of the pressure conditions for plagioclase crystallization as determined by MELTS are consistent with crystallization in the upper crust. Groundmass compositions were used as the input magma composition for MELTS thermodynamic models (Gualda and Ghiorso, 2015). We assume 0.1% water, consistent with relatively dry magmas in continental LIPs. The

pressure of plagioclase crystallization was determined by modulating the pressure of the system, equilibrating, then determining the liquidous phases. We utilize the maximum pressure at which plagioclase is the primary liquidous phase. We find the pressures where plagioclase is the primary stable phase to be between 0.05 and 0.15 Gpa, or ~1.5-5 km depth. These values are consistent with formation depths of plagioclase-rich intrusions of older continental LIPs such as the exhumed Keweenaw LIP in North America (Miller Jr and Ripley, 1996; Miller Jr and Weiblen, 1990), and those beneath the Siberian Traps (Arndt et al., 2003).

Utilizing the temperature and pressure constraints from thermodynamic calculations as inputs, equilibrium liquids were calculated using P-T-An dependent partition coefficients (Nielsen et al., 2017; Nielsen, pers comm. 2020). The calculated equilibrium liquids for the bulk dataset (Figure 3.5) fall within a reasonable range of concentrations for flood basalts in East Africa (e.g., George and Rogers, 2002; Kieffer et al., 2004). For most elements of interest, the equilibrium liquid compositions form a single data cluster and exhibit a flat to slightly negative correlation with anorthite content. However, Sr concentrations exhibit a bimodal distribution, forming two distinct equilibrium liquids: a high and low Sr liquid (Figure 3.5). The identification of these two distinct equilibrium liquids supports the conclusion that there also exists two compositional populations of plagioclase.

The identification of two populations of plagioclase crystals permits an exploration as to whether evidence of older crystal generations are preserved within individual lavas, as would be anticipated based upon the conceptual model presented above. We examined the stratigraphic variation of equilibrium liquid compositions (Figure 3.4) and found that individual lavas exhibit plagioclase populations that yield homogenous equilibrium liquid compositions; i.e., individual lavas appear to contain only one population of plagioclase crystals. This result is unexpected

given the open-system behavior as hypothesized, and could be interpreted as either: (1) the plagioclase cumulates being unavailable/destroyed after each pulse of magmatism, or (2) the erasure of the signature through diffusive equilibration with later magmas (Nielsen et al., 2020).

The upper crustal magmatic system could yield a homogenous plagioclase population in any given lava if the entirety of the pre-existing cumulate pile were removed during each high-flux period, prior to the formation of a new homogenous cumulate pile. Given evidence from exhumed upper crustal continental LIP magmatic systems (i.e., gabbros and anorthosites), distinct layers are preserved, in conflict with a model of cumulate pile destruction from pulse to pulse (Charlier et al., 2015). Within the Lokitaung Gorge, evidence for the persistence of the cumulate pile comes from the Middle Basalts where the lack of a high flux episode resulted in the preservation of diverse crystal populations that were not sampled in the subsequent pulses of magmatism. Alternatively, the sequestering of the cumulate material could provide an explanation as to the lack of diverse crystal populations within individual lavas at Lokitaung. In this conceptual model, the glomerophyric plagioclase in the erupted lavas is interpreted solely as being derived from cumulate piles generated during the previous hiatus. Prior cumulate material is still present within the magmatic system but may be armored beneath the most recent phase of crystallization and so is unavailable for remobilization. While this mechanism could explain the crystal populations observed in the Lokitaung Gorge, the complete absence of plagioclase cumulate material from prior crystallization events, despite the continual recharge of magmas into the system, would be somewhat serendipitous. The difficulties presented by these conceptual models in explaining the observations at Lokitaung necessitates a closer examination of the potential to alter the primary chemical signature of plagioclase crystals through diffusive equilibration.

3.5.3 Elemental diffusion and homogenization of plagioclase compositions

Insights gained from the examination of the stratigraphic distribution of crystal populations in the Lokitaung Gorge argue for potential overprinting of plagioclase crystals by diffusive equilibration. Assessing the potential for, and degree of, diffusive equilibration requires the examination of geochemical variation within individual crystals. We have previously shown that the Ab-An variation within individual plagioclase crystals record a differentiating magmatic system (see Streck, 2008; Vance, 1962). Assuming the plagioclase crystals faithfully record the composition of the liquid that formed them during this differentiation process, it is reasonable to expect trace element concentrations in the equilibrium liquids to reflect a parallel trend of a gradually more evolved system (Singer et al., 2011, 1995; Tepley et al., 2000). However, when observing intra-crystal variation of equilibrium liquid compositions, we see little variation in trace element concentrations (Figure 3.6). For example, for Sr and Ti, it would be expected for equilibrium liquids to have less Sr in the outer (later forming) parts of the crystals, due to removal of Sr from the residual liquid during fractionation of plagioclase (Nielsen et al., 2017). Conversely, Ti should increase in the residual liquid and, therefore, be more abundant in the outer portions of the crystals. The observation of limited variation in trace elements, despite evidence from An zoning of an evolving system (Figure 3.6), indicates a decoupling of the major and trace elements in the magmatic system. This decoupling of An-zoning and trace elements in plagioclase requires that compositions are controlled by more than just an evolving liquid, and may constitute evidence of diffusive equilibration.

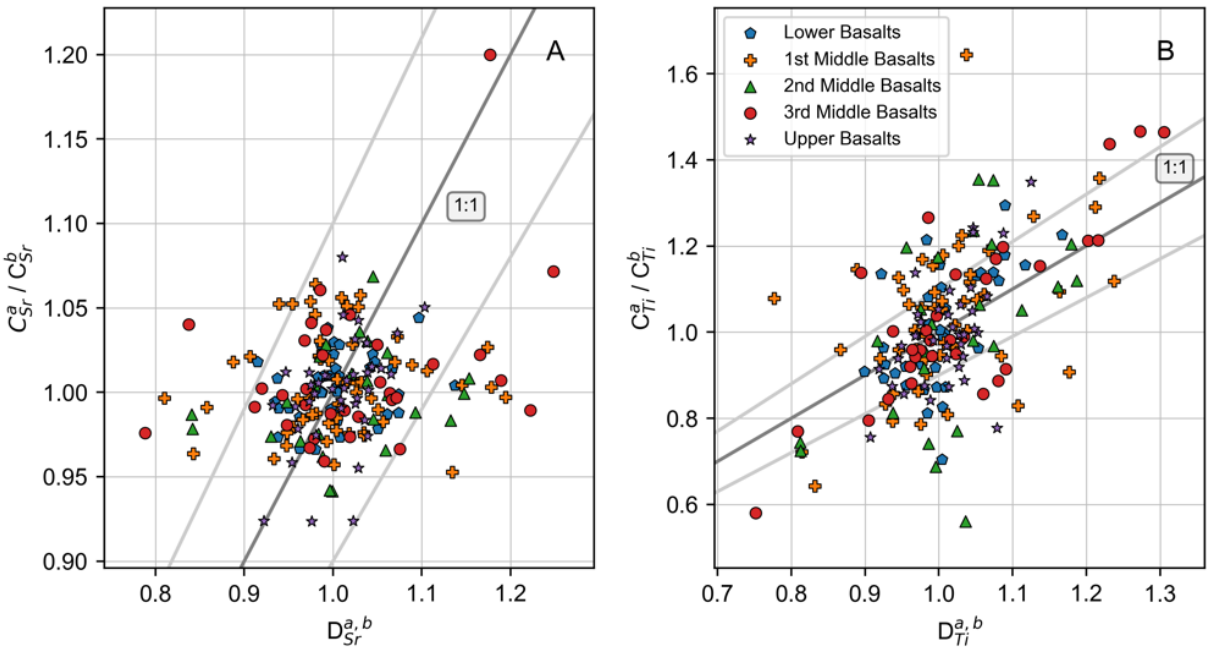

Figure 3.6 - Assessment of the internal equilibrium state of Sr (A) and Ti (B) for a large population of crystals where multiple ablations were sampled on the same crystal. The ratio of the liquid partition coefficients (X-axis) is compared to the ratio of the observed concentrations (Y-axis). Where the two ratios are equal, as shown by the 1:1 line, the pair of analyses are considered to be at equilibrium. A ±10% deviation from the 1:1 line is considered be the threshold for internal equilibrium between a pair of analyses.

Chemical diffusion of Sr in plagioclase is well studied and provides a means to examine the potential for crystals to have reached a state of internal chemical equilibrium (Cherniak and Watson, 2020; Costa and Dungan, 2005; Giletti and Casserly, 1994; Zellmer et al., 2003). Here, we test for internal chemical equilibrium by examining the bulk-traverse equilibrium (Zellmer et al., 2003, 1999) of crystals from the Lokitaung Gorge (Figure 3.6). This approach compares the intra-crystal partition coefficient ($D^{a,b}$; Zellmer et al., 1999: eqn 3) for an element between two

zones (a, b) of a crystal (each with different An contents) to the ratio of the measured concentration (C^a/C^b) of the same element in each zone (Zellmer et al., 2003, 1999). Where the ratio of the concentrations is equal to the partition coefficient, the two zones are in internal equilibrium (Zellmer et al., 2003: eqn. 4). Given the ±5% measurement error in this dataset, we consider a deviance between C^a/C^b and $D^{a,b}$ of ±10% from unity to be in equilibrium. We find that detailed LA-ICPMS transects of plagioclase in the Lokitaung Gorge basalts exhibit less than 10% variance between the calculated $D^{a,b}$ and the observed compositional ratios for neighboring analyses (Figure 3.6). This observation suggests crystals are in internal equilibrium with respect to Sr, although these crystals represent a limited subset of the total number of crystals analyzed. To more fully explore the internal equilibrium state of Sr in plagioclase throughout the Lokitaung Gorge basalts, we examine a larger population of crystals (190 pairs of analyses) where core and rim compositions were analyzed but were not collected as detailed transects. We find that the ratio of observed Sr compositions and the internal partition coefficients for most analytical pairs are within ±10% of the unity (Figure 3.7). We can, therefore, conclude that the majority of plagioclase crystals from the Lokitaung Gorge are in internal equilibrium with respect to Sr, thereby erasing primary magmatic signatures.

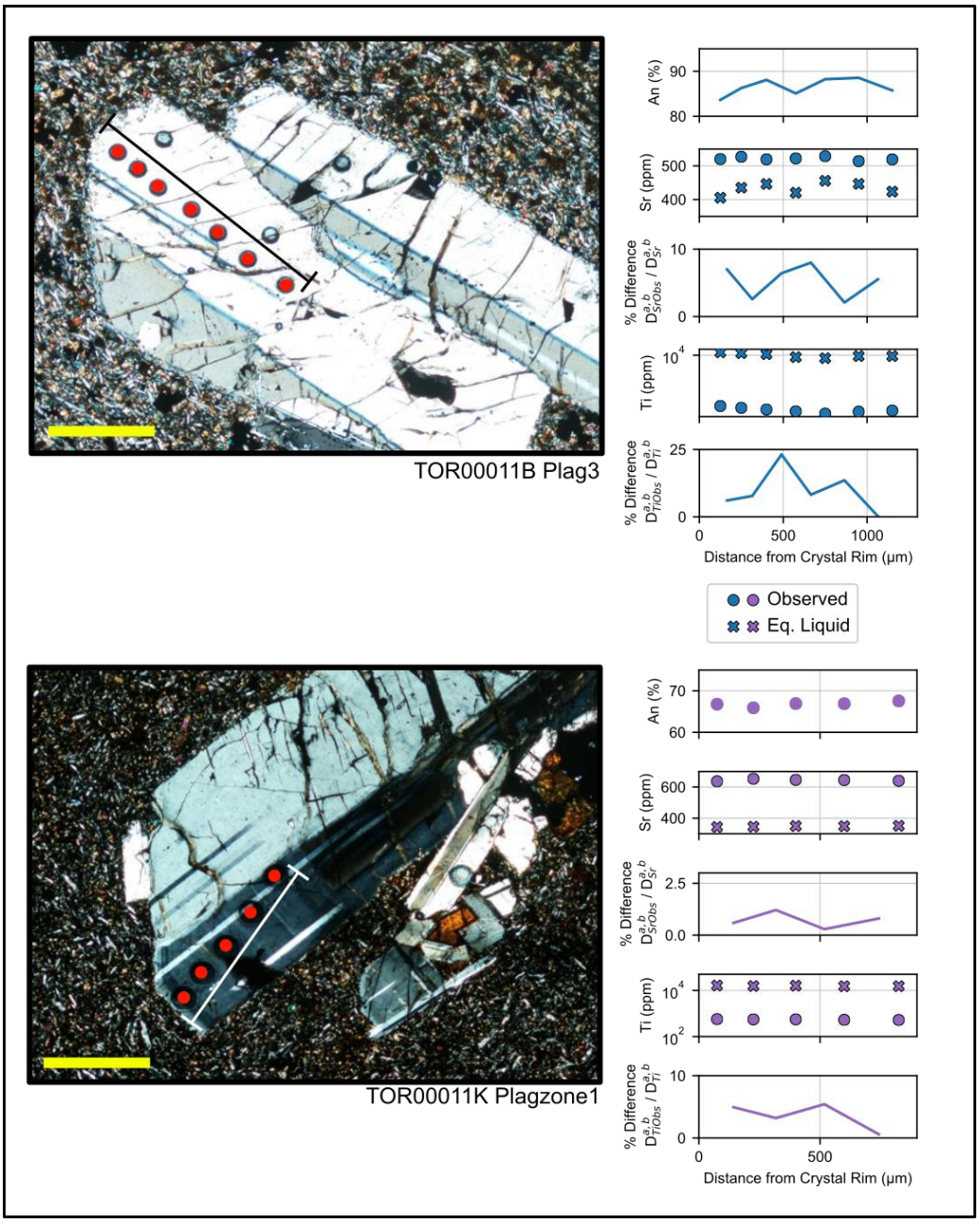

Figure 3.7 - Assessing the internal equilibrium for Sr and Ti in select plagioclase crystals. Example are selected from older (TOR00011B) and younger flows (TOR00011K). Crystal compositions were collected as a series of ablation spots from the crystal rim to the interior. The An, Sr, and Ti content of each spot is presented as a function of the distance from the crystal rim. Neighboring ablation spots were compared in terms of the ratio of liquid-crystal partition

Figure 3.6 (cont'd)

coefficient (function of the An content) and the observed ratio of elemental concentrations. These two ratios, partition coefficients and the observed concentrations between two analyses, are compared as an absolute value of the percent difference. Values <10% are considered to be at equilibrium.

Sr diffusion in plagioclase occurs over relatively short timescales (Cherniak, 2010; Zellmer et al., 1999). However, other elements that diffuse more slowly could still preserve evidence of disequilibrium (Cherniak and Watson, 2020). Critically, Ti requires 10^2-10^4 years longer than Sr for primary zoning to be lost, thus providing valuable constraints on the duration crystal storage in the continental LIP magma plumbing system (Cherniak and Watson, 2020). We explore the internal equilibrium state of Ti in plagioclase by examining a large subset of crystals (190 pairs of analyses) where core and rim compositions were analyzed. We find that the ratio of observed Ti compositions and the internal partition coefficients for most analytical pairs are within ±10% of the ideal 1:1 values (Figure 3.7). When Ti is compared to Sr, there are more crystal pairs that are out of the ±10% window for equilibrium, indicating that there may be some degree of disequilibrium in particular crystals. Crystals in disequilibrium are distributed throughout the section and are not correlated with specific lavas, nor are these crystals compositionally distinctive enough to represent a unique crystal population. These observations suggests that most plagioclase crystals in the Lokitaung Gorge are at or near internal equilibrium with respect to Ti; however, the observations noted above require that some crystals have not fully equilibrated, implying a shorter residence time suspended within the magma.

We have shown that both relatively fast diffusing Sr and relatively slow diffusing Ti have undergone diffusive equilibration within most plagioclase crystals at Lokitaung, thereby providing potential constraints on the duration these crystals were held at magmatic temperatures. The erasure of primary trace element zonation is strongly dependent on the element in question, the An content of the crystal, and the size of the crystal (Cherniak and Watson, 2020; Costa and Dungan, 2005; Dohmen and Blundy, 2014; Zellmer et al., 1999). Plagioclase in the Lokitaung Gorge basalts range from An_{60}-An_{80}, typically reach maximum crystals sizes of 1-2mm, and are shown to have formed at temperatures of 1140-1170°C. For Sr, the erasure of primary zonation under these conditions occurs between 10^3 years for small or lower An crystals, to 10^4 years for larger, more An rich crystals (Cherniak and Watson, 2020; Zellmer et al., 1999). Diffusion of Ti requires 10^4 to 10^5 years, respectively, for primary trace element zoning to be lost (Cherniak and Watson, 2020). Given that the majority of the crystal-pairs are at or near internal equilibrium in terms of Sr and Ti, we can conclude that plagioclase crystals in the Lokitaung section have spent 10^4 to 10^5 years at magmatic temperatures. The implication of these conclusions is that geochemical evidence for antecrystic material in flood basalt lavas can be erased due to the long timescales of crystals in hot storage. Storage of plagioclase at magmatic temperatures $>10^4$ years would homogenize the trace element concentrations but retain the primary An-zoning, which diffuses on the order of millions of years (Grove et al., 1984; Liu and Yund, 1992; Robb and Mungall, 2020).

Recent geochronological examination of Deccan Traps may support the prolonged interval (10^4 to 10^5 years) of hot storage of crystals that is required to homogenize the crystal compositions. Zircon U-Pb geochronology of the stratigraphically well constrained Western Ghats in India reveal eruptive pulses defined by episodes of high and low magmatic flux

(Schoene et al., 2019). Critically, the quiescent periods may last for up to several hundred thousand years (Schoene et al., 2019). These conclusions are parallel to our interpretations of high and low periods of magmatic flux and the requirement that crystals be stored at high temperatures for the same 10^5 year intervals. It is therefore evident that high-precision geochronologic constraints from the Deccan Traps, and the geochemical data presented in this contribution, result in a consistent narrative of storage and cyclic eruption over 10^5 year timescales.

3.5.4 Numerical modeling of Equilibrium Crystallization in Open Systems

We have demonstrated that plagioclase crystals from the Lokitaung Gorge basalts are derived from pulsed magmatism, and that the primary compositions of those crystals have been modified through intracrystalline diffusive equilibration. The open-system behavior adds complexity when estimating the conditions and processes active within the magmatic system. Existing open-system geochemical models (Bohrson et al., 2014; Kimura and Kawabata, 2015; Lee et al., 2014) calculate a liquid line of descent that constrains the trace element variation in open magmatic systems. These models operate under the assumption that during magma differentiation, all crystals are instantaneously segregated from the liquid and do not interact with that liquid after formation. We have demonstrated that the crystals at Lokitaung exhibit limited intrasample compositional variability with respect to trace elements, which may be explained by continual re-equilibration of crystal phases with an evolving liquid component. This interpretation precludes pure fractional crystallization, requiring calculations of liquid lines of descent to include interactions between already formed crystals and the liquid which may be accommodated by equilibrium crystallization. Recent work by Nishimura (2020, 2019, 2009) provide a means to

examine the vectors of differentiation where crystals react with the liquid component of the magma chamber under a range of REAFC conditions.

We have proposed a mass-balance conceptual magmatic model for the Lokitaung Gorge basalts whereby the variation in the plagioclase compositions is controlled by changes in the REAFC conditions within the shallow magmatic system. The core of this conceptual magmatic model is a persistent reservoir composed of magma and suspended crystals. The mass of this reservoir may be increased by the addition of recharging magma or the assimilation of wall rock. Conversely, the mass of the reservoir may be reduced by the sequestration of crystals and the evacuation of magma by eruption. In order to test these ideas, we varied the proportions of inputs and outputs, thereby modifying the composition of the reservoir. Upon completion of each model, the calculated equilibrium composition of the plagioclase suspended within the reservoir was compared with our measured plagioclase data from the Lokitaung Gorge. Model construction followed the methods of Nishimura (2020), where we solve the mass balance partial differential equation (Nishimura 2020: equation 1) utilizing their equations 4, 6, 7, and 8. We use these equations to calculate the equilibrium liquid and crystal compositions in a reservoir after modification by the input and output processes described above (see appendix 3).

The proposed model of pulsed magmatic activity through the Lokitaung Gorge basalts is unlikely to result from a single set of input and output parameters, but instead likely requires a series of interlinked models whereby such parameters can be modified as needed. We implement this model structure by constructing a series of interlinked analytical solutions. For example, an initial set of calculations (Model A) is performed under constant model parameters, yielding a range of output equilibrium liquid and crystal compositions. The vector of the crystal compositions produced by this model is matched to the observed crystal compositions. When the

vector of the observed plagioclase compositions changes, a new set of model conditions is required. Then, the output of Model A at this change point transitions to a new model – Model B – with the model parameters adjusted to produce calculated crystal outputs that match the new observed plagioclase vector. It is important to note that the calculated mass of sequestered crystals is also carried on to the next set of calculations via a running sum of accumulated material. This interlinked approach is consistent with previous work (Nishimura, 2019, 2009; Shaw, 2006) and provides for flexible model construction.

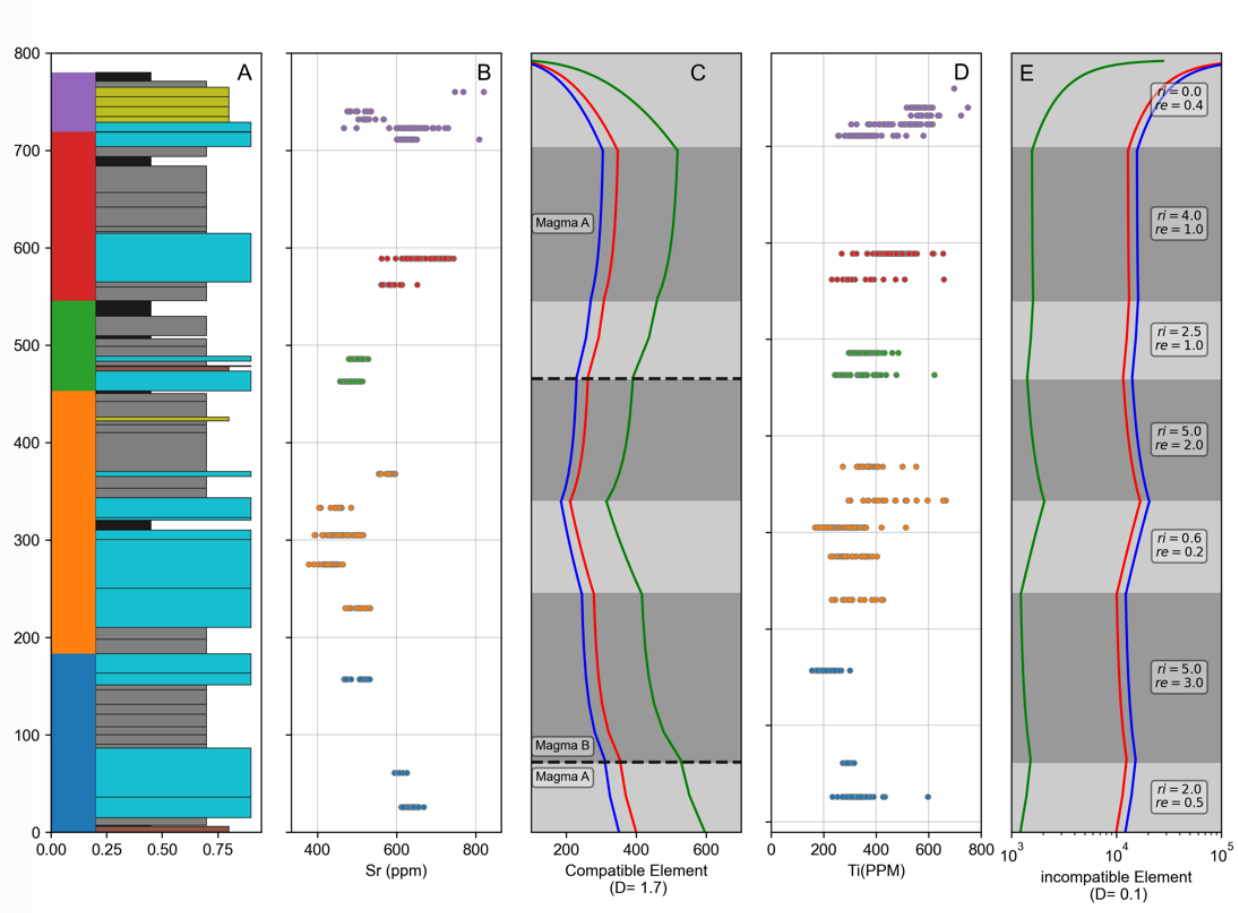

Figure 3.8 - Model calculations of the chemical evolution of the magmatic system at Lokitaung. Modeled liquid, mineral, and bulk magma compositions are calculated from equations in Nishimura (2020, 2019). Model calculations were performed as a series of seven interlinked models, denoted by shaded blocks in (C) and (E). The proportions of magma recharge and

Figure 3.8 (cont'd)

evacuation for each individual model is in part (E). (A) Petro-stratigraphic column of Lokitaung derived from petrographic observations. (B) Observed Sr concentrations of plagioclase crystals. (C) calculated Sr concentrations for the bulk magma, crystals, and liquid plotted against the accumulated mass of fractionated crystals (Nishimura, 2019). The magma composition utilized by each model is delineated by dashed lines and labels. (D) Observed concentration of Ti in plagioclase crystals. (E) Modeled calculated concentrations for Ti for the bulk magma, crystals, and liquid plotted against the accumulated mass of fractionated crystals (Nishimura, 2019).

To replicate the observed data in the Lokitaung Gorge basalts, we have created seven interlinked models that modulate the rates of magma recharge and magma evacuation in order to approximate the vectors of crystal compositions; the rate of assimilation and crystallization are held constant (Figure 3.8). We utilize two recharging magma compositions: (1) the first magma composition was calculated as being that liquid in equilibrium with the first crystals in the reservoir. This magma composition was used for models 1 and 5-7. (2) the second magma composition was iteratively adjusted in order to match the trend of the observed data, and contains ~25% less Sr and ~20% less Ti than the first model. This magma composition was used for models 2-4. We use the average partition coefficient for plagioclase crystals calculated in section 5.2 (D_{Sr} = 1.7 and D_{Ti} = 0.1), which are held constant throughout the modelling. We hold the proportion of suspended crystals constant, as sensitivity tests produced results whereby changes in the proportion of suspended crystals resulted in identical compositional vectors, but with differing mass accumulation in the system to achieve those vectors.

Models 1 and 2 are used to replicate the plagioclase compositional trends in the Lower Basalts (Figure 3.8). As an initial assumption, we presume that a common composition of

primitive magma is entering the Lower Basalts magmatic system; we therefore explore the compositional trends in the Lower Basalts by adjusting variables in the models. Plagioclase in the Lower Basalts initially exhibits incompatible trace element behavior consistent with a system where crystallization is evolving the magma toward greater incompatible trace element abundances. This observation is implemented in model 1 by varying the proportion of recharge to crystallization to permit an increase in the incompatible trace element concentrations in the liquid. Model 2 examines trends at higher levels in the Lower Basalts stratigraphy. Here, a strong deviation toward more primitive An-rich plagioclase is observed. Model 2 attempts to replicate this behavior by both increasing the recharge of primitive magma and the rate of magma evacuation (Figure 3.8). The combined effects of increased recharge and evacuation drives the incompatible trace elements to lower concentrations (i.e., toward the primitive parental magma composition; Figure 3.8c, e). However, adjustments in these model parameters alone could not replicate the magnitude of the observed trace element dilution in the younger flows of the Lower Basalts, suggesting potentially greater heterogeneity in the composition of the recharging magma. We therefore make the recharging magma composition more primitive for the younger flows of the Lower Basalts and retain this composition for the first cycle of the Middle Basalts.

The first cycle of the Middle Basalts is represented by models 3 and 4 in figure 8. The plagioclase-rich lavas at the onset of the Middle Basalts indicate a preceding hiatus in volcanism that may be commensurate with a reduction in magmatic flux into the shallow system. Model 3 reflects the reduction in magmatic flux early in first cycle of the Middle Basalts (plagioclase-rich lavas) by reducing the amount of recharge (and evacuation), thereby shifting the balance of the system toward crystallization. Model 3 predicts the observed increase in incompatible trace elements (Ti) and decrease in compatible elements (Sr). The remainder of the first cycle of the

Middle Basalts is comprised of aphyric lavas and thus offer no direct constraints on the magmatic system except for the requirement of higher flux (Krans et al., 2018). However, the vector of plagioclase compositions from the last porphyritic flow analyzed in the first and second cycles of the Middle Basalts requires a system where the incompatible trace elements are being diluted, and Sr is being enriched (Figure 3.3). Model 4 (Figure 3.8) implements this observed reversal of compatible and incompatible elements by increasing the recharge of primitive magma throughout this aphyric phase.

Model 5 addresses the observed plagioclase variability within the second cycle of the Middle Basalts. This cycle is coincident with a return more primitive An-rich plagioclase compositions (Figure 3.3), which we interpret as resulting from the high-flux interval during the prior aphyric phase. Plagioclase compositions become more evolved through the second cycle in terms of both major and incompatible trace elements. However, compatible trace elements (Sr) increase with younger flows (Figure 3.3, 8). No model parameters were found to accommodate the increase in concentration for both compatible and incompatible elements requiring a change in the recharging magma composition of Model 5 towards more evolved values (Figure 3.8). The deep parts of the magmatic plumbing system, from which these recharging magmas are derived, are dominated by the crystallization of clinopyroxene and olivine (Larsen et al., 2018; Morse, 1980; Rooney et al., 2017), neither of which accommodate significant Sr in their structure. Thus, these more evolved Sr-enriched liquids rise and enter the plagioclase forming portion of the system resulting in plagioclase that is more enriched in Sr.

Model 6 examines the variability within the third cycle of the Middle Basalts. Magma recharge increases with the onset of the third cycle, a condition supported by the predominance of aphyric lavas with only limited occurrences of plagioclase-phyric lavas. Neither Sr or Ti

change significantly from the onset of the third cycle to the beginning of the Upper Basalts. This observation is consistent with a system that has reached a steady state with respect to both compatible (Sr) and incompatible (Ti) elements. While it is possible to achieve a steady state during equilibrium crystallization for compatible elements at low recharge rates, the effect of partial crystal segregation causes the incompatible elements to increase exponentially (Nishimura, 2020: Figure 2 and 3). Steady state behavior in both a compatible and incompatible element requires a high proportion of recharge (Nishimura, 2020: Figure 4 and 5). We therefore explain the limited variation through the third cycle of the Middle Basalts along with the transition to the Upper Basalts to be the result of voluminous recharge into the shallow magmatic system.

Model 7 examines the final stages of the Lokitaung system preserved within the Upper Basalts. We interpret the Upper Basalts as the result of the final collapse of the magmatic system due the cessation of magma recharge from the deeper system. We implement the cessation of recharge in model 7 by eliminating the recharge fraction but maintaining an eruptive component. Accordingly, the modelled system rapidly shifts toward evolved compositions. The modelled compositions are consistent with the more evolved plagioclase compositions that are observed in these youngest lavas. However, Ba and La do not exhibit an increase in concentrations comparable to Ti, possibly due to additional (not modelled) crystallizing phases (alkali feldspar and/or apatite).

We have demonstrated that a magmatic system undergoing REAFC where a proportion of the crystals are able to interact with the magma can replicate the observed plagioclase compositions in the Lokitaung Gorge basalts. Based on petrography, those crystals that may interact with the liquid portion of the magmatic system, include cumulate materials. These

cumulates would be the source material for antecrysts that, when entrained in new magma pulses, equilibrate both internally and with the new hybrid magma. The apparent lack of antecrysts in the Lokitaung lavas can be explained by a process in which antecrysts react with the new hybrid magma for sufficiently long periods of time as to establish new internal equilibrium within the crystals. Plagioclase that may be antecrystic has reacted with the evolving liquid component of the system, thereby homogenizing crystal compositions which are then erupted in the compositionally homogenous plagioclase-rich lavas.

3.6 Summary and Conclusions

The basalts preserved at Lokitaung Gorge provide important insights into the temporal evolution of the magmatic differentiation system of a continental LIP. We define a series of magmatic pulses delineated by the cyclic occurrence of plagioclase-rich and aphyric lavas. Such observations indicate system-wide changes in magmatic flux, such that the transition from groups of aphyric lavas to plagioclase-rich lavas marks a disconformity that is the result of a volcanic hiatus. The hiatus is interpreted to represent a reduction in magmatic flux such that removal by eruption of material from the differentiation system is reduced, thus allowing crystals to accumulate in the chamber. A subsequent increase in magmatic flux remobilizes those cumulates and erupts them in the form of plagioclase-rich lavas.

Our petrographic observations are consistent with a polybaric fractionation system, wherein the deep system is clinopyroxene-olivine dominant, while the shallow system is plagioclase dominant. When interpreted within the context of the several cycles discussed above, it is apparent that the shallow fractionation system modulates the eruptive cycles and thus constitutes a critical component of continental LIPs. Using plagioclase trace element signatures,

we show that individual lavas comprise homogenous crystal populations. These populations vary throughout the stratigraphy and are consistent with a model of continual re-equilibration with a gradually evolving liquid component. This stratigraphic variability in plagioclase composition demonstrates that each magmatic cycle commences with a pulse of primitive magma originating deep from within the differentiation system, which is then followed by a period of lower flux prior to the commencement of another cycle.

The observation that plagioclase crystals exhibit compositional equilibrium in multiple trace elements indicates that crystals within the erupted magmas spent significant periods of time ($>10^5$ years) at magmatic temperatures. These timescales are consistent with known eruptive cycles reported from continental LIPs worldwide, which are on the order of $10^4 – 10^5$ years. This evidence of compositional equilibrium has implications for models describing the magmatic evolution of continental LIPs. Using a series of seven interlinked models, we have shown that the re-equilibrating mineral phases within a magma chamber not only modify the final crystal compositions, but may also have a profound impact on the final erupted liquid.

Our results clearly demonstrate the interaction between crystals and liquid during the evolution of a well-constrained stratigraphic section of continental flood basalt. Given this interaction, and the large mass of the reservoir constituting the crystal products of such systems (e.g., Duluth Complex), more consideration of equilibrium crystallization processes will improve future models describing the evolution of flood basalt magmatism.

4. CHEMOSTRATIGRAPHY OF THE EOCENE FLOOD BASALT PROVINCE: EPISODIC ERUPTIONS AND THE CHEMICAL EVOLUTION OF THE MAGMATIC PLUMBING

4.1 Introduction

Continental flood basalt provinces are fundamentally composed of two components: (1) a extrusive component that is composed of a stack of mafic lavas and, (2) an intrusive component comprised of layered intrusions and magma conduits (Charlier et al., 2015; Cox, 1980; Ernst, 2014). This division is essentially reflective of the differentiation process flood basalt magmas undergo within the continental lithosphere prior to eruption. Central to this differentiation is the separation of the solid and liquid phases as these magmas cool and crystallize. As liquids extracted at various stages in the differentiation process, stratiform mafic lavas in continental flood basalt provinces provide a temporal window into differentiation systems.

Numerical simulations of magma differentiation typically operate through the separation of crystals from an evolving liquid (fractional crystallization) or the growth of crystals in-situ without the separation of liquid and solid phases (equilibrium crystallization). Further complexity in the differentiation process is introduced by open-system behavior wherein the introduction of new magmas into a persistent magma chamber (recharge), the extraction of differentiated magmas and crystals (evacuation), and assimilation of wall rock (assimilation) modify the bulk composition of the system. Box models detailing recharge-evacuation-assimilation-fractional crystallization (REAFC) are an important advance in probes of continental flood basalt evolution (Bohrson et al., 2014; Davis et al., 2021; Lee et al., 2014; Steiner et al., 2021; Yu et al., 2015).

Observations from mid-ocean ridge systems where persistent magma chambers exist reveal important interactions between the solid crystal phases and the evolving liquids (e.g.,

Lissenberg and MacLeod, 2016; Nielsen et al., 2020) that are not simulated by current REAFC models. The crystals in such systems have been shown to have undergone diffusive equilibration, thereby modifying both the crystal and the liquid composition. In particular, basalts that have undergone this process may have resolvably different incompatible trace element concentrations in comparisons to those have undergone simple fractional crystallization (Lissenberg and MacLeod, 2016). With increasing interest in connecting the solid and liquid phases in complex magmatic systems, new numerical modelling strategies have emerged. Diffusive equilibration has been modelled between discrete zones within crystals to provide time constraints of diffusive processes (Costa et al., 2020; Zellmer et al., 2003, 1999). Equally, recent work in constraining the Sr isotope variability in plagioclase used mass-balance models to approximate the composition of plagioclase crystals in equilibrium with an evolving liquid during open-system magma evolution (Nishimura, 2020). While these studies provide important constraints on the composition of crystals within these systems, they also provide information on the composition of the coexisting liquid. Despite the utility of such models in probing magma differentiation processes, they have yet to be used to simulate the evolution of a continental flood basalt system in order to constrain the conditions of magma differentiation in such systems.

Here we utilize the mass-balance equations of Nishimura (2020) to explore the conditions of magma differentiation during the eruption of an exceptionally well-constrained flood basalt sequence. We present a geochemical dataset of 54 sequential flood basalt lavas from the Lokitaung Gorge (Turkana, northern Kenya), that are part of the Eocene Initial Phase of the East African large igneous province (Rooney, 2017; Steiner et al., 2021). Prior work on this suite of lavas has created a petro-stratigraphic framework in which we interpret our data (Chapter 3). We find that the geochemical variability within the lava flows parallels the existing petro-

stratigraphic framework: stratigraphic trends in lava compositions have inflection points at the boundaries between petro-stratigraphic units. When combined with observations on incompatible element profiles insensitive to differentiation that require common source magmas, we interpret the variability in lava compositions as reflecting open-system magma differentiation processes. We use the open-system magma differentiation equations of Nishimura (2020) to construct numerical solutions to resolving the petro- and chemo-stratigraphic variability of the lava compositions at Lokitaung. We find that the three volcano-stratigraphic units differ in terms of magma recharge: the Lower Basalts represent the initiation of the system (first 200m of stratigraphy) and are the period of highest magma recharge, occurring over the first; the Middle Basalts, though the main phase of flood basalt activity (500m thickness), are a period of lower magma recharge; the Upper Basalts represent the termination of flood basalt activity (uppermost 64m), and are the period of the least magma recharge. This cycle of activity parallels similar petrographic observations from the younger Oligocene Traps Phase of the NW Ethiopian Plateau therefore illustrating a similar progression in the development of a continental flood basalt magma plumbing system at both locales.

4.2 Background

4.2.1 Chemical Diffusion

Chemical diffusion is an important property of geologic materials with recent advances in analytical techniques and constraints on diffusion parameters providing new opportunities to probe magmatic processes (e.g., Bradshaw and Kent, 2017; Costa et al., 2020; Danyushevsky, 2002; Lynn et al., 2017; Nielsen et al., 2017). Recognition of diffusive re-equilibration of melt inclusions and the development of methods to back-calculate original compositions of those

inclusions has allowed for the examination of the pressure, temperature, and magma compositions during crystallization (e.g., Danyushevsky et al., 2000; Kent, 2008) (Metrich and Wallace, 2008; Rasmussen et al., 2020). Primary crystal zonation may be gradually overwritten by diffusive re-equilibration with new magma compositions that may result from assimilation, magma mixing, or simply fractionation of the early magma (Dohmen and Chakraborty, 2007; Nakamura, 1995; Tepper and Kuehner, 1999). Where primary zonation is not fully overwritten, the degree to which diffusive equilibration has occurred provides information on the timescales of crystal residence (Christensen and DePaolo, 1993; Hawkesworth et al., 2000; Zellmer et al., 1999), rates of magma ascent (Demouchy et al., 2006; Li et al., 2020), and cooling histories of magmatic systems (Costa et al., 2020).

These new insights into magmatic processes provide constraints on trans-crustal magma plumbing systems that may extend from the surface to the mantle and store magmas in many chambers and conduits (Cashman et al., 2017; Ernst et al., 2019). Such chambers and conduits often form layered mafic intrusions, where crystals may be held at high-temperature due to latent heat of crystallization and thermal mass of the solidifying crystal mushes (Morse, 2011) (hot-storage). The combination of high-temperature and prolonged storage provides an opportunity for crystals to undergo diffusive equilibration, often termed a trapped-liquid-shift in cumulus minerals (Barnes, 1986). The effect of a trapped liquid shift is commonly documented in minerals where diffusion happens rather quickly for the major elements in the mineral, such Fe and Mg as olivine (Nakamura, 1995) rather than the slower diffusion of Ca, Al, and Na through plagioclase (Morse, 1984). However, some recent studies of plagioclase compositions in the Bushveld complex have observed diffusive equilibration in the Ca, Al, and Na and have attributed equilibration to prolonged hot-storage of crush mushes (Robb and Mungall, 2020).

Therefore, diffusive chemical equilibration is in operation large open magmatic systems, like flood basalt provinces, and therefore represents a potential chemical reservoir that may impact erupted lava compositions.

Plagioclase is a ubiquitous phenocryst phase in flood basalt lavas (Annells, 1973; Berg and Klewin, 1988; Cox, 1980; Duraiswami et al., 2001; Lightfoot et al., 1990) and has been utilized as a means to probe the magma plumbing system in continental LIPs (e.g., Borges et al., 2014; Krans et al., 2018; Singer et al., 2011; Streck, 2008; Tepley et al., 2000; Vance, 1962). Textural examination of plagioclase in flood basalt lavas has shown how crystals accumulate in chambers and conduits before being erupted (Beccaluva et al., 2009; Óskarsson et al., 2017), and how pulses of magmatism are delineated by plagioclase-rich flows (Hansen and Grönvold, 2000; Higgins and Chandrasekharam, 2007; Krans et al., 2018). Primary crystal zonation of plagioclase has been used to elucidate changing conditions within the magma plumbing system (Singer et al., 2011, 1995; Tepley et al., 2000). However, given the potentially long duration between eruptive episodes in LIPs and the relatively high magma flux (Hansen and Grönvold, 2000; Schoene et al., 2019), plagioclase may be held in "hot storage" for an extended interval and thereby undergo diffusive equilibration. Such equilibration complicates the interpretation of primary crystal zonation, especially for trace elements that may diffuse much faster (Cherniak, 2010; Cherniak and Watson, 2020) than Ca, Al, and Na (Morse (1984). While such diffusive exchanges are dominantly considered in terms of how crystal compositions may be impacted, 'reactive porous flow' of magmas through extensive crystal cumulates can also modify the composition of the magma (Lissenberg & MacLoed, 2016). These observations suggest that plagioclase cumulates within the plumbing system of a continental LIP may represent a chemical reservoir with which flood basalt magmas may react with and modify erupted lava compositions.

4.2.2 Regional Geology

The Turkana region of northern Kenya is located in a depression between the Kenya and Ethiopian plateaus and thus contains one of the most complete records of Cenozoic volcanism in East Africa, extending from Eocene to recent in age (Brown and McDougall, 2011; Zanettin et al., 1983). Recent synthesis of Cenozoic magmatism in East Africa has identified a series of pulses of mafic volcanism, many of which are recorded in the Turkana region, that are related to periods of crustal extension within the East Africa Rift system and/or interaction of the mantle thermochemical anomalies and the African Lithosphere (Rooney, 2017, 2020a). Younger pulses of mafic magmatism in the Turkana region were primarily influenced by extension of African lithosphere and include the Axial Phase (0.5 Ma-present), the Stratoid Phase (4 Ma – 0.5 Ma), the Mid Miocene Resurgence (12 Ma – 9 Ma), Flood Phonolite Phase (16 Ma – 12 Ma), and the Samburu Phase (~20 Ma – 16 Ma) (Rooney, 2020a). However, prior to 20 Ma, a combination of nascent rift development and the strong influence of the interaction of a mantle thermochemical anomaly with the African lithosphere generated three pulses of mafic magmatism in Turkana: the Early Miocene Resurgence (~24 Ma – 17 Ma), the Oligocene Traps Phase (~33.9 Ma - 27 Ma; (Abbate et al., 2014; Baker et al., 1996; Hofmann et al., 1997; Ukstins et al., 2002)), and the Eocene Initial Phase (49 Ma – 31 Ma; (Brown and McDougall, 2011; Davidson, 1983; Furman et al., 2006; McDougall and Watkins, 2006; WoldeGabriel et al., 1991)). The Oligocene Traps Phase and the Eocene Initial Phase manifest as two distinct flood basalt provinces where the Oligocene Traps phase is centered on the Ethiopian plateau and the Eocene Initial Phase is centered on southern Ethiopia and northern Kenya (Figure 4.1; Rooney, 2017; Steiner et al., 2021). In Turkana, the Oligocene event is poorly preserved in the rock record, however, the earlier Eocene Initial Phase is preserved as several sections of stratiform mafic lavas (Brown and

McDougall, 2011; Furman et al., 2006; McDougall and Watkins, 2006; Walsh and Dodson, 1969). The preservation of Eocene Initial Phase lavas in Turkana in particularly useful to gain additional insight into the earliest phases of Cenozoic magmatism in East Africa.

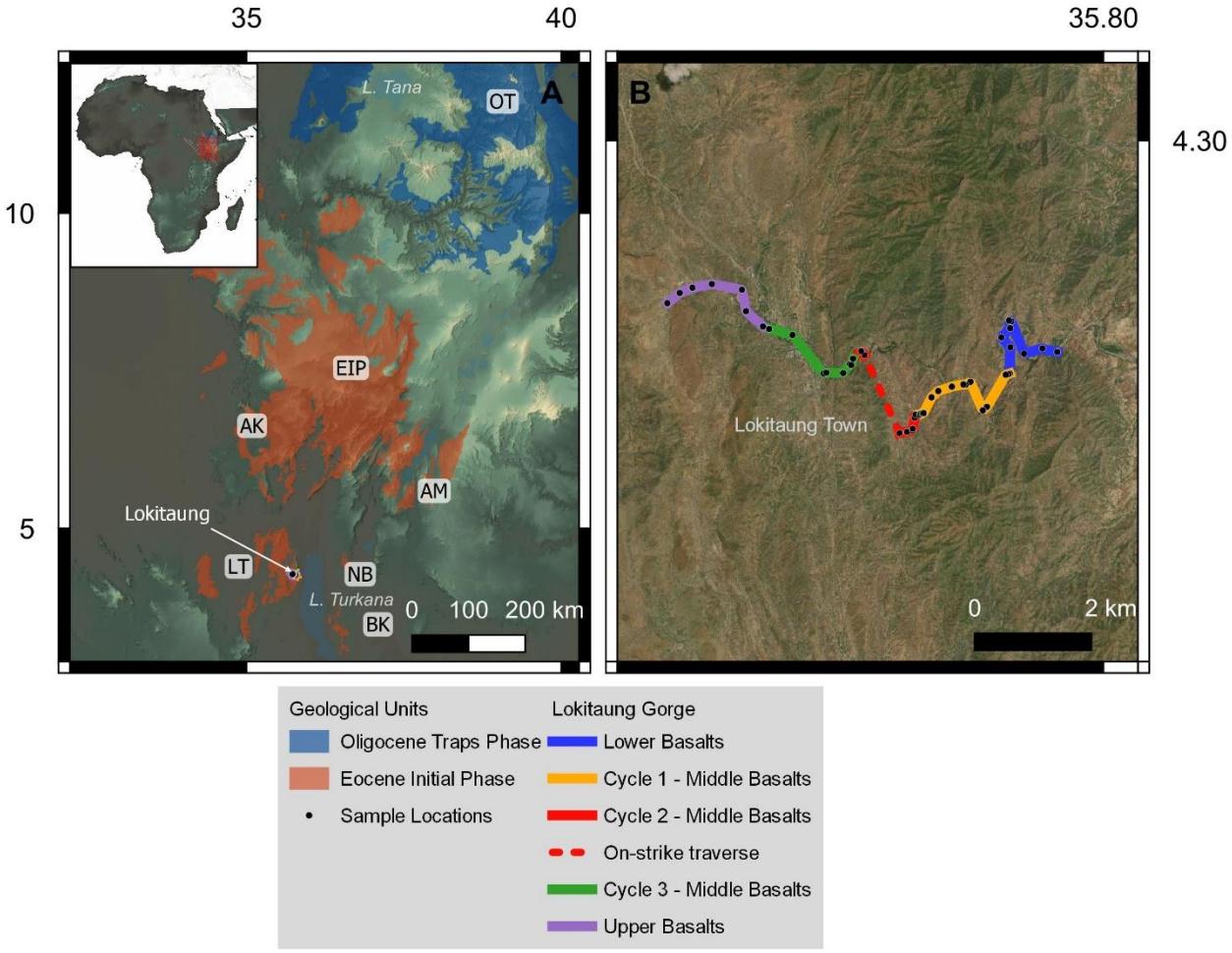

Figure 4.1 - (a) Distribution of Eocene and Oligocene flood basalt provinces in East Africa. Abbreviations: AK, Akobo Basalts; AM Amaro Region; BK, Balsea Koromto; EIP, Eocene Initial Phase; OT Oligocene Traps. (b) sampling transect through the Lokitaung gorge showing sample locations and respective stratigraphic units. An along-strike transect to bypass a waterfall is shown as a dashed line.

Volcanism during the Eocene Initial Phase began outside of Turkana at ~49 Ma and continued to 31 Ma (Davidson, 1983; Ebinger et al., 1993; George et al., 1998; WoldeGabriel et al., 1991). Recent work (Steiner et al., 2021) has broadly divided magmatism during the Eocene Initial Phase into periods that parallel the progression of flood basalt activity (Steiner et al., 2021). The earliest period of volcanism is characterized by small-volume alkaline, clinopyroxene-rich lavas of the Akobo basalts (AK in Figure 4.1; 49 Ma: Davidson, 1983). The commencement of flood basalt activity (early Main Phase of Steiner et al., 2021) is represented by the 45-39 Ma Amaro Basalts (Ebinger et al., 1993; George et al., 1998; Steiner et al., 2021; Stewart and Rogers, 1996). The most and the extensive, thick sequence of lavas termed the Gamo-Makonnen (36-31Ma: Abbate et al., 2014; Davidson, 1983; George et al., 1998; Steiner et al., 2021; Stewart and Rogers, 1996). Geochemical REAFC modeling of the broad temporal windows represented by each magmatic unit demonstrated periods of high and low magmatic flux correlative to eruptive phases with high and low volumes, respectively. These observations of the Eocene Initial Phase provide valuable insights into the broad temporal evolution of the magma plumbing system feeding flood basalt lavas during the Eocene Initial Phase, particularly those erupted in southern Ethiopia where the greatest volume of lavas from this period reside. However, there are additional contemporary stratiform mafic lavas to south in the Turkana region of northern Kenya.

Exposures of Eocene Initial Phase flood basalt lavas are found throughout the Turkana region. The earliest lavas are the Balsea Koromto basalts of the Kajong region (BK in Figure 4.1; 39.2-35.2 Ma: Furman et al., 2006; Wilkinson, 1988). The alkaline Balsea Koromto basalts were merged with the similarly alkaline Akobo basalts (AK in Figure 4.1) of southern Ethiopia and assigned to the initial phase of flood basalt volcanism (Jerram and Widdowson, 2005; Steiner et

al., 2021) at the onset of the Eocene Initial Phase. Main phase flood basalt volcanism is hypothesized to be represented by the Nabwal Formation (34.3 Ma: McDougall and Watkins, 2006) in the Nabwal hills (NB in Figure 4.1) and the Turkana Volcanics (LK in Figure 4.1; ~36-35 Ma; Bellieni et al., 1981; McDougall and Brown, 2009; Morley et al., 1992; Tiercelin et al., 2012) of the Laburr range due to similarities in timing and stratigraphic thickness. However, very little geochemical data exists for the stratiform mafic lavas in Turkana, lending some degree of ambiguity regarding their origin (Rooney, 2017; Steiner et al., 2021). Additional geochemical data from the Turkana volcanics can provide valuable insight into the relationship between the Turkana lavas and those better geochemically characterized lavas from southern Ethiopia as well as the initiation of Cenozoic Magmatism in East Africa.

4.3 Methods

4.3.1 Sampling

The 54 basalt samples utilized in this study were collected from a nearly continuous stratigraphic section of flood basalt lavas located east of the town of Lokitaung, Kenya. The lavas and interflow sediments of the Lokitaung section dip ~10° to the WNW and have been incised into a deep gorge that permits clear distinctions between successive flows. Thickness of flows were estimated in the field, though several exceptionally thick flows (>30m) required calculation of flow thickness based upon the dip and surface exposure. Steep waterfalls at 529m required an along-strike transect utilizing a marker horizon to ensure stratigraphic position was maintained. Sampling of lavas focused upon the dense, least weathered cores of massive or lobed flows. However, especially in the area surrounding the town of Lokitaung, deeply weathered lavas required the sampling of corestones that were less weathered. All sample metadata

including location information were recorded with the System for Earth Sample Registration and is accessible through the International Geo Sample Number (IGSN) found in the appendix.

4.3.2 Analytical Methods

Whole Rock lava compositions were determined by X-ray fluorescence (XRF) and laser ablation inductively coupled mass spectrometry (LA-ICPMS) at Michigan State University. Samples were cut from field samples into 30g billets which were then polished to remove saw marks and cleaned in an ultrasonic bath to remove any contamination from the cutting process. Billets were then crushed in a steel jaw crusher and powdered in a BICO flat plate pulverizing mill using ceramic milling plates. Powdered samples were fused into lithium-tetraborate glass discs using the method of Rooney et al. (2012). Glass discs were analyzed for major element compositions using a Bruker S4 Pioneer XRF calibrated with a range of rock powder reference materials fused into lithium-tetraborate discs. Trace element compositions of glass discs were determined via LA-ICPMS utilizing a Photon Machines Excimer G2 laser and Thermo ICap-Q following the methodology of Rooney et al. (2015). Trace element compositions were determined over six sessions where standards BHVO-1 and JB2 were analyzed at regular intervals as unknowns. LOI values were calculated from the mass deficit after major, minor, and most abundant trace elements were summed. For data plotting, major elements were recalculated to anhydrous values. Results and standard deviations for replicate analyses of standard reference materials and sample compositions are presented in the supplemental materials.

4.4 Results

The Lokitaung Section comprises ~780m meters of stratigraphy consisting of 54 mafic lava flows intercalated with paleosols, tuffs, and sedimentary horizons (Figure 4.2). The section has

been divided into three chemo and petro-stratigraphic groups based upon modal mineralogy and geochemistry (Steiner et al. *in review*). Individual lavas range in thickness from 0.5m to 50m with an average flow thickness of ~13m. Lava morphologies include massive flows, lobed flows, and columnar flows with entablature in particularly thick lavas. Petrographic observations presented in chapter 3 show the dominant texture to be aphyric with several groundmass types including granular, trachytic, and weakly ophitic all with variable amounts of volcanic glass. Plagioclase rich lavas are the second most abundant lava texture and occur at or near the boundaries between stratigraphic units. Less common textures include coarse clinopyroxene rich flows and "bowtie" glomerocrysts of plagioclase and late forming clinopyroxene. The basal stratigraphic unit at Lokitaung is Lower Basalts consisting of 13 lavas totaling 200m of stratigraphic thickness (Figure 4.2). The Middle Basalts are the largest grouping, composed of 33 lavas over 500m of stratigraphy. The Middle Basalts are further subdivided into three sub-units or cycles (Cycles 1 – 3) based upon similarity of lava compositions and petrographic markers such as plagioclase rich lavas (Figure 4.2). The Upper Basalts occur after a hiatus in volcanism marked by a thick tuff and contain 8 lava flows and a capping ignimbrite flow in 67m of stratigraphy. Here, we describe the geochemical characteristics of each group.

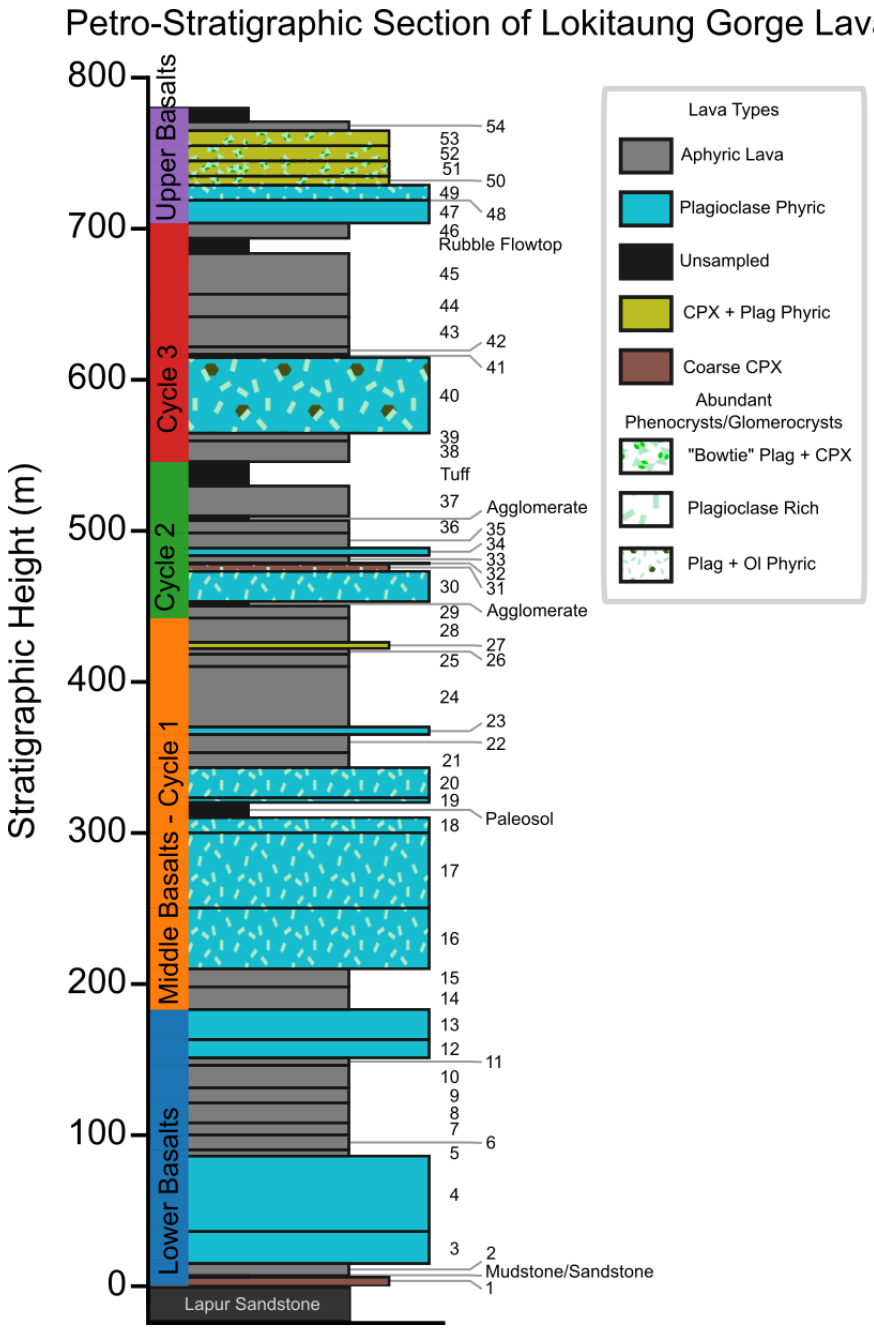

Figure 4.2 – Petro-stratigraphic column of the flood basalt sequence in the Lokituang Gorge. The basal flow is shown erupted atop the Cretaceous Lapur sandstone (Turkana Grits) and the terminal ignimbrite caps the section. Stratigraphic height is indicated in meters along left side of the column and flow numbers are listed adjacent to the respective flow along the right. Unsampled horizons are labelled with the lithology/material present.

4.4.1 Geochemistry

Lava compositions from the Lokitaung gorge can be divided, based upon major elements, into a coherent tholeiitic group and a scattered, subordinate population of alkaline lavas (Le Bas et al., 1986). The tholeiitic group represents 49 of the 54 lavas from the section (Figure 4.3). The tholeiitic lavas range from 4.25-7.75 wt. % MgO (Figure 4.4), gradually decreasing in MgO concentration in younger lavas. Most of the tholeiitic lavas plot within the basalt field (Le Bas et al., 1986). Compatible elements, such as Ni and Cr, range from ~10ppm-105ppm and ~10ppm-255pm, respectively, and exhibit a positive slope with MgO (Figure 4.5). Sr ranges from 200-400ppm have a flat slope versus MgO (Figure 4.5). Incompatible major and trace elements, including La and Nb are positively correlated with MgO, having a much steeper slope at less than 5 wt.% MgO (Figure 4.5). Chondrite normalized REE patterns for the tholeiitic group re broadly parallel, smooth REE patterns with a negative slope (Figure 4.6). Primitive mantle normalized diagrams have coherent pattern with moderate to strong negative Th-U anomaly, positive Nb-Ta anomaly, and a very strong negative K anomaly consistent with hybrid Type 4 to Type 3 magmas of Rooney (Rooney, 2020b) (Figure 4.7). All tholeiitic lavas from the Lokitaung section plot at HT1 magmas, as defined by Pik et al. (1998), near the HT-LT boundary (Figure 4.3).

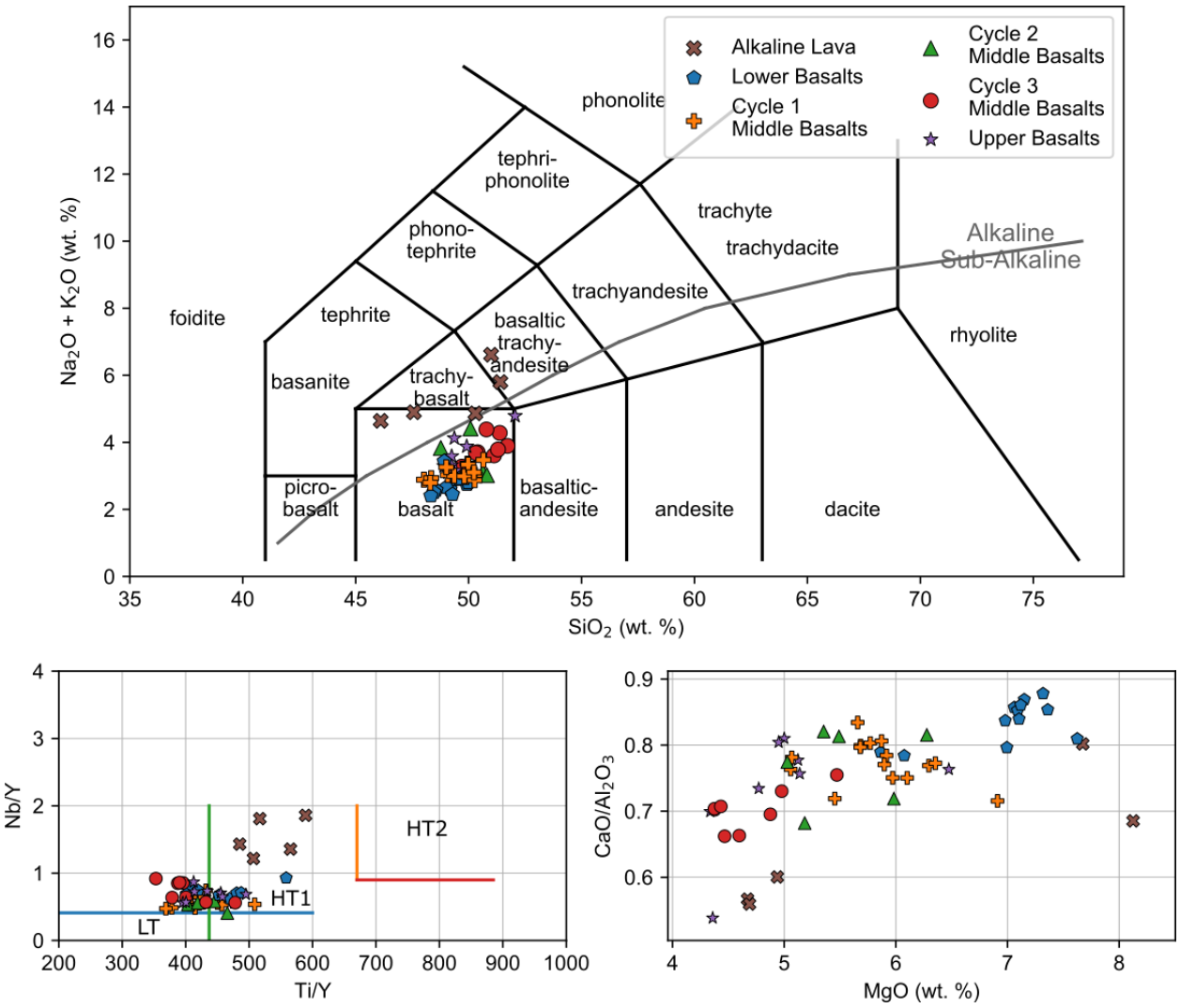

Figure 4.3 – Selected bivariant diagrams showing classifications diagrams and ratio plots for Lokitaung Lavas. Total Alkali Silica diagram from Le Bas et al. (1986) and HT-LT classification diagram from Pik et al. (1998).

The alkaline group is composed of 5 lavas from the Middle and Lower Basalts (flows 1, 27, 31, 33, 38), three of which are basaltic and two are basaltic-trachy-andesite (Le Bas et al., 1986). The alkaline group of lava exhibits a comparable range in MgO content as the tholeiites extending from 4.75 – 8.1 wt. % MgO (Figure 4.4). The alkaline group are moderately to

strongly depleted in Sc (Figure 4.5) and have lower CaO/Al_2O_3 ratios than the tholeiitic lavas (Figure 4.3). Chondrite normalized REE diagrams for the alkaline lavas show a smooth, negative slope REE profile that is steeper than the tholeiitic group (Figure 4.6), consistent with greater La/Yb (6-10) ratios of the alkaline lavas. Primitive mantle normalized trace element spider diagrams show the alkaline group is highly enriched in incompatible trace elements compared to the tholeiitic lavas (Figure 4.7). Three of the alkaline lavas have a negative K anomaly and positive Nb-T anomaly like Type IV magmas of Rooney (2020b). However, two alkaline lavas from Cycle 2 of the Middle Basalts have a weak positive K anomaly and strong negative P-Sr troughs that are more similar to Type IIb magmas (Rooney, 2020b). All of the alkaline lavas plot within the HT1 field of Pik et al. (1998) but are displaced to high Nb/Y and Ti/Y ratios than the tholeiites (Figure 4.3).

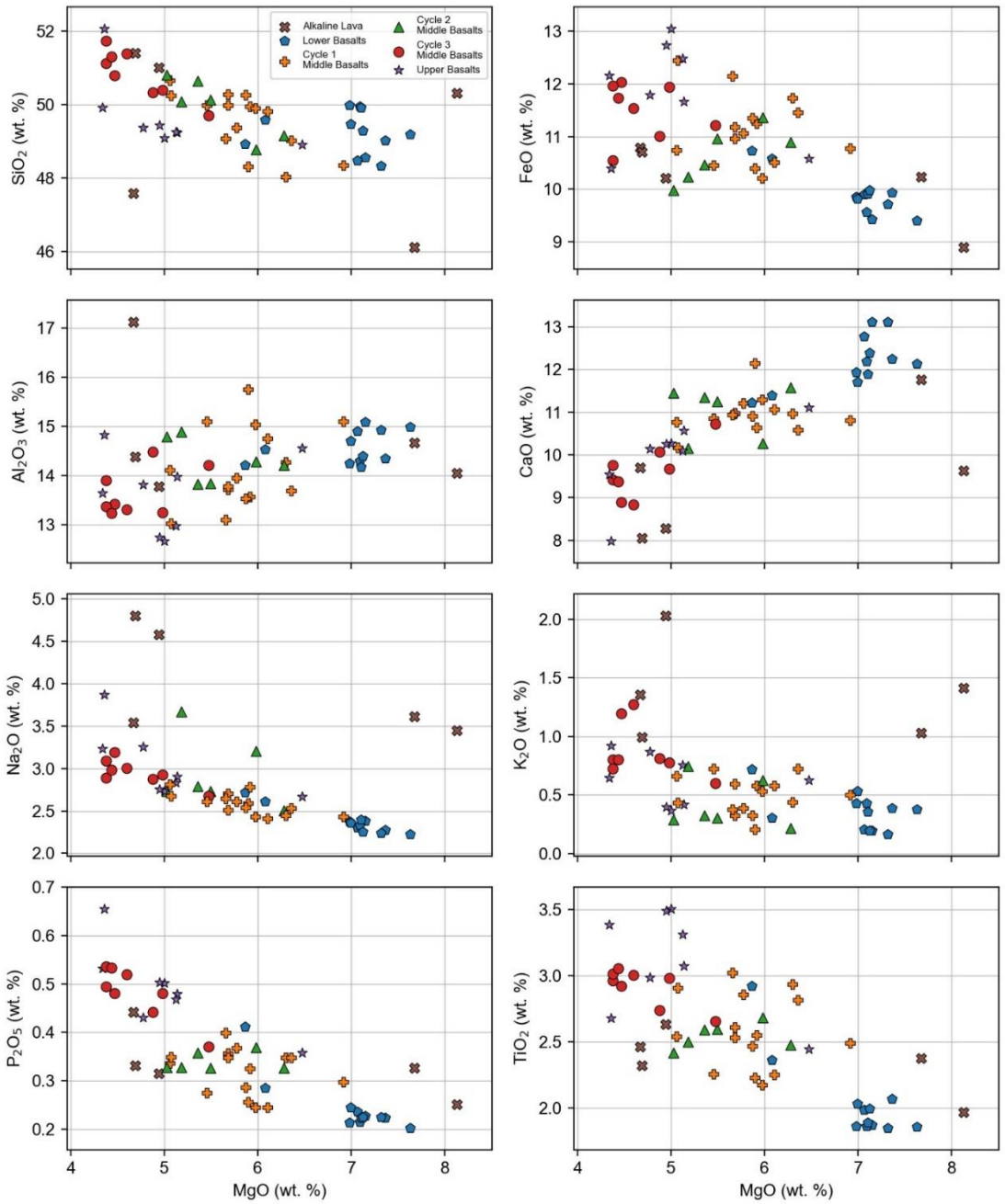

Figure 4.4 – Selected bivariant plots showing major and minor element concentrations relative to MgO for Lokitaung section lavas.

4.4.1.1 Lower Basalts (flows 1 – 13)

The Lower Basalts exhibit more primitive compositions compared to other units in the Lokitaung section. The degree of primitiveness is evident in the higher concentrations of MgO (avg. ~7 wt. %) and CaO (avg. ~12.1 wt. %) alongside the lower concentration of P_2O_5 (avg. 0.25 wt. %) and TiO_2 (avg. ~2 wt. %) (Figure 4.4). Incompatible trace elements Zr (avg. 152ppm) and La (avg. 19.4 ppm; Figure 4.5) are similarly depleted, though Zr is more so than La. Compatible trace elements, like Cr (avg. 156ppm) and Ni (avg. 66ppm), are relatively abundant compared to other stratigraphic units. Moderately compatible Sr and Sc have average concentrations of 360ppm and 39ppm, respectively. REE spider diagrams (Figure 4.6) and primitive mantle normalized trace element spider diagrams (Figure 4.7) both show broad depletion in trace elements compared to other stratigraphic units. Primitive mantle normalized trace element spider diagrams (Figure 4.7) show a broad, convex upward profile with a modest negative Th-U anomaly and strong negative-K and negative P anomalies consistent with type III and type IV magmas of Rooney (Rooney, 2020b). Chondrite normalized REE diagrams (Figure 4.6) show flat, gently sloping profile with LREE abundances comparable throughout the Lower Basalt unit, but flows higher in the unit are depleted in MREE and HREE, evident in the greater La/Yb ratio for those lavas.

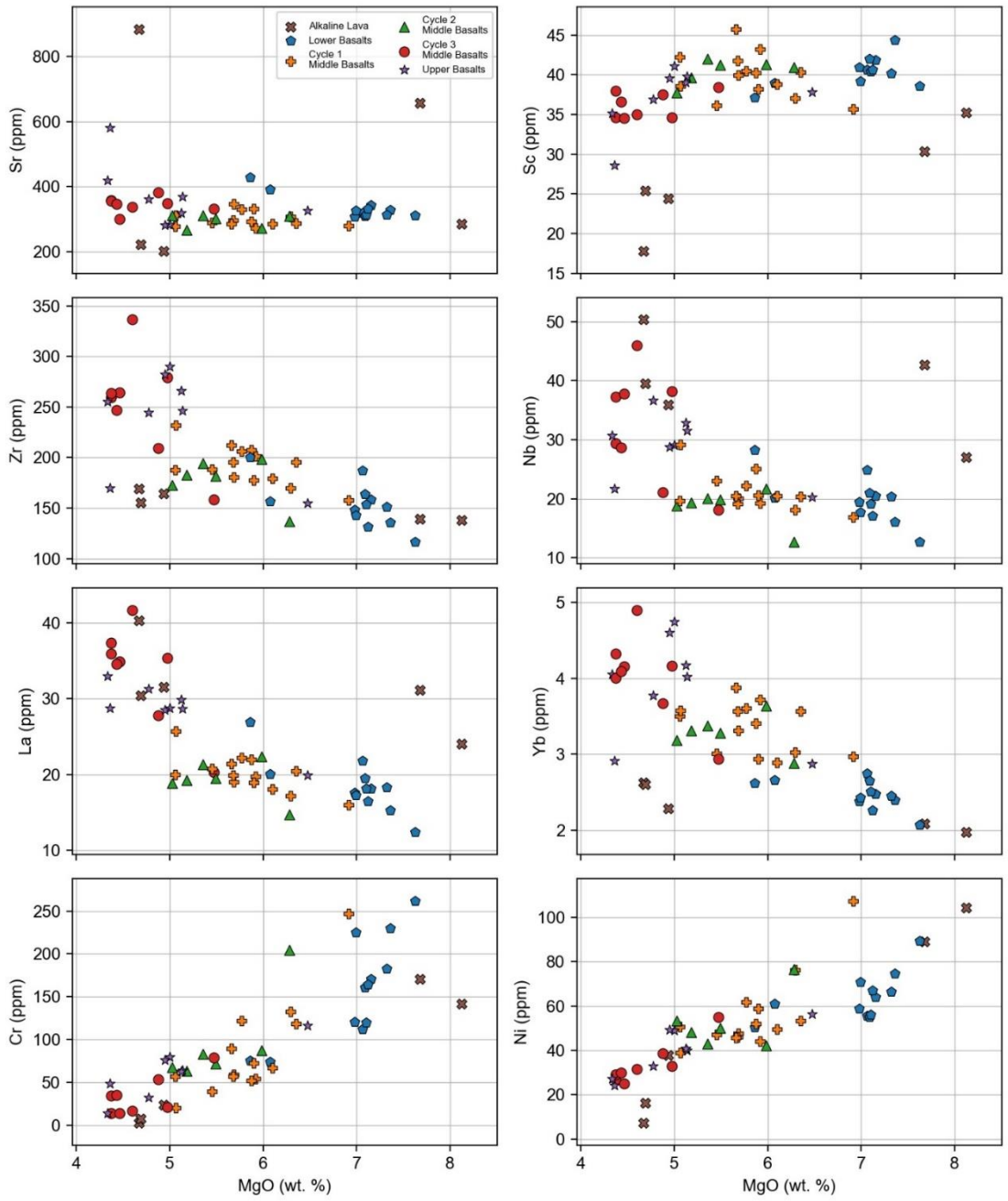

Figure 4.5 – Selected bivariant plots showing trace element concentrations relative to MgO for Lokitaung section lavas.

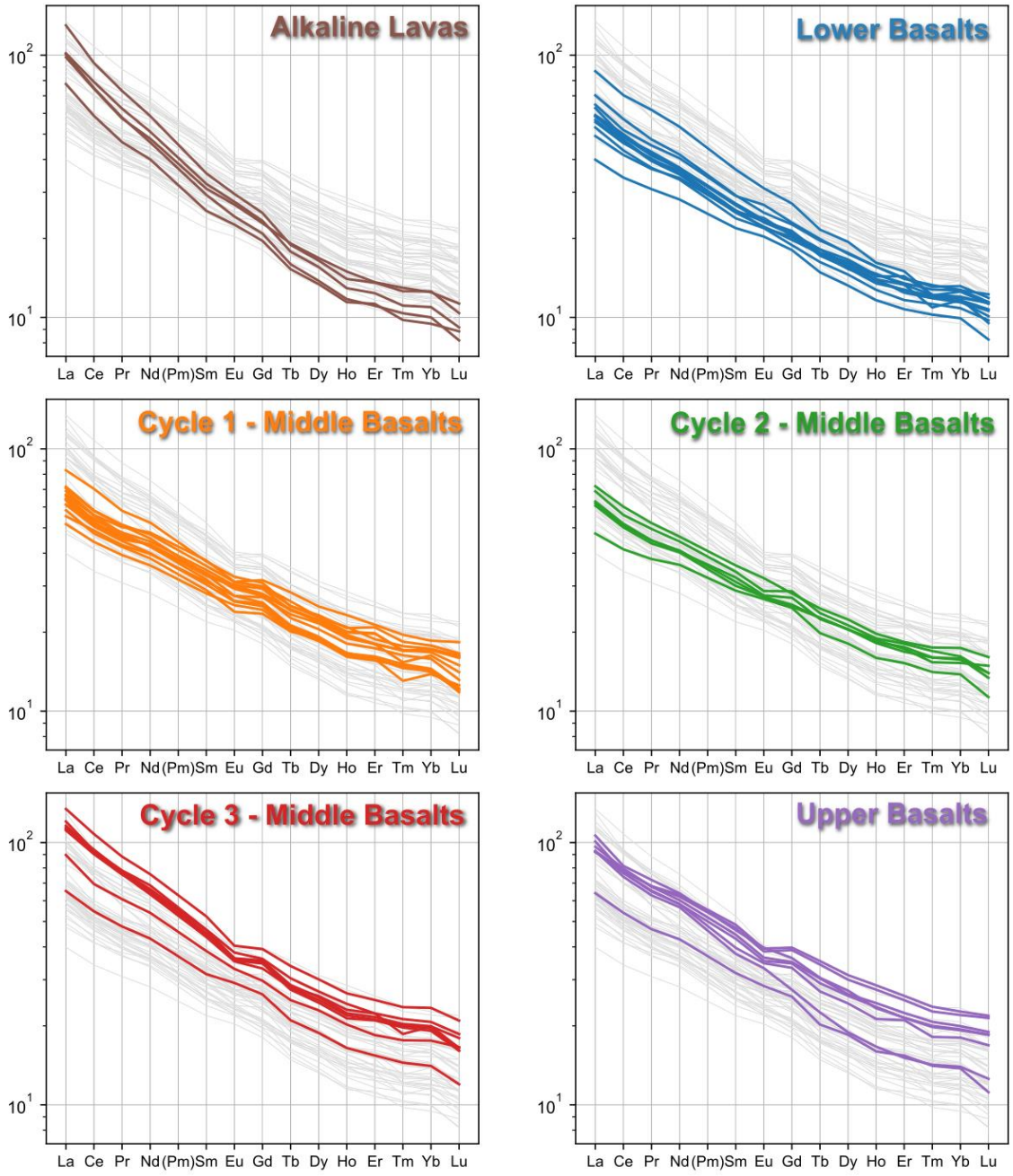

Figure 4.6 – Chondrite normalized spider diagrams showing REE patterns for lava samples from the Lokitaung section. Shaded grey patterns in background show all samples in the dataset. Chondrite normalization is from Boynton (1984). Pm was calculated from the geometric mean of Nd-Sm and does not represent analytical values.

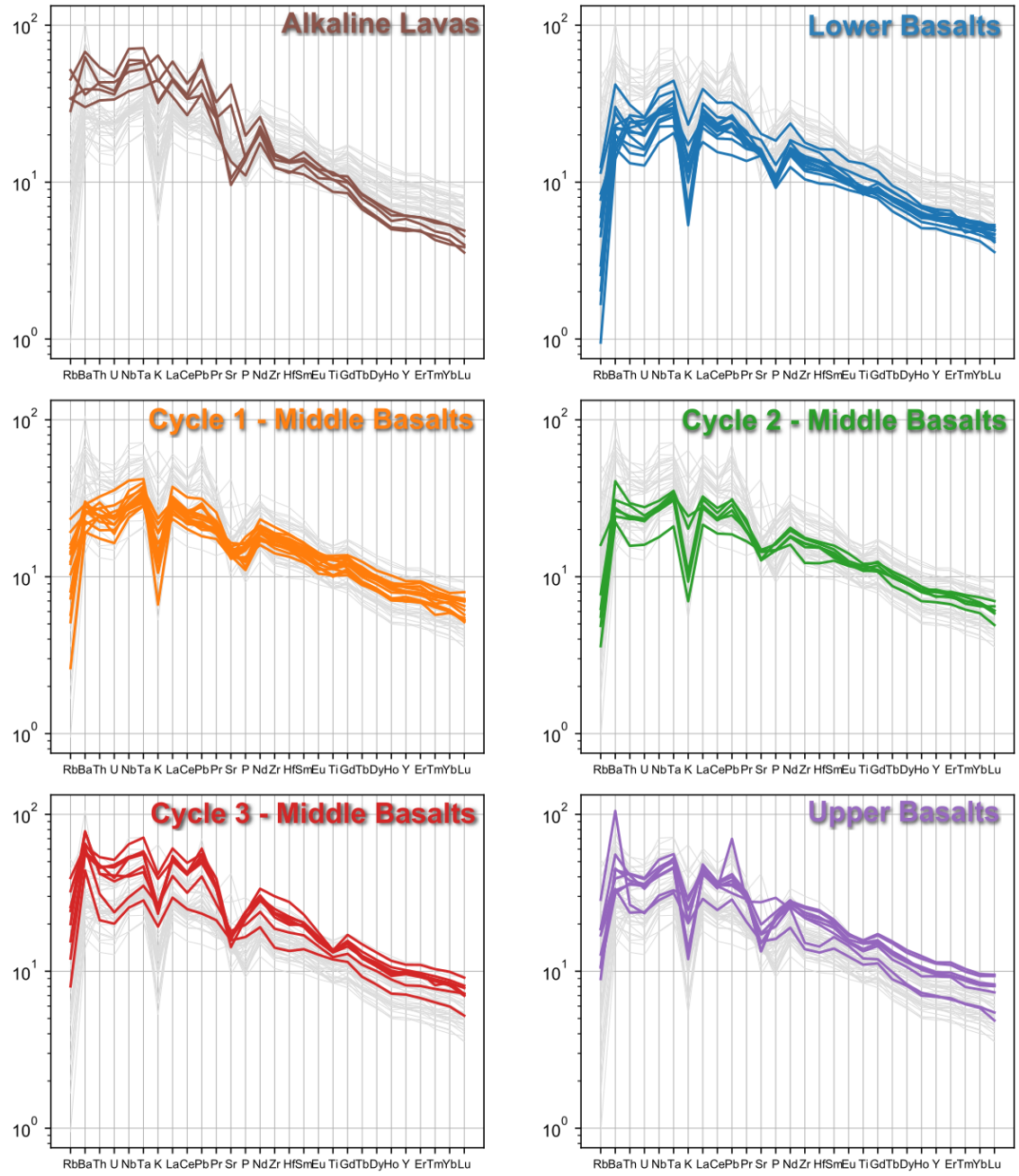

Figure 4.7 – Primitive-mantle-normalized spider diagrams showing incompatible element patterns for lava samples from the Lokitaung section. Shaded grey patterns in background show all samples in the dataset. Primitive mantle normalizations utilize compositions from (Sun and McDonough, 1989).

4.4.1.2 Middle Basalts (flows 14-46)

The Middle Basalts are divided into three cycles, based upon the cyclic occurrence of plagioclase porphyritic lavas. The tripartite divisions of the Middle Basalts are termed Cycle 1 (flows 14-28), Cycle 2 (flows 29-37), and Cycle 3 (flows 38-46) (Figure 4.2). The Cycles 1 and 2 of the Middle Basalts are more evolved than the Lower Basalts but are more primitive than Cycle 3 lavas or the Upper Basalts with lower average MgO (~5.7 wt. %), CaO (10.6 wt. %) (Figure 4.4), Cr (81ppm), and Ni (52ppm). Average P_2O_5 (0.31 wt. %), TiO_2 (2.5 wt. %), Zr (189ppm), and La (20.8ppm) are greater than the Lower Basalts but less than Cycle 3 or the Upper Basalts (Figure 4.4 and 4.5). Sr and Sc concentrations are less than the Lower Basalts at 315ppm and 37ppm, respectively. Incompatible trace elements concentrations in the Cycles 1 and 2 are slightly more enriched resulting in the displacement of primitive mantle patterns toward higher abundances when compared to the Lower Basalts, though the overall pattern remains consistent (Figure 4.7). Similar strong negative K-anomalies and positive Nb-Ta anomalies are observed in Cycles 1 and 2 making them similar to Type III and Type IV magmas (Rooney, 2020b). Chondrite normalized spider diagrams are broadly flat with a gently sloping profile to the HREE (Figure 4.6), however, the slope of the REE profile is somewhat shallower than the Lower Basalts due to enrichment of HREE in Middle Basalt lavas. The Cycle 3 of the Middle Basalts are more evolved than the earlier two cycles, with lower average MgO (4.6 wt. %), CaO (9.6 wt. %), Cr (33ppm), and Ni (33ppm) and greater average P_2O_5 (0.48 wt. %), TiO_2 (2.9 wt. %), Zr (252ppm), and La (33ppm) (Figure 4.4 and 4.5). Enrichment in incompatible element is reflected in primitive mantle normalized patterns and REE patterns which are displaced to higher abundances but continued to be parallel to sub-parallel to the Lower Basalts and Cycles 1 and 2 (Figure 4.6 and 4.7).

4.4.1.3 Upper Basalts (flows 47-54)

The lavas of the Upper Basalts are compositionally similar to the Cycle 3 of the Middle Basalts, though indicator of the degree of evolution are inconsistent. The Upper Basalts have slightly greater average MgO (5 wt %) and Cr (61ppm) but less CaO (9.9 wt. %) and Ni (39ppm) (Figure 4.4 and 4.5). The Upper Basalts contain greater P_2O_5 (0.49 wt. %) and TiO_2 (3.1 wt. %) but less Zr (238ppm) and La (28.5ppm) compared to the Cycle 3. REE's and HFSE exhibit a similar degree of enrichment as Cycle 3 of the Middle Basalts, though LIL elements are slightly less enriched (Figure 4.6 and 4.7). Notably, the negative K anomaly in the Upper Basalts is less extreme than in previous pulses (Figure 4.7).

4.5 Discussion

4.5.1 Numerical Modelling of Equilibrium Crystallization in Open Systems

To examine the processes active within the transcrustal magmatic system that fed flood basalt eruptions at Lokitaung, and how these processes may have changed through time, we implemented a series of open-system models. We took this modelling approach due to the growing recognition that the large, high-flux magmatic systems feeding flood basalt provinces are not accurately represented by closed system differentiation (Bohrson et al., 2020, 2006; Krans et al., 2018; Paces, 1990; Steiner et al., 2021; Streck and Grunder, 2012; Turner et al., 1999; Yu et al., 2015). Flood basalt magmatic systems are open systems, where differentiation occurs primarily through crystallization and subordinate assimilation of crustal material (Bohrson and Spera, 2001; Spera and Bohrson, 2001). However, the flood basalt magmatic system also undergoes periods of magma recharge and eruption/evacuation of voluminous lavas that can result in unexpected geochemical consequences. For example, periods of high magmatic

flux may introduce primitive, less evolved magmas into a magmatic system that contains more evolved magmas and the mixing/hybridization of those two magma compositions will perturb the system toward more primitive compositions. During periods of lower magma flux, it may be possible to reach a steady-state, where compatible elements become buffered, such that the extraction of those elements into a fractionating solid is balanced by the input of new primitive magma into the system (Bohrson et al., 2014; Lee et al., 2014; Nishimura, 2019). Incompatible elements, however, may never reach a buffered state and, because little of those elements are removed in the solid, may become highly enriched in the residual liquid – despite there being little to no change in the abundance of compatible elements. The effect of magma evacuation is dependent on the amount of recharge. If there is no magma recharge, the effect of evacuation may not be observable as fractional crystallization would continue to differentiate magmas. However, when evacuation takes place in the presence of recharge, the net effect is to remove incompatible elements through the evacuating magma and replace those magmas with incompatible element poor primitive magma. The system then more strongly deviates toward primitive compositions comparted to magma recharge alone. The shifting balance of magma recharge/assimilation/evacuation/fractional crystallization through time may explain the geochemical and chemostratigraphic trends observed in the lavas of the Lokitaung section.

4.5.1.1 Recharge, evacuation, assimilation, and fractional crystallization models (REAFC)

REAFC models have been previously used to explore the temporal variability of flood basalt lava compositions in other regions (Emeishan province (Yu et al., 2015); the Keweenaw Province (Davis et al., 2021); and the Eocene Initial Phase in East Africa (Steiner et al., 2021). These studies implemented REAFC models that are built upon the presumption of fractional crystallization – i.e., crystals are instantaneously segregated from the liquid magma and do not

interact further that liquid (Bohrson et al., 2014; Kimura and Kawabata, 2015; Lee et al., 2014). In chapter 3 we have shown that plagioclase does continue to interact with the remaining liquid, even equilibrating with subsequent pulses of magma. Such interactions will change the composition of the residual liquid. This process is consistent with observations from layered mafic intrusions (considered the remnants of the transcrustal magmatic systems), where crystals continue to interact with the liquid fraction in the form of trapped liquid shifts (Barnes, 1986; Robb and Mungall, 2020). The intercumulus liquid may migrate through the crystal mush (Marsh, 1996) to react with crystals or be liberated to mix with the liquid component of a magma chamber (Lissenberg and MacLeod, 2016). Therefore, pure fractional crystallization may not fully accommodate the processes active in the magma plumbing system feeding flood basalt lavas such as those of the Lokitaung Section.

4.5.1.2 Open-System Differentiation with Diffusive Equilibration, mass-balance model

To overcome these difficulties we present the first practical implementation of the theoretical equilibrium crystallization, mass-balance model of Nishimura (2020). Using this model, we explore the impact of open system behavior by modulating the proportions of magma recharge, assimilation, evacuation, and partial crystal segregation on erupted lava compositions (Figure 4.8). We also examine the effect of variable recharge magma compositions. Model outputs describe the geochemical evolution of the liquid magma and the crystal composition in equilibrium with that liquid for a given set of open-system parameters. To monitor model outputs, we examined a suite of compatible and incompatible elements that are sensitive to crystallization of phases common in continental flood basalts. MgO was chosen as a proxy for the degree of differentiation. Ni and Cr were chosen due to their compatibility in olivine and clinopyroxene, respectively, making them sensitive to the extraction of mafic phases. Sr was

chosen due to its relative compatibility in plagioclase. La was chosen due to its incompatibility in all expected crystallizing phases that were determined by thermodyanmic MELTS calculations (Gualda and Ghiorso, 2015). Partition coefficients for all but MgO are described by: Bougault and Hekinian (1974), Ewart and Griffen (1994), Green et al. (2000), McCallum and Charette (1978), McKenzie and O'Nions (1991), Nielsen et al. (1992), Paster et al. (1974), Ringwood and Essene (1970). The partition coefficient for MgO is assumed to be 2 (Lee et al., 2014; O'Neill and Jenner, 2012). Bulk partition coefficients for each element (except MgO) are calculated by the weighted average of the crystallizing assemblage.

4.5.1.3 Model setup for the Lokitaung Transcrustal Magmatic System

The conceptual model for the magma plumbing system feeding the Lokitaung flood basalts is one where magmas first differentiate at depth before being released to higher crustal levels to differentiate a second time under different conditions. Therefore, each numerical solution that approximates the open-system conditions for a volcano-stratigraphic unit at Lokitaung will require at least two sets of model calculations, one deep and one shallow. The two sets of model calculations simulate different depths of crystallization by modulating the modal proportion of stable phases based upon MELTS phase stability calculations (Gualda and Ghiorso, 2015) at deep (10kb) and shallow (2kb) depths. Broadly, crystallization in the deep system is dominated by the formation of clinopyroxene and olivine (or orthopyroxene) with very little plagioclase while the shallow system crystallizes plagioclase and clinopyroxene with lesser olivine. A critical component of the conceptual transcrustal magmatic system is the interconnectivity of magma chambers such that the lower system releases magma to the upper thereby linking the two sets of model calculations. The paired model calculations are connected by the methodology of Nishmura (2019) and Shaw (2006) where calculated compositions from one model are used as

the inputs for subsequent models. We thus simulate the release of magma from the lower system and subsequent injection into the upper by setting the initial and recharge magma composition for the upper system to a liquid composition along the evolution pathway of the lower system model.

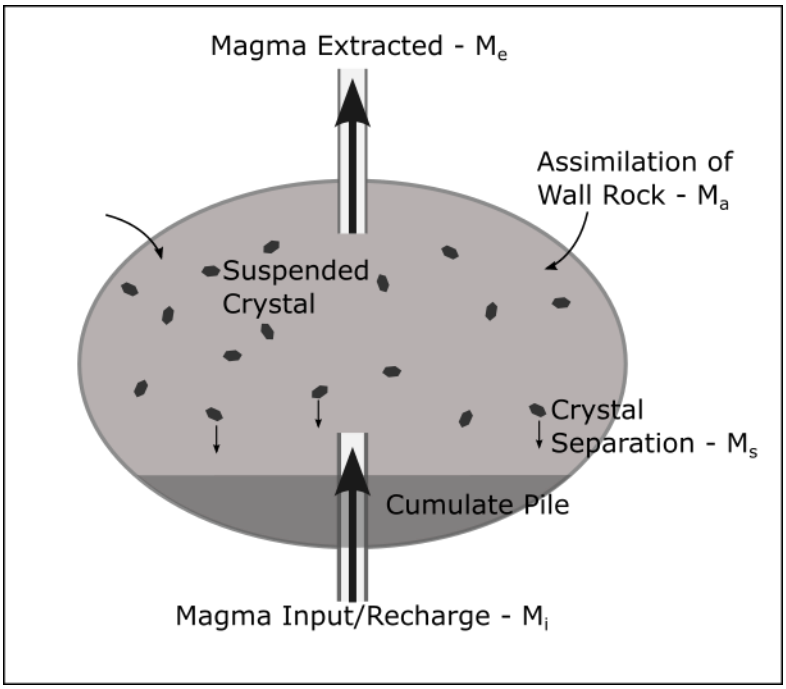

Figure 4.8 – Schematic of mass balance open system model after Nishimura (2020). Shows the open-system parameters that are modulated in numerical solutions. Suspended crystals may be homogenous due to equilibration or zoned where no equilibration occurs.

Input of magma into the lower system requires a primitive magma. However, no lavas in the Lokitaung section are sufficiently primitive (>9 wt. % MgO) to be used as the initial input. Because the Lokitaung basalts are considered to be part of the Eocene Initial Phase, we use the same primitive input magma used by Steiner et al. (2021): a hybrid Amaro Basalt. Because no single Amaro basalt composition can capture all the variation in the data, we have instead chosen

a primitive magma determined by iterating element concentrations and open-system conditions to achieve a best fit, while ensuring elemental variation was within the range of primitive Amaro Basalt compositions. For all model runs, the composition for a crustal assailant was assumed to be a middle crustal composition (Rudnick and Gao, 2003).

4.5.1.4 Comparison Partial Fractional Crystallization Models with and without Chemical Diffusion

There are two different varieties of open-system models in which a fraction of the formed crystals are held in contact with the host magma: one where diffusive equilibration of the crystal and liquid takes place and a second where diffusive equilibration does not take place. A comparison of open-system differentiation with and without chemical re-equilibration of crystal phases is necessary to fully evaluate subsequent numerical calculations that approximate the processing of magmas in the magmatic plumbing system that formed the flood basalts at Lokitaung. Here we compare the "zoned crystal" or disequilibrium model of Nishimura (2019) and the "homogeneous crystal" or equilibrium model of Nishimura (2020) (Figure 4.9). We use the same open-system proportions (recharge = 1.6, assimilation = 0.02, evacuation = 0.2), recharge magma (derivative liquid from Model 1, *see section 5.2.1*), starting magma composition (derivative liquid from Model 1, see *section 5.2.1*), and mineral mode (see Model 4 in *Cycle 3* of *section 5.2.2*). To a first order, the disequilibrium and equilibrium models are similar (Figure 4.9), both calculate an evolving liquid the becomes depleted in compatible elements (Ni, Cr, and MgO) and enriched in incompatible elements. Moderately compatible Sr varies little through the range of MgO concentrations from both models. The primary difference between the two models is the rate at which compatible elements are removed. Consistent with observations of Nishimura (2020), equilibration with crystal phases suppresses the removal of compatible elements from the

liquid portion of the magma, resulting in, for example, greater MgO concentrations for a given La concentration (Figure 4.9). This effect is particularly acute during the early stages of fractionation and is most easily observed by examining the Cr versus MgO plot in figure 9. Chromium is rapidly removed from the liquid early in the disequilibrium model before increasing slightly and reaching a steady state. This effect is consistent with observations of Nishimura (2020) for compatible elements where magma recharge is high (recharge + assimilation – evacuation > 1). For both compatible and incompatible elements, when recharge is high, both models reach the same steady state concentrations for each respective element. Both the disequilibrium and equilibrium models should be considered end-members of magmatic systems where crystals are suspended in or otherwise exposed to an evolving liquid (Nishimura, 2020). We did not find a significant difference in the outputs between the two models over the range of MgO contents recorded in the Lokitaung Lavas but choose to implement the equilibrium crystallization model due to recent work presented in chapter 3, that identified continued chemical interactions between plagioclase crystals and a host magma.

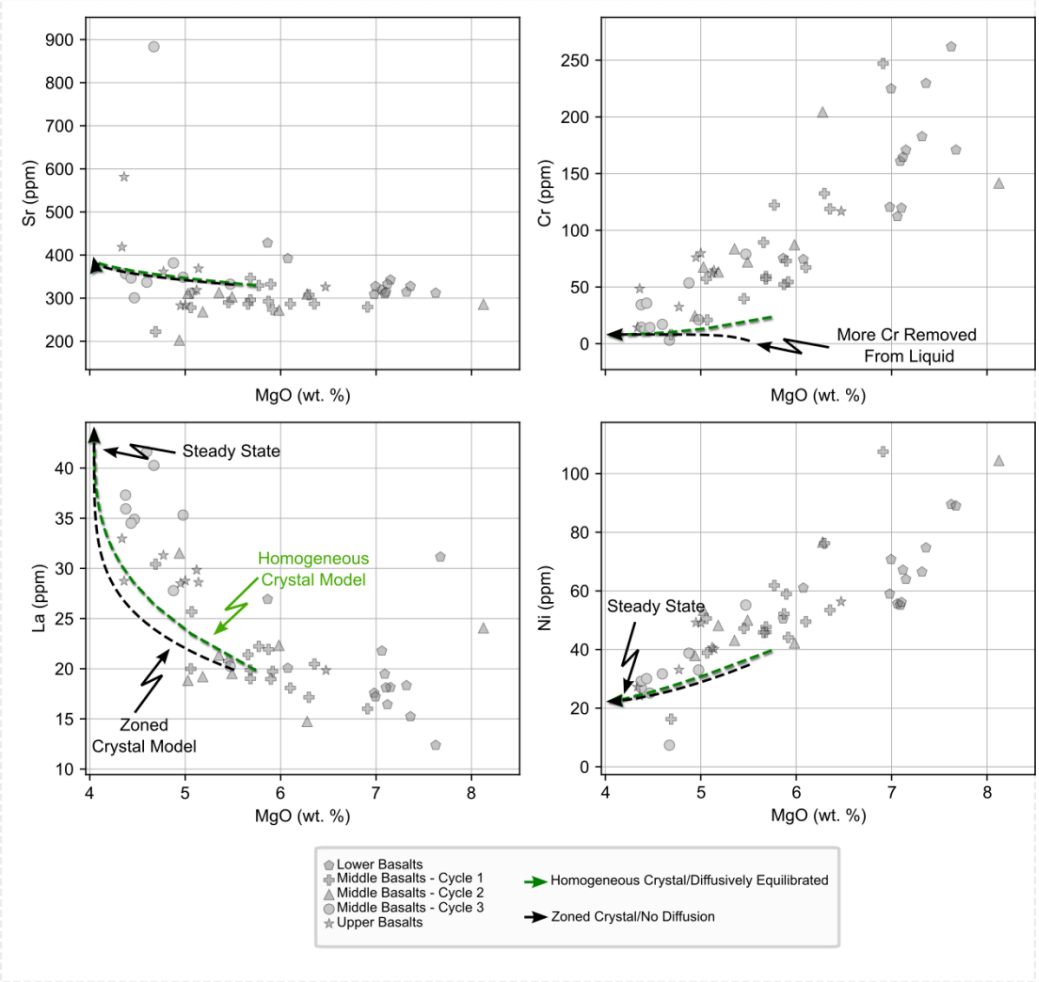

Figure 4.9 – Open-system model outputs comparing the evolving liquid compositions where the suspended fraction of the crystals continuously equilibrate with the evolving liquid (homogeneous crystal modal, green curve; Nishimura, 2020) and where the suspended crystals do not continuously equilibrate with the evolving liquid (zoned crystal model, black curve; Nishimura, 2019). The model parameters are identical for both set of calculations. The starting liquid composition utilized in figure 9 are the same composition used in model 3. Endpoint of model curves are the point at which both MgO and the element on the y-axis reach steady state and longer change composition in the system. Cr versus MgO best highlights the difference between the calculations, where the equilibration model parallels the positive slope of the data but the zoned crystal model exhibits a negative slope.

4.5.2 Magmatic Evolution of the Lokitaung Flood Basalts

Previous examination of the Lokitaung section created a tripartite division based upon the approach of Krans et al. (2018) where new magma pulses are marked by the occurrence of plagioclase-rich lavas. The Lokitaung section is divided into the: Lower Basalts, Middle Basalts, and the Upper Basalts where the Middle Basalts are then subdivided into three cycles. In chapter 3 we proposed that plagioclase compositions in plagioclase rich lavas could be replicated by a magmatic system undergoing differing proportions magma recharge, evacuation, and assimilation. Here we apply the same tripartite divisions from prior studies to the Lokitaung section and interpret the geochemical characteristics of lavas as a result of changes in the proportions of magma recharge, evacuation, and assimilation within the magma plumbing system. Importantly, we utilize whole-rock geochemical compositions for aphyric lavas providing valuable context to the periods of magmatism that may not be well represented by prior studies of porphyritic lavas.

4.5.2.1 Lower Basalt Magmatic System (200 m, flows 1 – 13)

The Lower Basalt magmatic system provides critical information as how a trans-crustal magmatic system was created during the initial stages of the flood basalt magmatism. Stratigraphically constrained observations derived from our geochemical results and prior petrographic studies provide an important temporal framework upon which we construct our numerical models exploring the early formation of the magmatic system. The most significant observation is that the Lower Basalts erupted as primarily aphyric flows (with some exceptions), and exhibit a geochemical trend of becoming more primitive over time. However, the specific details of how the geochemical and petrographic characteristics of these basalts changed over time are important for model construction.

The onset of the Lower Basalt is marked by the eruption of an ankarmatic flow (flow 1) that is strongly alkaline in composition and exhibits a trace element profile that is steeper than the others of the Lower Basalts. The alkaline composition, steep REE profile, and elevated trace elements are consistent with derivation from the fusion of amphibole bearing lithospheric metasomes that were destabilized by the impinging mantle thermochemical anomaly (Furman et al., 2016; Rooney, 2017, 2010) which is a very different than subsequent plume-derived tholeiitic lavas of the Lower Basalt. This clinopyroxene-rich lava likely transited the African lithosphere before an open system was established, otherwise the crystal-rich magma would have been captured by the magmatic system and lost its crystal cargo (Krans et al., 2018). Given the unusual parental magma composition and fractionation history, this lava is omitted from our open-system modelling that focuses upon the sustained period of plume-derived volcanism during the main phase.

The onset of the main phase of volcanism at Lokitaung is marked by lavas that initially contain abundant plagioclase phenocrysts before transitioning to aphyric lavas (Figure 4.2). These lavas are separated from the ankaramatic basal flow by several meters of clastic sediments, which when combined with the observation of abundant plagioclase phenocrysts in the overlying flows is indicative of a hiatus in volcanism, during which magmas may have become trapped in the lithosphere and differentiated (Krans et al., 2018). Such a period of differentiation is consistent with observations that flows 2 and 3 (the first erupted after the hiatus) being the most evolved in the Lower Basalts (MgO: 5.86 - 6.01 wt. %; Figure 4.10). We posit that this hiatus was terminated by renewed magmatism or an increase in magma flux, which initially caused the eruption of these crystal-rich lavas. During sustained magma flux any residual crystals that can be mobilized are removed (Hansen and Grönvold, 2000; Krans et al.,

2018) and results in the eruption of the aphyric lavas that dominate the remaining Lower Basalts (Figure 4.2). Increasing magma flux results in a gradual trend of progressively more primitive lava compositions beginning at flow 4 (7 wt. % MgO; fig 10) and continuing through the remainder of the Lower Basalts (7.6 wt. % MgO in flow 13; Figure 4.10). Minor and incompatible trace elements concentrations exhibit deviation from the typical correlation with MgO (Figure 4.11) suggesting additional complexity in the magmatic system beyond an increase in magma flux. For example, while MgO remains somewhat consistent from flows 5 – 9 incompatible trace element concentrations increase (Figure 4.11). This pattern is typically indicative of a system that is simultaneously undergoing both magma recharge and fractional crystallization (Bohrson et al., 2014; Davis et al., 2021; Lee et al., 2014; Steiner et al., 2021).

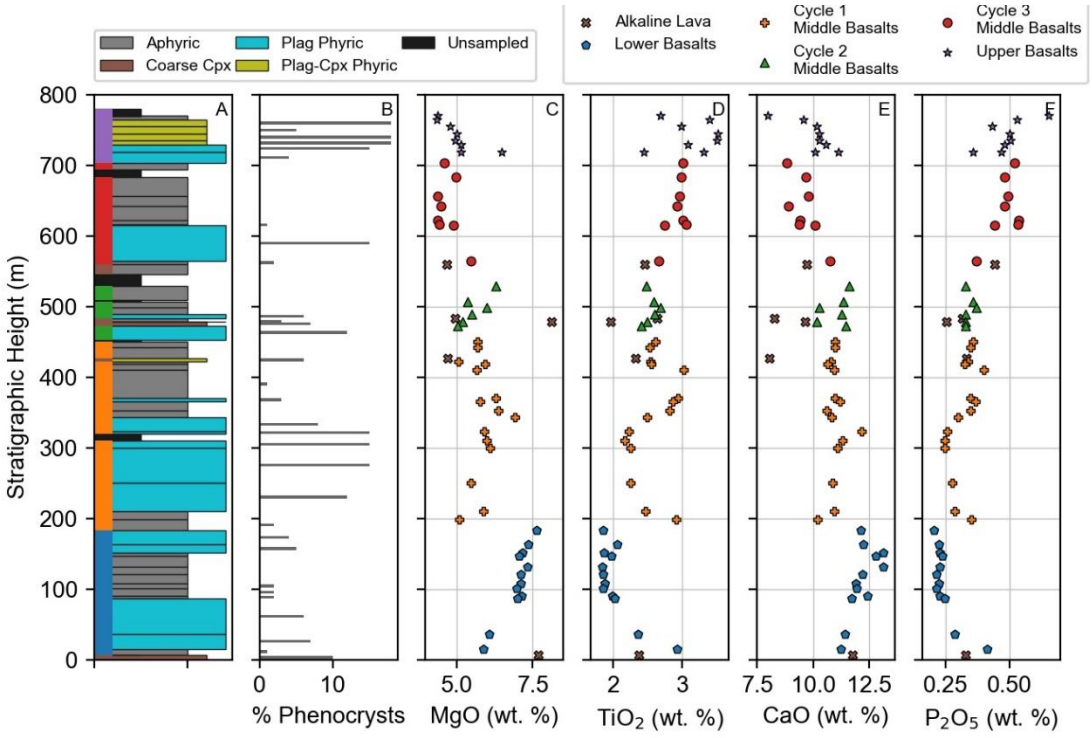

Figure 4.10 – (a) volcano-stratigraphic column showing lava textures. (b) phenocrysts abundance in porphyritic lavas. (c-f) strip logs of select major and minor element compositions.

In order to test the conceptual model outlined above, we utilize a series of interconnected numerical calculations to calculate liquid lines of descent that best approximate the observed data as described in section 5.1. Briefly, our model is comprised of two connected magma differentiation systems located in the lower and upper crust that are undergoing magma recharge, evacuation (eruption), and crystallization. The relative influence of each of these differentiation systems on erupted lavas is implemented by adjusting the proportion of phases that have been modelled to have crystallized. Deeper systems are dominated by olivine and clinopyroxene forming very little plagioclase, while shallower systems are dominated by plagioclase.

We reproduce the initiation of the trans-crustal magmatic system in the Lokitaung section with Model 1, which simulates differentiation of the early erupted magmas in the Lower Basalts

as occurring in an immature magmatic system dominated by the lower crustal differentiation system. Such systems are controlled by the fractionation of clinopyroxene and olivine, resulting in a depletion in the magma of Cr, Ni, and MgO, with an enrichment in La, and Sr. The liquid line of descent calculated for Model 1 (fig.12) captures the most-evolved compositions observed in the Lower Basalts (flows 2 and 3). It is important to note that an upper crustal system must have existed contemporaneously given the occurrence of transported plagioclase in these lavas. It is envisaged that during the hiatus, differentiation of unerupted lavas resulted in an upper crustal system with abundant plagioclase and such a requirement is accommodated by small proportion of plagioclase in the modal assemblage for Model 1 (Figure 4.13). However, the lavas that transported these crystal cumulates to the surface dominantly evolved within the lower crustal system.

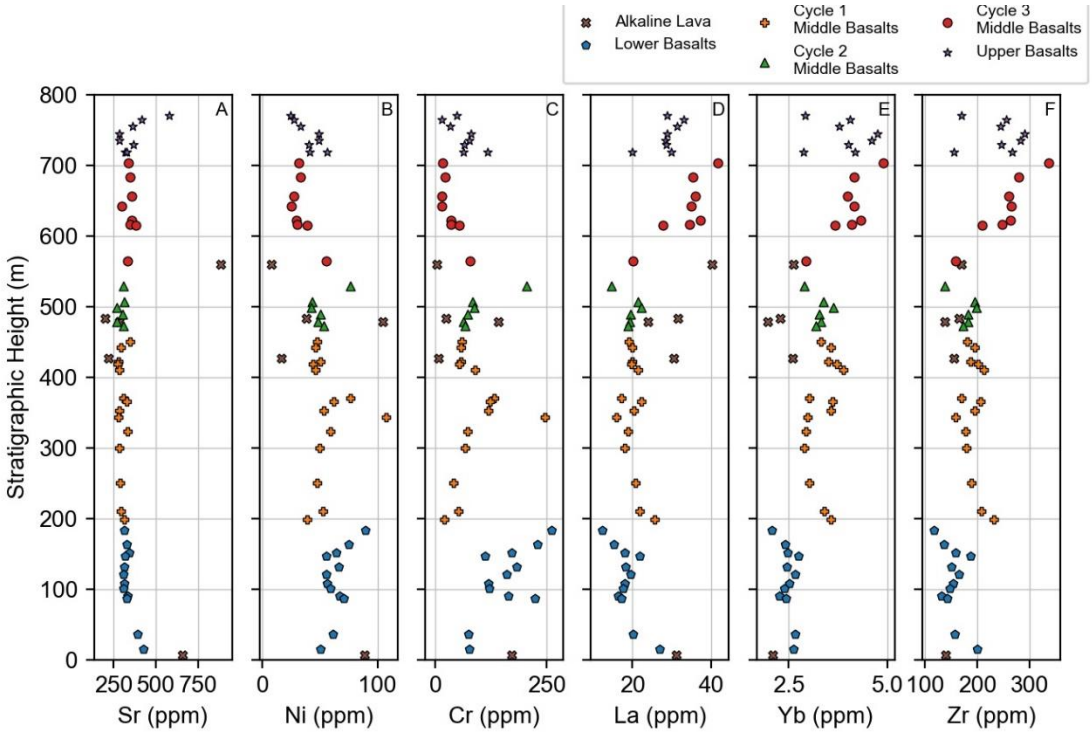

Figure 4.11 – Strip logs showing trace element concentrations in Lokitaung lavas relative to stratigraphic position.

Models 1-1 to 1-4 represent a shift in the conditions of magma differentiation of the Lower Basalts and simulate a progressively maturing magmatic system that eventually results in Model 2 (Figure 4.12). This evolving system has a greater proportion of recharging magma (6.6 times greater flux; table 1) in comparison to Model 1 and incorporates much greater amounts of plagioclase into the crystallizing assemblage, marking the establishment of a shallow magmatic system (table 1). This change in the magmatic system is consistent with the observed changes in behavior of Cr, Ni, MgO, and Sr up section in Lokitaung (Figure 4.11). Models 1-1 to 1-4 gradually increase the mode of plagioclase crystallization to simulate the greater influence of the shallow magmatic system during periods of high magma flux (fig 12 and 14). Model 1-1 introduces ~6% modal plagioclase to the system, representing a small upper system; Model 1-2

adds another 6% plagioclase simulating the continued growth of the upper system. Models 1-3 to 1-4 continue to add 6% modal plagioclase to the crystallizing assemblage while maintaining a high magma flux to support the transcrustal system (Figure 4.12). By the time Model 2 is reached (Figure 4.12), magma recharge has driven compositions toward the most primitive in the sequence and established a mature transcrustal magma differentiation system (Figure 4.14).

			Magma Composition		Open System Parameters			Crystallizating Mode					
Model Number	Modelled System	Stratigraphic Unit	Starting Magma	Recharge Magma	Recharge	Assimilation	Evacuation	Ol	OPX	CPX	PLAG	MT	ILM
1	Lower	Lower Basalts	Amaro Hybrid	Amaro Hybrid	1.5	0.02	0	0.52	0	0.41	0.04	0.005	0.025
1-1	Lower + Upper	Lower Basalts	Lower System Derivative (Model 1)	Amaro Hybrid	10	0.02	1	0.58	0	0.33	0.06	0.005	0.025
1-2	Lower + Upper	Lower Basalts	Lower System Derivative (Model 1-1)	Amaro Hybrid	10	0.02	1	0.56	0	0.29	0.12	0.005	0.025
1-3	Lower + Upper	Lower Basalts	Lower System Derivative (Model 1-2)	Amaro Hybrid	10	0.02	1	0.54	0	0.25	0.18	0.005	0.025
1-4	Lower + Upper	Lower Basalts	Lower System Derivative (Model 1-3)	Amaro Hybrid	10	0.02	1	0.52	0	0.21	0.24	0.005	0.025
2	Lower + Upper	Lower Basalts	Lower System Derivative (Model 1-4)	Amaro Hybrid	10	0.02	1	0.5	0	0.17	0.3	0.005	0.025
3	Upper	Middle Basalts: Cycle 1 and 2	Lower System Derivative	Lower System Derivative	1.7	0.02	0.2	0.1	0	0.37	0.48	0.045	0.005
3-1	Upper	Middle Basalts: Cycle 1 and 2	Lower System Derivative	Amaro Hybrid	1.2	0.02	0.2	0.1	0	0.37	0.48	0.045	0.005
4	Upper	Middle Basalts: Cycle 3	Lower System Derivative	Lower System Derivative	1.6	0.02	0.2	0	0.1	0.45	0.37	0.07	0.01
5	Upper	Upper Basalts	Lower System Derivative	Lower System Derivative	0	0.02	0.2	0	0	0.25	0.7	0.045	0.005

Table 1 – Open-system model parameters used for model runs.

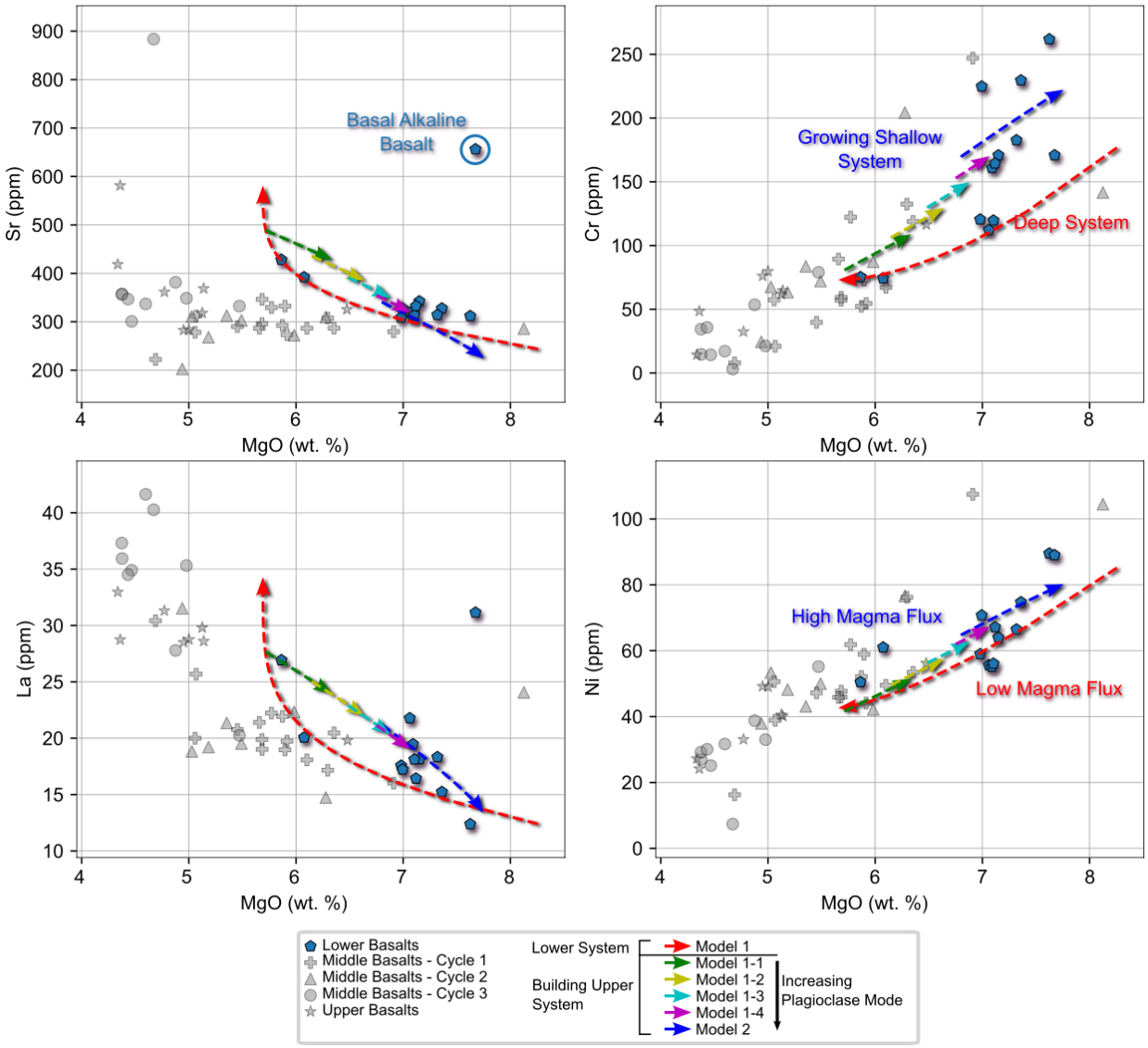

Figure 4.12 – Open system models were calculated to simulate the differentiation of magmas in the lower crust (Model 1). The proportion of plagioclase was then gradually increased for Models 1-1, 1-2, 1-3, 1-4, and 2 to simulate the gradual construction of a transcrustal, open magmatic system.

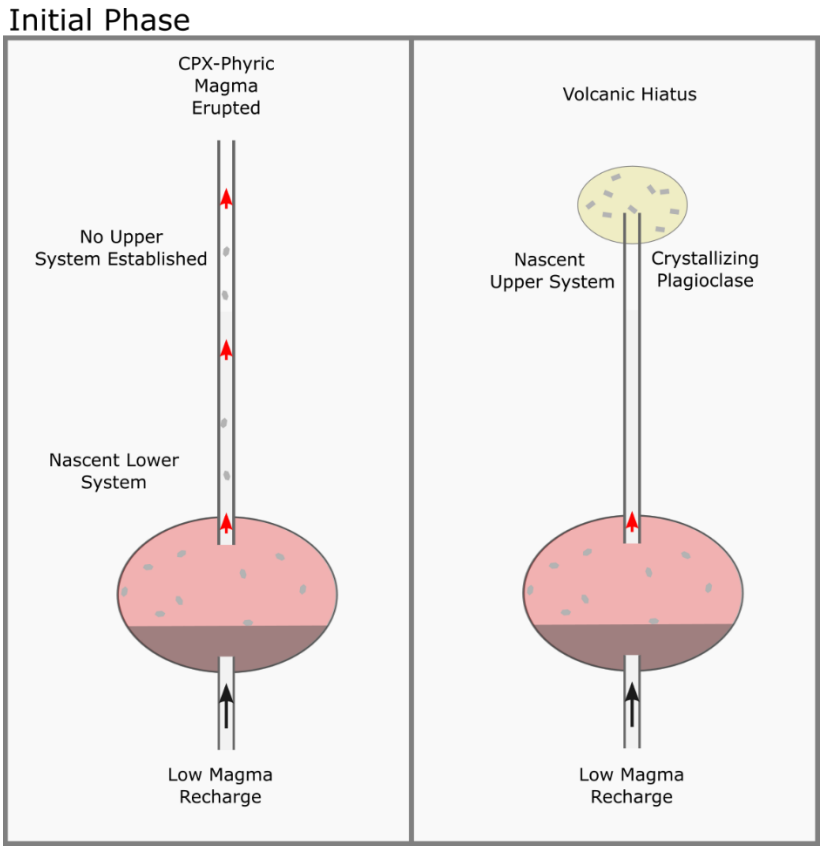

Figure 4.13 – Cartoon describing the magma plumbing system at Lokitaung during the eruption of the basal flow and subsequent hiatus in volcanism that occurred at the onset of volcanism. The clinopyroxene rich basal lava formed crystals at depth and erupted through a magmatic system with no upper system. The nascent upper system must have been established during the subsequent volcanic hiatus, forming plagioclase crystals that would be erupted during renewed volcanism.

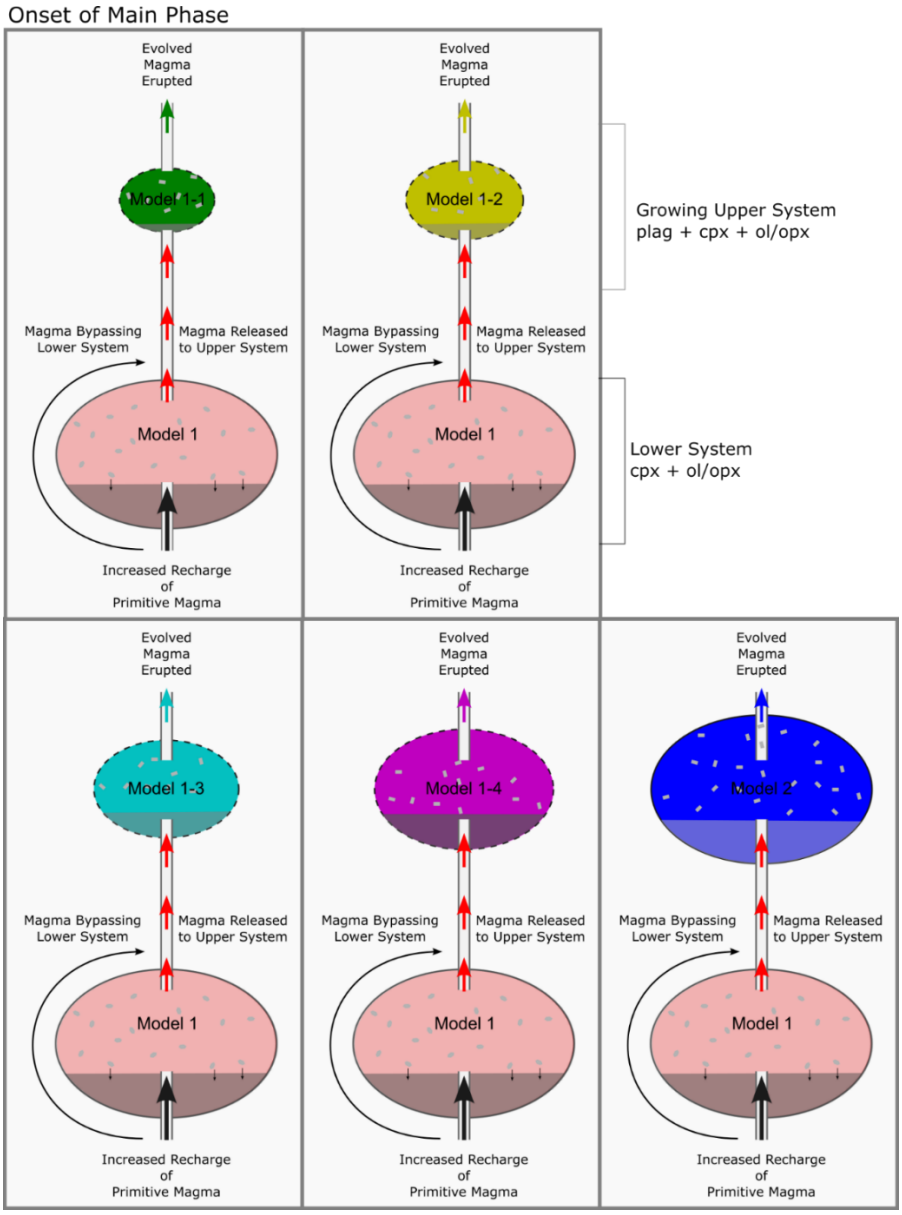

Figure 4.14 – Cartoon describing the evolution of the magma plumbing system during the eruption of the lower basalts. The color of the upper magma system in each cartoon panel corresponds to model outputs in figure 12 (see arrow color in Figure 4.12). Renewed volcanism during model 1-1 erupts plagioclase rich magmas trapped during the prior volcanic hiatus and injects fresh magma into the nascent upper magma system. Sustained high magma flux expands the upper magma system during models 1-2,1-3, and 1-4. By Model 2, Lower Basalt magmas reached their most primitive and the upper magmatic system was fully established.

4.5.2.2 Middle Basalt Magmatic System (500 m, flows 13 – 46)

The Middle Basalts, comprise the majority of the Lokitaung stratigraphy and are divided into three sub-units: Cycles 1, 2, and 3. The Middle Basalts are composed predominantly of stratiform aphyric mafic lavas, with subordinate thick-plagioclase rich flows, and intercalations of thin tuffaceous horizons (Figure 4.2). Compositionally, the Middle Basalts are broadly less primitive than the Lower Basalts, indicating a greater degree of processing in the magmatic system.

***Cycle 1**, 250 m, flows 13 – 28:* The Middle Basalts are separated from the Lower Basalts by a group of highly plagioclase porphyritic lavas (>10% phenocrysts) with relatively evolved compositions (5 wt. % MgO; Figure 4.10). Such lava characteristics suggest a magmatic hiatus between the termination of the Lower Basalts and the commencement of Cycle 1 of the Middle Basalts wherein plagioclase was able to accumulate within the shallow magmatic system before being transported to the surface in the initial lavas of Cycle 1. The MgO content of Cycle 1 lavas gradually increase from 5 wt. % to a maximum of 6.9 wt. % from flows 14 to 20 before decreasing again to between 4.6 and 5.6 wt. % in the youngest flows (Figure 4.10). Strong C-shapes profiles through incompatible elements (TiO2, P2O5, and REE) are observed from flows 14 to 20, reflecting a transition from evolved magmas, to more primitive, then back to evolved. The transition from evolved to more primitive back to evolved compositions from flows 14-20 is evidence for a magmatic system was fractionating magmas, creating more evolved compositions observed at the onset of Cycle 1, before a period of increased magmatic flux (recharge) perturbed the system toward more primitive compositions. The flux of magma then gradually decreased, allowing more evolved lavas to erupt forming the youngest flows in Cycle 1.

Cycle 2*, 107 m: flows 29 – 37:* The onset of second cycle is marked by a combination of plagioclase porphyritic and coarse clinopyroxene lavas (Figure 4.2). The crystal cargo in these flows suggest magmas are being extracted from multiple crustal levels where plagioclase is derived from shallow parts of the magmatic system and clinopyroxene crystals from deeper reaches of the system (Krans et al., 2018; Steiner et al., 2021). Lava compositions become more MgO rich up-section, increasing from 5 wt. % to 6.25 wt. % (excluding the clinopyroxene rich lava near the base whose composition is more MgO rich due to clinopyroxene cumulates; Figure 4.10), that could be interpreted as magma recharge. However, the incompatible elements (Na2O, P2O5, REEs; Figure 4.10 and 11) do not exhibit a complementary decrease in concentration that would be expected during magma recharge. The lack of systematic patterns supports the petrographic observations of significant phase heterogeneity and suggests that the lavas erupted during Cycle 2 may have bypassed parts of the magmatic system, preventing homogenization and common liquid lines of descent. We suggest that this change in the magmatic system results from magma chambers and conduits becoming isolated is due to a period of low magmatic flux – the input of fresh magma was unable to support the crustal-scale differentiation system developed during Cycle 1.

Cycle 3*, 140 m; flows 38 – 46*: The start of Cycle 3 of the Middle basalt marks a shift in the magmatic system that manifests in the eruption more evolved lavas then prior magma pulses. The first lava of Cycle 3 is highly-porphyritic and contains a unique assemblage of plagioclase-olivine with lesser clinopyroxene glomerocrysts that is not observed elsewhere in the Lokitaung section (Figure 4.2). This mineral assemblage is evidence that magmas have reached multiple phase saturation at shallow depths, in contrast to mono-mineralic plagioclase formation in previous pulses and is, therefore, representative of more advanced differentiation. The

compositions of later lavas in Cycle 3 support this conclusion; nearly all aphyric lavas in this cycle are below 5 wt. % MgO, have the lowest Cr and Ni (<50 ppm) and the highest P2O5, TiO2, and REE concentrations compared to prior lavas (Figure 4.10 and 4.11). Notably, the Sc concentration of Cycle 3 lavas are among the lowest in the section, which may be the result of additional clinopyroxene fractionation at depth, into which Sc will partition during crystallization. Such a conclusion is supported by CaO/Al2O3 ratio observed in third cycle lavas (Figure 4.3) which would be anticipated decrease during clinopyroxene fractionation. Therefore, Cycle 3 lavas were erupted from a magmatic system where deep fractionation of clinopyroxene evolved magmas to a greater degree, compared to prior pulses, before releasing them to higher crustal levels and eventual eruption.

Model construction: The model used to simulate the Middle Basalts parallels that of the Lower Basalts. Cycles 1 and 2 of the Middle Basalts exhibit initial plagioclase-rich lavas that transition to younger aphyric flows (Figure 4.2), paralleling similar observations from the Lower Basalts, and interpreted as sustained magma flux thereby requiring magma recharge. Lava compositions in the Middle Basalts, do not strongly deviate toward more primitive compositions as observed in the Lower Basalts, suggesting the proportion of magma recharge is likely less than during the Middle Basalt event (Figure 4.10). The Model 3 (dark blue field in Figure 4.15) captures much of the data for Cycles 1 and 2 of the Middle Basalts where the proportion of assimilation was set to 0.02, evacuation was set to 0.2 and magma recharge set to 1.7. This is an 83% decrease in magma recharge compared to the Lower Basalts. The greater degree of differentiation observed in Cycles 1 and 2 compared to the Lower Basalts is consistent with the lower magma flux during this period which would allow magmas to progress to more evolved compositions.

While Model 3 is capable of replicating much of the lava compositions in Cycles 1 and 2, lavas with elevated Ni and Cr contents could not be replicated. We model these higher Ni and Cr lavas as primitive melts that bypass the lower differentiation system (Figure 4.16) and inject directly into the upper system (Figure 4.15: Model 3-1, cyan field). This process drives the Cr and Ni contents of magmas to higher values and limits the extent to which incompatible trace elements become enriched. The amount of magma recharge in Model 3-1 was reduced by ~30% from Model 3 to prevent liquid compositions from becoming too primitive. Therefore, amount of primitive magma entering the upper differentiation system have been subordinate to the more differentiated magmas released from the lower differentiation system. Two lavas were extremely enriched in Cr and Ni compared to other Middle Basalt lavas (Figure 4.15) and could not be simulated through modelling, suggesting that these lavas may have bypassed the magmatic plumbing system and erupted as more primitive lavas.

Cycle 3 of the Middle Basalts contain lavas that are notably more evolved than the earlier two pulses. They contain greater Sr, lower Sc, and higher CaO/Al_2O_3 consistent with a larger proportion of clinopyroxene fractionation (Figure 4.3). The model for Cycle 3 (Figure 4.17, Model 4, green field) has been modified from that of Cycles 1 and 2 to incorporate more differentiated magmas coming from the lower system (increasing the overall abundance of clinopyroxene in the model) and to add magnetite to the phase assemblage as suggested by thermodynamic calculations described earlier. The green field in figure 3 shows the best fit Open-system model calculations that replicate Cycle 3 of the Middle Basalts. This model had slightly reduced recharge, consistent with the more evolved composition of Cycle 3 lavas (model parameters were assimilation 0.2, evacuation, 0.2, and recharge 1.6).

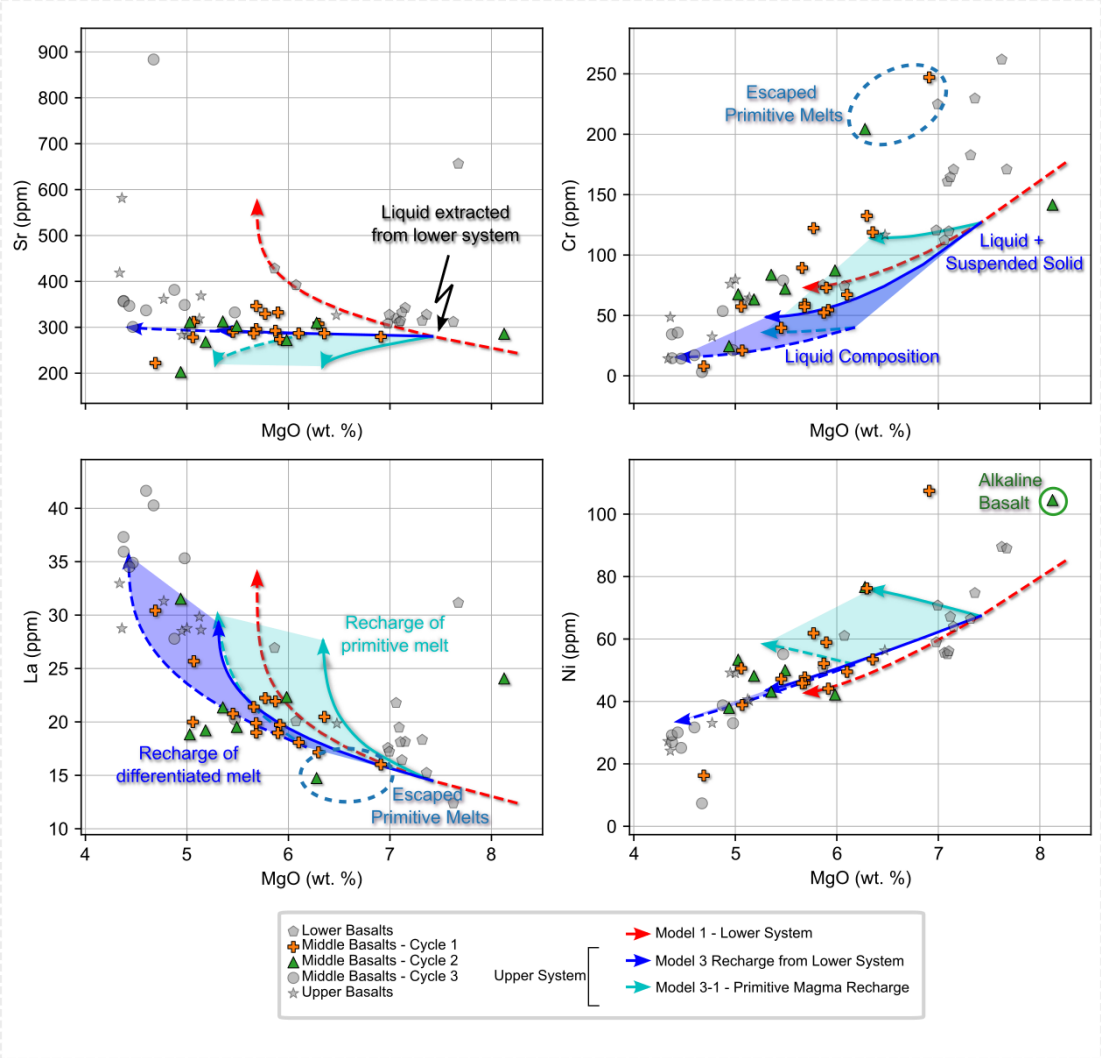

Figure 4.15 – Interconnected open system models were calculated to simulate the differentiation of magmas in a transcrustal magma plumbing system where differentiation occurs first in a lower system (Model 1) then an upper system (Models 3 and 3-1). Model 3 utilizes starting and recharging magmas of the composition released from the lower system while Model 3-1 utilizes a primitive recharge magma compositions to simulate the magmas that may bypass the lower system. Two Cr, Ni, and MgO rich lavas cannot be replicated by Models 3 or 3-1 and are primitive magmas that bypassed both the lower and upper systems and, therefore, experienced little differentiation.

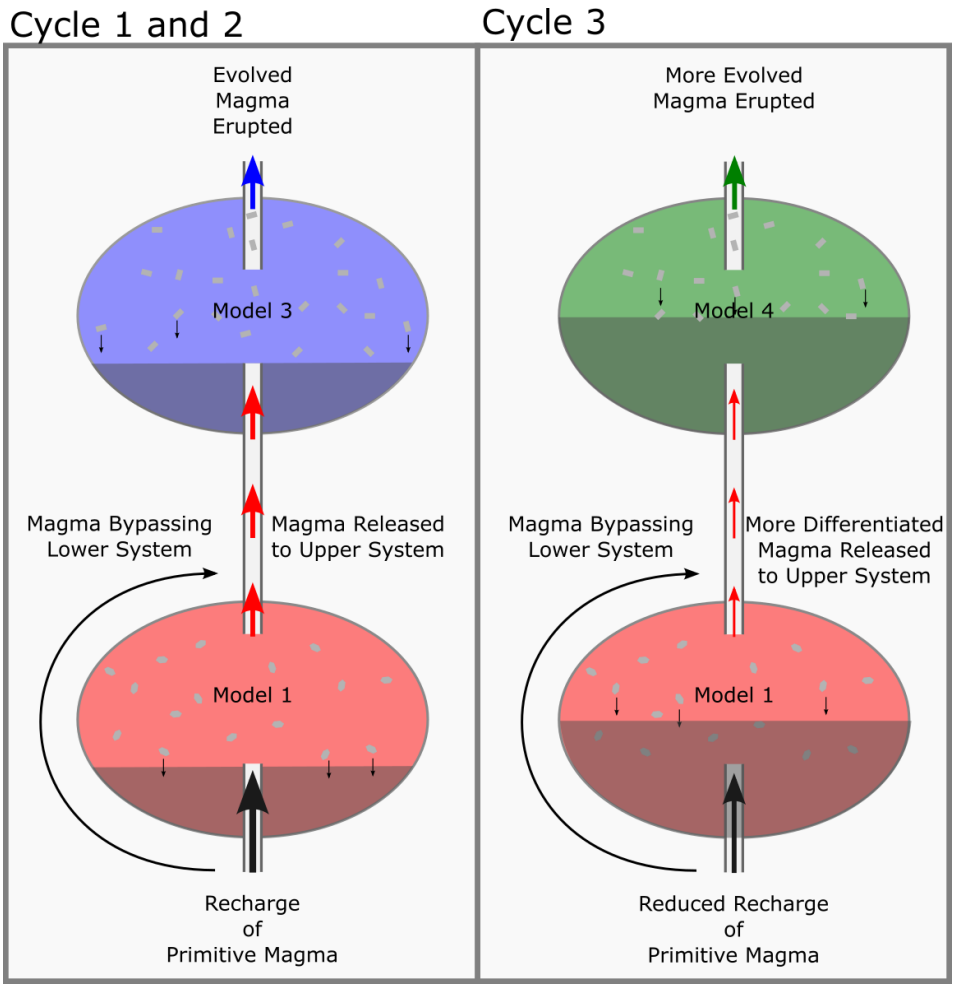

Figure 4.16 – Cartoon describing the transcrustal magmatic system models that represent the Middle Basalt sequence. Cycles 1 and 2 of the Middle Basalts are more primitve than Cycle 3, suggesting higher magma flux during Cycles 1 and 2 (Model 3). The magmas released from the lower system during Cycle 3 (Model 4) are more evolved suggesting magmas are differentiating more in the lower system during this time.

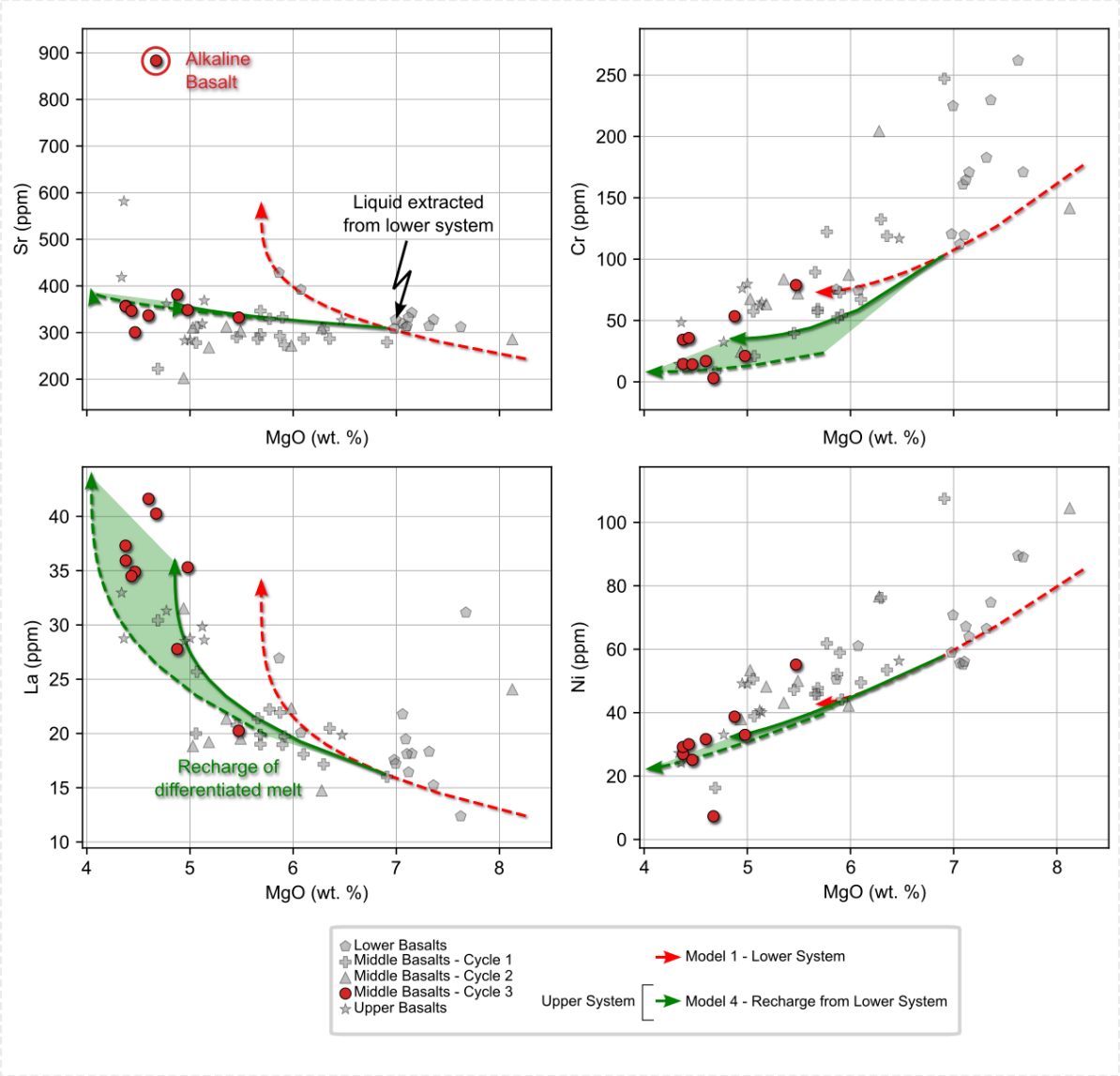

Figure 4.17 - Interconnected open system models were calculated to simulate the differentiation of magmas in a transcrustal magma plumbing system where differentiation occurs first in a lower system (Model 1) then an upper system (Models 4). The starting and recharge magma in Model 4 is more differentiated than Model 3 to accommodate the increased Sr abundances in the Upper Basalt lavas. An exceptionally Sr enriched magma is alkaline in composition and not considered part of the open-system fractionation modelled here.

4.5.2.3 Upper Basalt Magmatic System (67 m, flows 47 – 54)

The Upper Basalt sequence of eight lavas began with the eruption of two plagioclase rich flows followed by a series of plagioclase-clinopyroxene glomerophyric lavas. These abundant plagioclase-clinopyroxene glomerocrysts are consistent with advanced, shallow, gabbroic crystallization (Thy, 1983). The first and second lavas in the Upper Basalts contain 6.5 and 5 wt. % MgO, respectively, and Cr and Ni contents that are slightly greater than those of Cycle 3 of the Middle Basalts (Figure 4.10). Such an observation of increased primitiveness of lava compositions combined with the plagioclase crystal cargo is consistent with a renewed pulse of fresh magma at the onset of the Upper Basalts. However, unlike prior pulses where sustained flux of fresh magma continued resulting in a buffered system or drove the system toward more primitive compositions, the Upper Basalts become more evolved. MgO concentrations decrease from the initial 6.5 wt. % to 4 wt. % (Figure 4.10), paralleled by decreases in Ni and Cr (Figure 4.11). P_2O_5, TiO_2, (Figure 4.10) and REEs (Figure 4.11) increase in concentrations with stratigraphic height. The coupled increase in incompatible elements and decrease in compatible elements along with petrographic evidence of advanced fractionation is consistent with a model where the Upper Basalts erupted from a magmatic system that was no longer undergoing magma recharge. Thus, while magmatism in the Upper Basalts may have been initiated by a fresh magma pulse, the lack of sustained fresh magma allows the system to differentiate through fractional crystallization, eventually resulting in a thick ignimbrite atop the section, marking the end of flood basalt activity in the Lokitaung Section (Figure 4.2).

The numerical model simulating the Upper Basalts differs from previous iterations in that it does not undergo any magma recharge. The yellow field in figure 18 represent a magmatic system with no recharge allowing magmas to differentiate through partial fractional

crystallization, assimilation, and evacuation (model parameters: assimilation = 0.2, evacuation = 0.2, magma recharge = 0). The extraction point for the starting magma that enters the upper system from the lower system is advanced further along the lower system's liquid line of descent (i.e., the magma is more evolved).

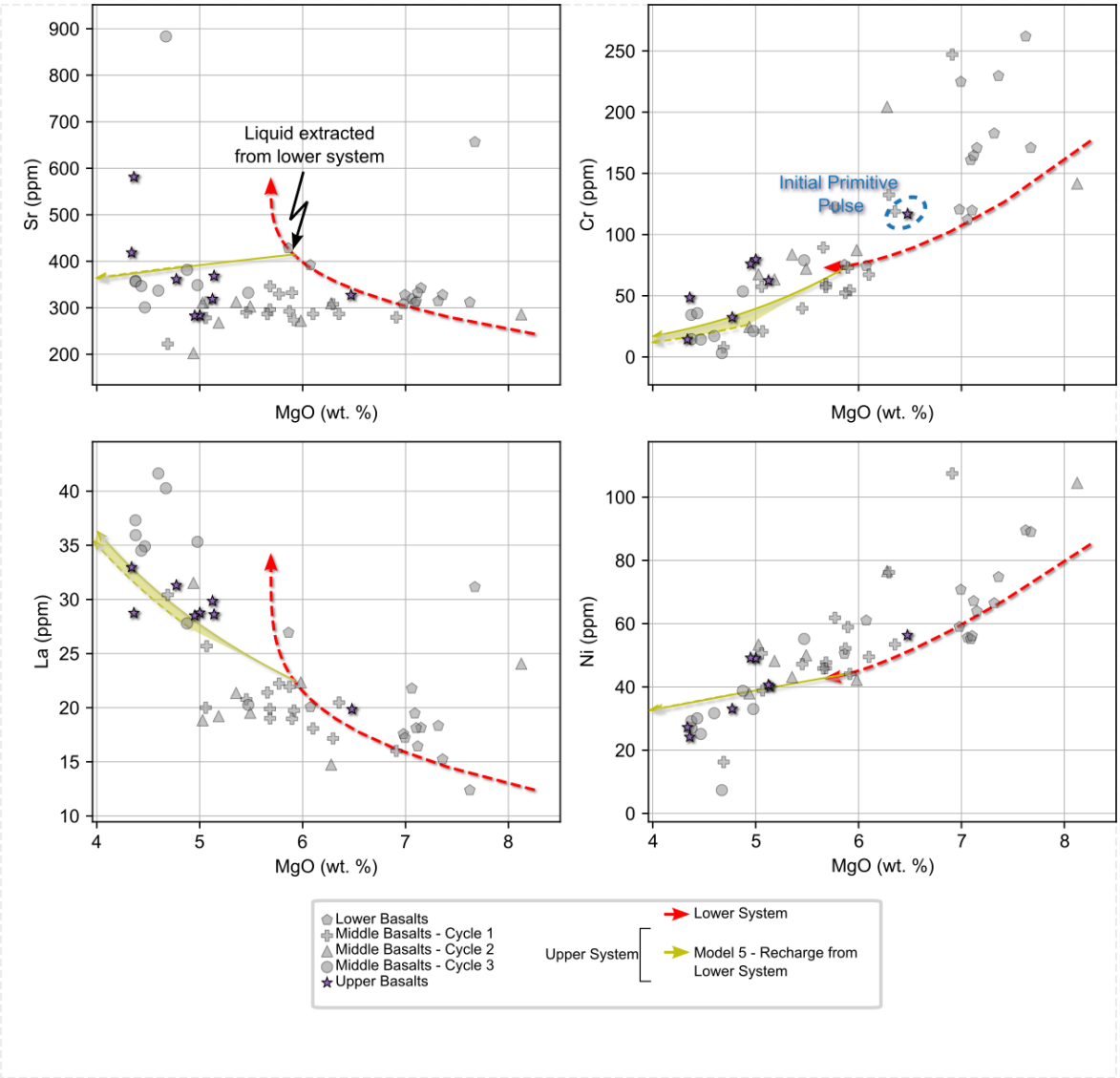

Figure 4.18 - Interconnected open system models were calculated to simulate the differentiation of magmas in a transcrustal magma plumbing system where magma recharge has ceased. Model 5 calculates differentiation in the upper system without magma recharge such that only partial fractional crystallization, assimilation, and evacuation is occurring.

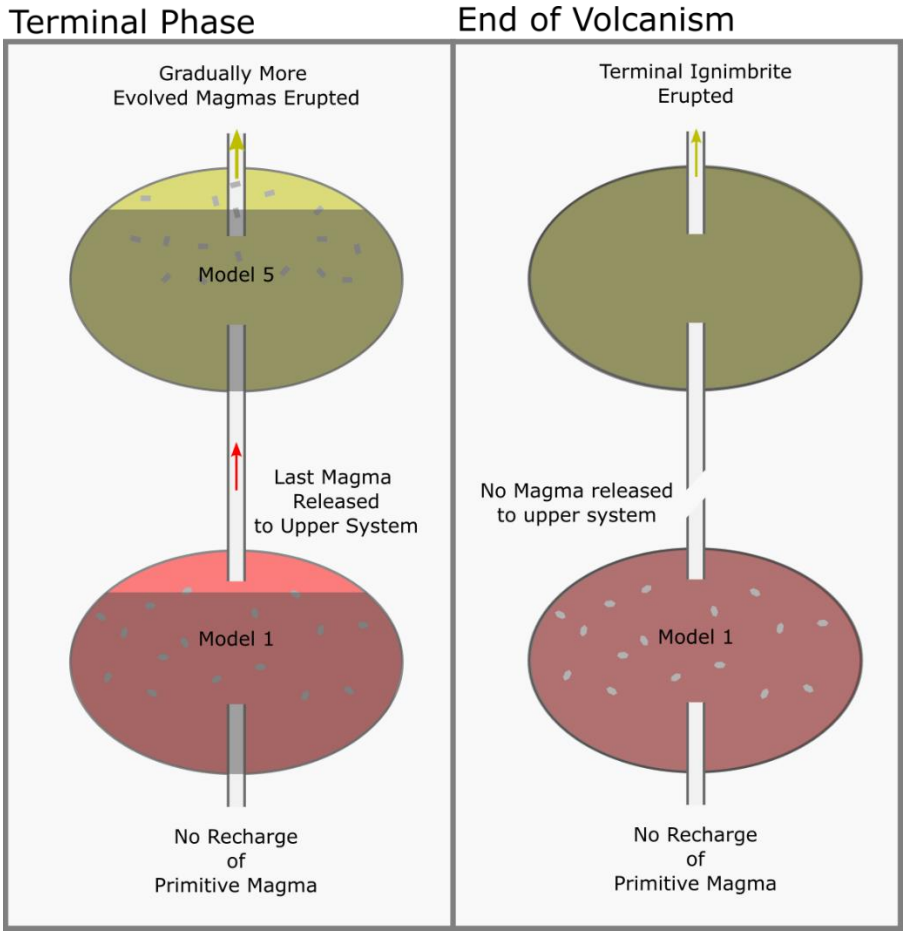

Figure 4.19 – Cartoon describing the terminal phase of flood basalt activity. Loss of recharge from the mantle causes the lower system to lose the capacity to transmit fresh magma to the upper system. The loss of recharge to the upper system causes the remaining magmas to differentiate, eventually culminating in the eruption of the terminal ignimbrite.

4.5.2.4 Summary

Examination of the geochemical data and open-system models from lavas from the Lokitaung Gorge reveals that the dynamic magma plumbing system is controlled primarily by the flux of magma into the magmatic system. An early, high flux period during the eruption of the Lower Basalts formed a transcrustal magma plumbing system (Figure 4.14) where magmas

are stored and differentiated throughout the crust. The flux of new magma into the transcrustal magma pluming system during the eruption of the Lower Basalts was sufficiently high (10x the mass of material crystallizing in the magma differentiation system) to progressively shift the magmatic system towards erupting increasingly primitive lavas (fig 10). A hiatus in magmatism at the end of the Lower Basalts caused magmas to be retained within the transcrustal magma pluming system and differentiate before renewed magmatism at the onset of the Middle Basalts.

The eruption of the Middle Basalts marks a new pulse of magma entering the transcrustal magma pluming system, thereby restarting open-system processes (fig 16). The flux of new magma into the system was significantly less (83% reduction) than that of the Lower Basalts. This decreased flux results in heterogeneity in the magmas released from the lower differentiation system into the upper and eventually a more evolved composition of the erupted lavas (figure 16). A final volcanic hiatus occurs at the top of the Middle Basalts.

A resurgence in volcanism follows the hiatus at the top of the Middle Basalts and forms the Upper Basalts. The Upper Basalts exhibit geochemical behavior consistent with a system undergoing fractionation crystallization without significant recharge (compatible elements and incompatible elements are negatively correlated). Without the recharge of fresh magma into the into the transcrustal magma pluming system, the system progresses toward more evolved compositions culminating in the eruption of a thick felsic tuff that marked the end of flood basalt eruption at Lokitaung (Figure 4.19).

4.5.3 Regional Context

4.5.3.1 The Lokitaung Basalts and the Eocene Initial Phase

The geochemical data presented here represents a significant addition to the sparse geochemical characterizations of the flood basalt lavas from Turkana, providing an opportunity to compare

the these with the geochemical datasets from the Eocene Initial Phase in southern Ethiopia. We find that there are compositional similarities between Lokitaung and the lavas in southern Ethiopia and the Lokitaung section parallels the existing volcano-stratigraphic framework for Eocene volcanism. To the first order, the flood basalts of the Eocene Initial Phase in southern Ethiopia are divided into an early strongly alkaline unit (49 Ma; Akobo Basalts), a tholeiitic group (ca. 45-39 Ma; Amaro Basalts), and a later alkaline group (ca. 38-28 Ma; Gamo-Makonnen unit). At Lokitaung, the basal lava is petrographically very similar to the Akobo Basalt (Davidson, 1983) and is similarly alkaline (Figure 4.20) and exbibits the same elevated incompatible element pattern as the Akobo Basalt in primitive mantle normalized spider diagrams (Figure 4.21). These observations are consistent with basal lava at Lokitaung representing the initial phase of Eocene flood basalt volcanism in northern Turkana. The Lower Basalts are the most primitive lavas at Lokitaung and are the next eruptive event to occur after the basal lava, supporting the idea that the Lower Basalts may correlate to the Amaro Basalts. Indeed, the Lower Basalts are tholeiitic like the Amaro Basalts (Figure 4.20) and have similar patterns and elemental abundances in primitive mantle normalized spider diagrams (Figure 4.21). However, the Lower Basalts are more evolved (lower MgO and greater incompatible element concentrations) and exhibit greater coherence in trace element patterns compared to the characteristically heterogeneous Amaro Basalts (George and Rogers, 2002; Steiner et al., 2021) (Figure 4.21). Steiner et al. (2021) interpreted the lack of coherence between Amaro Basalts' trace element patterns as the result of an immature magmatic that is not yet capable of efficiently hybridizing and homogenizing magmas. The coherent patterns and lower MgO of the Lower Basalts (and the rest of the Lokitaung section), therefore, is evidence that the Lower Basalts are likely derived from a more mature magmatic system than the Amaro Basalts and that a

correlative unit to the Amaro Basalts is not present at Lokitaung. The Middle Basalts and the Gamo-Makonnen were erupted contemporaneously, and both represent the main phase of flood basalt volcanism, erupting the thickest lava sequences in their respective sections. The Middle Basalts and the Gamo-Makonnen have the same narrow range of MgO concentrations (Figure 4.20; ~4-6 wt. %) and coherent trace element patterns (Figure 4.21) consistent with derivation from an open magmatic system that is hybridizing magmas. Open system models presents here and in previous studies (Steiner et al., 2021) show both the Middle Basalts and the Gamo-Makonnen unit are both controlled by open system differentiation, consistent with main phase magmatism. The terminal stages of mafic volcanism are not well documented in southern Ethiopia due to a lack of flow-by-flow sampling of flood basalt sections. As a result, the Upper Basalts do not have a direct correlative unit Eocene Initial Phase exposed in southern Ethiopia. However, both the flood basalts in southern Ethiopia and Lokitaung are capped by ignimbrites that mark the termination of flood basalt activity (Davidson, 1983; Ebinger et al., 1993; Tefera et al., 1996).

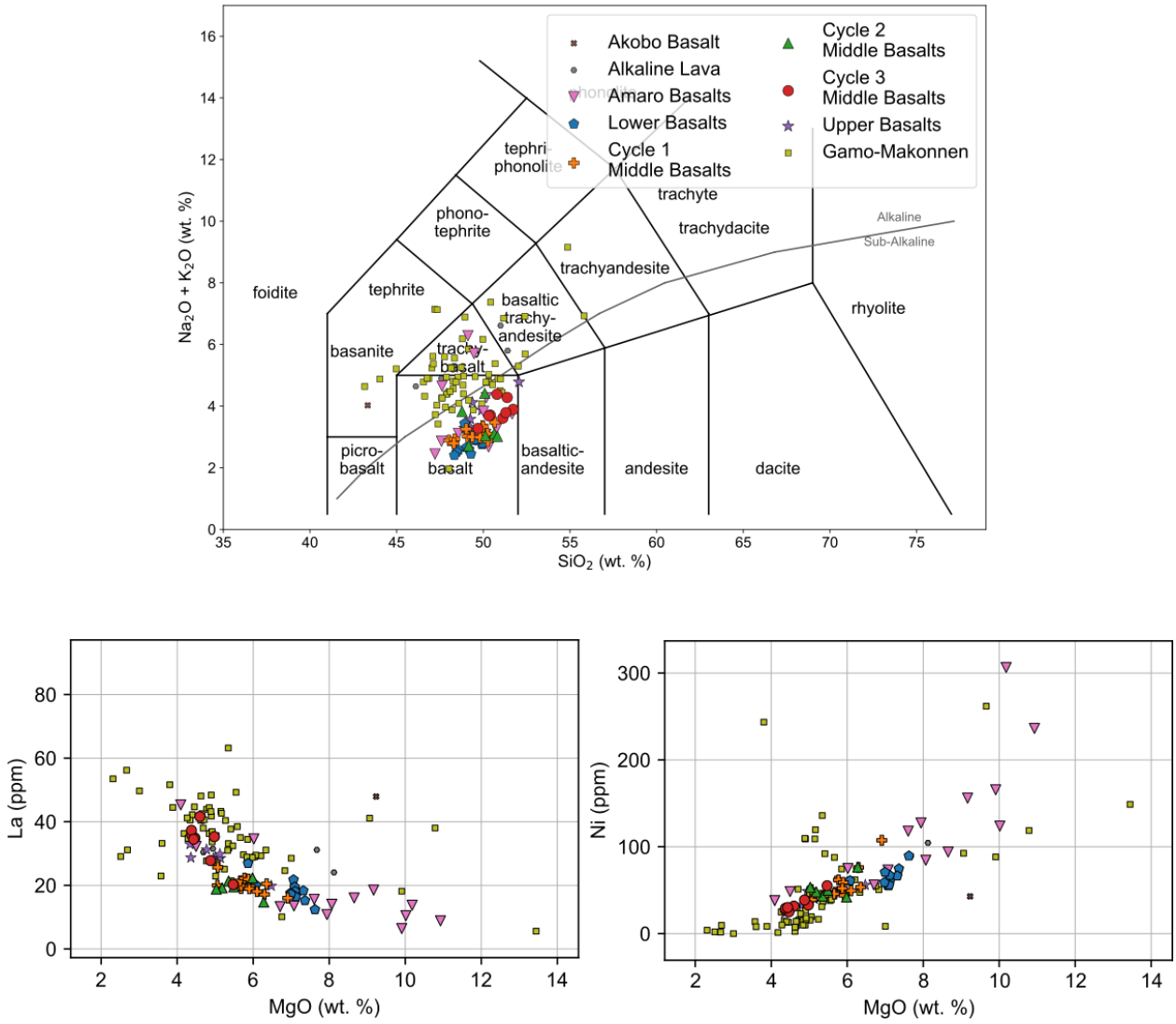

Figure 4.20 – TAS diagram and select bivariant plots comparing lava samples from the Eocene Initial Phase of the East African LIP.

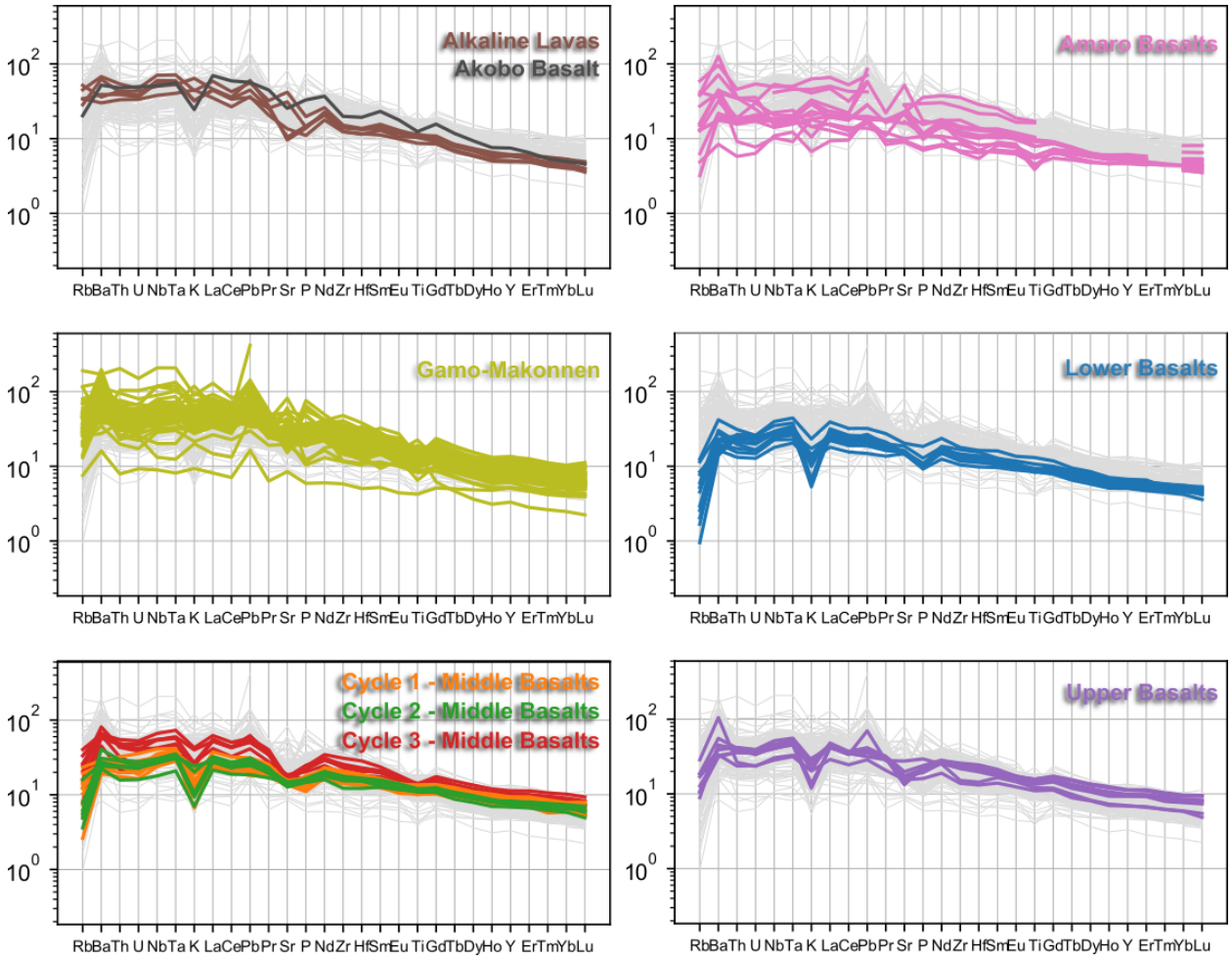

Figure 4.21 - Primitive-mantle-normalized spider diagrams showing incompatible element patterns for lava samples from the Eocene Initial Phase. Shaded grey patterns in background show all samples in the dataset. Primitive mantle normalizations utilize compositions from (Sun and McDonough, 1989).

4.5.3.2 Stratigraphic Comparison of Flood Basalt Sections in East Africa

The flow-by-flow volcano-stratigraphic section collected at Lokitaung is the only one of its kind within the Eocene Initial Phase, providing a valuable opportunity to explore the changes in the flood basalt magma plumbing system throughout the main phase of Eocene volcanism and

compare that to a similar volcano-stratigraphic section to from the Oligocene Traps. The existing coarse magmatic stratigraphy for the Eocene Initial Phase was developed utilizing a geographically widely distributed dataset that resolved the phases of flood basalt volcanism and the broad magmatic conditions contributing to each phase's formation but could not resolve the fine-scale variation imparted by episodic flood basalt eruptions such as those observed by Krans et al. (2018). Krans et al. (2018) collected and examined the only other flow-by-flow volcano-stratigraphic section of flood basalts in East Africa, focusing upon the Oligocene Traps near Lake Tana (Figure 4.1). Both sections reveal episodic flood basalt events with high-flux pulses separated by periods of volcanic hiatus. The pulses of volcanism in the Oligocene Traps section are divided into three major magmatic units: a Lower flood basalt, Middle flood basalts, and Upper flood basalt and, like the Middle Basalts of the Lokitaung Section, the Middle flood basalts in the Oligocene Traps feature a tripartite sub-division termed groups A, B, and C. Using petrographic observations of the mode of the crystal cargo in erupted lavas show the Lower flood basalt of the Oligocene section contains the most olivine, suggesting those lavas are the most primitive. Such an observation parallels the more primitive compositions observed in the Lower Basalts of the Lokitaung Section. The mode of the crystal cargo gradually shifts to greater abundance of plagioclase through the Lower flood basalts and into the Middle flood basalts mirroring increasingly evolved compositions with time observed in the Lokitaung Section as well as the establishment of a trans crustal system magma plumbing system. The terminal lavas of both sections contain evidence of a waning magmatic flux identified by the absence of clinopyroxene glomerocrysts in Upper flood basalts of the Oligocene Traps (Krans et al., 2018) and the shift toward yet more evolved compositions in the Upper Basalts at Lokitaung. These similarities in volcano-stratigraphy between these two sections is notable, given the temporal

(Lokitaung Section ~36 Ma; Oligocene Traps 31 Ma) and spatial separation (900km) of the two sections it is unlikely that they were derived from the same magmatic system. Instead, the episodic nature of flood basalt volcanism, broad progression toward more evolved magma compositions, and establishment of a persistent trans crustal magma system are properties of flood basalt magmatic systems in East Africa.

4.6 Conclusions

This study represents the first complete flow-by-flow geochemical stratigraphy of the flood basalt sequence of the Eocene Initial Phase of magmatism in East Africa. We find that the geochemical variability within the lava flows parallels the existing petro-stratigraphic framework, dividing the flood basalt sequence into three pulses of activity:

Lower Basalts – The initial phase of flood basalt activity. These lavas are the most primitive in the sequence and become more primitive with time. We interpret the geochemical and petrographic characteristics of these lavas as representing differentiation within a dominantly lower-crustal system coincident with a high-flux event during the construction of the transcrustal magma plumbing system. Open-system numerical solutions support this conclusion – the Lower Basalts require the greatest proportion of magma recharge and the most mafic crystallizing assemblage to approximate lava compositions.

Middle Basalts – The main phase of flood basalt activity and the thickest sequence at Lokitaung. The Middle Basalts are subdivided into three cycles. Cycles 1 and 2, which occur at the base of the Middle Basalts, are more evolved that the Lower Basalts. Lava compositions become more evolved in the, younger, Cycle 3 lavas. We interpret the geochemical and petrographic characteristics of these lavas as representing differentiation

within a transcrustal magma plumbing system during moderate magma-flux. Open-system numerical solutions support this conclusion – the Middle Basalt lava compositions require less magma recharge (83% less than the Lower Basalts). The transcrustal differentiation system is modelled by interlinked numerical solutions to simulate the transfer of magma from a lower magma system (clinopyroxene and olivine rich) to a shallow magma system (plagioclase rich).

Upper Basalts – The terminal phase of flood basalt activity. The Upper Basalts are initially slightly more primitive than Cycle 3 of the Middle Basalts, but they become more evolved with time. We interpret the geochemical and petrographic characteristics of these lavas as a terminal magmatic system where magma recharge has ceased and differentiation by fractional crystallization is occurring. Open-system numerical modelling solutions support this conclusion – the compositional evolution of the Upper Basalts can be simulated by fractional crystallization, assimilation, and evacuation without the input of recharging magma.

When compared to other flood basalt lavas from the Eocene Initial Phase, we find that the Amaro Basalts do not have a correlative magmatic unit at Lokitaung. However, the main phase of volcanism at Lokitaung (Middle Basalts) and in Southern Ethiopia (Gamo-Makonnen) is contemporaneous. A correlative of the Upper Basalts is not known from southern Ethiopia, but the two sequences are capped by ignimbrites.

The petro-stratigraphic observations we have made at Lokitaung parallel that of the Oligoecene Traps Phase of the NW Ethiopian Plateau. Both the Oligocene Traps and the Lokitaung section record an early primitive magma pulse during the initial phase of activity, which is followed by a volcanic hiatus. Renewed magmatism at the onset of the main phase of

volcanism in both provinces produces the bulk of flood basalt lavas over a series of cyclic pulses. Magma flux during the main phase is sufficiently high to maintain a transcrustal differentiation system in both flood basalt provinces. Finally, a sequence of lavas that is characterized by low magma flux from the deeper magma systems, terminates flood basalt volcanism in both provinces.

This study represents the first practical application of the open-system partial-fractional crystallization model in which diffusive equilibration of suspended crystals occurs (Nishimura, 2020). We find that this model is capable of approximating the geochemical variation in the Lokitaung section, and preserves information on the composition of crystals interacting with these lavas. We suggest that more widespread use of this modelling approach will yield a needed database of how crystal-liquid interactions in such systems may generate the array of crystal compositions seen in layered mafic intrusions, unifying the currently disparate plutonic and volcanic components in the study of large igneous provinces.

REFERENCES

REFERENCES

Abbate, E., Bruni, P., Ferretti, M.P., Delmer, C., Laurenzi, M.A., Hagos, M., Bedri, O., Rook, L., Sagri, M., Libsekal, Y., 2014. The East Africa Oligocene intertrappean beds: Regional distribution, depositional environments and Afro/Arabian mammal dispersals. Journal of African Earth Sciences 99, 463–489. https://doi.org/10.1016/j.jafrearsci.2013.11.001

Anderson, D.L., 2005. Large igneous provinces, delamination, and fertile mantle. Elements 1, 271–275.

Annells, R.N., 1973. Proterozoic flood basalts of eastern Lake Superior: The Keweenawan volcanic rocks of the Mamainse Point area, Ontario. Can. Geol. Surv. Pap. 72-10.

Armitage, J.J., Ferguson, D.J., Goes, S., Hammond, J.O., Calais, E., Rychert, C.A., Harmon, N., 2015. Upper mantle temperature and the onset of extension and break-up in Afar, Africa. Earth Planet Sc Lett 418, 78–90.

Arndt, N.T., Czamanske, G.K., Walker, R.J., Chauvel, C., Fedorenko, V.A., 2003. Geochemistry and origin of the intrusive hosts of the Noril'sk-Talnakh Cu-Ni-PGE sulfide deposits. Economic Geology 98, 495–515.

Baker, B.H., Williams, L.A.J., Miller, J.A., Fitch, F.J., 1971. Sequence and geochronology of the Kenya rift volcanics. Tectonophysics 11, 191–215. https://doi.org/10.1016/0040-1951(71)90030-8

Baker, J., Snee, L., Menzies, M., 1996. A brief Oligocene period of flood volcanism in Yemen: implications for the duration and rate of continental flood volcanism at the Afro-Arabian triple junction. Earth and Planetary Science Letters 138, 39–55. https://doi.org/10.1016/0012-821X(95)00229-6

Barnes, S.J., 1986. The effect of trapped liquid crystallization on cumulus mineral compositions in layered intrusions. Contrib. Mineral. Petrol. 93, 524–531.

Bastow, I., Nyblade, A., Stuart, G., Rooney, T., Benoit, M., 2008. Upper mantle seismic structure beneath the Ethiopian hot spot: Rifting at the edge of the African low-velocity anomaly. Geochemistry, Geophysics, Geosystems 9.

Beccaluva, L., Bianchini, G., Natali, C., Siena, F., 2009. Continental flood basalts and mantle plumes: a case study of the Northern Ethiopian Plateau. J Petrol 50, 1377–1403.

Bellahsen, N., Faccenna, C., Funiciello, F., Daniel, J.M., Jolivet, L., 2003. Why did Arabia separate from Africa? Insights from 3-D laboratory experiments. Earth and Planetary Science Letters 216, 365–381. https://doi.org/10.1016/S0012-821X(03)00516-8

Bellieni, G., Brotzu, P., Morbidelli, L., Piccirillo, E.M., Traversa, G., 1986. Petrology and Mineralogy of Miocene Fissural Volcanism of the East Kenya Plateau. Neues Jb Miner Abh 154, 153–178.

Bellieni, G., Visentin, E.J., Zanettin, B., Piccirillo, E.M., Radicati di Brozolo, F., Rita, F., 1981. Oligocene transitional tholeiitic magmatism in northern Turkana (Kenya): comparison with the coeval Ethiopian volcanism. Bull. Volcanol. 44, 411–427.

Bennett, M., Emblin, S., Robins, B., Yeo, W., 1986. High-temperature ultramafic complexes in the North-Norwegian Caledonides. I: Regional setting and field relationships. Bulletin-Norges geologiske undersokelse 1–40.

Berg, J.H., Klewin, K.W., 1988. High-MgO lavas from the Keewenawan midcontinent rift near Mamainse Point, Ontario. Geology 16, 1003–1006.

Blundy, J.D., Annen, C.J., 2016. Crustal magmatic systems from the perspective of heat transfer. Elements 12, 115–120.

Bohrson, W.A., Spera, F.J., 2001. Energy-constrained open-system magmatic processes II: Application of energy-constrained assimilation-fractional crystallization (EC-AFC) model to magmatic systems. J Petrol 42, 1019–1041.

Bohrson, W.A., Spera, F.J., Ghiorso, M.S., Brown, G.A., Creamer, J.B., Mayfield, A., 2014. Thermodynamic Model for Energy-Constrained Open-System Evolution of Crustal Magma Bodies Undergoing Simultaneous Recharge, Assimilation and Crystallization: the Magma Chamber Simulator. Journal of Petrology 55, 1685–1717. https://doi.org/10.1093/petrology/egu036

Bohrson, W.A., Spera, F.J., Ghiorso, M.S., Fowler, S.J., 2006. The Magma Chamber Simulator: A comprehensive tool for modeling the evolution of magmatic systems. AGUFM 2006, V11A-0566.

Bohrson, W.A., Spera, F.J., Heinonen, J.S., Brown, G.A., Scruggs, M.A., Adams, J.V., Takach, M.K., Zeff, G., Suikkanen, E., 2020. Diagnosing open-system magmatic processes using the Magma Chamber Simulator (MCS): part I—major elements and phase equilibria. Contributions to Mineralogy and Petrology 175, 1–29.

Boone, S.C., Kohn, B.P., Gleadow, A.J., Morley, C.K., Seiler, C., Foster, D.A., 2019. Birth of the East African Rift System: Nucleation of magmatism and strain in the Turkana Depression. Geology 47, 886–890.

Borges, M.R., Sen, G., Hart, G.L., Wolff, J.A., Chandrasekharam, D., 2014. Plagioclase as recorder of magma chamber processes in the Deccan Traps: Sr-isotope zoning and implications for Deccan eruptive event. Journal of Asian Earth Sciences 84, 95–101. https://doi.org/10.1016/j.jseaes.2013.10.034

Boschetto, H.B., Brown, F.H., McDougall, I., 1992. Stratigraphy of the Lothidok Range, northern Kenya, andK/Ar ages of its Miocene primates. Journal of Human Evolution 22, 47–71. https://doi.org/10.1016/0047-2484(92)90029-9

Bosworth, W., 1992. Mesozoic and early Tertiary rift tectonics in East Africa. Tectonophysics 209, 115–137. https://doi.org/10.1016/0040-1951(92)90014-W

Bosworth, W., Morley, C.K., 1994. Structural and stratigraphic evolution of the Anza rift, Kenya. Tectonophysics 236, 93–115.

Bougault, H., Hekinian, R., 1974. Rift Valley in the Atlantic Ocean near 36°50′N: petrology and geochemistry of basaltic rocks. Earth and Planetary Science Letters 24, 249–261. https://doi.org/10.1016/0012-821X(74)90103-4

Boyce, A., Bastow, I.D., Cottaar, S., Kounoudis, R., Guilloud De Courbeville, J., Caunt, E., Desai, S., 2021. AFRP20: New P-Wavespeed Model for the African Mantle Reveals Two Whole-Mantle Plumes Below East Africa and Neoproterozoic Modification of the Tanzania Craton. Geochemistry, Geophysics, Geosystems 22, e2020GC009302.

Boynton, W.V., 1984. Cosmochemistry of the Rare Earth Elements: Meteorite Studies, in: Developments in Geochemistry. Elsevier, pp. 63–114. https://doi.org/10.1016/B978-0-444-42148-7.50008-3

Bradshaw, R.W., Kent, A.J.R., 2017. The analytical limits of modeling short diffusion timescales. Chem. Geol. 466, 667–677. https://doi.org/10.1016/j.chemgeo.2017.07.018

Brotzu, P., Morbidelli, L., Nicoletti, M., Piccirillo, E.M., Traversa, G., 1984. Miocene to quaternary volcanism in eastern Kenya: Sequence and geochronology. Tectonophysics 101, 75–86. https://doi.org/10.1016/0040-1951(84)90043-X

Brown, F.H., Jicha, B.R., 2016. New high-precision 40Ar/39Ar ages on Oligocene volcanic rocks of northwestern Kenya. Journal of African Earth Sciences 114, 63–66. https://doi.org/10.1016/j.jafrearsci.2015.11.012

Brown, F.H., McDougall, I., 2011. Geochronology of the Turkana Depression of Northern Kenya and Southern Ethiopia. Evolutionary Anthropology: Issues, News, and Reviews 20, 217–227. https://doi.org/10.1002/evan.20318

Bryan, W.B., 1979. Regional Variation and Petrogenesis of Basalt Glasses from the FAMOUS Area, Mid-Atlantic Ridge. Journal of Petrology 20, 293–325. https://doi.org/10.1093/petrology/20.2.293

Camp, V.E., Reidel, S.P., Ross, M.E., Wolff, J.A., Martin, B.S., Tolan, T.L., Wells, R.E., 2013. Origin of Columbia River Basalt: Passive rise of shallow mantle, or active upwelling of a deep-mantle plume. The Columbia River Flood Basalt Province: Geological Society of America Special Paper 497, 181–199.

Campbell, I.H., Griffiths, R.W., 1990. Implications of mantle plume structure for the evolution of flood basalts. Earth Planet Sc Lett 99, 79–93.

Cashman, K.V., Sparks, R.S.J., Blundy, J.D., 2017. Vertically extensive and unstable magmatic systems: A unified view of igneous processes. Science 355, eaag3055. https://doi.org/10.1126/science.aag3055

Chambers, E.L., Harmon, N., Keir, D., Rychert, C.A., 2019. Using ambient noise to image the northern East African Rift. Geochemistry, Geophysics, Geosystems 20, 2091–2109.

Chang, S.-J., Kendall, E., Davaille, A., Ferreira, A.M., 2020. The evolution of mantle plumes in East Africa. Journal of Geophysical Research: Solid Earth 125, e2020JB019929.

Charlier, B., Namur, O., Latypov, R., Tegner, C. (Eds.), 2015. Layered Intrusions, Springer Geology. Springer Netherlands, Dordrecht. https://doi.org/10.1007/978-94-017-9652-1

Cherniak, D.J., 2010. Cation Diffusion in Feldspars. Reviews in Mineralogy and Geochemistry 72, 691–733. https://doi.org/10.2138/rmg.2010.72.15

Cherniak, D.J., Watson, E.B., 2020. Ti diffusion in feldspar. American Mineralogist 105, 1040–1051. https://doi.org/10.2138/am-2020-7272

Christensen, J.N., DePaolo, D.J., 1993. Time scales of large volume silicic magma systems: Sr isotopic systematics of phenocrysts and glass from the Bishop Tuff, Long Valley, California. Contrib. Mineral. Petrol. 113, 100–114. https://doi.org/10.1007/BF00320834

Cooper, K.M., Reid, M.R., 2008. Uranium-series crystal ages. Reviews in Mineralogy and Geochemistry 69, 479–544.

Costa, F., Dungan, M., 2005. Short time scales of magmatic assimilation from diffusion modeling of multiple elements in olivine. Geology 33, 837–840. https://doi.org/10.1130/G21675.1

Costa, F., Shea, T., Ubide, T., 2020. Diffusion chronometry and the timescales of magmatic processes. Nat. Rev. Earth Environ. 1, 201–214. https://doi.org/10.1038/s43017-020-0038-x

Corti, G., Cioni, R., Franceschini, Z., Sani, F., Scaillet, S., Molin, P., Isola, I., Mazzarini, F., Brune, S., Keir, D., Erbello, A., Muluneh, A., Illsley-Kemp, F., Glerum, A., 2019. Aborted propagation of the Ethiopian rift caused by linkage with the Kenyan rift. Nat Commun 10, 1309. https://doi.org/10.1038/s41467-019-09335-2

Cox, K.G., 1980. A Model for Flood Basalt Vulcanism. Journal of Petrology 21, 629–650. https://doi.org/10.1093/petrology/21.4.629

Danyushevsky, L.V., 2002. Melt Inclusions in Olivine Phenocrysts: Using Diffusive Re-equilibration to Determine the Cooling History of a Crystal, with Implications for the Origin of Olivine-phyric Volcanic Rocks. J. Petrol. 43, 1651–1671. https://doi.org/10.1093/petrology/43.9.1651

Danyushevsky, L.V., Della-Pasqua, F.N., Sokolov, S., 2000. Re-equilibration of melt inclusions trapped by magnesian olivine phenocrysts from subduction-related magmas: petrological implications. Contrib. Mineral. Petrol. 138, 68–83. https://doi.org/10.1007/PL00007664

Davidson, A., Moore, J., Davies, J., Alemu Shiferaw, M.T., 1973. Preliminary report on the geology and geochemistry of parts of Sidamo, Gemu Gofa, and Kefa Provinces. Rept. Omo River Project 1.

Davidson, A., Rex, D.C., 1980. Age of volcanism and rifting in southwestern Ethiopia. Nature 283, 657–658. https://doi.org/10.1038/283657a0

Davidson, A.C., 1983. The Omo RIver Project, Reconaissance geology and geochemistry of parts of Ilubabor, Kefa, Gemi Gofa, and Sidamo. Ministry of Mines and Energy: Ethiopian Institute of Geological Surveys Bulletin 2, 1–89.

Davis, W.R., Collins, M.A., Rooney, T.O., Brown, E.L., Stein, C.A., Stein, S., Moucha, R., 2021. Geochemical, petrographic, and stratigraphic analyses of the Portage Lake Volcanics of the Keweenawan CFBP: implications for the evolution of main stage volcanism in continental flood basalt provinces. Geological Society, London, Special Publications SP518-2020–221. https://doi.org/10.1144/SP518-2020-221

De Min, A., Callegaro, S., Marzoli, A., Nardy, A.J., Chiaradia, M., Marques, L.S., Gabbarrini, I., 2018. Insights into the petrogenesis of low-and high-Ti basalts: Stratigraphy and geochemistry of four lava sequences from the central Paraná basin. Journal of Volcanology and Geothermal Research 355, 232–252.

Demouchy, S., Jacobsen, S.D., Gaillard, F., Stern, C.R., 2006. Rapid magma ascent recorded by water diffusion profiles in mantle olivine. Geology 34, 429. https://doi.org/10.1130/G22386.1

Ding, X., Ripley, E.M., Li, C., 2012. PGE geochemistry of the Eagle Ni–Cu–(PGE) deposit, Upper Michigan: constraints on ore genesis in a dynamic magma conduit. Mineralium Deposita 47, 89–104. https://doi.org/10.1007/s00126-011-0350-y

Dohmen, R., Blundy, J., 2014. A predictive thermodynamic model for element partitioning between plagioclase and melt as a function of pressure, temperature and composition. American Journal of Science 314, 1319–1372.

Dohmen, R., Chakraborty, S., 2007. Fe–Mg diffusion in olivine II: point defect chemistry, change of diffusion mechanisms and a model for calculation of diffusion coefficients in natural olivine. Phys. Chem. Miner. 34, 409–430. https://doi.org/10.1007/s00269-007-0158-6

Dufek, J., Bergantz, G.W., 2005. Lower crustal magma genesis and preservation: A stochastic framework for the evaluation of basalt-crust interaction. J Petrol 46, 2167–2195.

Duraiswami, R., Bondre, N., Dole, G., Phadnis, V., Kale, V., 2001. Tumuli and associated features from the western Deccan Volcanic Province, India. Bulletin of Volcanology 63, 435–442. https://doi.org/10.1007/s004450100160

Ebinger, C.J., 2020. Recipe for Rifting: Flavors of East Africa.

Ebinger, C.J., Keir, D., Bastow, I.D., Whaler, K., Hammond, J.O., Ayele, A., Miller, M.S., Tiberi, C., Hautot, S., 2017. Crustal structure of active deformation zones in Africa: Implications for global crustal processes. Tectonics 36, 3298–3332.

Ebinger, C.J., Sleep, N.H., 1998. Cenozoic magmatism throughout east Africa resulting from impact of a single plume. Nature 395, 788–791. https://doi.org/10.1038/27417

Ebinger, C.J., Yemane, T., Kelley, S., Rex, D.C., 2000. Rift deflection, migration, and propagation: Linkage of the Ethiopian and Eastern rifts, Africa. Geological Society of America Bulletin 14.

Ebinger, C.J., Yemane, T., Woldegabriel, G., Aronson, J.L., Walter, R.C., 1993. Late Eocene–Recent volcanism and faulting in the southern main Ethiopian rift. Journal of the Geological Society 150, 99–108. https://doi.org/10.1144/gsjgs.150.1.0099

Elkins-Tanton, L.T., Draper, D.S., Agee, C.B., Jewell, J., Thorpe, A., Hess, P.C., 2007. The last lavas erupted during the main phase of the Siberian flood volcanic province: results from experimental petrology. Contrib Mineral Petr 153, 191–209.

Emishaw, L., Abdelsalam, M.G., 2019. Development of Late Jurassic-Early Paleogene and Neogene-Quaternary Rifts Within the Turkana Depression, East Africa From Satellite Gravity Data. Tectonics 38, 2358–2377.

Ernst, R.E., 2014. Large Igneous Provinces. Cambridge University Press, Cambridge, United Kingdom.

Ewart, A., Griffin, W.L., 1994. Application of proton-microprobe data to trace-element partitioning in volcanic rocks. Chemical Geology 117, 251–284.

Faccenna, C., Glišović, P., Forte, A., Becker, T.W., Garzanti, E., Sembroni, A., Gvirtzman, Z., 2019. Role of dynamic topography in sustaining the Nile River over 30 million years. Nat. Geosci 12, 1012–1017.

Farnetani, C.G., Richards, M.A., Ghiorso, M.S., 1996. Petrological models of magma evolution and deep crustal structure beneath hotspots and flood basalt provinces. Earth Planet Sc Lett 143, 81–94.

Ferguson, D.J., Maclennan, J., Bastow, I.D., Pyle, D.M., Jones, S.M., Keir, D., Blundy, J.D., Plank, T., Yirgu, G., 2013. Melting during late-stage rifting in Afar is hot and deep. Nature 499, 70–73. https://doi.org/10.1038/nature12292 http://www.nature.com/nature/journal/v499/n7456/abs/nature12292.html#supplementary-information

Furman, T., Kaleta, K.M., Bryce, J.G., Hanan, B.B., 2006. Tertiary Mafic Lavas of Turkana, Kenya: Constraints on East African Plume Structure and the Occurrence of High-μ Volcanism in Africa. Journal of Petrology 47, 1221–1244. https://doi.org/10.1093/petrology/egl009

Furman, T., Graham, D., 1999. Erosion of lithospheric mantle beneath the East African Rift system: geochemical evidence from the Kivu volcanic province 26.

Furman, T., Nelson, W.R., Elkins-Tanton, L.T., 2016. Evolution of the East African rift: Drip magmatism, lithospheric thinning and mafic volcanism. Geochimica et Cosmochimica Acta 185, 418–434. https://doi.org/10.1016/j.gca.2016.03.024

Gathogo, P.N., Brown, F.H., McDougall, I., 2008. Stratigraphy of the Koobi Fora Formation (Pliocene and Pleistocene) in the Loiyangalani region of northern Kenya. Journal of African Earth Sciences 51, 277–297. https://doi.org/10.1016/j.jafrearsci.2008.01.010

George, R., Rogers, N., 2002. Plume dynamics beneath the African plate inferred from the geochemistry of the Tertiary basalts of southern Ethiopia. Contributions to Mineralogy and Petrology 144, 286–304. https://doi.org/10.1007/s00410-002-0396-z

George, R., Rogers, N., Kelley, S., 1998. Earliest magmatism in Ethiopia: Evidence for two mantle plumes in one flood basalt province. Geology 26, 923. https://doi.org/10.1130/0091-7613(1998)026<0923:EMIEEF>2.3.CO;2

Giletti, B.J., Casserly, J.E.D., 1994. Strontium diffusion kinetics in plagioclase feldspars. Geochimica et Cosmochimica Acta 58, 3785–3793.

Grant, T.B., Larsen, R.B., Anker-Rasch, L., Grannes, K.R., Iljina, M., McEnroe, S., Nikolaisen, E., Schanche, M., Øen, E., 2016. Anatomy of a deep crustal volcanic conduit system; the Reinfjord ultramafic complex, Seiland Igneous Province, northern Norway. Lithos 252, 200–215.

Green, T.H., Blundy, J.D., Adam, J., Yaxley, G.M., 2000. SIMS determination of trace element partition coefficients between garnet, clinopyroxene and hydrous basaltic liquids at 2–7.5 GPa and 1080–1200 C. Lithos 53, 165–187.

Griselin, M., Arndt, N.T., Baragar, W.R.A., 1997. Plume–lithosphere interaction and crustal contamination during formation of Coppermine River basalts, Northwest Territories, Canada. Can. J. Earth Sci. 34, 958–975. https://doi.org/10.1139/e17-080

Grove, T.L., Baker, M.B., Kinzler, R.J., 1984. Coupled CaAl-NaSi diffusion in plagioclase feldspar: Experiments and applications to cooling rate speedometry. Geochimica et Cosmochimica Acta 48, 2113–2121. https://doi.org/10.1016/0016-7037(84)90391-0

Guth, A.L., 2013. Spatial and Temporal Evolution of the Volcanics and Sediments of the Kenya Rift. Michigan Technological University.

Gualda, G.A.R., Ghiorso, M.S., 2015. MELTS_Excel: AMicrosoft Excel-based MELTS interface for research and teaching of magma properties and evolution. Geochemistry, Geophysics, Geosystems 16, 315–324. https://doi.org/10.1002/2014GC005545

Hackman, B.D., Charsley, T.J., Key, R.M., Wilkinson, A.F., 1990. The development of the East African Rift system in north-central Kenya. Tectonophysics 184, 189–211. https://doi.org/10.1016/0040-1951(90)90053-B

Hansen, H., Grönvold, K., 2000. Plagioclase ultraphyric basalts in Iceland: the mush of the rift. J. Volcanol. Geotherm. Res. 98, 1–32. https://doi.org/10.1016/S0377-0273(99)00189-4

Harry, D.L., Sawyer, D.S., 1992. Basaltic volcanism, mantle plumes, and the mechanics of rifting: The Parana flood basalt province of South America. Geology 20, 207–210.

Hawkesworth, C.J., Blake, S., Evans, P., Hughes, R., Macdonald, R., Thomas, L.E., Turner, S.P., Zellmer, G., 2000. Time Scales of Crystal Fractionation in Magma Chambers—Integrating Physical, Isotopic and Geochemical Perspectives. J. Petrol. 41, 991–1006. https://doi.org/10.1093/petrology/41.7.991

Hendrie, D.B., Kusznir, N.J., Morley, C.K., Ebinger, C.J., 1994. Cenozoic extension in Northern Kenya - A quantitative model of rift basin development in the Turkana region. Tectonophysics 236, 409–438.

Hibbard, M.J., 1995. Petrography to petrogenesis.

Higgins, M.D., Chandrasekharam, D., 2007. Nature of Sub-volcanic Magma Chambers, Deccan Province, India: Evidence from Quantitative Textural Analysis of Plagioclase Megacrysts in the Giant Plagioclase Basalts. Journal of Petrology 48, 885–900. https://doi.org/10.1093/petrology/egm005

Hofmann, C., Courtillot, V., Féraud, G., Rochette, P., Yirgu, G., Ketefo, E., Pik, R., 1997. Timing of the Ethiopian flood basalt event and implications for plume birth and global change. Nature 389, 838–841. https://doi.org/10.1038/39853

Itaya, T., Sawada, Y., 1987. K-Ar ages of volcanic rocks in the Samburu Hills area, northern Kenya.

Jean, M.M., Shervais, J.W., Champion, D.E., Vetter, S.K., 2013. Geochemical and paleomagnetic variations in basalts from the Wendell Regional Aquifer Systems Analysis (RASA) drill core: Evidence for magma recharge and assimilation–fractional crystallization from the central Snake River Plain, Idaho. Geosphere 9, 1319. https://doi.org/10.1130/GES00914.1

Jerram, D., Mountney, N., Holzförster, F., Stollhofen, H., 1999. Internal stratigraphic relationships in the Etendeka group in the Huab Basin, NW Namibia: understanding the onset of flood volcanism. Journal of Geodynamics 28, 393–418. https://doi.org/10.1016/S0264-3707(99)00018-6

Jerram, D.A., Mountney, N.P., Howell, J.A., Long, D., Stollhoffen, H., 2000. Death of a sand sea: an active aeolian erg systematically buried by the Etendeka flood basalts of NW Namibia. Journal of the Geological Society 157, 513. https://doi.org/10.1144/jgs.157.3.513

Jerram, D.A., Widdowson, M., 2005. The anatomy of Continental Flood Basalt Provinces: geological constraints on the processes and products of flood volcanism. Lithos 79, 385–405. https://doi.org/10.1016/j.lithos.2004.09.009

Kappelman, J., Tab Rasmussen, D., Sanders, W.J., Feseha, M., Bown, T., Copeland, P., Crabaugh, J., Fleagle, J., Glantz, M., Gordon, A., Jacobs, B., Maga, M., Muldoon, K., Pan, A., Pyne, L., Richmond, B., Ryan, T., Seiffert, E.R., Sen, S., Todd, L., Wiemann, M.C., Winkler, A., 2003. Oligocene mammals from Ethiopia and faunal exchange between Afro-Arabia and Eurasia. Nature 426, 549–552. http://www.nature.com/nature/journal/v426/n6966/suppinfo/nature02102_S1.html

Karakas, O., Dufek, J., 2015. Melt evolution and residence in extending crust: Thermal modeling of the crust and crustal magmas. Earth and Planetary Science Letters 425, 131–144. https://doi.org/10.1016/j.epsl.2015.06.001

Karlstrom, L., Richards, M., 2011. On the evolution of large ultramafic magma chambers and timescales for flood basalt eruptions. Journal of Geophysical Research: Solid Earth 116.

Kent, A.J.R., 2008. Melt Inclusions in Basaltic and Related Volcanic Rocks. Rev. Mineral. Geochem. 69, 273–331. https://doi.org/10.2138/rmg.2008.69.8

Key, R.M., Watkins, R.T., 1988. Geology of the Sabarei area. Republic of Kenya Ministry of Environment and Natural Resources, Mines and Geological Department Report 111.

Kieffer, B., Arndt, N., Lapierre, H., Bastien, F., Bosch, D., Pecher, A., Yirgu, G., Ayalew, D., Weis, D., Jerram, D.A., Keller, F., Meugniot, C., 2004. Flood and Shield Basalts from Ethiopia: Magmas from the African Superswell. Journal of Petrology 45, 793–834. https://doi.org/10.1093/petrology/egg112

Kimura, J.-I., Kawabata, H., 2015. Ocean B asalt S imulator version 1 (OBS 1): Trace element mass balance in adiabatic melting of a pyroxenite-bearing peridotite. Geochemistry, Geophysics, Geosystems 16, 267–300.

Kounoudis, R., Bastow, I.D., Ebinger, C.J., Ogden, C.S., Ayele, A., Bendick, R., Mariita, N., Kianji, G., Wigham, G., Musila, M., Kibret, B., 2021. Body-wave tomographic imaging of the Turkana Depression: Implications for rift development and plume-lithosphere interactions. Geochem Geophys Geosyst. https://doi.org/10.1029/2021GC009782

Krans, S.R., Rooney, T.O., Kappelman, J., Yirgu, G., Ayalew, D., 2018. From initiation to termination: a petrostratigraphic tour of the Ethiopian Low-Ti Flood Basalt Province. Contributions to Mineralogy and Petrology 173. https://doi.org/10.1007/s00410-018-1460-7

Larsen, R.B., Grant, T., Sørensen, B.E., Tegner, C., McEnroe, S., Pastore, Z., Fichler, C., Nikolaisen, E., Grannes, K.R., Church, N., ter Maat, G.W., Michels, A., 2018. Portrait of a giant deep-seated magmatic conduit system: The Seiland Igneous Province. Lithos 296–299, 600–622. https://doi.org/10.1016/j.lithos.2017.11.013

Lassiter, J.C., DePAOLO, D.J., Mahoney, J.J., 1995. Geochemistry of the Wrangellia Flood Basalt Province: Implications for the Role of Continental and Oceanic Lithosphere in Flood Basalt Genesis. Journal of Petrology 36, 983–1009. https://doi.org/10.1093/petrology/36.4.983

Latypov, R., Chistyakova, S., Costin, G., Namur, O., Barnes, S., Kruger, W., 2020. Monomineralic anorthosites in layered intrusions are indicators of the magma chamber replenishment by plagioclase-only-saturated melts. Scientific reports 10, 1–14.

Lavayssière, A., Rychert, C., Harmon, N., Keir, D., Hammond, J.O., Kendall, J.-M., Doubre, C., Leroy, S., 2018. Imaging lithospheric discontinuities beneath the Northern East African Rift using S-to-P receiver functions. Geochemistry, Geophysics, Geosystems 19, 4048–4062.

Le Bas, M.J., Le Maitre, R.W., Streckeisen, A., Zanettin, B., 1986. A chemical classification of volcanic rocks based on total Alkali-Silica diagram. J. Petrol. 27, 745–750.

Lee, C.-T.A., Lee, T.C., Wu, C.-T., 2014. Modeling the compositional evolution of recharging, evacuating, and fractionating (REFC) magma chambers: Implications for differentiation of arc magmas. Geochimica et Cosmochimica Acta 143, 8–22. https://doi.org/10.1016/j.gca.2013.08.009

Li, W., Chakraborty, S., Nagashima, K., Costa, F., 2020. Multicomponent diffusion of F, Cl and OH in apatite with application to magma ascent rates. Earth Planet. Sci. Lett. 550, 116545. https://doi.org/10.1016/j.epsl.2020.116545

Lightfoot, P.C., Naldrett, A.J., Gorbachev, N.S., Doherty, W., Fedorenko, V.A., 1990. Geochemistry of the Siberian Trap of the Noril'sk area, USSR, with implications for the relative contributions of crust and mantle to flood basalt magmatism. Contr. Mineral. and Petrol. 104, 631–644. https://doi.org/10.1007/BF01167284

Lissenberg, C.J., MacLeod, C.J., 2016. A Reactive Porous Flow Control on Mid-ocean Ridge Magmatic Evolution. J. Petrol. 57, 2195–2220. https://doi.org/10.1093/petrology/egw074

Liu, M., Yund, R.A., 1992. NaSi-CaAl interdiffusion in plagioclase. American Mineralogist 77, 275–283.

Lynn, K.J., Garcia, M.O., Shea, T., Costa, F., Swanson, D.A., 2017. Timescales of mixing and storage for Keanakāko'i Tephra magmas (1500–1820 C.E.), Kīlauea Volcano, Hawai'i. Contrib. Mineral. Petrol. 172, 76. https://doi.org/10.1007/s00410-017-1395-4

Maguire, P.K.H., Keller, G.R., Klemperer, S.L., Mackenzie, G.D., Keranen, K., Harder, S., O'Reilly, B., Thybo, H., Asfaw, L., Khan, M.A., Amha, M., 2006. Crustal structure of the northern Main Ethiopian Rift from the EAGLE controlled-source survey; a snapshot of incipient lithospheric break-up. Geological Society, London, Special Publications 259, 269–292. https://doi.org/10.1144/GSL.SP.2006.259.01.21

Maitre, L., 1989. A classification of igneous rocks and glossary of terms. Recommendations of the international union of geological sciences subcommission on the systematics of igneous rocks 193.

Marsh, B.D., 1996. Solidification fronts and magmatic evolution. Mineral. Mag. 60, 5–40. https://doi.org/10.1180/minmag.1996.060.398.03

McCallum, I.S., Charette, M.P., 1978. Zr and Nb partition coefficients: Implications for the genesis of mare basalts, KREEP and sea floor basalts. Geochimica et Cosmochimica Acta 42, 859–869. https://doi.org/10.1016/0016-7037(78)90098-4

McDougall, I., Brown, F.H., 2009. Timing of volcanism and evolution of the northern Kenya Rift. Geological Magazine 146, 34–47.

McDougall, I., Watkins, R.T., 2006. Geochronology of the Nabwal Hills: a record of earliest magmatism in the northern Kenyan Rift Valley. Geological Magazine 143, 25–39. https://doi.org/10.1017/S0016756805001184

McKenzie, D., O'Nions, R.K., 1991. Partial Melt Distributions from Inversion of Rare-Earth Element Concentrations. J Petrol 32, 1021–1091.

Metrich, N., Wallace, P.J., 2008. Volatile Abundances in Basaltic Magmas and Their Degassing Paths Tracked by Melt Inclusions, in: Putirka, K.D., Tepley, F.J. (Eds.), Minerals, Inclusions and Volcanic Processes, Reviews in Mineralogy & Geochemistry. pp. 363–402

Mechie, J., Keller, G.R., Prodehl, C., Gaciri, S., Braile, L.W., Mooney, W.D., Gajewski, D., Sandmeier, K.-J., 1994. Crustal structure beneath the Kenya Rift from axial profile data. Tectonophysics 236, 179–200.

Miller Jr, J., Ripley, E., 1996. Layered intrusions of the Duluth complex, Minnesota, USA. Layered intrusions 257–301.

Miller Jr, J.D., Weiblen, P.W., 1990. Anorthositic rocks of the Duluth Complex: Examples of rocks formed from plagioclase crystal mush. Journal of Petrology 31, 295–339.

Mohr, P., 1983. Ethiopian flood basalt province. Nature 303, 577–584.

Mohr, P., Zanettin, B., 1988. The Ethiopian flood basalt province, in: MacDougall, J.D. (Ed.), Continental Flood Basalts. Kluwer Academic, Dordrecht, pp. 63–110.

Montési, L.G., 2013. Fabric development as the key for forming ductile shear zones and enabling plate tectonics. Journal of Structural Geology 50, 254–266.

Morley, C.K., Bosworth, W., Day, R.A., Lauck, R., Bosher, R., Stone, D.M., Wigger, S.T., Wescott, W.A., Haun, D., Bassett, N., 1999a. AAPG Studies in Geology# 44, Chapter 4: Geology and Geophysics of the Anza Graben.

Morley, C.K., Karanja, F.M., Wescott, W.A., Stone, D.M., Harper, R.M., Wigger, S.T., Day, R.A., 1999b. AAPG Studies in Geology# 44, Chapter 2: Geology and Geophysics of the Western Turkana Basins, Kenya.

Morley, C.K., Wescott, W.A., Stone, D.M., Harper, R.M., Wigger, S.T., Karanja, F.M., 1992. Tectonic evolution of the Northern Kenyan rift. Journal of the Geological Society 149, 333–348.

Morse, S.A., 2011. The fractional latent heat of crystallizing magmas. Am. Mineral. 96, 682–689. https://doi.org/10.2138/am.2011.3613

Morse, S.A., 1980. Basalts and phase diagrams: an introduction to the quantitative use of phase diagrams in igneous petrology. Springer-Verlag.

Mungall, J.E., Kamo, S.L., McQuade, S., 2016. U–Pb geochronology documents out-of-sequence emplacement of ultramafic layers in the Bushveld Igneous Complex of South Africa. Nature Communications 7, 1–13.

Nakamura, M., 1995. Continuous mixing of crystal mush and replenished magma in the ongoing Unzen eruption. Geology 23, 807–810. https://doi.org/10.1130/0091-7613(1995)023<0807:cmocma>2.3.co;2

Naldrett, A.J., 2010. Secular Variation of Magmatic Sulfide Deposits and Their Source Magmas. Economic Geology 105, 669–688. https://doi.org/10.2113/gsecongeo.105.3.669

Natali, C., Beccaluva, L., Bianchini, G., Ellam, R.M., Savo, A., Siena, F., Stuart, F.M., 2016. High-MgO lavas associated to CFB as indicators of plume-related thermochemical effects: The case of ultra-titaniferous picrite–basalt from the Northern Ethiopian–Yemeni Plateau. Gondwana Research 34, 29–48.

Natali, C., Beccaluva, L., Bianchini, G., Siena, F., 2013. The Axum–Adwa basalt–trachyte complex: a late magmatic activity at the periphery of the Afar plume. Contrib Mineral Petr 166, 351–370. https://doi.org/10.1007/s00410-013-0879-0

Natali, C., Beccaluva, L., Bianchini, G., Siena, F., 2011. Rhyolites associated to Ethiopian CFB: clues for initial rifting at the Afar plume axis. Earth Planet Sc Lett 312, 59–68.

Nelson, W.R., Hanan, B., Graham, D.W., Shirey, S.B., Yirgu, G., Ayalew, D., Furman, T., 2019. Distinguishing plume and metasomatized lithospheric mantle contributions to post-flood basalt volcanism on the southeastern Ethiopian Plateau. Journal of Petrology.

Nielsen, R.L., Gallahan, W.E., Newberger, F., 1992. Experimentally determined mineral-melt partition coefficients for Sc, Y and REE for olivine, orthopyroxene, pigeonite, magnetite and ilmenite. Contributions to Mineralogy and Petrology 110, 488–499.

Nielsen, R.L., Ustunisik, G., Lange, A.E., Tepley, F.J., Kent, A.J.R., 2020. Trace Element and Isotopic Characteristics of Plagioclase Megacrysts in Plagioclase Ultraphyric Basalts (PUB). Geochem. Geophys. Geosyst. 21. https://doi.org/10.1029/2019GC008638

Nielsen, R.L., Ustunisik, G., Weinsteiger, A.B., Tepley, F.J., Johnston, A.D., Kent, A.J.R., 2017. Trace element partitioning between plagioclase and melt: An investigation of the impact of experimental and analytical procedures: IMPACT OF ANALYTICAL PROCEDURES ON D. Geochem. Geophys. Geosyst. 18, 3359–3384. https://doi.org/10.1002/2017GC007080

Nishimura, K., 2020. Open-system Magma Chamber Processes under Equilibrium Crystallization Conditions. Journal of Toyo University Natural Sciences 64, 33–51. http://id.nii.ac.jp/1060/00011481/

Nishimura, K., 2019. Chemical mass balance equations for open-system magma chamber processes that result in crystal zoning. Journal of Volcanology and Geothermal Research 374, 181–196. https://doi.org/10.1016/j.jvolgeores.2019.02.012

Nishimura, K., 2009. A trace-element geochemical model for imperfect fractional crystallization associated with the development of crystal zoning. Geochimica et Cosmochimica Acta 73, 2142–2149. https://doi.org/10.1016/j.gca.2009.01.011

O'Neill, H.S.C., Jenner, F.E., 2012. The global pattern of trace-element distributions in ocean floor basalts. Nature 491, 698–704. https://doi.org/10.1038/nature11678

Óskarsson, B.V., Andersen, C.B., Riishuus, M.S., Sørensen, E.V., Tegner, C., 2017. The mode of emplacement of Neogene flood basalts in Eastern Iceland: The plagioclase ultraphyric basalts in the Grænavatn group. Journal of Volcanology and Geothermal Research 332, 26–50.

Paces, J.B., 1990. Magmatic processes, evolution and mantle source characteristics contributing to the petrogenesis of midcontinent rift basalts: Portage Lake volcanics, Keweenaw Peninsula, Michigan.

Paster, T.P., Schauwecker, D.S., Haskin, L.A., 1974. The behavior of some trace elements during solidification of the Skaergaard layered series. Geochimica et Cosmochimica Acta 38, 1549–1577. https://doi.org/10.1016/0016-7037(74)90174-4

Pearce, T.H., 1994. Recent work on oscillatory zoning in plagioclase, in: Feldspars and Their Reactions. Springer, pp. 313–349.

Pearce, T.H., Kolisnik, A.M., 1990. Observations of plagioclase zoning using interference imaging. Earth-Science Reviews 29, 9–26.

Peng, Z.X., Mahoney, J., Hooper, P., Harris, C., Beane, J., 1994. A role for lower continental crust in flood basalt genesis? Isotopic and incompatible element study of the lower six formations of the western Deccan Traps. Geochimica et Cosmochimica Acta 58, 267–288. https://doi.org/10.1016/0016-7037(94)90464-2

Pik, R., Deniel, C., Coulon, C., Yirgu, G., Hofmann, C., Ayalew, D., 1998. The northwestern Ethiopian Plateau flood basalts: Classification and spatial distribution of magma types. Journal of Volcanology and Geothermal Research 81, 91–111. https://doi.org/10.1016/S0377-0273(97)00073-5

Pik, R., Deniel, C., Coulon, C., Yirgu, G., Marty, B., 1999. Isotopic and trace element signatures of Ethiopian flood basalts; evidence for plume-lithosphere interactions. Geochim Cosmochim Ac 63, 2263–2279.

Pik, R., Marty, B., Carignan, J., Yirgu, G., Ayalew, T., 2008. Timing of East African Rift development in southern Ethiopia: Implication for mantle plume activity and evolution of topography. Geology 36, 167–170.

Priestley, K., McKenzie, D., Debayle, E., Pilidou, S., 2008. The African upper mantle and its relationship to tectonics and surface geology. Geophys J Int 175, 1108–1126.

Purcell, P.G., 2018. Re-imagining and re-imaging the development of the East African Rift. Petroleum Geoscience 24, 21–40. https://doi.org/10.1144/petgeo2017-036

Putirka, K.D., 2008. Thermometers and barometers for volcanic systems. Reviews in Mineralogy and Geochemistry 69, 61–120.

Rasmussen, D.J., Plank, T.A., Wallace, P.J., Newcombe, M.E., Lowenstern, J.B., 2020. Vapor-bubble growth in olivine-hosted melt inclusions. Am. Mineral. 105, 1898–1919. https://doi.org/10.2138/am-2020-7377

Reed, C.A., Gao, S.S., Liu, K.H., Yu, Y., 2016. The mantle transition zone beneath the Afar Depression and adjacent regions: Implications for mantle plumes and hydration. Geophysical Journal International 205, 1756–1766.

Ridley, V.A., Richards, M.A., 2010. Deep crustal structure beneath large igneous provinces and the petrologic evolution of flood basalts. Geochemistry, Geophysics, Geosystems 11. https://doi.org/10.1029/2009GC002935

Ringwood, A.E., Essene, E., 1970. Petrogenesis of Apollo 11 basalts, internal constitution and origin of the moon. Geochimica et Cosmochimica Acta Supplement 1, 769.

Rochette, P., Tamrat, E., Féraud, G., Pik, R., Courtillot, V., Ketefo, E., Coulon, C., Hoffmann, C., Vandamme, D., Yirgu, G., 1998. Magnetostratigraphy and timing of the Oligocene Ethiopian traps. Earth and Planetary Science Letters 164, 497–510. https://doi.org/10.1016/S0012-821X(98)00241-6

Robb, S.J., Mungall, J.E., 2020. Testing emplacement models for the Rustenburg Layered Suite of the Bushveld Complex with numerical heat flow models and plagioclase geospeedometry. Earth and Planetary Science Letters 534, 116084.

Rogers, N.W., Thomas, L.E., Macdonald, R., Hawkesworth, C.J., Mokadem, F., 2006. U-238-Th-230 disequilibrium in recent basalts and dynamic melting beneath the Kenya rift. Chem Geol 234, 148–168. https://doi.org/DOI 10.1016/j.chemgeo.2006.05.002

Rooney, T., Franceschi, P., Hall, C., 2011. Water-saturated magmas in the Panama Canal region: a precursor to adakite-like magma generation? Contrib Mineral Petr 161, 373–388. https://doi.org/10.1007/s00410-010-0537-8

Rooney, T.O., 2020a. The Cenozoic magmatism of East Africa: Part II – Rifting of the mobile belt. Lithos 360–361, 105291. https://doi.org/10.1016/j.lithos.2019.105291

Rooney, T.O., 2020b. The Cenozoic magmatism of East Africa: Part III – Rifting of the craton. Lithos 105390. https://doi.org/10.1016/j.lithos.2020.105390

Rooney, T.O., 2020c. The Cenozoic Magmatism of East Africa: Part IV–The Terminal Stages of Rifting Preserved in the Northern East African Rift System. Lithos 105381.

Rooney, T.O., 2020c. The Cenozoic magmatism of East Africa: part V–magma sources and processes in the East African Rift. Lithos 360, 105296.

Rooney, T.O., 2017. The Cenozoic magmatism of East-Africa: Part I — Flood basalts and pulsed magmatism. Lithos 286–287, 264–301. https://doi.org/10.1016/j.lithos.2017.05.014

Rooney, T.O., 2010. Geochemical evidence of lithospheric thinning in the southern Main Ethiopian Rift. Lithos 117, 33–48. https://doi.org/10.1016/j.lithos.2010.02.002

Rooney, T.O., Herzberg, C., Bastow, I.D., 2012. Elevated mantle temperature beneath East Africa. Geology 40, 27–30. https://doi.org/10.1130/G32382.1

Rooney, T.O., Lavigne, A., Svoboda, C., Girard, G., Yirgu, G., Ayalew, D., Kappelman, J., 2017. The making of an underplate: Pyroxenites from the Ethiopian lithosphere. Chemical Geology 455, 264–281.

Rooney, T.O., Morell, K.D., Hidalgo, P., Fraceschi, P., 2015. Magmatic consequences of the transition from orthogonal to oblique subduction in P anama. Geochemistry, Geophysics, Geosystems 16, 4178–4208. https://doi.org/10.1002/2015GC006150

Rooney, T.O., Nelson, W.R., Ayalew, D., Hanan, B., Yirgu, G., Kappelman, J., 2017. Melting the lithosphere: Metasomes as a source for mantle-derived magmas. Earth and Planetary Science Letters 461, 105–118. https://doi.org/10.1016/j.epsl.2016.12.010

Rooney, T.O., Nelson, W.R., Dosso, L., Furman, T., Hanan, B., 2014. The role of continental lithosphere metasomes in the production of HIMU-like magmatism on the northeast African and Arabian plates. Geology 42, 419–422. https://doi.org/10.1130/G35216.1

Rudnick, R., Gao, S., 2003. Composition of the continental crust, in: Rudnick, R. (Ed.), The Crust, Treatise on Geochemistry. Elsevier-Pergamon, Oxford, pp. 1–64.

Schmeling, H., Wallner, H., 2012. Magmatic lithospheric heating and weakening during continental rifting: A simple scaling law, a 2-D thermomechanical rifting model and the East African Rift System. Geochemistry, Geophysics, Geosystems 13.

Schoene, B., Eddy, M.P., Samperton, K.M., Keller, C.B., Keller, G., Adatte, T., Khadri, S.F., 2019. U-Pb constraints on pulsed eruption of the Deccan Traps across the end-Cretaceous mass extinction. Science 363, 862–866.

Self, S., Thordarson, T., Keszthelyi, L., 1997. Emplacement of continental flood basalt lava flows. Geophysical Monograph-AGU 100, 381–410.

Self, S., Thordarson, T., Widdowson, M., 2005. Gas fluxes from flood basalt eruptions. Elements 1, 283–287.

Shaw, D.M., 2006. Trace elements in magmas: a theoretical treatment. Cambridge University Press.

Shcherbakov, V.D., Plechov, P.Yu., Izbekov, P.E., Shipman, J.S., 2011. Plagioclase zoning as an indicator of magma processes at Bezymianny Volcano, Kamchatka. Contrib Mineral Petrol 162, 83–99. https://doi.org/10.1007/s00410-010-0584-1

Singer, B.S., Dungan, M.A., Layne, G.D., 1995. Textures and Sr, Ba, Mg, Fe, K, and Ti compositional profiles in volcanic plagioclase: clues to the dynamics of calc-alkaline magma chambers. American Mineralogist 80, 776–798.

Singer, B.S., Smith, K.E., Jicha, B.R., Beard, B.L., Johnson, C.M., Rogers, N.W., 2011. Tracking open-system differentiation during growth of Santa María volcano, Guatemala. J Petrol 52, 2335–2363.

Spera, F.J., Bohrson, W.A., 2001. Energy-constrained open-system magmatic processes I: General model and energy-constrained assimilation and fractional crystallization (EC-AFC) formulation. J Petrol 42, 999–1018.

Steiner, A., Streck, M.J., 2019. Voluminous and compositionally diverse, middle Miocene Strawberry Volcanics of NE Oregon: Magmatism cogenetic with flood basalts of the Columbia River Basalt Group, in: Field Volcanology: A Tribute to the Distinguished Career of Don Swanson. Geological Society of America. https://doi.org/10.1130/2018.2538(03)

Steiner, R.A., Rooney, T.O., Girard, G., Rogers, N., Ebinger, C., Peterson, L., Phillips, R., 2021. Initial Cenozoic Magmatic Activity in East Africa: New Geochemical Constraints on Magma Distribution within the Eocene Continental Flood Basalt Province. Geological Society, London, Special Publications SP518-2020–262. https://doi.org/10.1144/SP518-2020-262

Stewart, K., Rogers, N., 1996. Mantle plume and lithosphere contributions to basalts from southern Ethiopia. Earth and Planetary Science Letters 139, 195–211. https://doi.org/10.1016/0012-821X(96)00015-5

Streck, M.J., 2008. Mineral Textures and Zoning as Evidence for Open System Processes. Reviews in Mineralogy and Geochemistry 69, 595–622. https://doi.org/10.2138/rmg.2008.69.15

Streck, M.J., Grunder, A.L., 2012. Temporal and crustal effects on differentiation of tholeiite to calcalkaline and ferro-trachytic suites, High Lava Plains, Oregon, USA. Geochemistry, Geophysics, Geosystems 13. https://doi.org/10.1029/2012GC004237

Sun, S. s-, McDonough, W.F., 1989. Chemical and isotopic systematics of oceanic basalts: Implications for mantle composition and processes., in: Saunders, A.D. (Ed.), Magmatism in the Ocean Basins. Geological Society of London Special Publication 42, pp. 313–345.

Talbot, M.R., Morley, C.K., Tiercelin, J.-J., Le Hérissé, A., Potdevin, J.-L., Le Gall, B., 2004. Hydrocarbon potential of the Meso-Cenozoic Turkana Depression, northern Kenya. II. Source rocks: quality, maturation, depositional environments and structural control. Marine and Petroleum Geology 21, 63–78.

Tatsumi, Y., Kimura, N., 1991. Secular variation of basalt chemistry in the Kenya Rift: Evidence for the pulsing of asthenospheric upwelling. Earth and Planetary Science Letters 104, 99–113. https://doi.org/10.1016/0012-821X(91)90241-9

Tefera, M., Chernet, T., Haro, W., Teshome, N., Woldie, K., 1996. Geological map of Ethiopia. Geological Survey of Ethiopia.

Tepper, J.H., Kuehner, S.M., 1999. Complex zoning in apatite from the Idaho Batholith; a record of magma mixing and intracrystalline trace element diffusion. Am. Mineral. 84, 581–595. https://doi.org/10.2138/am-1999-0412

Tepley, F.J., Davidson, J.P., Tilling, R.I., Arth, J.G., 2000. Magma Mixing, Recharge and Eruption Histories Recorded in Plagioclase Phenocrysts from El Chichón Volcano, Mexico. Journal of Petrology 41, 1397–1411. https://doi.org/10.1093/petrology/41.9.1397

Thompson, D.A., Hammond, J.O.S., Kendall, J.-M., Stuart, G.W., Helffrich, G.R., Keir, D., Ayele, A., Goitom, B., 2015. Hydrous upwelling across the mantle transition zone beneath the Afar Triple Junction. Geochemistry, Geophysics, Geosystems 16, 834–846.

Thy, P., 1983. Phase relations in transitional and alkali basaltic glasses from Iceland. Contr. Mineral. and Petrol. 82, 232–251. https://doi.org/10.1007/BF01166618

Thybo, H., Artemieva, I.M., 2013. Moho and magmatic underplating in continental lithosphere. Tectonophysics 609, 605–619.

Tiercelin, J.-J., Potdevin, J.-L., Thuo, P.K., Abdelfettah, Y., Schuster, M., Bourquin, S., Bellon, H., Clément, J.-P., Guillou, H., Nalpas, T., 2012. Stratigraphy, sedimentology and diagenetic evolution of the Lapur Sandstone in northern Kenya: Implications for oil exploration of the Meso-Cenozoic Turkana depression. Journal of African Earth Sciences 71, 43–79.

Turner, S.P., Kirstein, L.A., Hawkesworth, C.J., Peate, D.W., Hallinan, S., Mantovani, M.S.M., 1999. Petrogenesis of an 800 m lava sequence in eastern Uruguay: insights into magma chamber processes beneath the Parana flood basalt province. Journal of Geodynamics 28, 471–487.

Ukstins, I.A., Renne, P.R., Wolfenden, E., Baker, J., Ayalew, D., Menzies, M., 2002. Matching conjugate volcanic rifted margins: 40Ar/39Ar chrono-stratigraphy of pre- and syn-rift bimodal flood volcanism in Ethiopia and Yemen. Earth and Planetary Science Letters 198, 289–306. https://doi.org/10.1016/S0012-821X(02)00525-3

Vance, J.A., 1962. Zoning in igneous plagioclase; normal and oscillatory zoning. American Journal of Science 260, 746–760.

Vanderkluysen, L., Mahoney, J.J., Hooper, P.R., Sheth, H.C., Ray, R., 2011. The feeder system of the Deccan Traps (India): insights from dike geochemistry. J Petrol 52, 315–343.

Villiger, S., Ulmer, P., Muntener, O., 2004. The Liquid Line of Descent of Anhydrous, Mantle-Derived, Tholeiitic Liquids by Fractional and Equilibrium Crystallization--an Experimental Study at 1{middle dot}0 GPa. Journal of Petrology 45, 2369–2388. https://doi.org/10.1093/petrology/egh042

Walsh, J., Dodson, R.G., 1969. Geology of northern Turkana, degree sheets 1, 2, 9, and 10. Geological Survey of Kenya.

Wescott, W.A., Wigger, S.T., Stone, D.M., Morley, C.K., 1999. Geology and geophysics of the Lotikipi Plain. Geoscience of Rift Systems-Evolution of East Africa, American Association of Petroleum Geologists Studies in Geology 44, 55–65.

Wilkinson, A.F., 1988. Geology of the Allia Bay area. Report of the Mines and Geology Department, Kenya 54.

WoldeGabriel, G., Yemane, T., Suwa, G., White, T., Asfaw, B., 1991a. Age of volcanism and rifting in the Burji-Soyoma area, Amaro Horst, southern Main Ethiopian Rift: geo- and biochronologic data. Journal of African Earth Sciences (and the Middle East) 13, 437–447. https://doi.org/10.1016/0899-5362(91)90107-A

Wolff, J.A., Ramos, F.C., Hart, G.L., Patterson, J.D., Brandon, A.D., 2008. Columbia River flood basalts from a centralized crustal magmatic system. Nat Geosci 1, 177–180.

Wolfenden, E., Ebinger, C., Yirgu, G., Renne, P.R., Kelley, S.P., 2005. Evolution of a volcanic rifted margin: Southern Red Sea, Ethiopia. Geological Society of America Bulletin 117, 846–864.

Yemane, T., Yohunie, T., 1987. Geological Report on sub-sheets A, B, and C (Agere Mariam NG-37-10).

Yu, X., Lee, C.-T.A., Chen, L.-H., Zeng, G., 2015. Magmatic recharge in continental flood basalts: Insights from the Chifeng igneous province in Inner Mongolia: MAGMATIC RECHARGE IN FLOOD BASALT. Geochem. Geophys. Geosyst. 16, 2082–2096. https://doi.org/10.1002/2015GC005805

Zanettin, B., 1978. The evolution of the Chencha escarpment and the Ganjuli graben (lake Abaya) in southern Ethiopian rift. Neues Jahrb. Geol. Paleontol. Monatshefte 8, 473–490.

Zanettin, B., Justin Visentin, E., Bellieni, G., Piccirillo, E.M., Rita, F., 1983. Le volcanisme du Bassin du Nord-Turkana (Kenya): Age, succession et évolution structurale. BCREDP 7, 249–255.

Zanettin, B., Justin-Visentin, E., Nicoletti, M., Piccirillo, E.M., 1980. Correlations among Ethiopian Volcanic Formations with Special References to the Chronological and Stratigraphical

problems of the “Trap Series.” Accademia Nazionale dei Lincei: Geodynamic Evolution of the Afro-Arabian Rift System: Meeting 47, 231–252.

Zellmer, G.F., Blake, S., Vance, D., Hawkesworth, C., Turner, S., 1999. Plagioclase residence times at two island arc volcanoes (Kameni Islands, Santorini, and Soufriere, St. Vincent) determined by Sr diffusion systematics. Contributions to Mineralogy and Petrology 136, 345–357.

Zellmer, G.F., Hawkesworth, C.J., Sparks, R.S.J., Thomas, L.E., Harford, C.L., Brewer, T.S., Loughlin, S.C., 2003. Geochemical evolution of the Soufriere Hills volcano, Montserrat, Lesser Antilles volcanic arc. Journal of Petrology 44, 1349–1374.